**The Dissertation Committee for Adam Joseph Berro Certifies that this is the approved version of the following dissertation:**

# Catalysis and Materials Development in Organic Chemistry

**Committee:**

C. Grant Willson, Supervisor

Brent L. Iverson

Dionicio R. Siegel

David A. Vanden Bout

Paul A. Zimmerman

# Catalysis and Materials Development in Organic Chemistry

**by**

**Adam Joseph Berro, B.S.**

**Dissertation**

Presented to the Faculty of the Graduate School of

The University of Texas at Austin

in Partial Fulfillment

of the Requirements

for the Degree of

**Doctor of Philosophy**

**The University of Texas at Austin**

**August, 2009**

# Dedication

Dedicated to Wendy Marriner, my family, and in memory of Emil C. Berro.

## Acknowledgements

First and foremost, I would like to thank my advisor, C. Grant Willson, to whom I owe a great deal of gratitude and without whom I would not be writing this dissertation. I have learned a lot in your lab and it has been an honor to work for you. To all who I have worked in collaboration with on the double exposure project, including Dr. Saul Lee, Dr. Kane Jen, Dr. Toshi Ogata (TOK), Dr. Younjin Cho (Cheil), Xinyu Gu, and Tomoki Nagai (JSR) at the University of Texas at Austin, I owe many thanks. There is far more work than one person could conceivably accomplish, and without them, there would be far less data to present. Thank you to Dr. Paul Zimmerman (SEMATECH and Intel), Dr. Robert Bristol (Intel), Prof. Nicholas Turro, as well as the Columbia University post-docs Dr. Naphtali O'Connor and Dr. Steffen Jockusch, for all of their help on the double exposure project and the great deal of knowledge on photochemistry that they shared with us.

To all of the people I have worked with over my graduate career, including Prof. Nathan Bauld, Dr. Jinkui Yang and Dr. David Cauble, I thank you for all of the work done on the [2+2] cycloaddition project and for all of the knowledge they passed on to a first year graduate student working on his first organic chemistry project.

To my coworkers, Jeff Strahan, Michael Jacobsson, Jacob Adams, Mikey Lin, and Sidd Chauhan, for making work bearable on days when it would otherwise not have been.

To Kathleen, as nothing here would ever get done without someone to keep us all going in the right direction and meeting our deadlines. To Ivan Jewett and Anna Smith in the Martin group, thank you for all of the helpful conversations on synthetic challenges that I have encountered and the search for ways around them. To Tom in the Fast lab, thank you for the HPLC help at the bitter end.

To my undergraduate students Elizabeth Adolph, Tony Gonzalez, and Travis Byargeon, best of luck in your future endeavors and thank you for all the hours of work that you put in. The added help has been much appreciated. Elizabeth, I hope that you find your graduate career at Vanderbilt to be rewarding

And to Wendy, while graduate school has been a long journey, I'm glad that we were able to do it together.

# Catalysis and Materials Development in Organic Chemistry

Publication No._____

Adam Joseph Berro, Ph.D.

The University of Texas at Austin, 2009

Supervisor: C. Grant Willson

The field of organic chemistry is divided into many subfields, which include polymer design and synthesis, transition metal catalysis and organocatalysis among a variety of others. Challenges in polymer design and synthesis can be highlighted pointedly in the use of photoresists for lithographic processing. Recent challenges in development of shorter wavelength sources has led to the need to develop new photoresist materials that can be exposed twice without any development steps in between. Two methods for addressing double exposure materials will be presented. Additionally, the areas of catalysis, whether transition metal or organic in nature, are important methods in organic synthesis. The mechanism of the addition of Gilman reagents to enones has been the subject of debate, and efforts to elucidate this mechanism will be presented. Finally, organocatalysis has expanded its scope into a variety of reactions previously only conducted with transition metal catalysts. Work towards an enantioselective allylic amination reaction using organocatalysis as well as absolute stereochemistry of the product will be explored.

# Table of Contents

# List of Tables

# List of Figures

## List of Schemes and Equations

# Chapter 1 *Introduction to Photolithography and Double Exposure Lithography*

## 1.1 DEVELOPMENT OF THE TRANSISTOR

From the humble beginnings of the transistor in the Bell Laboratories in 1947, the transistor has arguably become one of the most important inventions in the last century. It has enabled a vast array of electronic devices that now serve as indispensable components in daily life. This semiconductor-based device operates as both an electronic switch and as an amplifier, thus taking the place of much larger equipment, namely vacuum tubes. Incorporating these components into a smaller sized device allowed for the reduction of size for a computer from the size of a house down to a device capable of being placed onto the average desk. This in turn led to the incorporation of transistors into all manner of devices that have become ubiquitous with the information age.

Transistors were first placed into integrated circuits (ICs) in 1959 by Jack Kilby of Texas Instruments and Robert Noyce of Fairchild Semiconductor. This then lead to the development of digital logic, thus leading to the central processing units (CPUs) that drive the computer power of the personal computer. Transistors began to take over the electronics world in part because of the ability to mass-produce them onto wafers of ultrapure silicon along with the necessary additional components (i.e. capacitors, resistors, etc). This also had the added side benefit that the components themselves could be shrunk further from their initial sizes in the 1960s.

## 1.2 DRIVE TOWARDS SMALLER FEATURES

The semiconductor industry has continued to mature over the course of the last several decades with the size of features on semiconductor chips decreasing at a rapid pace. The continual decrease in feature size has allowed for the inclusion of semiconductor devices to expand from use in mainframe computers to the plethora of devices, such as cellular phones,

portable MP3 players, GPS devices, etc. This trend was accurately extrapolated by Intel co-founder and former CEO Gordon Moore in a publication in 1965,[1] which has become over the years to be known as "Moore's Law." While it is not a law per se, it has been the *de facto* standard by which the industry has measured its progress against not only previous years but also against competitors. In this publication, Moore asserted the density of transistors on an integrated device would double every 18-24 months (Figure 1.1).

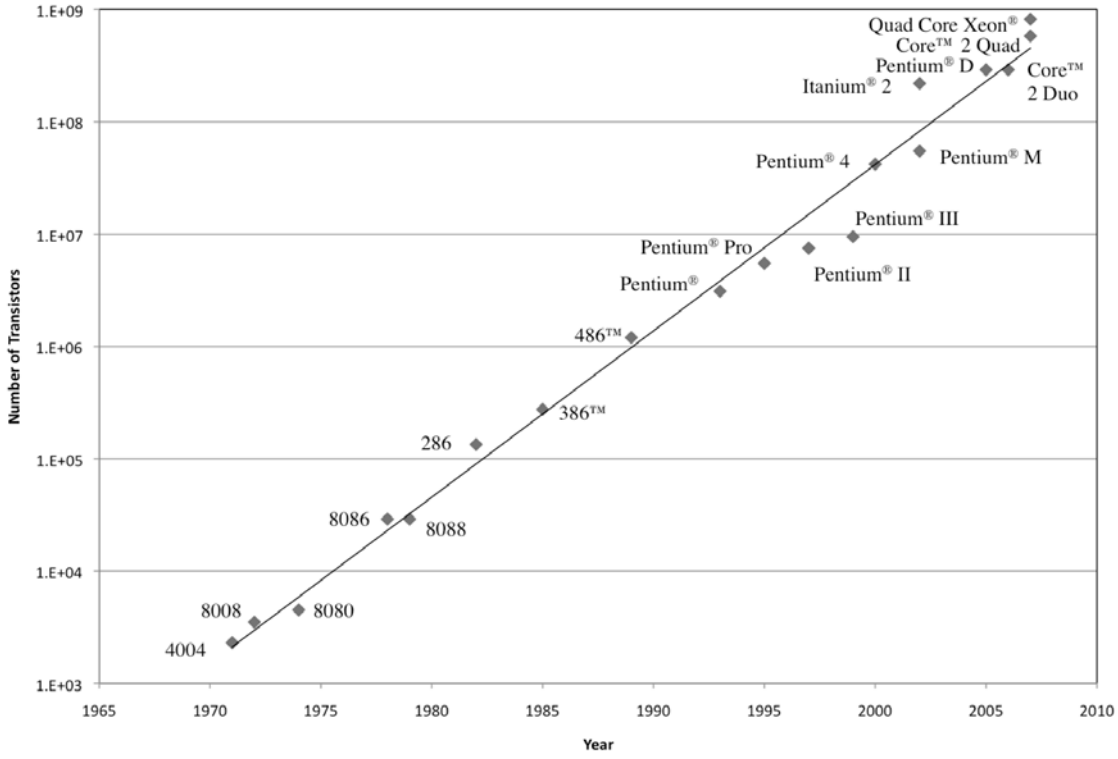


Figure 1.1. Transistor count for Intel microprocessors 1970-2007

In large part, this trend continues in the present; an astonishing run of 45 years. While the statement itself seems quite simple, the technological advances required to maintain this trend are largely masked to a more general audience. Inherent in these technological shifts is a continuing need to produce devices that work at faster speeds as well as the ability to maintain high device yield. It is this balance that has provided the many challenges that have had to be met in order to keep pace with Moore's Law.

As feature density has increased on semiconductor chips, there has been a corresponding dramatic decrease in feature size. Feature sizes *ca.* 1980 were on the order of 1-5 microns that today are routinely printed in the range of 45-60 nanometers. To place this size into perspective, at 80 nm, the width of a feature is now less than 600 carbon atoms wide as determined by the average distance of a carbon-carbon bond. Each density doubling has come in what the industry calls a technology node, defined by a length scale. Each of these technology nodes has required a modification in process, materials, equipment, or some combination to faithfully reproduce features onto silicon wafers. The confluence of these components is an area where engineering, chemistry and physics combine to form the discipline known as photolithography.

## 1.3 PHOTORESIST AND THE PHOTOLITHOGRAPHIC PROCESS

The photolithographic process is the means by which features are patterned onto silicon substrates. The word photolithography comes from a term used for the printing invention of Alois Senefelder in 1798.[2] Lithography originally referred to the process of applying a coating of grease to a limestone plate and transferring ink to a substrate, such as paper. The grease attracted the hydrophobic ink to the coated areas, thus allowing for contrast and reproduction of both writing as well as artistic work. In many ways, the photolithographic process is similar, however the means by which the pattern is transferred is quite different. Here, the limestone has been replaced with a photomask, which blocks light in regions that are coated with chromium, and allows light to pass through the uncoated regions, facilitating contrast and pattern transfer. The substrate in this case is a highly purified crystalline silicon wafer. The "ink" is represented as photoresist (also referred to as resist). The word photoresist itself reflects the dual purpose of this material. First, it must be photochemically reactive to the exposure wavelength, and second, it must be resistive to chemical etching.

For photoreactivity, there are two potential pathways (Figure 1.2). The exposed areas can become more soluble in a basic solution or developer, in which case one ends up with a positive tone resist. Conversely, the exposed areas can become less soluble in developer, leaving the opposite tone as before (negative tone). In most cases today, positive tone resists are favored due

to pattern fidelity and swelling issues that often accompany negative tone resists. The developed resist can then be etched, which transfers the image into the substrate. Finally, the remaining resist is stripped, resulting in the desired image. In this repetitious manner, the features of a semiconductor can be built up layer by layer.

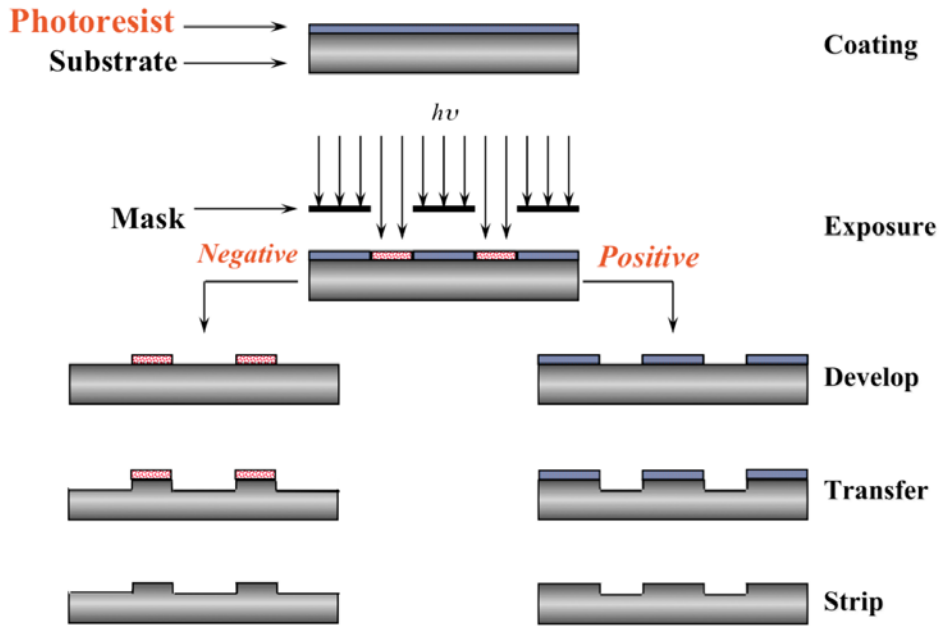


Figure 1.2. Positive and negative tone photoresist

While the process can be easily explained in a straightforward manner, in practice the procedures required to meet the desired specifications of the final product are quite difficult. As feature sizes have decreased, these tolerance levels have likewise shrunk.

## 1.4 LITHOGRAPHY PROCESSING

While the photoresist itself is extremely important to the overall lithographic processes, there are many steps that take place both before and after exposure that directly effect the overall outcome of the process. In fact, several steps must occur prior to the introduction of the photoresist. Since positive tone resist dominates manufacturing presently, the flow will be described as it pertains to these systems.

### Substrate Preparation

Before any work begins to apply the photoresist, the silicon wafer itself must be prepared to optimize resist performance. The first of these preparation steps is to treat the wafer to make adhesion of the photoresist more efficient. For this, a silicon-containing compound (referred to as an adhesion promoter) is coated onto wafer.[3] This layer reduces the hydrophilicity of the silicon wafer and allows for better adhesion from the primarily organic (and hydrophobic) layers that will be subsequently coated. Having now prepared the wafer for further coating, a bottom antireflective coating (BARC) is then coated to reduce the reflectance of the underlying silicon, which arises from the highly polished, mirror-like nature of the wafer. Reflected waves produce what is called the standing wave effect, the result of two waves traveling in opposite directions that combine.[4] The observable result of this combination is a wavy appearance in the developed image. To combat this effect, the BARC is coated to absorb or internally reflect the wave from the wafer. There is wavelength dependence to the standing wave phenomenon, and therefore the thickness of the antireflective coating is adjusted accordingly to minimize the light reflected back into the resist. Having now addressed the issues of adhesion and light reflection, the wafer is now ready for photoresist application.

### Photoresist Coating

The treated wafer is then brought into a spin-coating tool where the resist is applied as a solution in a low volatility solvent, such as propylene glycol methyl ether acetate (PGMEA), 2-heptanone, or various halogenated benzene compounds (Figure 1.3). These solutions come premixed from photoresist vendors, and contain far more than just resist resin. These formulations for a standard 193 nm photoresist (the current state-of-the-art exposure wavelength and toolset) contain predominantly photoresist (~90%), but also photoacid generators (PAG) used to alter the solubility of the polymer, as well as basic quenchers to control and stabilize the photoresist polymer, and in some cases, dissolution inhibitors to alter the reactivity of the resin.

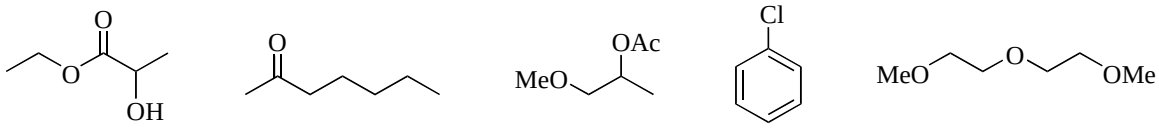


Figure 1.3. Structures of common casting solvents (ethyl lactate, 2-heptanone, PGMEA, chlorobenzene and diglyme left to right)

These different additives give lithographers a variety of "knobs" with which the resist characteristics can be tuned to the specific process requirements for the fabrication of specific products. The final composition is then diluted with solvent to approximately 10-20% weight ratio of resist to solvent.

The choice of solvent is quite important to this process, as it must be sufficiently solubilizing to the resist components, low enough volatility to allow for even coverage in the spin-coating process and low enough boiling point to facilitate easy removal during a short baking process conducted after coating.[3,5] The solution of resist and the accompanying components is dispensed onto the wafer, and coating across the whole wafer is accomplished by spinning the wafer at high speed. This allows the solution to spread and most of the solvent to be driven off. In recent years, this process has become quite efficient, with very low amounts of solution (in some cases, less than one milliliter) to coat an 8" diameter wafer. Through control of the spinning speed and the concentration of the initial solution, the thickness of the resulting film can be controlled down to the nanometer level with nanometer variability across the entire wafer.[6]

**Post-Apply or "Soft" Bake**

After coating, the wafer is then placed onto a heating plate to drive off most of the remaining solvent, which has large implications in diffusion path length of resist components.[5] Here, the temperature is tightly controlled to remove solvent but not exceed the temperature threshold for decomposition of the resist or any of the resist components.[7] This process additionally allows for better adhesion of the resist to the underlying layers. Post-apply bakes in a fabrication facility (or fab, as commonly referred to in the semiconductor industry) typically

lasts 30-90 s and is done at temperatures between 60 and 130 ºC. The wafer is now ready to be exposed.

**Lithographic Exposure**

The coated wafer is now moved into the exposure tool, where the wafer is precisely aligned not only in the x and y directions but also the z direction, as the exact focal length in the system is extremely important for faithful pattern replication.[8] Errors of more than a few nanometers can and often do result in nonfunctional devices. Modern exposure tools also utilize a small amount of water between the final lens element in the exposure optics and the resist itself, allowing for the use of higher numerical aperture lens systems, which allows for the printing of smaller features (*vida infra*). In addition to the precise nature of the alignment, the exposure dose (measured in $mJ/cm^2$) is also highly controlled so as to provide a uniform intensity of light exposure not only across a single wafer but across multiple wafers to ultimately give uniform pattern sizes on all finished devices. This is accomplished by utilizing a series of lens elements between the light source and the wafer. It is here the sensitivity of the resist plays a key role. Higher sensitivity leads to lower exposure doses required to print the desired pattern. Current resists rely on chemical amplification through the use of photochemically generated acid to deprotect blocking groups on the resist (in the case of a positive tone resist) and therefore provide gain in the ability of a small amount of light to provide a high number of chemical reactions (Scheme 1.1).

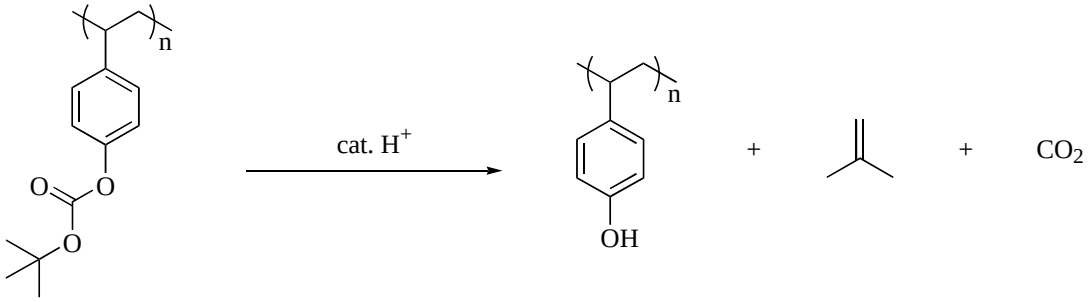


Scheme 1.1. Acid catalyzed deprotection of poly(*t*-BOC-styrene)

For the purposes of mass-production, lower exposure times are favored for higher throughput. The end result of the exposure is a latent image in resist, which is where gain is realized.

**Post Exposure or "Hard" Bake**

The exposed wafer is then moved to a hot plate where the chemical amplification process is exploited. By heating the wafer, the acid generated during exposure can diffuse through the polymer matrix and deprotect the blocking groups in a catalytic fashion. The higher the number of groups deprotected, the greater the dissolution rate in that area will be. Again, there is a balance that must be maintained, in this case between dissolution rate gain by deprotection and the unwanted sideways diffusion of the acid into unexposed regions called bias. For typical resists, the bake is done between 90 ºC (used for acetals and other low activation blocking groups) and 130 ºC (used for *t*-BOC blocking groups).[9]

**Development**

After the post exposure bake, the wafer is rinsed and developed. The developer is applied to the wafer and allowed to stand for 20-60 s. The developer solution sometimes contains additives to prevent collapse of the patterned features, decrease the roughness on the edges of the pattern, or to achieve wetting of the resist surface.[10] The wafer is then spun to remove the developer solution and subsequently baked to remove any remaining solvent before being etched.

**Ion Etching and Residual Resist Stripping**

In the final stages of patterning, the photoresist must peform the role of preventing ion bombardment in undesired areas. The wafer is placed into an etching chamber, where the atmosphere above the wafer itself contains etching gas (or mixture of gases) at low pressures that are subjected to a high electric field. This electric field turns the etching gas(es) into a plasma, which is then directed towards the wafer via this same electric field. This is done in a highly anisotropic fashion, so as to allow for more accurate pattern transfer into the unprotected

substrate.[11] This bombardment creates volatile products from the exposed portions that diffuse away in the high vacuum environment. The resist must block any of the reactive etch ions to reach the wafer surface in the areas that it remains, meaning the integrity of the film must be high towards the chosen etching components. Once the etching has proceeded to sufficient depth in the substrate, the wafer is moved to a second etching tool, where in most cases an oxygen plasma is used to remove the organic layers (namely, the resist) from the wafer surface without reacting with the silicon.[12] The combined processes provide the desired three-dimensional structure.

## 1.5 LIMITS TO RESOLUTION

Imaging of resist can be accomplished using many sources of irradiation, such as electron beam (e-beam), X-ray, ion beam, and ultraviolet. However, for the purposes of mass manufacture of semiconductor devices, ultraviolet irradiation has been the preferred method based upon the speed, cost, and availability of different source wavelengths. It should be noted that while X-ray and e-beam irradiation can provide higher resolution images, the cost of the source (X-ray illumination) and the speed of write (e-beam) have prevented these technologies from becoming industry standards. Electron beam writing has however become the standard method for fabrication of photomasks, the source of the patterns exposed onto the wafers, since the need for high resolution is great, while speed is a far lesser concern.[13]

The wavelength of exposure has a direct effect upon minimum feature size one can print. Lower wavelengths can allow the lithographer to produce smaller images, as governed by the Rayleigh equation (Equation 1.1).

$$R = \frac{k_1 \lambda}{NA} \quad (NA = n \sin\theta)$$

Equation 1.1. Rayleigh equation

In this equation, the resolution limit R is equal to the processing factor $k_1$, a dimensionless value related to the photoresist itself multiplied by the wavelength of light λ, divided by the numerical aperture of the lens system *NA*. *NA* is determined to be *n* multiplied by the sine of the angle Θ, where *n* is the refractive index of the medium (for reference, *n* of air =1.00) and Θ is the maximum angle from incident that the light can be captured by the lens.

As can be seen from this relationship, reducing the wavelength of light used or the processing factor for the resist material or increasing the numerical aperture of the lens system will allow for the resolution of smaller features. However, there are limits to each of these factors. First, the $k_1$ factor has a theoretical limit of 0.25. The wavelength is restricted by the availability of sources with sufficient power to provide adequate illumination, and the lens's *NA* is limited by the medium through which the light will travel. This includes not only the lens itself but also the material between the lens and the photoresist as well as the photoresist itself. Historically, these issues have not prevented feature size reductions, although these problems have begun to manifest themselves recently.[14] Lithographers particularly have focused upon advances in materials for resists to maintain adequate levels of transparency and etch resistance to keep up with lens materials and exposure technology, while optics engineers have focused on the latter two. It should be noted that *NA* is also limited due to processing factors. This stems from the fact that not every exposure will be at exactly the same distance from the lens element, even though this parameter is controlled quite well in current exposure tools. In order to have the high product yields, there must be some tolerance for variance in the focal point of the system, where if the focus depth is inaccurate by some small factor that it will not affect the final pattern. In processing terms, this is called depth of focus (DOF), which can be determined by the following equation (Equation 1.2).

$$DOF = \frac{k_2 \lambda}{NA^2} \quad (NA = n \sin\theta)$$

Equation 1.2. Depth of Focus

Because of the inverse relation between depth of focus and the square of numerical aperture, it has largely been the case that higher resolution is preferably achieved with decreasing exposure wavelength when possible because of the direct relationship between DOF and wavelength.

As the push to decrease feature size continues, lithography technology continues to advance by finding new materials that retain the desirable characteristics of past systems while improving upon photospeed (to lower dose requirements) and to work with ever shrinking wavelengths of exposure. While new challenges arise to push feature size below the current state-of-the-art 45 nm processes, it is imperative that lithographers continue to develop creative solutions to overcome current process limitations.

## 1.6 PHOTORESIST CHEMISTRY

The earliest photoresists used for semiconductor manufacture were based upon an isoprene rubber resin and a *bis*-arylazide (Figure 1.4).

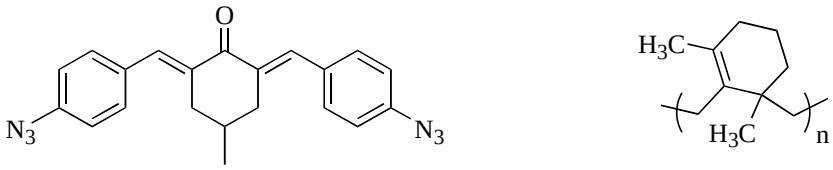


Figure 1.4. Example *bis*-arylazide and cyclized isoprene polymer

The isoprene polymer resin in these systems is partially cyclized, in order to increase the glass transition ($T_g$) of the material for processing purposes. When exposed to UV light, the *bis*-arylazide decomposes to form a nitrene and expel nitrogen gas (Scheme 1.2). In this manner, a reactive intermediate is generated that is capable of cross-linking adjacent polymer chains. This renders the exposed area insoluble in developer, resulting in a negative tone resist.[2] This can occur through formation of aziridines (as shown in Scheme 1.2), as well as several other modes.

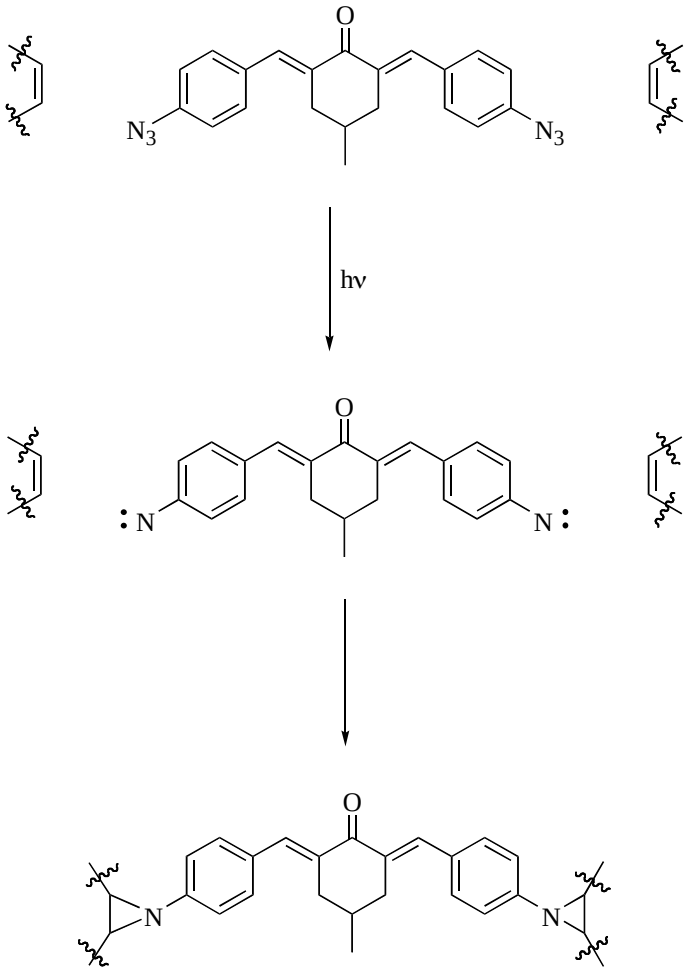


Scheme 1.2. Formation of cross-links from photochemical aziridine formation

Gradually, these *bis*-arylazide systems were phased out in favor of using positive tone systems due to their enhanced resolution capabilities as well as higher thermal stability and resistance to dry etching.[2] The first resist of this type was the novolac-diazonaphthoquinone (DNQ) system (Scheme 1.3).[15] These resists took advantage of the solubility in basic media of the novolac, a resin comprised of repeating phenol units and the dissolution inhibition properties of the DNQ. Additionally, novolac was found to not only be soluble in a large number of organic solvents but also can be spin-coated into highly uniform glassy films.

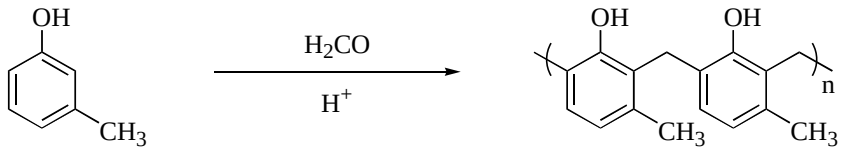


Scheme 1.3. Synthesis of novolac

With the addition of sufficient quantities of DNQ (roughly 15 to 20% by weight), the dissolution rate of novolac becomes orders of magnitude slower in basic developer.[2] The key component of this system is the photoreactivity of the DNQ unit. Upon exposure to ultraviolet light, the DNQ undergoes a Wolff rearrangement to form a ketene and releases nitrogen gas (Scheme 1.4).[16] Because there is a small amount of water present, the reactive ketene forms a carboxylic acid, becoming highly base soluble. Because of this switch, there is no longer any inhibition of the novolac from dissolving in the basic developer, and thus the exposed areas dissolve very quickly to provide a positive tone resist.

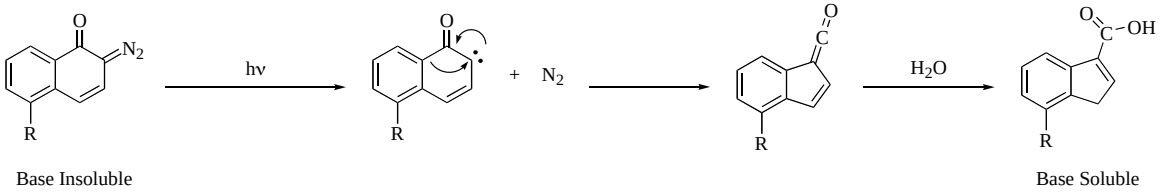


Scheme 1.4. Photochemical Wolff rearrangement of DNQ

These novolac/DNQ systems have proved to be very valuable in semiconductor manufacturing, as they are still in use for layers that do not require the smallest possible features (on the order of microns). Combined with the intensity from mercury arc lamps fitted with the proper filters, corresponding to the g (436 nm) and i-line (365 nm) emissions, lithographers have the setup that took some of the opening steps in pushing society into the information age.

While these systems were quite effective in the near UV region, this resist system became too absorbing for effective exposure to be conducted at reasonable dosages when moving to the lower wavelengths required to push feature sizes to smaller dimensions. Additionally, the quantum yield of the Wolff rearrangement is between 0.1 and 0.3,[2] which was acceptable when utilizing extremely bright sources such as mercury arc lamps, but is much too inefficient to

provide a acceptable printing speed at sub 250 nm exposure wavelengths where light sources are comparatively dim. A new type of system was needed to overcome these limitations.

## 1.7 DEVELOPMENT OF CHEMICALLY AMPLIFIED RESISTS (CARS)

With the development of excimer lasers, a source that was powerful enough for lithography was now in hand, however a new type of resist that could effectively image at significantly lower dosage (measured in tens of millijoules instead of hundreds of millijoules, as was the case in g and i-line resists) still had to be developed. In order for this to occur, there must be a mechanism by which each photon was able to initiate more than one reaction, resulting in amplification. In the best of cases, a DNQ based system would only afford one Wolff rearrangement per photon. Along these lines, ionic compounds were being developed simultaneously at 3M[17] and at General Electric[18] that would radically alter the way in which photoresists operate. Being pursued for the purposes of cationic polymerizations, these compounds would generate acid upon exposure to deep UV irradiation[19] and came in two different types, iodonium salts and triarylsulfonium salts (Figure 1.5).[19]

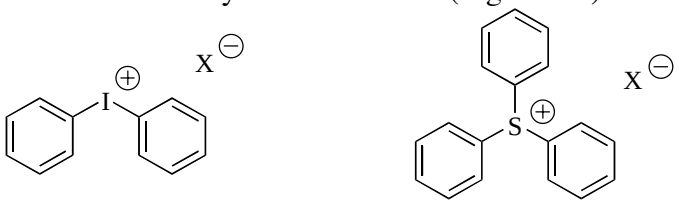


Figure 1.5. Generic Structures of Iodonium and Sulfonium PAG compounds

In both cases, the anion is the conjugate base from a superacid.[20] For the cationic polymerization reactions they were meant to initiate, acid strength was key to the overall yield of the reaction, and it turned out this fortuitous overlap in material requirements would help propel the semiconductor industry into its modern form.

Work being conducted at International Business Machines (IBM) at the time was focused on the challenge of developing a new photoresist that would work at 248 nm, the exposure wavelength generated from a krypton fluoride (KrF) excimer laser source. The new resist was based upon *tert*-butoxycarbonyl (*t*-BOC) protected poly(*p*-hydroxystyrene), which could be

deblocked (Scheme 1.1) and thus change its solubility characteristics when heated in the presence of acid.[21,22] The development of photoacid generators (PAGs) allowed for the use of this new type of resist, which takes advantage of chemical amplification, as a small amount of generated acid could deblock a large number of *t*-BOC groups. This type of resist has become known in the lithography world as a chemically amplified resist (CAR), which remains today the standard resist type for all deep UV (DUV) exposures.[23]

This idea has since been extended to 193 nm exposure through the use of non-aromatic containing polymers, a switch that was made in order to decrease the absorbance of the resist, as ideally the only absorbing component in the resist system is the PAG. Currently, CARs utilize acetals and tertiary esters as the acid-sensitive blocking groups attached to a methacrylate backbone (Figure 1.6).

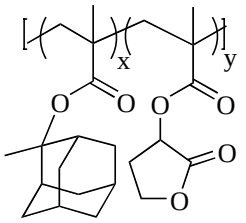


Figure 1.6. Example of 193 nm resist polymer

## 1.8 THE END OF OPTICAL LITHOGRAPHY?

As mentioned in a previous section, the resolution limit of an optical exposure tool is related to the processing factor $k_1$ multiplied by the wavelength divided by the *NA* of the lens system (Equation 1.1). Until recently, a typical dry 193 nm exposure tool, that is, one which has air as the medium between the lens system and the resist, was near the fundamental limit for a lens system with *NA* of slightly lower than 1.00. To circumvent this problem, 193 nm immersion exposure tools (193i) were implemented to allow for higher *NA* lens systems. While this modification extended resolution limits down to 45 nm, these systems are now encountering their resolution limits as well.[24] The processing factor in modern processes is now running near the theoretical limit of $k_1$=0.25 (though it should be noted that $k_1$=0.27 is the generally accepted limit for manufacturing purposes)[25] and efforts to alter the lens stack, interstitial medium, and resist's

refractive index have been dropped from industry consideration.[26] Earlier this decade, work to lower the exposure wavelength to 157 nm using fluorine excimer laser sources met with a similar fate. This has left lithographers with a significant challenge in order to reduce feature sizes for the next manufacturing node. Presently, 45 nm processes are the smallest in production with 32 nm processes being ramped up for commercial manufacture at major semiconductor fabs.

Other options, such as extreme ultraviolet (EUVL) and imprint lithography have been deemed not ready by the industry, again reducing the number of potential solutions to the feature size reduction down to the 22 nm node.[32] One potential way around the limitations presented by the Rayleigh equation would be to split the pattern into two parts, with each part patterned in a separate exposure step. In order to accomplish this, one must develop some alternative methods. A traditional photoresist exposed twice with the same pattern shifted to half the pitch on the second exposure will provide no image, as the latent image produced from the exposure is not a step function, but instead resembles a sine wave. When the two images are put together, they appear to be that of a sine and cosine wave, which when added together produce a value of 1. There is no intensity modulation, which results in complete development of the resist and no residual features (Figure 1.7).

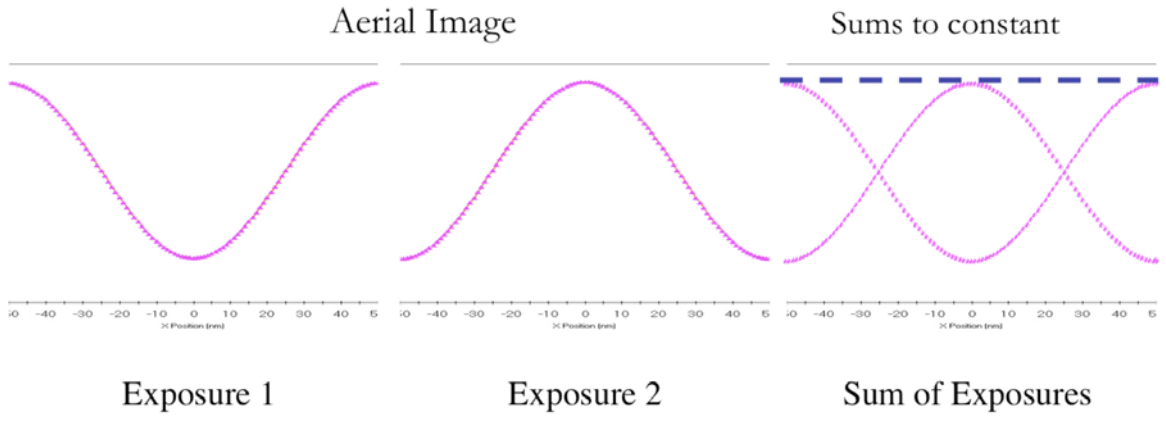


Figure 1.7. Summation of exposure passes offset by one period

This has left two solutions remaining to solve this sizeable technical challenge: double patterning lithography (DPL) and double exposure lithography (DEL). In a double patterning

approach, a standard 193 nm resist is used, but only half of the desired pattern is printed in the exposure. The resist is then processed as normal. A second coating of resist is applied after the development and etching steps, and the wafer is exposed a second time to add the second half of the desired pattern. After a second round of development and etching steps, the final pattern emerges (Figure 1.8). This allows for the features to be placed at an effective spacing closer than would be allowed in a single pass due to the Rayleigh equation.

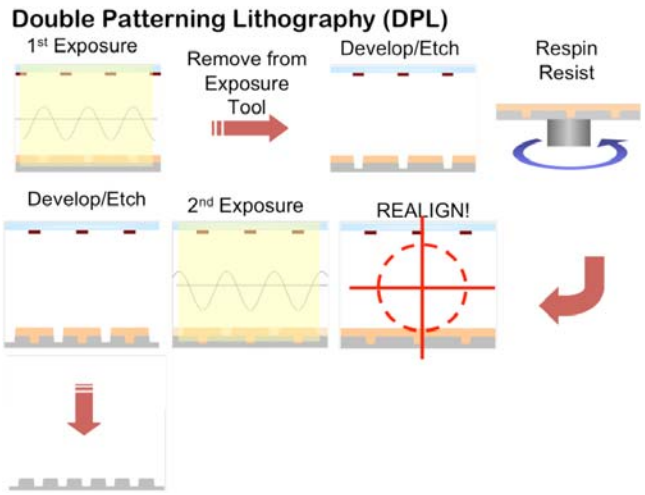


Figure 1.8. Process flow for DPL

In the DEL approach, there are also two exposure steps, but in this case, the exposures occur in the same exposure tool. By using this approach, the development and etching steps would only need to be done once, saving a significant number of steps and consequently, saving time as well which reduces the cost of the process (Figure 1.9). There is, of course, a caveat to this approach. Unlike in a DPL setup where only standard, available materials are needed for both exposures, a DEL approach requires a new sort of resist material that possesses a nonlinear response to exposure dose, so as to avoid the summation effect due to the sine wave nature of the aerial image. This means the simple model of chemical amplification used up to this point for DUV resists will not be useful in a DEL system.

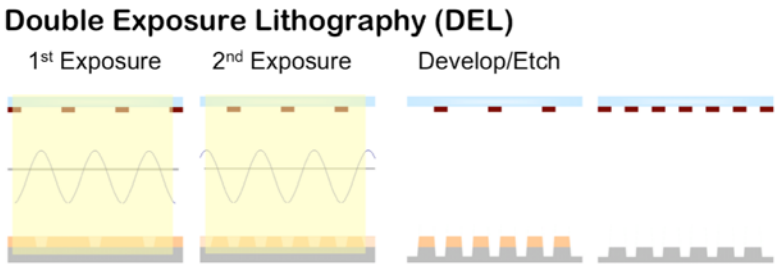


Figure 1.9. DEL process flow

## 1.9 DOUBLE EXPOSURE LITHOGRAPHY OPTIONS

At the outset of this project, a few different ways to approach the challenge of developing a system with a nonlinear relationship between the dose applied and the response of the resist were considered. For the purposes of this project, it made sense to evaluate these options first through simulation work, as it would allow us to eliminate possibilities that appeared to have a lower likelihood for success and to focus on the more promising avenues of research. To accomplish this engineering side of the project, simulations were undertaken using industry standard simulation software called ProLith™, with some modifications to the acid generation behavior of the resist. In several of the possibilities for double exposure materials there is no acid generation *per se*, so code must be written in such a fashion as to interface with the software in a manner it understands, thus the somewhat unusual terminology for the actual reactions occurring in the system itself. ProLith™ was not written in such a way that anticipated double exposure projects, so this code was generated as a collaboration between our group and SEMATECH, the semiconductor research consortium, particularly through the efforts of Dr. Jeffrey Byers from SEMATECH and Saul Lee and Kane Jen in the Willson group.[24,25,27] This code takes the output of the latent image in resist from ProLith™ and replaces the standard acid generation code, allowing for a nonlinear response to the input dose. This response is fed back into the simulation software, which then allows the generation of standard exposure latitude plots, showing the effects of minor variations in depth of focus and Bossung plots, which show

the effects of minor variations in dose on feature size, commonly referred to as critical dimension or CD (Figure 1.10).

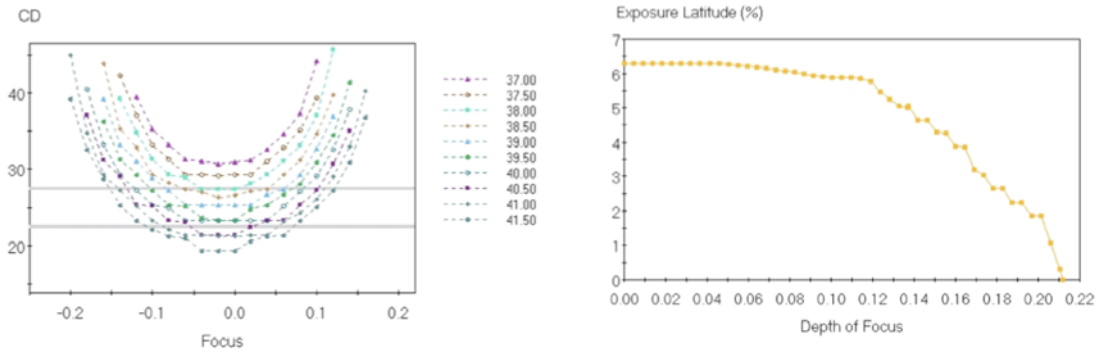


Figure 1.10. Examples of Bossung (left) and depth of focus (right) plots

We chose to look at four different approaches to DEL: reversible contrast enhancement layers (rCEL), a two-stage photoacid generator (referred to as an intermediate-state two-photon photoacid generator or ISTP), simultaneous two-photon photoacid generators, and optical threshold layers (OTL), all of which will be explained in the following sections.

## 1.10 REVERSIBLE CONTRAST ENHANCEMENT LAYERS

The first of the approaches evaluated by simulation was the reversible contrast enhancement layer (rCEL). Nonreversible variants of this concept are already in existence,[28] so no custom code was necessary for ProLith™ simulation to evaluate these materials. For these materials, the layer is coated on top of the photoresist and is initially opaque to the exposure wavelength. During exposure, the layer bleaches progressively as the dose increases, resulting in the areas of highest exposure becoming almost completely transparent and allowing exposure in the underlying photoresist. This should in practice take the sine wave-like image in resist and modify it to look more like a step function in the resist (Figure 1.11).

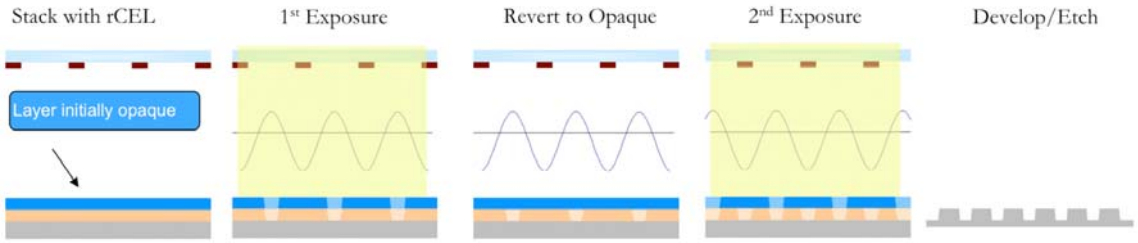


Figure 1.11. rCEL concept

This approach requires a rapid bleaching effect in the rCEL material, going from an effectively opaque film to a largely transparent one. In lithography, the key values related to absorbance are presented in slightly different fashion than would be the case in chemistry. The resist response is broken into three components, called Dill parameters,[29,30] which relate to the initial absorbance of the material (Dill A), the absorbance after exhaustive exposure (Dill B), and the rate at which the absorbance changes (Dill C). In the case of an rCEL material for double exposure, the simulation was run using several Dill A values (measured $\mu m^{-1}$) to find a useful initial absorbance value that would afford reasonable images in the underlying resist (Figure 1.12).

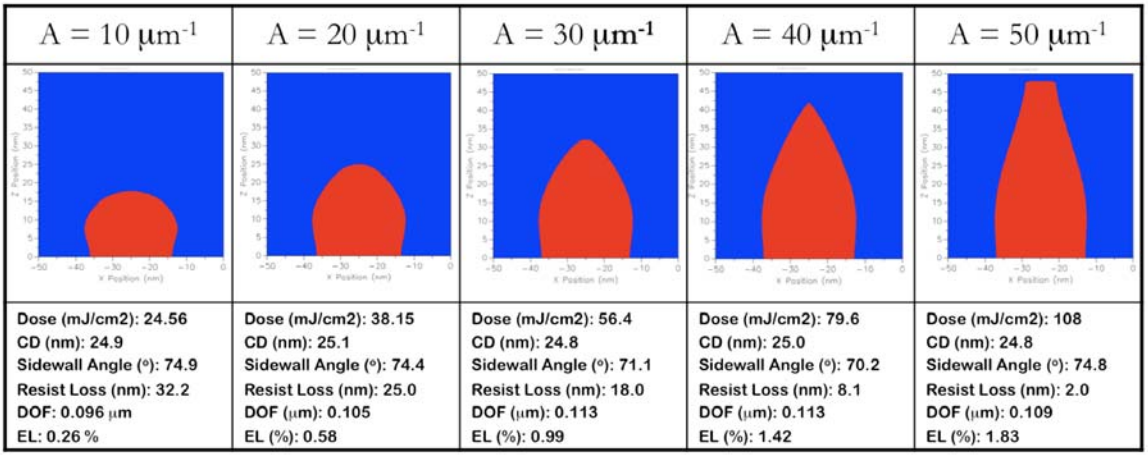


Figure 1.12. Reversible CEL simulation results. The red area represents the features that would remain after the exposure and development steps, while the blue area is the initial resist removed during development.

As shown above with an absorbance of 10 $\mu m^{-1}$, the resulting image generated in the resist is unacceptable due to a high amount of resist loss as well as the poor shape of the resolved features, which under ideal circumstances would more closely resemble rectangular structures than the highly rounded shape seen at this absorbance level. When moving to higher absorbance values, predictably the dose requirement increases quite substantially, though a reasonable image can be obtained with a Dill A value of 50 $\mu m^{-1}$. This however poses a significant problem, as absorbance is on the order of a metal layer similar to the type used in photomasks. Keeping in mind this layer must be capable of bleaching to allow light to penetrate to the underlying resist for an image to be formed, in essence one would be required to develop a bleachable chromium-based material; a daunting challenge that seemed to be an undesirable avenue of research. Neglecting the material challenge of developing what amounts to a bleachable metal, the dosage required to image such a system was calculated to be on the order of ~70 $mJ/cm^2$, nearly an order of magnitude higher than dosages commonly used in present 193 nm immersion systems. This means not only would there be a speed penalty for two exposures, but that each exposure itself would be quite slow. Due to these factors, it was decided to abandon efforts to develop such materials and to focus on more promising avenues.

## 1.11 SIMULTANEOUS TWO-PHOTON PHOTOACID GENERATORS

A second option for a double exposure system was to alter the PAG in such a way as to prevent it from generating acid without the absorbance of two photons. This would introduce nonlinearity to the acid production and allow for a pitch divided imaging regime. Such materials have been proposed in lithographic systems previously in semiconductor fabrication to improve contrast in single exposure systems.[31] These systems unfortunately suffer from poor quantum yield, and thus require high exposure doses for image generation. By calculating the laser power/pulse in a standard 193 nm exposure tool, it was determined the number of laser pulses required to generate acid from ~20% of the PAG present in the film was on the order of $10^{12}$ pulses; a figure untenable without significant advances in laser output, ruling this out as a potential approach.[25]

## 1.12 INTERMEDIATE-STATE TWO-PHOTON PAG

While simultaneous absorption of two photons appeared to be impractical, it was thought that by allowing for the two photons to be absorbed in a sequential fashion that the issue of laser power could in large part be avoided. This type of arrangement would require the generation of a short-lived intermediate with a first photon that upon absorption of a second photon could then go on to produce acid. If no second photon is encountered, the intermediate would either decay to some inactive state or decay back to the initial state either by using ambient energy or through exposure at some different wavelength. While more complicated than a simultaneous two photon PAG, having time to absorb the second photon dramatically improves the viability of this approach (Figure 1.13).

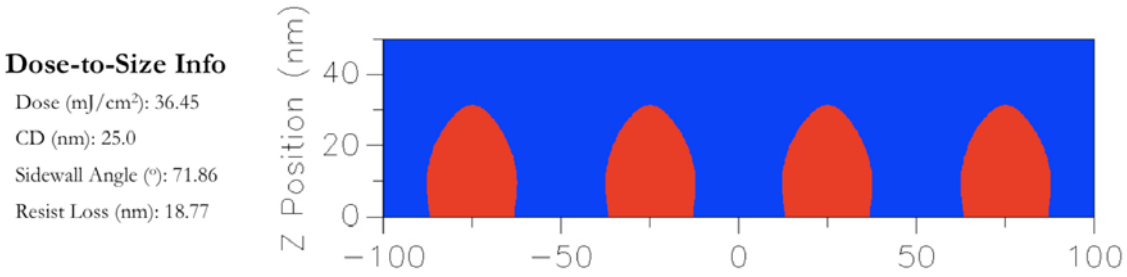


Figure 1.13. ISTP simulation results

As seen from the above representation of these results, the dosage required for this approach is in a far more reasonable range (~30 mJ/cm). Again, the image in resist is of lower quality than a typical 193 nm resist and there is still significant resist loss. However it is likely that optimization could provide a higher contrast as well as a more manufacturing friendly image in resist. This approach was deemed promising enough for further study and will be discussed in Chapter 2.

## 1.13 OPTICAL THRESHOLD LAYER

Perhaps the most ambitious of the possible approaches to a double exposure lithographic solution, the optical threshold layer (OTL) concept would require a completely different way of resist function. Thermal resists rely on a thresholding concept, using energy from phonons in

place of photons. It works in a method that is much like the melting of a solid, where a threshold level of energy is required in order for the state change to occur. If a dose just below this threshold is applied and the sample removed from the energy source, one must still input the threshold level of energy in order for the melting event to occur. In current resist systems, the inability to do this is commonly referred to as resist "memory," which prevents two exposure passes to one resist. Presently in photoresists, exposures are additive, so for this concept to work, a way to obtain this threshold response using photons as the energy source must be determined (Figure 1.14).

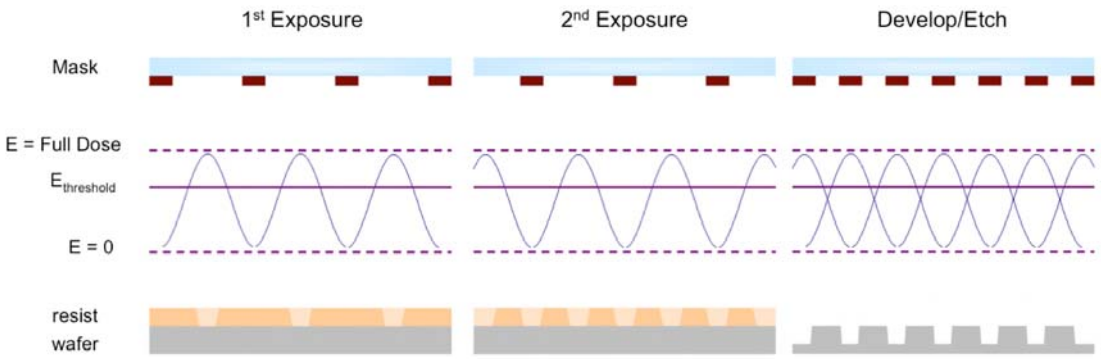


Figure 1.14. Optical Threshold Layer concept

Simulation indicated this approach to be the most promising of the methods tested. For this approach, the acid generation code was altered so that no acid generation occurs in areas that receive sub-threshold dose. As can be seen in the simulation output (Figure 1.15), the sidewall angles were reasonable for a first pass (angles approaching 90° are preferred), and the amount of calculated resist loss was far lower than in any other method simulated. In spite of the amount of materials development required for this approach, the simulation results were strong enough to justify effort conducted into this area to attempt to find materials that could satisfy the threshold requirements the OTL would require, and our efforts in this area will be detailed in Chapter 3.

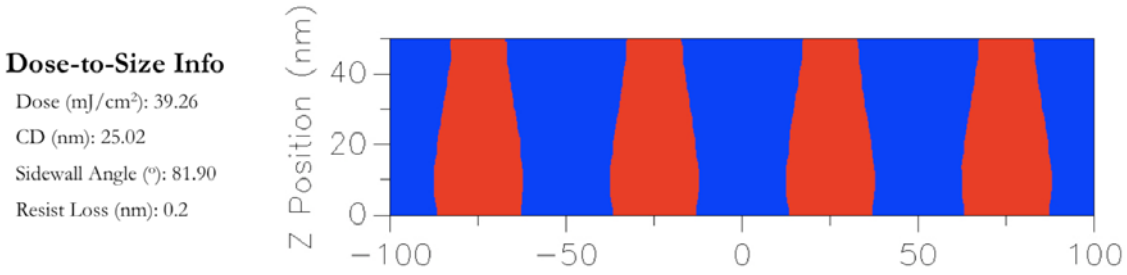


Figure 1.15. OTL simulation results

## 1.14 CONCLUSION

The photolithographic process has been a highly efficient technology enabler. First it allowed for computing power that required machines the size of houses to be shrunk into a box that fits on a standard desk. Lithographers have been continually challenged to shrink the size of the features printed, incorporate new exposure technologies, and have routinely advanced the techniques in use all the way from near UV light sources to the present argon fluoride 193 nm excimer laser sources. The incremental improvement in resists, exposure sources, and processing techniques have served the industry well over the course of the last several decades, however because theoretical limits of processing techniques and the resolution limit of current source technology, more creative approaches to further feature size reduction, such as double exposure lithography, will be required going forward.

## 1.15 REFERENCES

(1) Moore, G. E. *Electronics* **1965**, *38*, 114-117.
(2) Willson, C. G. In *Introduction to Microlithography*; Thompson, L. F., Willson, C. G., Bowden, M. J., Eds.; American Chemical Society: Washington, D.C., 1983, p 87-159.
(3) Morneau, W. M. In *Semiconductor Lithography*; Plenum Press: New York, 1988, p 259-327.
(4) Mack, C. A. In *Fundamental Principles of Optical Lithography*; John Wiley & Sons: West Sussex, 2007, p 129-140.
(5) Thompson, L. F.; Bowden, M. J. In *Introduction to Microlithography*; Thompson, L. F., Willson, C. G., Bowden, M. J., Eds.; American Chemical Society: Washington, D.C., 1983, p 161-214.
(6) Mack, C. A. In *Fundamental Principles of Optical Lithography*; John Wiley & Sons: West Sussex, 2007, p 15-18.
(7) Morneau, W. M. In *Semiconductor Lithography*; Plenum Press: New York, 1988, p 329-353.
(8) Morneau, W. M. In *Semiconductor Lithography*; Plenum Press: New York, 1988, p 355-408.

(9) Mack, C. A. In *Fundamental Principles of Optical Lithography*; John Wiley & Sons: West Sussex, 2007, p 224-235.
(10) Thompson, L. F. In *Introduction to Microlithography*; Second Edition ed.; Thompson, L. F., Willson, C. G., Bowden, M. J., Eds.; American Chemical Society: Washington, D.C., 1994, p 332-341.
(11) Morneau, W. M. In *Semiconductor Lithography*; Plenum Press: New York, 1988, p 631-777.
(12) Morneau, W. M. In *Semiconductor Lithography*; Plenum Press: New York, 1988, p 779-812.
(13) Morneau, W. M. In *Semiconductor Lithography*; Plenum Press: New York, 1988, p 409-458.
(14) Matsumoto, K.; Costner, E. A.; Nishimura, I.; Ueda, M.; Willson, C. G. *Macromolecules* **2008**, *41*, 5674-5680.
(15) Kawabe, Y.; Tan, S.; Nishiyama, F.; Sakaguchi, S.; Kokubo, T.; Blakeney, A. J.; Ferreira, L. *Proc. SPIE Int. Soc. Opt. Eng.* **1996**, *2724*, 420-437.
(16) Willson, C. G. In *Introduction to Microlithography*; Thompson, L. F.; Willson, C. G.; Bowden, M. J., Eds.; American Chemical Society: Washington, D.C., 1983, p 87-159.
(17) Smith, G. H. US Patent 19830719.
(18) Crivello, J. V. US Patent 19760921.
(19) Crivello, J. V. *J. Polym. Sci., Part A: Polym. Chem.* **1999**, *37*, 4241-4254.
(20) Olah, G. A.; Surya Prakash, G. K. *Superacids*; Wiley: New York, 1985,7-8.
(21) Frechet, J. M. J.; Eichler, E.; Ito, H.; Willson, C. G. *Polymer* **1983**, *24*, 995-1000.
(22) Willson, C. G.; Ito, H.; Frechet, J. M. J.; Tessier, T. G.; Houlihan, F. M. *J. Electrochem. Soc.* **1986**, *133*, 181-7.
(23) Ito, H. *Adv. Polym. Sci.* **2005**, *172*, 37-245.
(24) Byers, J.; Lee, S.; Jen, K.; Zimmerman, P.; Turro, N. J.; Willson, C. G. *J. Photopolym. Sci. Technol.* **2007**, *20*, 707-717.
(25) Lee, S.; Byers, J.; Jen, K.; Zimmerman, P.; Rice, B.; Turro, N. J.; Willson, C. G. *Proc. SPIE* **2008**, *6924*, 69242A/1-69242A/12.
(26) Zimmerman, P. A.; Rice, B. J.; Piscani, E. C.; Liberman, V.; Harry, J. L., Mircea, V. D., Eds.; SPIE: 2009; Vol. 7274, p 727420.
(27) Lee, S.; Jen, K.; Willson, C. G.; Byers, J.; Zimmerman, P.; Turro, N. J. *J. Micro/Nanolithogr., MEMS, MOEMS* **2009**, *8*, 011011/1-011011/11.
(28) Grant, B. D.; Clecak, N. J.; Twieg, R. J.; Willson, C. G. *IEEE Transactions on Electron Devices* **1985**, *28*, 1300-1305.
(29) Dill, F. H. *IEEE Transactions on Electron Devices* **1975**, *22*, 440-444.
(30) Dill, F. H.; Hornberger, W. P.; Hauge, P. S.; Shaw, J. M. *IEEE Transactions on Electron Devices* **1975**, *22*, 445-452.
(31) Kuebler, S. M.; Braun, K. L.; Zhou, W.; Cammack, J. K.; Yu, T.; Ober, C. K.; Marder, S. R.; Perry, J. W. *J. Photochem. Photobiol., A* **2003**, *158*, 163-170.
(32) Wurm, S. *J. Photochem. Sci. Technol.* **2009**, *22*(1), 31-42.

# Chapter 2 *Development of Intermediate-State Two-Photon Photoacid Generator Systems*

## 2.1 INTRODUCTION

Having established through simulation studies that the ISTP concept could afford pitch doubled images, work then began to look at methods for achieving a system that would fit the necessary parameters.[1-3] It became clear early on in this process that the simplest approach would be to isolate the individual parameters. This allowed for isolation of individual response parameters (Figure 2.1), namely acid generation and photon absorption (sensitizer). It also had the added benefit of being able to draw directly from the literature for potential sensitizer components.

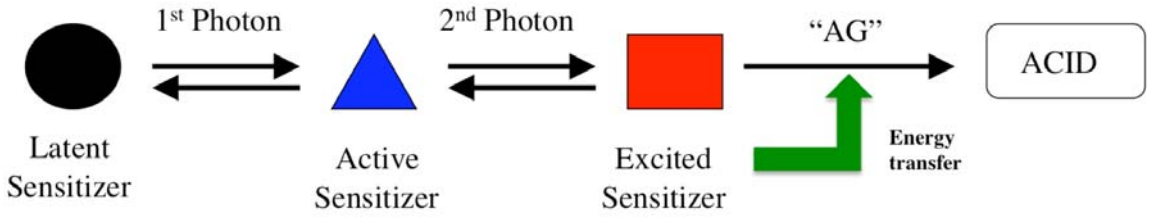


Figure 2.1. Schematic of ISTP concept

The first component required is a PAG that does not absorb light at the operational wavelength. For initial studies, we decided to work at higher wavelengths, namely 248 nm, in order to have a larger pool of known sensitizer compounds to work with. Operating at 248 nm also simplifies the task of generating compounds that are transparent, as more transparent functional groups are available at this wavelength.[4]

## 2.2 SYNTHESIS OF NON-ABSORBING PAG COMPOUNDS

It was decided to synthesize a pair of norbornane-based hydroxamic ester PAGs, where the acid component comes from a triflate functionality (Figure 2.2). This type of scaffold was known, however it was based on the norbornene rather than a norbornane molecule.[5,6]

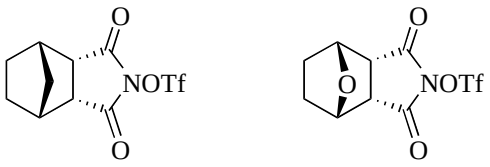


**2.1a** **2.1b**

Figure 2.2. PAG compounds targeted for synthesis

Because we wished to have a system that was non-absorbing, we needed to find a synthesis for this type of structure that does not incorporate the unwanted carbon-carbon double bond functionality. We started with the known *endo*-norbornene-dicarboxylic anhydride (synthesized via Diels-Alder reaction of furan and maleic anhydride), the double bond was reduced using Pd/C catalyst under modest pressure of hydrogen gas (Scheme 2.1).

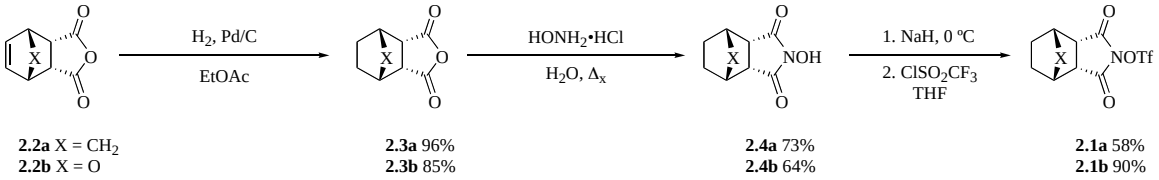


**2.2a** X = $CH_2$
**2.2b** X = O

**2.3a** 96%
**2.3b** 85%

**2.4a** 73%
**2.4b** 64%

**2.1a** 58%
**2.1b** 90%

Scheme 2.1. Synthesis of imide triflate PAG compounds

The *endo*-norbornane anhydride **2.3a** was then converted to the hydroxyimide **2.4a** by condensation with hydroxylamine in aqueous base at reflux. Finally, the latent acid functionality was installed by deprotonation of the hydroxyl group with sodium hydride and reacting the anion with trifluoromethanesulfonyl chloride. An analogous set of reactions was conducted with the oxo-bridged version of the starting material (**2.2b**). Both products were obtained as white solids. Having completed the synthesis, the UV-Vis absorbance of these compounds was measured, as they must be essentially transparent at the exposure wavelength. Gratifyingly, both of these compounds proved to be quite transparent across a range of deep UV wavelengths (Figure 2.3). These data were further corroborated by exposure to 254 nm radiation for several hours without any observable acid formed as indicated by addition of acid indicator. Armed with this

knowledge, appropriate sensitizer compounds needed to be indentified to detect acid generation from these PAGs.

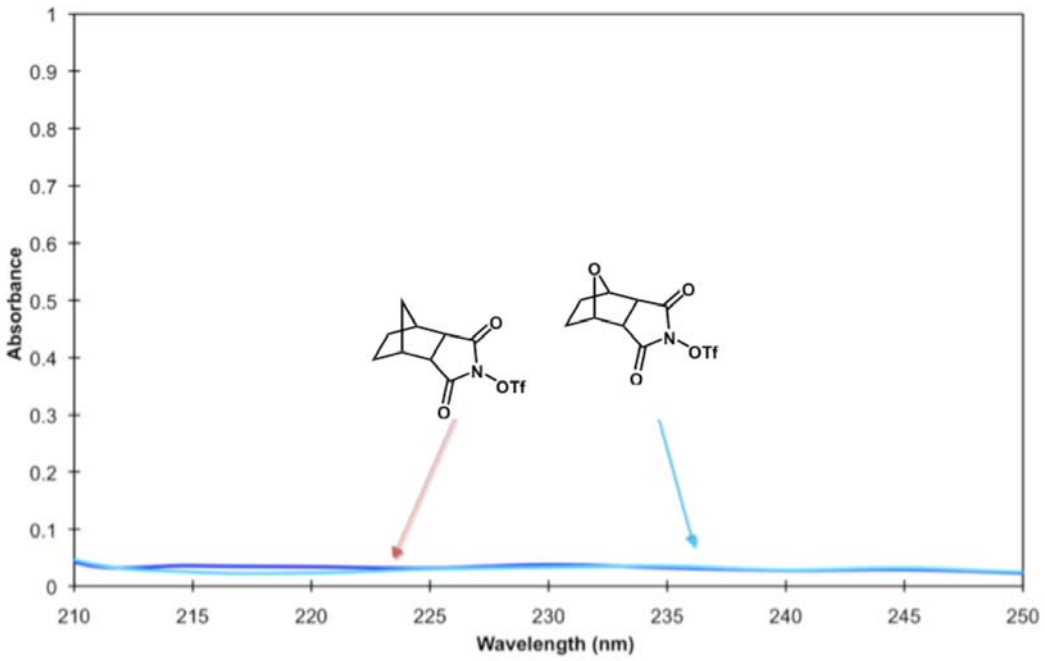


Figure 2.3. Absorbance of synthesized PAG compounds in MeCN (10 μM), 1 cm path length

## 2.3 IDENTIFICATION OF SENSITIZER COMPOUNDS

With two transparent acid generating species in hand, attention was turned towards finding compounds capable of facilitating energy transfer to them. This requires reduction potential measurements on the synthesized PAG compounds. We were advised that direct measurement of the reduction might be a more daunting challenge than previously thought.[7] We would not only need to gain access to specialized equipment for this measurement, but that the measurement itself is reportedly too difficult as these compounds were expected to have very high reduction potentials. To surmount this challenge, it was suggested that we undertake a simulation study. Using Spartan molecular modeling software, the Highest Occupied Molecular Orbital-Lowest Unoccupied Molecular Orbital (HOMO-LUMO) energy gap could be estimated

using quantum mechanical calculations. Several compounds for which the reduction potential was already known were simulated. This energy could then be correlated back to a known reduction potential, providing a calibration curve that would then be useful for the estimating the reduction potentials of our synthesized PAG compounds.

For the calibration curve, it was decided to use a variety of aromatic compounds, as there are a large number of sensitizers of this type reported in the literature.[8] The compounds chosen had energies minimized based upon calculation using the AM1 basis set, which was selected because of the short calculation time as well as the level of agreement exhibited between the the AM1 set and more detailed models (Figure 2.4).

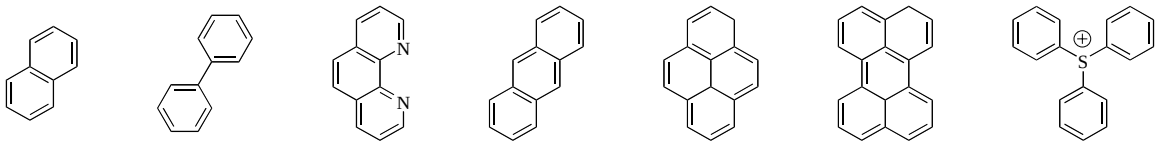


Figure 2.4. Compounds used for determining calibration curve

The orbital energies were then calculated to obtain HOMO and LUMO energies (Figure 2.5). Having obtained a calibration curve, our synthesized PAG compounds **2.1a** and **2.1b** were subjected to similar analysis. In addition to the PAG compounds in hand, we also modeled several compounds we hoped to synthesize to determine if these compounds were sufficiently easily reduced (Figure 2.6).

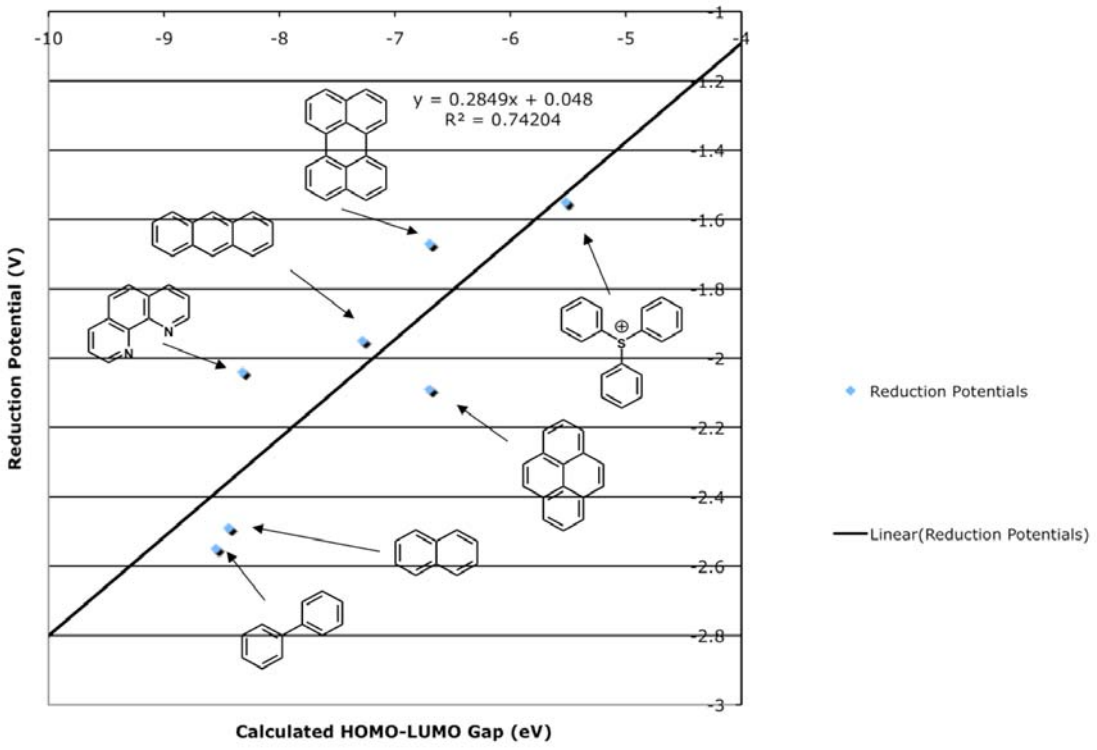


Figure 2.5. Calibration curve for PAG reduction potential

This analysis predicted the reduction potentials of the synthesized PAG compounds to be lower than expected. It should be noted that the oxo-bridged variant has a nearly identical predicted reduction potential as the methylene-bridged compound. As an added benefit of the simulation work, we now had identified sensitizer candidate compounds that could potentially engage in energy transfer and generate acid with our PAG compounds.

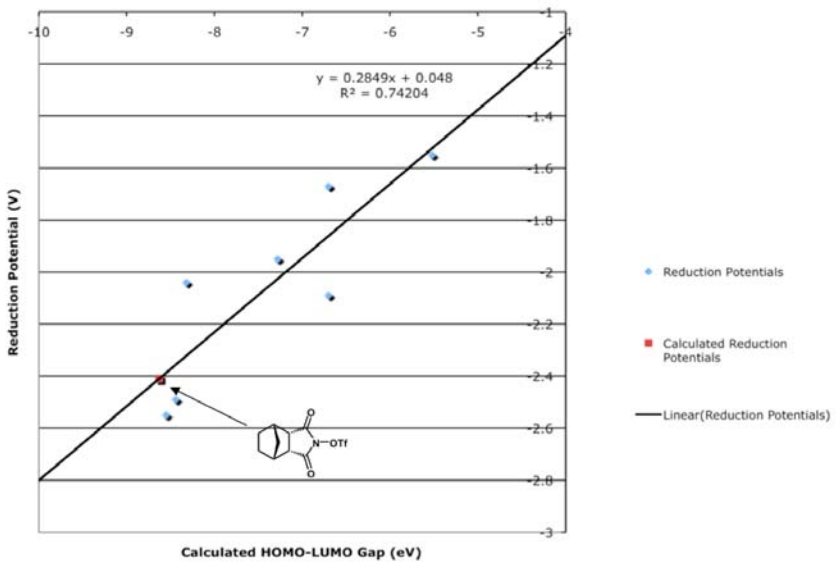


Figure 2.6. Calculated reduction potential for compound **2.1a**

## 2.4 SENSITIZER SCREENING

To establish the validity of the calibration curve, testing commenced on sensitizer candidates, including one control with a reduction potential calculated to be insufficient for energy transfer to occur. Ultimately, we settled upon 2-methoxynaphthalene, which based upon the calculations, should be sufficiently energetic to reduce our synthesized PAG compounds, and 9,10-dimethoxyanthracene, which should be insufficiently energetic to reduce our compounds.

These systems were tested at Columbia University by our collaborators through illumination of a solution containing our PAG compound (**2.1a** or **2.1b**) and the sensitizer in solution. However, we additionally required a method by which we could detect acid generation. For this, it was decided to use a method reported by Sciano *et al.*[9] in which fluorescein, an acid sensitive fluorescent molecule, was employed to detect acid in acetonitrile solution by monitoring the UV-Vis absorbance spectra (Figure 2.7). Acid can be detected in this system by the increase in absorbance between 400 and 450 nm. This system can be used in a quantitative fashion.

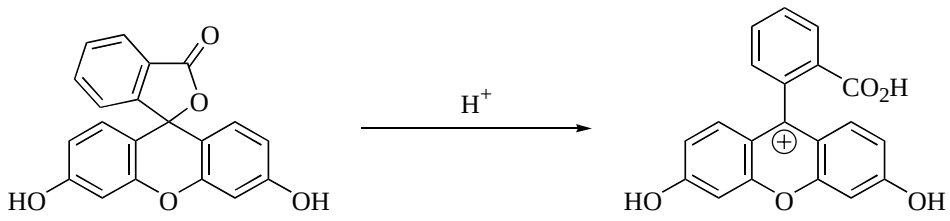


Figure 2.7. Fluorescein in closed and open (protonated) form

To test these systems, a broadband UV source outfitted with a bandpass filter (300 nm) was utilized to photochemically excite the sensitizer compounds (Scheme 2.2). Two control experiments were conducted to ensure that no acid would be produced by the inert PAG itself or directly by the sensitizer. In both cases, no acid production was observed, indicating the two components are individually inert.

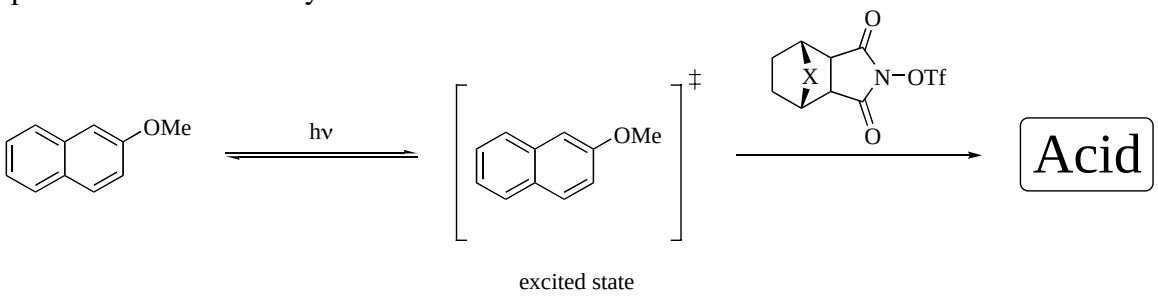


Scheme 2.2. Proposed pathway of acid generation

Gratifyingly, upon irradiation of the combined sample, there was a large increase in the absorbance of the sample between 400 and 450 nm, indicating acid generation had taken place (Figure 2.8).

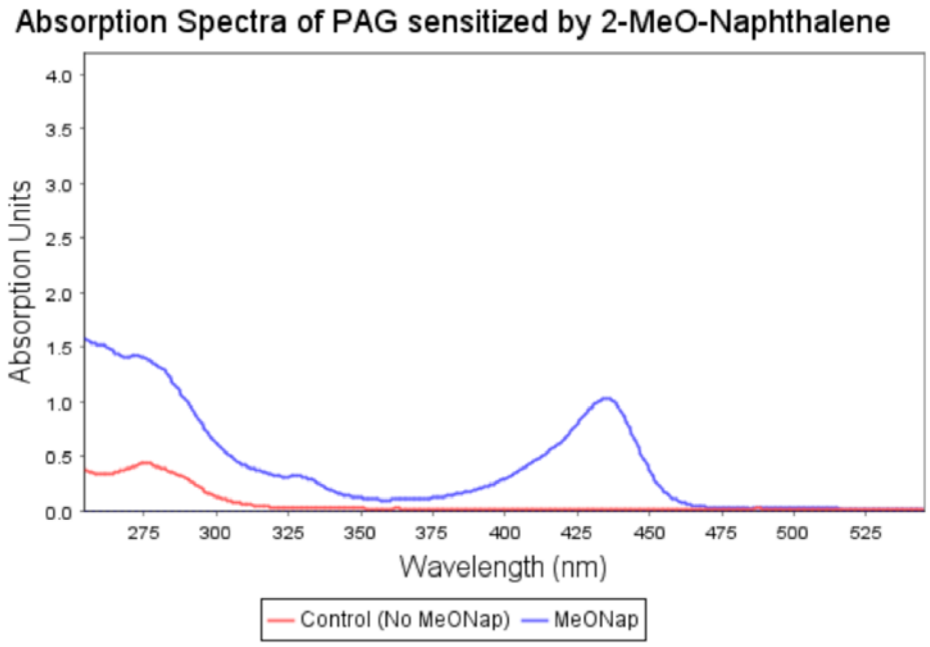


Figure 2.8. UV-Vis spectra for PAG (red) and PAG + sensitizer (blue) after irradiation

## 2.5 MECHANISM OF ACID GENERATION

Having now determined that acid could indeed be generated in this system, the mechanism was further investigated. It was postulated that for this system the sensitizer compound upon irradiation was being excited into an higher energy singlet state, at which point electron transfer from could occur to the PAG and acid liberated. This seemed reasonable, as other imide triflate compounds are known to decompose *via* excited singlet states.[10-12]

Additionally by using the calculated reduction potential of **2.1a** and **2.1b** in the Rehm-Weller relationship (Equation 2.1),[13] it was determined that when using sensitizers with higher energy excited-states (such as 2-methoxynaphthalene), the energetics of the electron transfer were favorable. The Rehm-Weller relationship defines the favorability of electron transfer to be related to the reduction potential of the sensitizer species ($E^o$ $[S^+/S]$), the quencher ($E^o$ $[Q^+/Q]$) and the available energy at the reaction temperature ($\Delta G_{00}$).

$$\Delta G_{el} = 23.06\left[E^{\circ}(S^{+}/S) - E^{\circ}(Q^{+}/Q)\right] - w_p - \Delta G_{00}$$

Equation 2.1. Rehm-Weller relationship

With this in mind, experiments were conducted to provide more evidence for an electron transfer mechanism. By altering our exposure solution to contain a triplet sensitizer, either acetophenone or anthraquinone, in place of 2-methoxynaphthalene, no acid was generated. This would seem to indicate that **2.1a** and **2.1b** are activated through a singlet state, which is in agreement with the literature.[10-12] When using lower energy singlet sensitizers, such as various anthracenes, perylene, pyrene, and phenothiazine, which were shown by calculations to be insufficiently energetic to induce electron transfer **2.1a** or **2.1b**, acid generation again was not observed. To confirm the possibility of electron transfer from a singlet state, sodium iodide was added to the exposure solution that contained PAG (**2.1b**), sensitizer (2-methoxynaphthalene) and acid indicator (fluorescein). Sodium iodide is known to serve as an electron scavenger,[14] and thus inhibit acid formation if an electron transfer pathway is active. Indeed, no acid was generated in this experiment, providing good evidence that electron transfer was the mechanism through which acid generation was occurring.

## 2.6 EFFORTS TOWARDS TWO-PHOTON ACID GENERATION

Having successfully demonstrated acid generation in a one-photon sense with **2.1a** and **2.1b**, the next step was to find a system that would work within the framework of a two-photon setup. Fortuitously, 2-methoxynaphthalene had been found by Bradshaw and Hammond to dimerize *via* [4+4] cycloaddition on exposure at 300 nm exposure (Scheme 2.3).[15] The major product of this photocyclization reaction is the *trans* isomer **2.5**, where the methoxy substituents are on opposite ends of the cycloadduct.

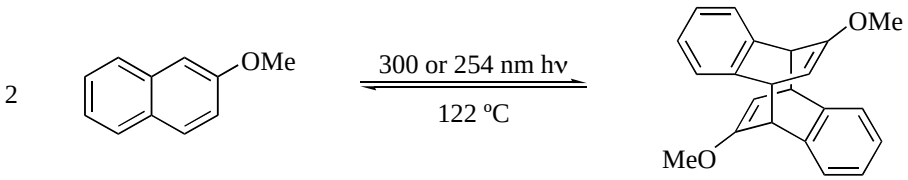


**2.5**

Scheme 2.3. Synthesis of 2-methoxynaphthalene cycloadduct **2.5**

Their report does not test the retro-[4+4] cycloaddition reaction to determine the extent of reversibility with respect to UV irradiation. Cycloadduct **2.5** was however known to undergo cycloreversion back to the monomeric species at 122 ºC with a $t_{1/2}$ of 8.25 h according to their findings. To this end, the [4+4] cycloaddition product was synthesized and the material exposed at both 300 nm and 254 nm (using a xenon lamp and monochromator) to establish the reversibility. The photochemical cycloreversion at both wavelengths does prove to be successful, meaning this system did have the potential to demonstrate a proof of principle of the two-photon acid generation behavior that was being pursued in this project.

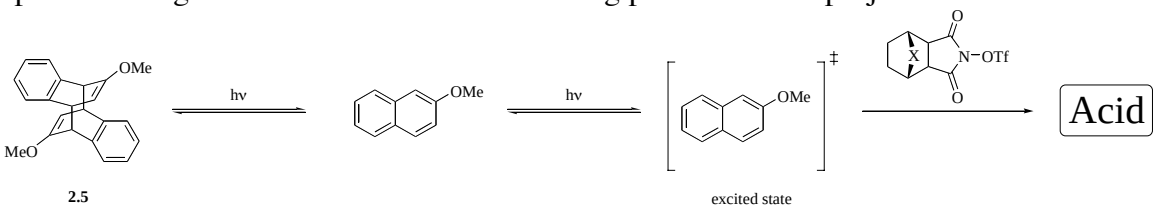


**2.5**

Figure 2.9. Two photon sequential acid generation

When replicating the acid generation experiment using cycloaddition product **2.5**, acid generation was detected, indicating the cycloadduct was competent in the generating a species that could conduct electron transfer with our PAG compounds **2.1a** and **2.1b** (Figure 2.9) or was capable of direct sensitization.

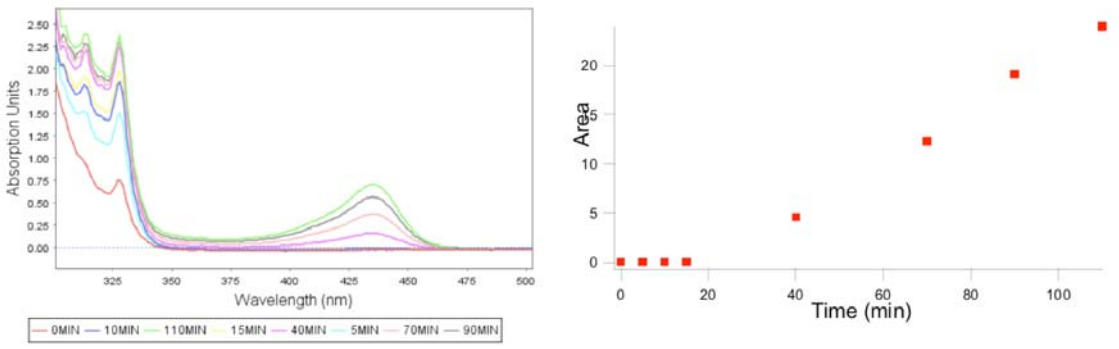


Figure 2.10. Acid production from cycloadduct **2.5**

By plotting the area of the new absorbance from the protonated fluorescein as a function of time, a time-dependent linear increase can be seen (Figure 2.10). It should be noted that the exposure time is quite high due to the low intensity of the Xenon light source at the 254 nm exposure wavelength. Exposures using a KrF excimer laser source at 248 nm would afford much shorter exposure times. Additionally while the increase in acid production after 20 minutes appears linear, it is likely that the nonlinearity that we hope to observe in this system would be present in the lower dosage ranges. It appears key to remain below saturation level of the active sensitizer in order to affect a nonlinear response in the system from these observations. What this system proved however was that it is possible to make a precursor compound that generates an active sensitizer *in situ* and conduct an electron transfer reaction to generate acid from the otherwise inert acid generating species.

## 2.7 CONTINUING WORK TOWARDS NONLINEAR ACID GENERATION

At this point, primary work in the area of new sensitizer compounds and acid generating species that would be more transparent at 193 nm shifted to other members of the project. It is important for the purposes of completeness to mention there have been a number of improvements made in the first generation system involving sensitizer precursor **2.5** and acid generators **2.1a** and **2.1b**.

In the area of sensitizer compounds, the biggest improvements on the initial design have related to the nature of the sensitizer itself. Studies in polymer films by collaborators have

shown tethered anthracene compounds (Figure 2.11) as well as tethered anthracene-naphthalene compounds can affect sensitization.

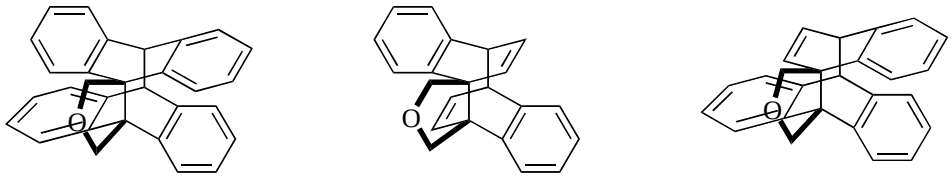

Figure 2.11. Tethered sensitizer candidates

The tethered nature of these materials has also increased the efficiency at which the cycloreversion reaction occurs due to the inability of the two components to diffuse away from one another, making these materials far more efficient at 193 nm exposure than the 2-methoxynaphthalene system.

Acid generators that are more transparent at 193 nm than compounds **2.1a** and **2.1b** have been synthesized and testing has begun on these compounds with the current generation of sensitizers (Figure 2.12). Additionally, testing has begun at Intel Corp. with several of these compounds to quantify the extent of nonlinearity.

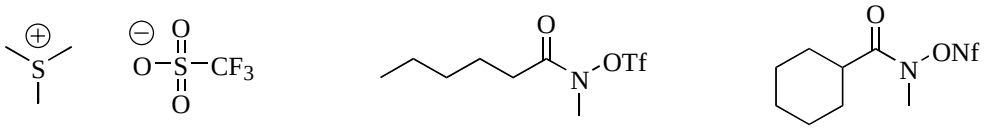

Figure 2.12. New acid generator compounds

## 2.8 CONCLUSION

Through the work conducted into ISTP materials, it has been shown that not only can the photon absorption and acid generation components can be separated while maintaining a functional system, but also sensitizer compounds can be generated and re-dimerized *in situ* using exposures at different wavelengths. This opens the door to more functional analogs that exhibit nonlinear dose response required for a successful DEL system. It has also been demonstrated that acid can be obtained from an acid generator that does not absorb at the exposure wavelength through electron transfer from the singlet excited-state of a sensitizer to the imide triflate PAG

compounds synthesized for this study. With continued work on the nonlinear response of the system, it remains possible that working double exposure process may be developed.[16]

## 2.9 EXPERIMENTAL

### General Methods

All reactions were conducted in flame-dried glassware under nitrogen atmosphere unless otherwise noted. Tetrahydrofuran was dried using sodium/benzophenone ketyl radical and distilled immediately prior to use. All chemicals were obtained from Sigma-Aldrich and were used without further purification. $^{1}$H NMR spectra were obtained on Varian Mercury (400 MHz), Varian MR (400 MHz) or Varian Unity (300 MHz) spectrometers and were referenced to deuteriochloroform (7.26 ppm) or dimethyl sulfoxide-*d*6 (2.49 ppm). $^{13}$C NMR spectra were obtained on Varian Mercury (100 MHz), Varian MR (100 MHz) or Varian Unity (75 MHz) spectrometers, referenced to the center of the deuteriochloroform (77 ppm) or dimethyl sulfoxide-*d*6 (39 ppm) and run with broadband decoupling. $^{19}$F NMR spectra were obtained on a Varian MR (376 MHz) spectrometer and are unreferenced. FT-IR spectra obtained on a Nicolet Avatar 360 FT-IR instrument. High resolution mass spectra (HRMS) are reported as *m*/*z* (relative intensity) and are calculated for M+1 peaks. Melting points were determined on a Meltemp II apparatus in open capillary tubes and are uncorrected. UV/Vis absorbance spectra for compounds **2.1a** and **2.1b** were obtained on a Cary 1E ultraviolet/visible spectrometer. For acid detection experiments, an Agilent 8453 spectrophotometer was used. UV flood exposures were conducted using a Rayonet RPR-100 low pressure mercury lamp photoreactor. Time resolved emission was measured on an OB920 from Edingburgh Analytical instruments by time-correlated single photon counting using a nitrogen flash lamp at 326 nm for excitation. For typical exposure experiments, 2 mL of 2-methoxynaphthalene (0.1 mM) in acetonitrile was titrated with 20 μL of imide triflate PAG **2.1a** or **2.1b** (1 M).

***4-Oxa-tricyclo[5.2.1.00,0]decane-3,5-dione (2.3a)***

Synthesized according to a modified literature procedure.[17] In a beaker containing **2.2a** (4.02 g, 24.00 mmol) and palladium on carbon (10 mg, 5% by wt.) was added ethyl acetate (40 mL). The reaction was placed into a bomb and charged with 3 atm of hydrogen gas. The reaction was stirred overnight at room temperature. Filtration through Celite, washing with ethyl acetate and concentration afforded a white solid. Recrystallization from methanol provided the desired product as white sheet-like crystals (3.90 g, 96%). **$^{1}$HNMR** (400 MHz, $CDCl_3$): 3.37-3.39 (m, 2H), 2.82-2.85 (m, 2H), 1.66-1.72 (m, 4H), 1.45-1.48 (m, 2H). **$^{13}$CNMR** (75 MHz, $CDCl_3$): 174.4, 45.5, 41.4, 38.8, 24.5. **FTIR** (thin film from DCM): 2967, 2884, 2691, 1776, 1688, 1316, 1230, 1184, 1091, 822 $cm^{-1}$. Melting point (130-132 ºC) and HRMS matched literature values.

***4-Hydroxy-4-aza-tricyclo[5.2.1.00,0]decane-3,5-dione (2.4a)***

Synthesized according to literature procedure.[18] To a round bottom flask under air containing hydroxylamine hydrochloride (660 mg, 9.50 mmol) and water (12.5 mL) was slowly added sodium carbonate (560 mg, 5.27 mmol). The norbornane compound (1.253 g, 7.54 mmol) was added slowly and then the reaction was heated to 100 ºC for 1 h. The hot reaction mixture was acidified to pH=1 using concentrated hydrochloric acid. The reaction was cooled to ambient temperature, then filtered and dried to afford the product as a white solid (991 mg, 73 %). **$^{1}$HNMR** (300 MHz, $CDCl_3$): 3.04 (s, 2H), 2.76 (s, 2H), 1.53-1.56 (m, 4H), 1.26-1.29 (q, 2H, $J$ = 7.9 Hz). **$^{13}$CNMR** (75 MHz, $CDCl_3$): 174.3, 45.5, 41.4, 38.8, 24.5. **FTIR** (thin film from DCM): 3425, 2955, 1688, 1649, 1217, 1204, 1090, 822 $cm^{-1}$. Melting point (153-154 ºC) and HRMS matched literature values.

***Trifluoro-methanesulfonic acid 3,5-dioxo-4-aza-tricyclo[5.2.1.00,0]dec-4-yl ester (2.1a)***

To a round bottom flask cooled to 0 ºC containing sodium hydride (186 mg, 4.63 mmol) and THF (38 mL) was added the hydroxamic acid (700 mg, 3.86 mmol). The reaction mixture was stirred at 0 ºC for 30 minutes and then trifluoromethanesulfonyl chloride (0.45 mL, 4.24

mmol) was added dropwise. The reaction was warmed to ambient temperature over ~1 h and stirred overnight at this temperature. The reaction mixture was quenched with water and diluted with ethyl ether. The layers were separated and the organic layer dried over sodium sulfate. The mixture was concentrated on a rotary evaporator and redissolved in dichloromethane. The solution was filtered through a plug of silica gel and concentrated to afford the desired product as a white solid (600 mg, 58 %). **$^{1}$HNMR** (400 MHz, $CDCl_3$): 3.16 (m, 2H), 2.85 (s, 2H), 1.2-1.6 (m, 4H). **$^{13}$CNMR** (100 MHz): 168.8, 113.7-123.39 (q, *J* = 322.3 Hz), 45.6, 41.4, 39.6, 24.6. **$^{19}$FNMR** (376 MHz): -83.4. **FTIR** (thin film from DCM): 2970, 2929, 2891, 1810, 1764, 1483, 1446, 1312, 1304, 1286, 1240, 1165, 1126, 1107, 1074, 1053, 960, 921, 902, 866, 812, 792, 772, 730, 653, 634, 589, 567, 510 $cm^{-1}$. **HRMS** (CI+) calculated for $C_{10}H_{11}F_3NO_5S$: 314.0310; found: 314.0312. **mp**: 56-57 ºC.

***Norcantharidin (2.3b)***

To a solution of exo-3,6-epoxy-1,2,3,6-tetrahydrophthalic anhydride (2.00 g, 12.0 mmol) in ethyl acetate (45 mL) was added 5% palladium on carbon (0.384 g), and the mixture was stirred at room temperature under a hydrogen atmosphere for 10 h. The reaction mixture was filtered through Celite and concentrated *in vacuo* to give a colorless crystal (1.73 g, 85%). **$^{1}$HNMR** (300 MHz, DMSO-*d*6): 1.61 (dt, 2H, *J* = 7.17, 3.07 Hz), 1.86-1.90 (m, 2H), 3.16 (s, 2H), 5.01 (dt, 2H, *J* = 3.20, 2.18 Hz). **$^{13}$CNMR** (75 MHz, DMSO-*d*6): 173.0, 79.7, 50.7, 27.5. **FTIR** (KBr): 3003, 2986, 2960, 2885, 1840, 1776, 1724, 1684, 1416, 1335, 1286, 1228, 1124, 1084, 999, 957 $cm^{-1}$. **HRMS** (CI+) calculated for $C_8H_9O_4$: 169.0501; found: 169.0501. **mp**: 118-119 °C.

***N-hydroxy-7-Oxabicyclo[2.2.1]heptane-2,3-dicarboximide (2.4b)***

A solution of hydroxylamine was prepared by adding sodium carbonate (0.574 g, 5.41 mmol) to an aqueous solution of hydroxylamine hydrochloride (0.689 g, 10.1 mmol, in 20 mL). Norcantharidin (1.30 g, 7.73 mmol) was added to the aqueous solution and the mixture heated at 70 °C for 1 h. The clear solution was added 10 mL of 1 M hydrochloric acid and cooled

overnight. The crystals were collected, washed twice with ice cold 1 M hydrochloric acid and dried under vacuum to afford the product as a white, crystalline solid (910 mg, 64%). **$^{1}$HNMR** (300 MHz, DMSO-*d*6): 11.7 (s, 1H), 4.65 (t, 2H, *J* = 1.92), 2.99 (s, 2H), 1.63 (s, 4H). **$^{13}$CNMR** (75 MHz, DMSO-*d*6): 172.6, 78.0, 46.8, 28.1. **FTIR** (KBr): 3427(br), 3483, 3115, 2968, 1786, 1716, 1531, 1470, 1321, 1217, 1194, 1072 $cm^{-1}$. **HRMS** (CI+) calculated for $C_8H_{10}NO_4$: 184.0610; found: 184.0609. **mp**: 231-232 °C.

***Oxabicycloheptane imide triflate (2.1b)***

In a 50 mL dry round bottom flask, sodium hydride (0.208 g) and 16 mL of THF was added and cooled to 0 °C, after which *N*-hydroxy-7-Oxabicyclo[2.2.1]heptane-2,3-dicarboximide **2.4b** (0.800 g, 4.37 mmol) was added slowly. The mixture was stirred at 0 °C for 0.5 h. Trifluoromethanesulfonyl chloride (0.138 g, 0.820 mmol) was added dropwise. The reaction mixture was stirred overnight at ambient temperature, after which water (20 mL) was added. The mixture was extracted with ethyl ether, washed with water and brine and dried over $MgSO_4$. The solution was filtered through silica gel. After filtration, the solvent was evaporated *in vacuo*, giving a white solid (1.24 g, 90%). **$^{1}$HNMR** (300 MHz, $CDCl_3$): 4.95 (t, 2H, *J* = 1.92), 3.05 (s, 2H), 1.66 (s, 4H). **$^{13}$CNMR** (75 MHz, $CDCl_3$): 167.1, 120.5, 116.2, 47.4, 29.7, 28.6. **FTIR** (KBr): 2995, 2953, 2920, 1749, 1452, 1234, 1213, 1174, 1124, 1045 $cm^{-1}$. **HRMS** (CI+) calculated for $C_9H_9F_3NO_6S$: 316.0103; found: 316.0105. **mp**: 153-154 °C.

## 2.10 REFERENCES


(1) Byers, J.; Lee, S.; Jen, K.; Zimmerman, P.; Turro, N. J.; Willson, C. G. *J. Photopolym. Sci. Technol.* **2007**, *20*, 707-717.
(2) Lee, S.; Byers, J.; Jen, K.; Zimmerman, P.; Rice, B.; Turro, N. J.; Willson, C. G. *Proc. SPIE* **2008**, *6924*, 69242A/1-69242A/12.
(3) Lee, S.; Jen, K.; Willson, C. G.; Byers, J.; Zimmerman, P.; Turro, N. J. *J. Micro/Nanolithogr., MEMS, MOEMS* **2009**, *8*, 011011/1-011011/11.
(4) Pretch, E.; Simon, W.; Seibl, J.; Clerc, T. In *Tables of Spectral Data for Structure Determination of Organic Compounds*; Second ed.; Springer-Verlag: New York, 1989, p U5-U155.
(5) Crivello, J. V. US Patent 19760921.
(6) Crivello, J. V. *J. Polym. Sci., Part A: Polym. Chem.* **1999**, *37*, 4241-4254.
(7) Bard, A. J. *private communication*
(8) Hoffmann, N. *J. Photochem. Photobiol., C* **2008**, *9*, 43-60.

(9) Pohlers, G.; Scaiano, J. C.; Sinta, R. *Chem. Mater.* **1997**, *9*, 3222-3230.
(10) Malval, J.-P.; Suzuki, S.; Morlet-Savary, F.; Allonas, X.; Fouassier, J.-P.; Takahara, S.; Yamaoka, T. *J. Phys. Chem. A.* **2008**, *112*, 3879-3885.
(11) Malval, J.-P.; Morlet-Savary, F.; Allonas, X.; Fouassier, J.-P.; Suzuki, S.; Takahara, S.; Yamaoka, T. *Chem. Phys. Lett.* **2007**, *443*, 323-327.
(12) Iwaki, J.; Suzuki, S.; Park, C.; Miyagawa, N.; Takahara, S.; Yamaoka, T. *J. Photopolym. Sci. Technol.* **2004**, *17*, 123-124.
(13) Rehm, D.; Weller, A. *Ber. Bunsen-Ges.* **1969**, *73*, 834-839.
(14) Jiang, Q.; Spehar, A.-M.; Hakansson, M.; Suomi, J.; Ala-Kleme, T.; Kulmala, S. *Electrochim. Acta* **2006**, *51*, 2706-2714.
(15) Bradshaw, J. S.; Hammond, G. S. *J. Am. Chem. Soc.* **1963**, *85*, 3953-3955.
(16) O'Connor, N. A.; Berro, A. J.; Lancaster, J. R.; Gu, X.; Jockusch, S.; Nagai, T.; Ogata, T.; Lee, S.; Zimmerman, P.; Willson, C. G.; Turro, N. J. *Chem. Mater.* **2008**, *20*, 7374-7376.
(17) Birney, D.; Tang, K. L.; Koh, J. H. P.; Pool, B. R.; White, J. M. *J. Am. Chem. Soc.* **2002**, *124*, 5091-5099.
(18) Elderfield, R. C.; Hydorn, A. E.; Schenker, E.; Wyckoff, K. K. *J. Org. Chem.* **1959**, *24*, 1296-1301.

# Chapter 3 *Progress Towards Double Exposure Lithography via Optical Threshold Layer Materials*

## 3.1 INTRODUCTION

While the ISTP system takes advantage of concepts that had been previously demonstrated in imaging studies, the optical threshold layer (OTL) system would mark a radical departure from a standard photoresist system. A material was needed that possessed a threshold tolerance ($E_{threshold}$) to light exposure before undergoing any sort of reaction. It must then be able to revert to its initial state and be exposed a second time (Figure 3.1).

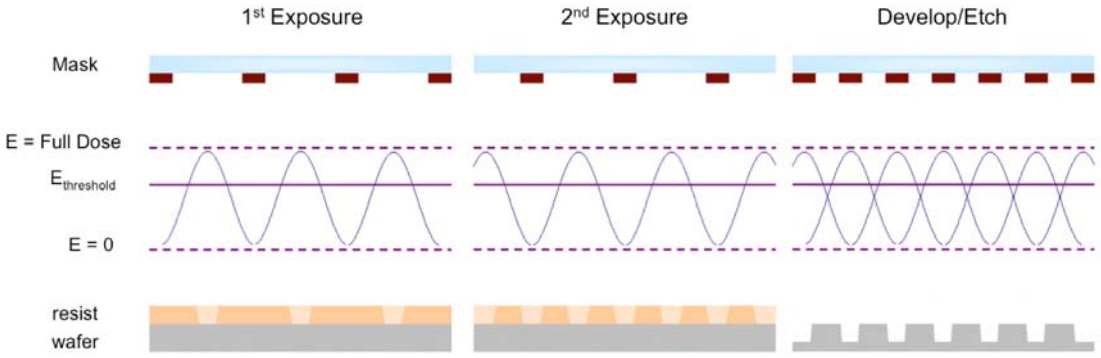


Figure 3.1. Optical Threshold Layer (OTL) schematic

Inspiration for this was found in physical state changes, as can be observed in the melting of solids, which has been exploited in the design of thermal resist systems.[1-3] However, simple calculations showed the amount of power available from the laser light source at the wafer was far too low to invoke a physical state change, such as a melt, on its own. The search then turned towards mechanisms that would afford these changes by altering the physical state of the material without changing temperature. For this, photochromic compounds could be used. A photochromic material is defined as any material that can be reversibly isomerized to a second form using light exposure, with the reversal occurring at a different wavelength due to a change in absorbance (Scheme 3.1).[4]

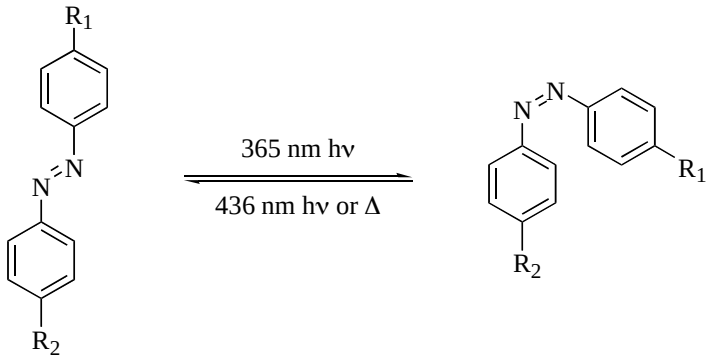


Scheme 3.1. Photochemical isomerism of azobenzene photochromics

Many photochromic compounds undergo significant structural changes when exposed to their isomerization wavelength, which in turn might be enough to alter some physical property of the material. It was felt that this change would make an OTL mechanism possible.

The final question before embarking upon material synthesis was the desired property to be altered. Several choices were available, however the alteration of melting temperature and the shifting of liquid crystalline states were chosen, the latter in large part due to the available literature focusing upon the state of the material containing photochromic groups.[5-14] Initial forays into OTL materials would be directed at known photochromic compounds, such as azobenzenes, since a large body of literature was available dealing with the isomerization characteristics of azobenzene analogs. Efforts towards developing photochromic compounds that are more active at 193 nm exposure wavelength would be undertaken after a successful system demonstration at higher wavelengths.

## 3.2 PHOTOCHROMIC COMPOUNDS

Photochromic compounds have been known for several decades, with perhaps the most prominent use coming in the last 20 to 30 years with the introduction of Photolite™ from American Optical in 1982 and later Transitions™ eyeglass lenses (Scheme 3.2).[15]

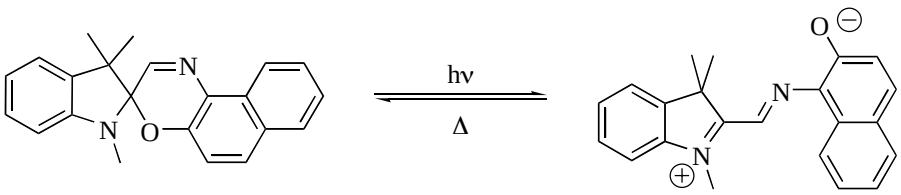


Scheme 3.2. Photochromic isomerism in spirooxazine from Photolite™ lenses

When worn indoors, the lens appears clear like a normal eyeglass lens. However, when worn outdoors in sunlight, the lens darkens, absorbing sunlight and acting as sunglasses. This has been a boon for many people who require corrective lenses for vision but did not want to carry a separate pair of sunglasses for going outdoors. The function was made possible by the utilization of a photochromic compound, specifically a spirooxazine, which upon exposure to UV irradiation undergoes a ring opening reaction to a more conjugated, and thus more absorbing form. This provides the darkening observed. This ring opening is easily reversed in the working system through thermal relaxation, although compounds of this type are also known to revert to their initial form through exposure at a second wavelength. Since the introduction of Photolite™, Transitions™ lenses have utilized new photochromic materials to improve response and coloration, such as the spironapthopyrans, a version of which is used in current versions of these lenses (Scheme 3.3).[15]

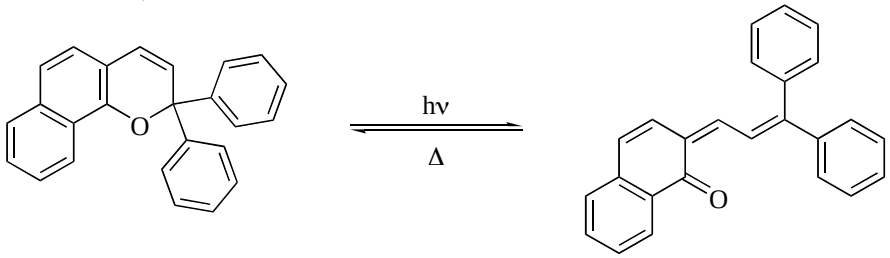


Scheme 3.3. Spironaphthopyran scaffold used in Transitions™ lenses

A similar phenomenon exists for azobenzene compounds, which undergo a photochemical isomerization. In this case the isomerization is from the more stable *trans* form to the *cis* form. This isomerization, as in the spironaphthopyrans, causes a shift in the absorbance spectrum (Figure 3.2).

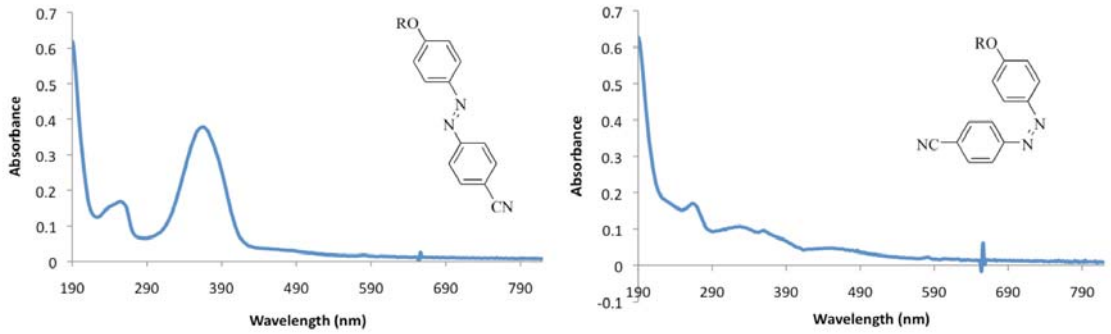


Figure 3.2. Example UV/Vis absorbance of azobenzene compound before (left) and after (right) exposure

## 3.3 SYNTHESIS OF SIDE-CHAIN CRYSTALLINE POLYMERS

The synthesis of a many azobenzene compounds and polymers are known,[16] however no work, to our knowledge, has been conducted specifically aimed at modulation of melting temperatures of substances with azobenzenes contained in the structure.

Work conducted at the University of Texas at Austin by Prof. Paul and coworkers demonstrated that alkyl side-chain containing methacrylate polymer films of long alkyl side-chain methacrylates were capable of preventing the diffusion of gas molecules when the side-chains were below their melting temperature.[17-23] However, when warmed beyond this transition, the diffusion of several different gases was increased by several orders of magnitude. It was thought that by synthesizing a corresponding copolymer of a long alkyl side-chain methacrylate and an azobenzene containing methacrylate, a system would be obtained that would allow for the alteration of the melting temperature of the copolymer through exposure to UV light (Figure 3.3).

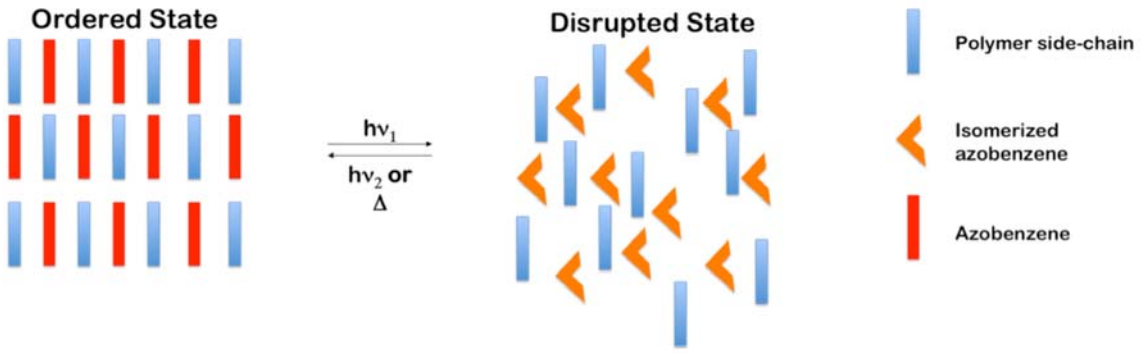


Figure 3.3. Disruption of crystalline state

Synthesis of these side-chain crystalline compounds is straightforward from cheap, commercially available starting materials. The $C_{18}$ alkyl side chain was chosen to adjust the melting temperature of the side-chain to near room temperature (Figure 3.4), with aspirations towards a workable system for industrial use.

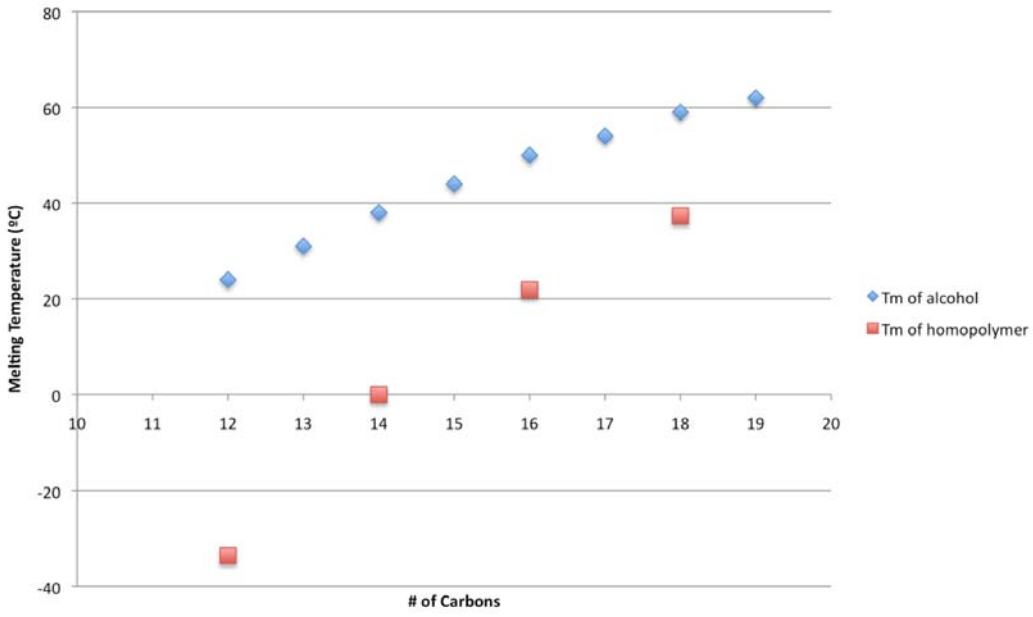


Figure 3.4. Melting Temperature of alkyl alcohols and related methacrylate homopolymers

Synthesis of the azobenzene containing monomer begins with diazonium salt formation of 4-aminobenzonitrile, followed by quenching with phenolate anion to provide azobenzene **3.1**.

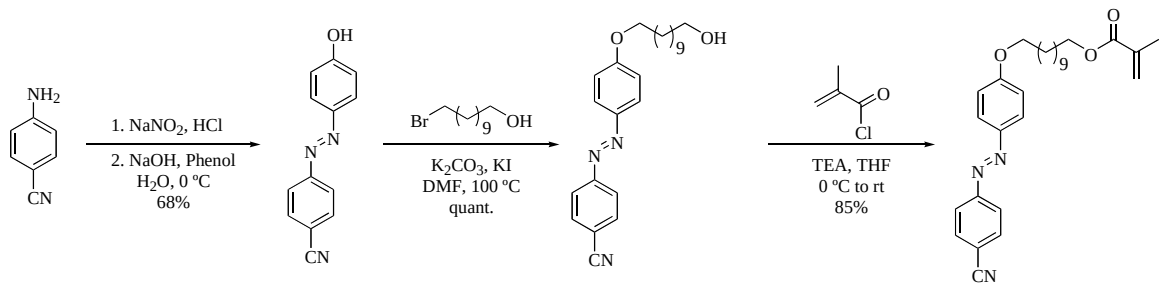


**3.1** **3.2** **3.3**

Scheme 3.4. Synthesis of methacrylate monomer **3.3**

With monomer **3.3** in hand, radical copolymerization with octadecylmethacrylate **3.4** in a feed ratio of 1:4 (**3.3**:**3.4**) provided the desired copolymer **3.5** with the same ratio (as determined by $^{1}$H NMR) as shown in Scheme 3.5. Other copolymer ratios were synthesized using the same method, though for the purposes of this study, polymer **3.5** was chosen as it incorporates an appropriate amount of azobenzene as well as a side-chain melting temperature near room temperature.

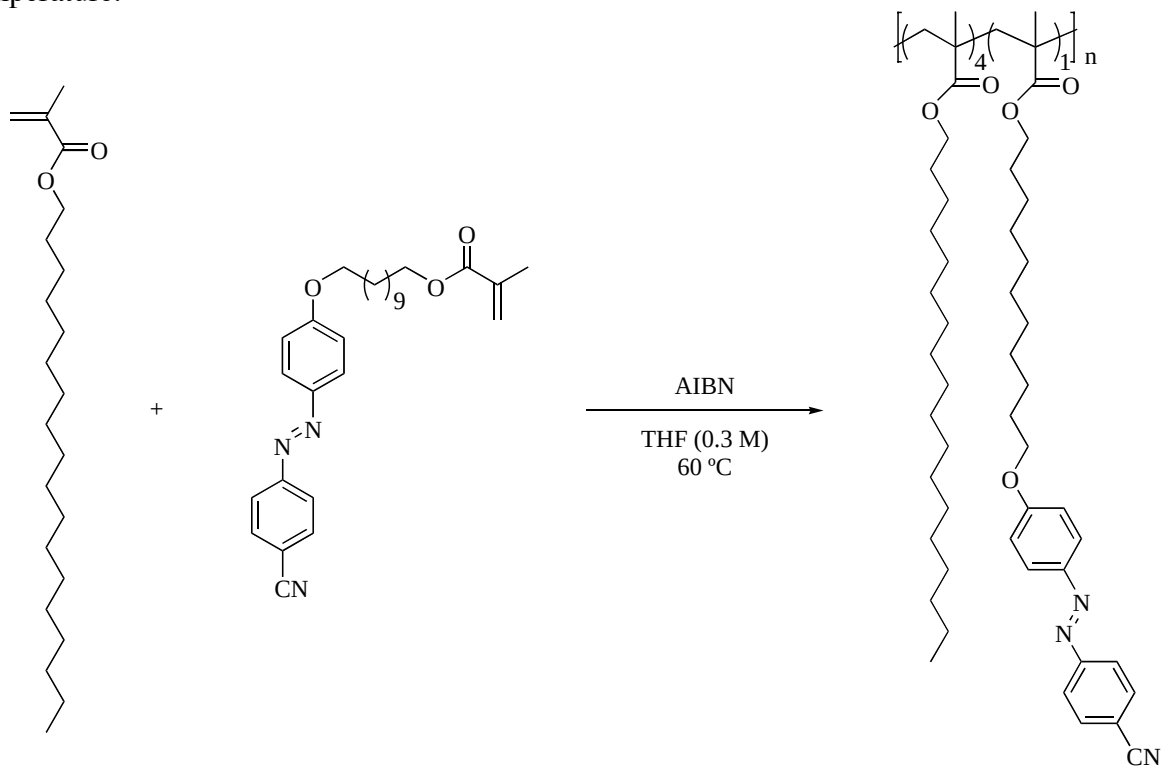


**3.4** **3.3** **3.5**

Scheme 3.5. Synthesis of copolymer **3.5**

## 3.4 MATERIALS TESTING OF SIDE-CHAIN CRYSTALLINE POLYMERS

Having the desired polymer in hand, work then turned towards the testing of the properties of these novel copolymers. First, the melting transitions of the copolymer side-chains were determined by differential scanning calorimetry (DSC). DSC operates by monitoring the difference in energy required to heat a reference pan from the sample pan to the same temperature. Spikes in the energy required indicate a material transition that is occurring, whether this transition is from a glassy state to an amorphous state ($T_g$), or a melting event ($T_m$). A $T_m$ shows up as a strong spike, while a $T_g$ is a smooth transition. In the case of polymer **3.5**, the melting temperature of the alkyl side-chains was found to be ~32 °C by this analysis method due to the large endothermic spike that occurs at that temperature (Figure 3.5). This process is conducted for a heating cycle and cooling cycle, resulting in a closed loop.

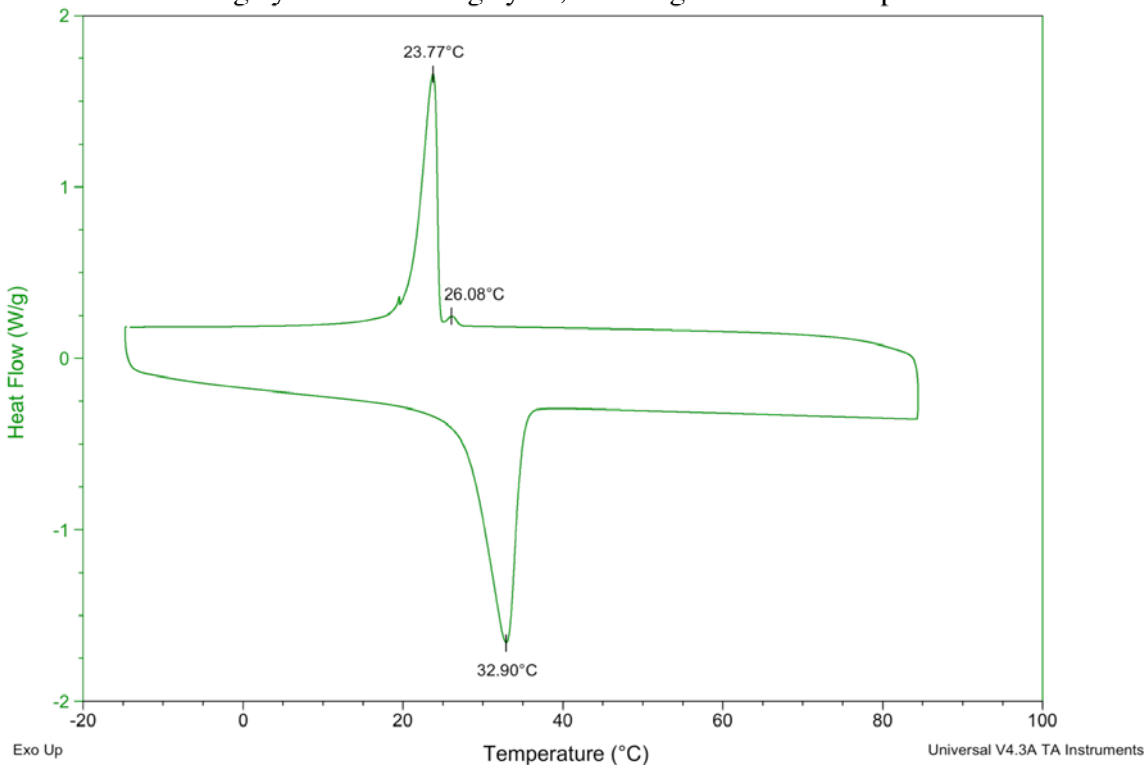


Figure 3.5. DSC thermogram of copolymer **3.5**. Lower portion is from heating cycle, while the upper portion is from the cooling cycle.

Next, the isomerization of the azobenzene component needed to be tested. For this, a thin film of the polymer was spin-coated onto a quartz wafer and exposed to 365 nm UV light from a

mercury arc lamp source through a bandpass filter in order to avoid exposure to the reversal wavelength also present in a mercury arc lamp output. The change in absorbance of the material in the ultraviolet region was monitored using UV-Vis. The dose dependent change in absorbance near 365 nm is clear evidence that a change is taking place in the material. This method also determines the saturation dose of the material, which will be needed for later exposure studies to determine the change in diffusion coefficient of the polymer film (Figure 3.6).

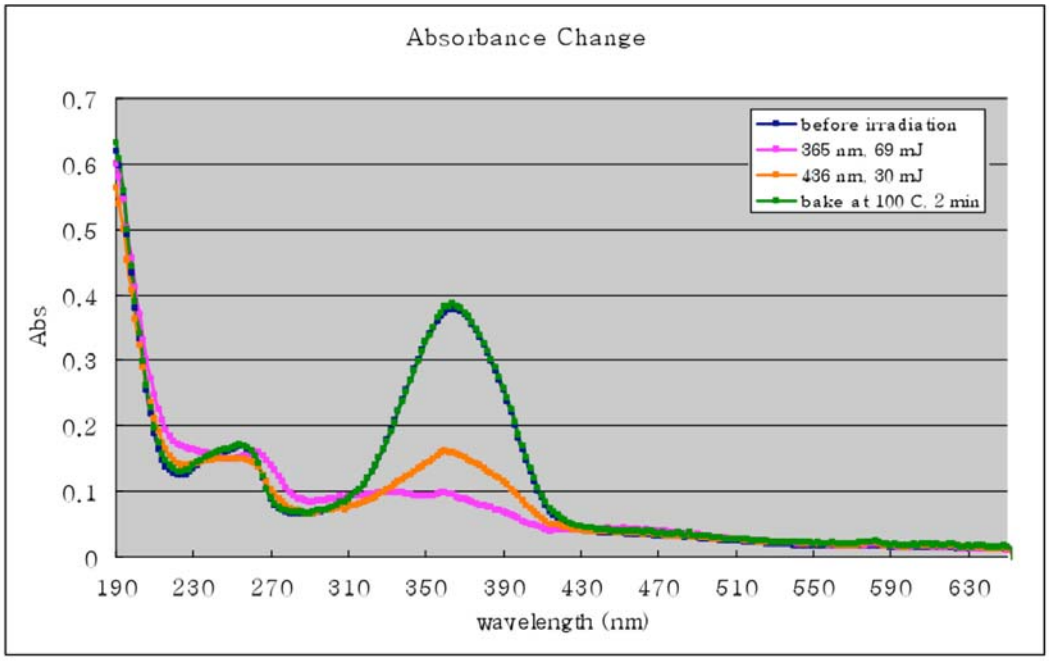


Figure 3.6. UV-Vis absorbance of polymer **3.5**

The spectrum shown in Figure 3.6 shows the saturation dose of polymer **3.5** is approximately 70 mJ/cm$^2$. As expected, the azobenzene functionality can be isomerized back to its *trans* form with 436 nm light, again from a mercury arc lamp outfitted with a bandpass filter. The absorbance of the material at 365 nm does not completely revert to its original level until baked at 100 ºC for 120 s. This data indicates the photochromic groups have isomerized to their original forms. Additionally, this process is repeatable with little additional loss.

Having established the reversibility of the photochromic isomerization in polymer system **3.5**, focus shifted to the determination of the ability to alter the melting temperature. This

measurement was difficult to make directly, as obtaining enough isomerized material to accurately conduct a DSC measurement was a daunting challenge. This was primarily due to the high absorbance of the polymer film at the exposure wavelength, meaning that only thin films, those on the order of a micron or less, can be assured to have isomerized the azobenzene units throughout the film. With such a thin film, obtaining the 5-10 mg of sample needed for DSC analysis required a large wafer to be coated and uniformly exposed, followed by removal of the film from the wafer and transfer to a DSC pan, itself a challenge. The decision was made to measure this change indirectly, through use of a spectroscopic ellipsometer (Figure 3.7). A spectroscopic ellipsometer works by aiming a beam of multiple wavelengths of light through a polarizer at the sample and collecting the reflective light, again through a polarizer and obtaining information about the surface it reflected off of.

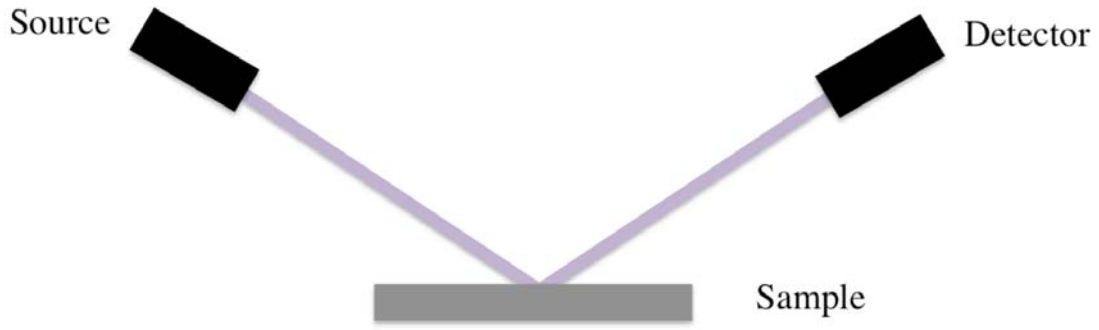


Figure 3.7. Ellipsometer schematic

The angle at which the light is aimed at the sample is adjusted in order to obtain the highest level of reflection. In the process of reflection, the phase ($\Psi$) and amplitude ($\Delta$) of the incident light wave are altered, and these changes are observed through the detector. The measured differences in these values can be correlated to the thickness of the film that reflected the light. In this manner, the film thickness is measured indirectly. This proves useful in this case, as materials undergoing state changes undergo a simultaneous thickness (density) change. Materials expand at a linear rate when the state remains the same, however a discontinuity is observed at the temperature where the material undergoes a transition.[13,14,24] This discontinuity can be observed by monitoring the thickness of the material as it is heated. By finding the

midpoint of the discontinuity (the inflection point), the melting point of the side-chains was observed (Figure 3.8). After demonstrating that this method can successfully determine the melting point in the unexposed system, the film was exposed to 365 nm light and subjected to the analysis. As shown in Figure 3.8, it can be clearly seen that the melting temperature of the side-chains in the film has been shifted to a lower temperature, in this case by approximately 2 ºC. It should be noted here the melting temperature determined by this method is slightly lower than that observed by DSC. This shift is consistent with shifts in other compounds tested during the course of this project and likely arises from poor adhesion of the thermocouple used in the measurement to the sample.

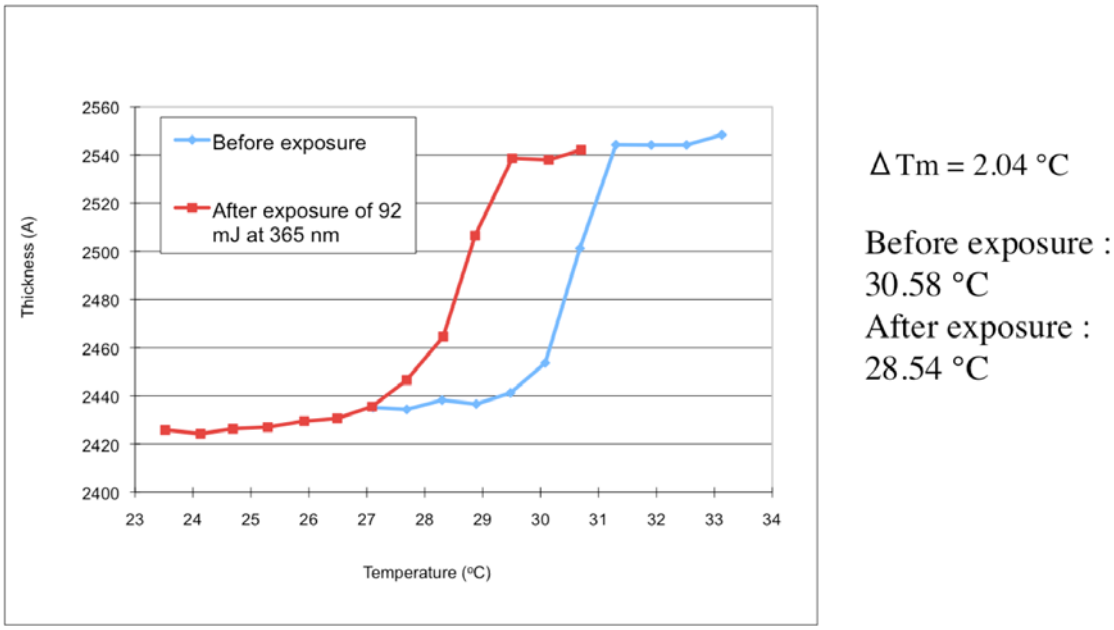


Figure 3.8. Melting temperature shift from UV exposure of polymer **3.5**

## 3.5 DIFFUSION EXPERIMENTS

Having successfully demonstrated a photoinduced change in the melting temperature of a photochromic-containing copolymer, work began on testing the change in permeability of the copolymer due to this physical change. Diffusion should occur far more rapidly in the exposed regions assuming the temperature of the film does not go above the original $T_m$ of the polymer

film. Before this could be tested, the difference in permeability of the material without exposure was fully characterized. This included measuring the diffusivity in the film below its $T_m$ as well as above. For this, a method for measuring was needed. Fortuitously, work previously conducted by Postnikov *et al* had found a trilayer film stack could be used to measure the diffusion of acid by the deprotection of the *t*-butoxycarbonyl group of poly(*t*-BOC-styrene) (Scheme 3.6).[25] The bottom layer of the stack was an inert polymer containing a PAG. The top layer was the previously mentioned protected styrene detector layer, while the middle layer was the polymer for which the diffusion properties are being observed. By using reflectance FT-IR, the stretching frequency of the carbonyl of the BOC group was monitored and as the reaction proceeded, the integrated area of this stretch decreased.

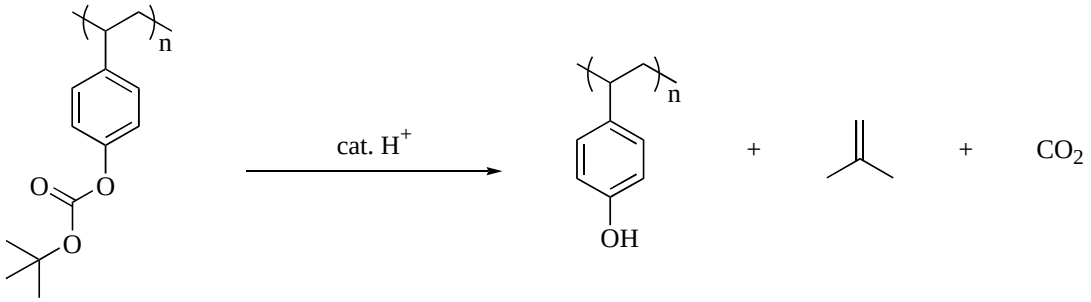


Scheme 3.6. BOC deprotection from PBOCST

This acidolysis reaction is catalytic, thereby increasing the signal-to-noise ratio and allowing for the collection of less ambiguous data. While poly(*t*-BOC-styrene) is a good detector layer for high temperature measurements, this work required working at temperatures much closer to ambient. Data from previous experiments showed that deprotection of the BOC group proceeds at a very slow rate at room temperature, meaning that a different detector layer would be required to observe changes in the synthesized systems.

A system was needed that would provide gain in the detection of the amount of acid diffused, but which did not require high temperatures to initiate the chemical change. One system that fit the necessary requirements was poly(phthaldialdehyde) (PPHA), a polyacetal.[26] This polymer has a ceiling temperature[27] of approximately -40 ºC,[28] meaning that if an active end

of the polymer was generated at any temperature above this point, the chain would depolymerize to its monomeric form. PPHA was synthesized and end-capped using acetic anhydride.[26] This polymer has the acid sensitive acetal functionality, which allowed for amplification of the acid diffused into the PPHA film and causes the depolymerization of the chain. Switching to PPHA also necessitated a switch in the method used for determining diffusion, as the IR signal was determined through testing to be too difficult to distinguish for either the acetal linkage of the forming aldehyde (loss of signal due to volatility and uneven distribution on the film). To circumvent these problems, UV-Vis detection was utilized, as the absorbance of the film changed quite dramatically due to the loss of the PPHA layer. For the purposes of uniform film formation, the PPHA was mixed with poly(butylmethacrylate) (PBMA).

Having found a suitable detector layer and method of detection, the next step of the process was to determine an appropriate acid feeder layer for the azobenzene containing copolymer. The feeder layer must be inert but also above its $T_g$ in order for diffusion to occur.[25] In this case, PBMA was chosen, as it has a low $T_g$ (20 ºC) as well as different solubility properties than the azobenzene containing copolymer. Triphenylsulfonium triflate was used as the PAG for these experiments. The new trilayer film stack (Figure 3.9) was exposed to 248 nm light from a krypton fluoride (KrF) excimer laser source in order to generate acid in the feeder layer.


Figure 3.9. Film stack for diffusion measurements

The PPHA/PBMA layer displays low absorbance at 248 nm and the azobenzene containing copolymer exhibiting the same for thin films (under 200 nm, as used for the purposes of this experiment) so only a minor correction to the exposure dose is necessary to ensure adequate acid generation from the PAG present in the acid feeder layer. After exposure, the

films were baked at, below, and above the melting temperature of the side-chains, in order to observe the difference in diffusion rates of the two states. Gratifyingly, the film stack is stable when the material is below the $T_m$ of the side-chains, but PPHA film decomposition is seen above this temperature.

### 3.6 IMAGING STUDIES USING SIDE-CHAIN CRYSTALLINE COPOLYMERS

Having observed the diffusion change in the unisomerized system, work then began on the exposed film. Here, the same film stack setup was used as in the unisomerized film. Film stacks were first flood exposed to 248 nm light (200 mJ/cm$^2$) to activate the PAG present in the feeder layer. A second exposure through a contact mask at 365 nm (210 mJ/cm$^2$) afforded the isomerization in selected areas of the barrier layer (azobenzene copolymer). The film stack was then baked at 28 ºC (below the $T_m$ of the unisomerized polymer) for 5 minutes and the film observed using optical microscopy (Figure 3.10).

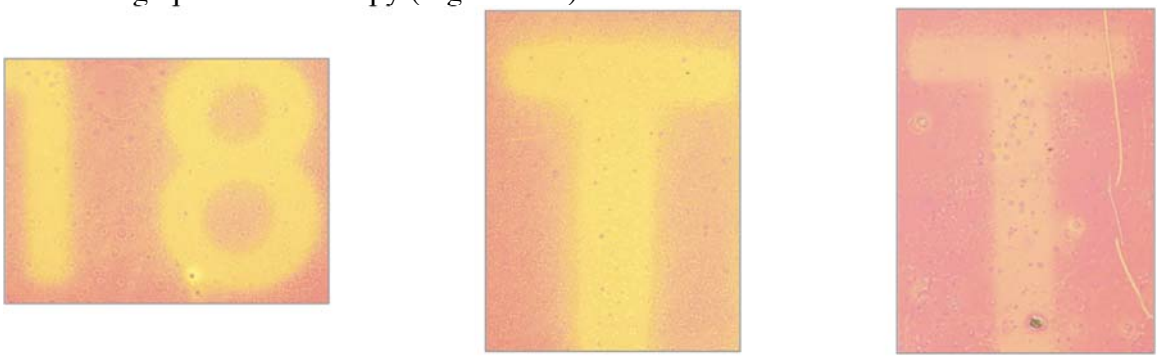

Figure 3.10. Images of exposed trilayer film stack (bright areas represent isomerized barrier layer **3.5** and acid-catalyzed depolymerization of PPHA)

As can be seen from these images, a distinct color change occured in the areas exposed to the 365 nm light. The increase in the brightness indicates areas where the PPHA film has been depolymerized, forming a thinner film. This allows for the brighter appearance. With this set of experiments, it has been shown the permeability of an azobenzene-long alkyl side chain methacrylate copolymer is altered by heating above the side-chain $T_m$. It has also been demonstrated that the permeability of the barrier layer is reversibly altered by 365 nm exposure, due to the isomerization of the azobenzene component from its *trans* form to the *cis* form.

## 3.7 LIQUID CRYSTALLINE POLYMER APPROACH TO OTL BEHAVIOR

In addition to the side-chain crystalline approach towards a suitable OTL barrier layer, work was also conducted on a liquid crystalline polymer that could meet the same goals. Liquid crystals were discovered serendipidously in 1888 by Reinitzner while observing cholesteryl benzoate. The compound turned into a cloudy liquid at 145 ºC and eventually a clear liquid at 178 ºC.[29] When these samples were sent out to be analyzed under polarizing optical microscopy, they appeared to have the optical properties of crystals but flowed like a liquid.[30] This study led to the coining of the term "liquid crystal." By definition, liquid crystals possess some degree of orientational order with either no or partial positional order.[31] While liquid crystals (LCs) appear in two main categories: calamitics (rod-like) and discotic (disc-like). For the purposes of this work, only calamitic-type LCs will be discussed.

Liquid crystals can exist in a variety of different mesophases, which arise from the nature of the order in the liquid crystal. These are commonly characterized by polarized optical microscopy (POM) and X-ray diffraction.[31] The most common mesophases observed are nematic (N) and smectic (S). Smectic phases come in several varieties, depending upon the orientation of the mesogens (Figure 3.11).[32] Smectic phases exhibit a higher degree of order, and in compounds that possess multiple LC phases, they generally appear closer to the crystalline state.[31]

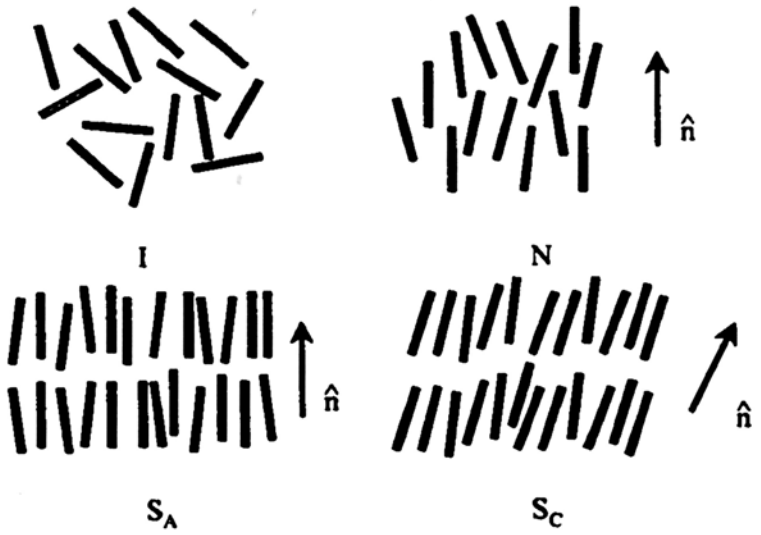


Figure 3.11. Orientation of mesogens in isotropic liquid (I), nematic (N), smectic A ($S_A$), and smectic C ($S_C$) phases

At the outset of this work, the exact mesophase of the LC material was not important, as the goal was to find a material sufficiently impermeable to essentially block small molecule diffusion. Due to the large body of literature addressing the reversibility of the isomerization,[16,33] our work would focus on azobenzene containing systems. Additionally, azobenzenes have been incorporated into liquid crystalline systems previously, highlighted by the work of Ringsdorf[34-37] and Ikeda.[11,38-41] It was also felt that liquid crystalline barrier layers in an OTL system would not suffer from as many line edge roughness issues associated with crystalline domain boundries as could be possible in a crystalline system. This was due to the ability of LC compounds to be homeotropically aligned through various methods, resulting in a single domain.[5,42,43] For the LC polymer barrier layer approach, the same idea behind the permeability switch would be used as in the side-chain crystalline system (Figure 3.3).

## 3.8 State Change of Liquid Crystals Through UV Exposure

Interestingly, the disruption of a LC state using a photochromic compound had been observed previously.[13,14,44] Work conducted by Paul *et al*[45] at the University of Texas at Austin demonstrated the effects of orientation and annealing,[46] as well as copolymer composition[47] on

gas transport through LC polyesters but had not utilized liquid crystalline polymers containing photochromic groups. Ikeda and coworkers have done extensive work looking specifically at photochemically induced isothermal phase changes of liquid crystalline polymers with azobenzene mesogens[8,10] as well as doped systems. They however did not look at permeability and additionally, were using polymers whose liquid crystalline transitions were above 50 ºC, making them less useful in the context of an OTL system. However, we were unable to find a case where the permeability of the material has been measured and the effects of the isomerization observed concurrently. With this in mind, work commenced to develop a LC system that contained an azobenzene as either a mesogen or dopant, which could be isomerized and that was also a LC at or near room temperature.

## 3.9 SYNTHESIS OF AZOBENZENE CONTAINING LIQUID CRYSTALLINE POLYMERS

The first compounds synthesized were polymers that utilized the azobenzene component as the LC mesogen. Polymers **3.11** and **3.12**, originally synthesized by Ringsdorf *et al*[35] for use in holographic storage were thought to be ideal candidates to test the diffusion properties. Both compounds were synthesized as shown in Scheme 3.7.

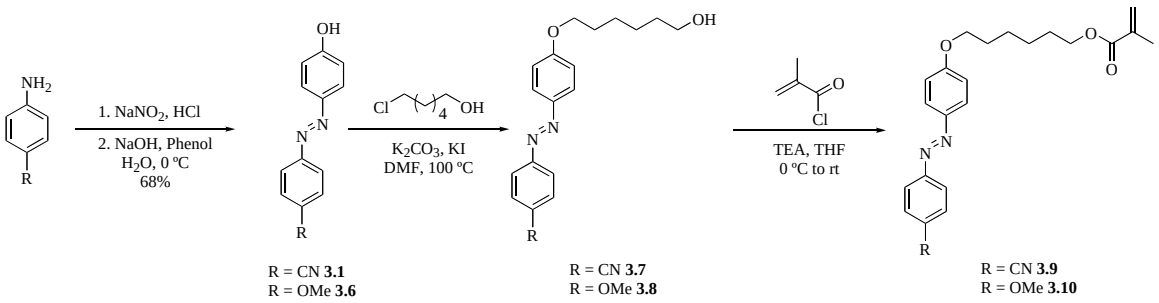


Scheme 3.7. Synthesis of azobenzene LC monomer **3.9, 3.10**

The desired starting aniline was made into the diazonium salt with nitrous acid and quenched with phenolate anion to afford the azobenzene (**3.1** or **3.6**), which was then alkylated with 6-chloro-1-hexanol in DMF to give the alcohol needed for ester formation (**3.7**, **3.8**). Reaction with methacryloyl chloride in the presence of triethylamine provided the azobenzene

monomer. Compounds **3.9**, **3.10** were polymerized using AIBN in toluene to afford homopolymers **3.11** and **3.12** (Figure 3.12).

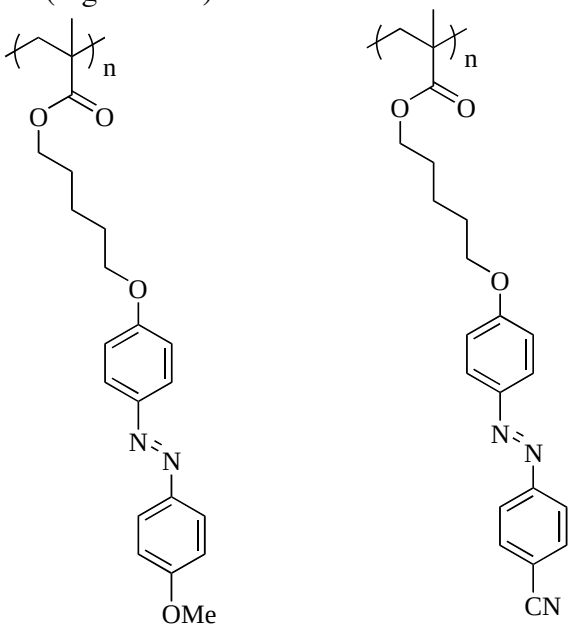


**3.11** **3.12**

Figure 3.12. Homopolymers for diffusion testing

## 3.10 CHARACTERIZATION OF LIQUID CRYSTALLINE POLYMERS

The LC polymers were characterized using standard protocols for both liquid crystals as well as polymers. The molecular weight of the polymers was determined by gel permeation chromatography (GPC) and the physical transitions determined by DSC. DSC thermograms can indicate not only melting transitions ($T_m$) and glass transitions ($T_g$) but also provide information on liquid crystalline transitions, although the energy changes for LC transitions were much lower (Figure 3.13).[31]

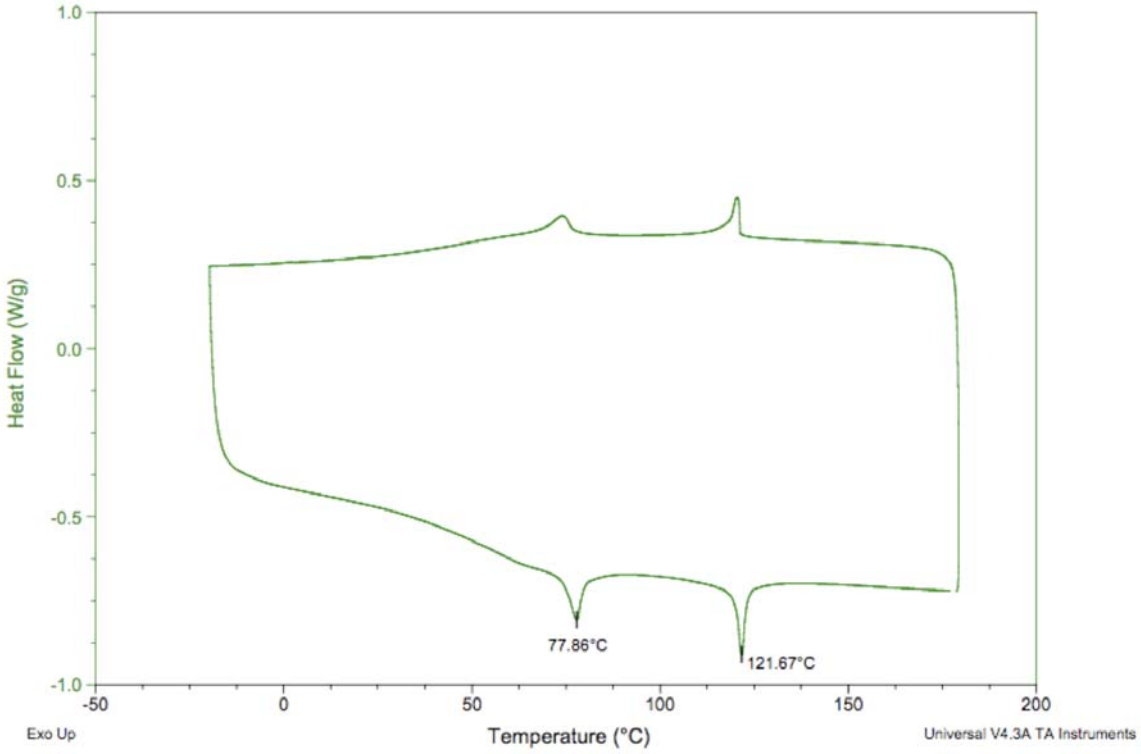


Figure 3.13. DSC thermogram of **3.11** showing LC transitions

A more definitive demonstration of LC behavior comes from POM observations. For POM the sample is placed onto a heated stage between two polarizers set at 90º to one another in order to block out any light not rotated by the sample (Figure 3.14),[32] which occurs when there is regular order as there is in either a LC or a crystalline solid. Due to the optical anisotropy of the LC sample, it possesses the ability to rotate the plane polarized light. The sample is then ramped either up or down through a range of temperatures so that the crystalline, liquid crystalline, and isotropic liquid states can be observed. Here, some indication of the mesophase for the material can be determined by observing the texture. Nematic phases typically are observed as colored strands whereas nematic phases exhibit fan-like shapes.[31]

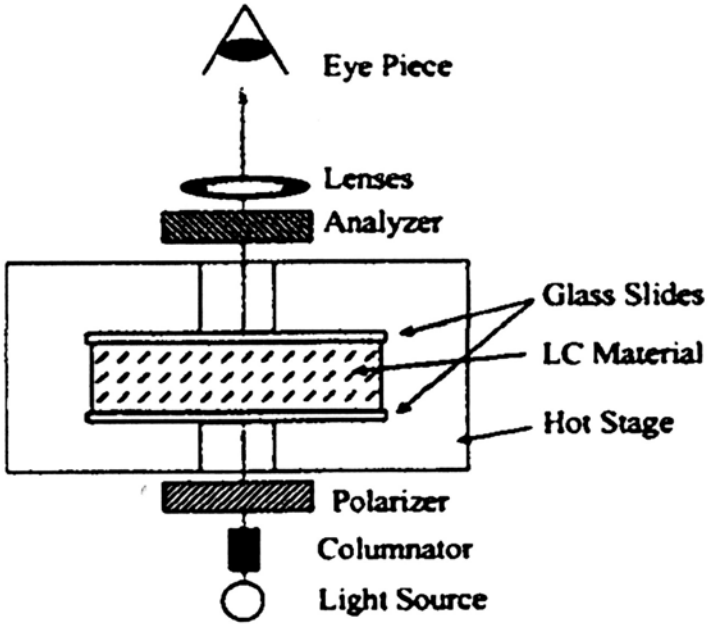


Figure 3.14. Schematic representation of POM setup

Homopolymer **3.11** exhibited a nematic phase between 77 and 121 ºC (Figure 3.15), roughly matching the literature values, although it lacked a smectic phase as had been reported.[35] This could be due to the higher molecular weight ($M_N$ = 26,000 kDa instead of 2,500 as reported), which was observed to change the occurrence of LC phases in these systems.

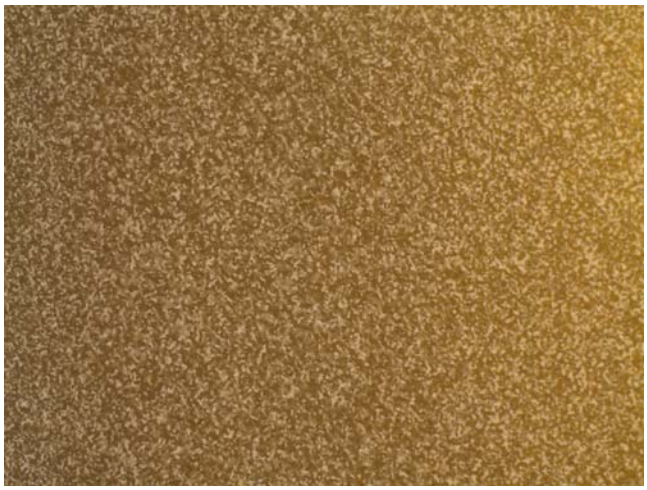

Figure 3.15. Nematic phase for polymer **3.11**

## 3.11 DIFFUSION STUDIES WITH LC AZOBENZENE HOMOPOLYMERS

Having identified polymers with LC states, diffusion measurements were conducted with small molecules to determine the permeability. While methods to measure this property of LC did exist using laser illumination to monitor absorbance,[13,14] our laboratory was not equipped with this capability. Instead, a new characterization method was employed, one similar to the setup employed for the side-chain crystalline polymers. The film stack used for this experiment was identical to the stack used for in the FT-IR experiments by Postnikov *et al*,[25] though with a different barrier layer. In this case, poly(*t*-BOC-styrene) could be used, as the transition temperatures were high enough to be conducive to its use (Figure 3.16).

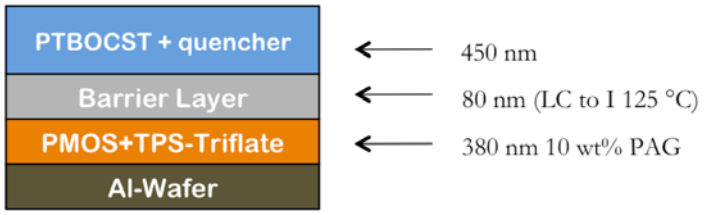


Figure 3.16. Film stack for LC diffusion measurements

To determine the rate of diffusion, the permeability was tested at several different temperatures (Figure 3.17). Two of these temperatures (107, 117 ºC) were chosen to test for diffusion below the LC to I transition. Additionally, in order to rule out decomposition of the detector layer, one trial did not have the exposure step to generate acid from the PAG in the acid-feeder layer. And finally, one trial was conducted at the transition temperature (125 ºC, as measured with the thermocouple used in the diffusion experiment), and one above (128 ºC). As can be seen in Figure 3.17, both trials where the LC barrier layer should remain in the LC state showed little change in the integrated area of the *t*-BOC carbonyl stretch, indicating little deprotection had occurred. The trial where no exposure to generate acid was conducted also showed little change. However when the temperature of the film stack was heated to the transition temperature, acid diffusion was observed by the decrease in the carbonyl stretch integration. Finally, at 128 ºC the diffusion of acid across the barrier layer and subsequent

deprotection of the *t*-BOC groups was so rapid that the acid front moving across the barrier layer could not be observed.

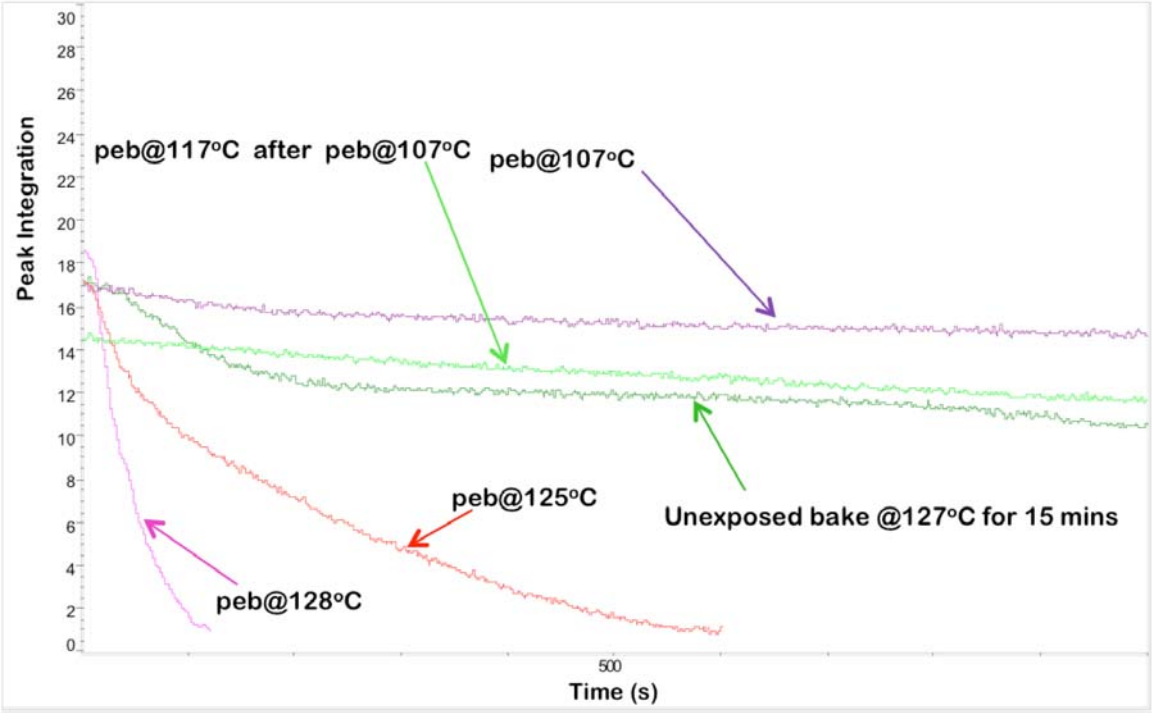


Figure 3.17. Carbonyl peak integration over time to detect acid diffusion using polymer **3.11** as the barrier layer

These results were quite encouraging, as it had now been established that LC polymers utilizing azobenzenes as mesogens could serve as a diffusion barrier to the acid generated in the feeder layer. Next, the change of the diffusion rate in an LC polymer through UV exposure had to be confirmed.

A measurement was again conducted using the ellipsometer, exposing the sample for 60 s (predetermined from previous exposure of this film) at 340 nm, and then measuring the film properties. For this measurement, the thickness and refractive indices at two wavelengths (460 and 634 nm) were measured, specifically to observe any changes that occured, which would provide adequate information about the material state. A 6% change in refractive index (Figure 3.18) was observed, with a corresponding change also seen in the thickness measurements during

the same trial (expansion from 260 nm to 280 nm). This evidence was strong enough to conclude a state change was indeed occurring. The material was seen at the testing temperature of 90 ºC to revert back from the isomerized *cis* state to the initial *trans* state. In fact, this backwards isomerization was observed to occur in less than 90 s at temperatures as low as 70 ºC in measurements by this technique.

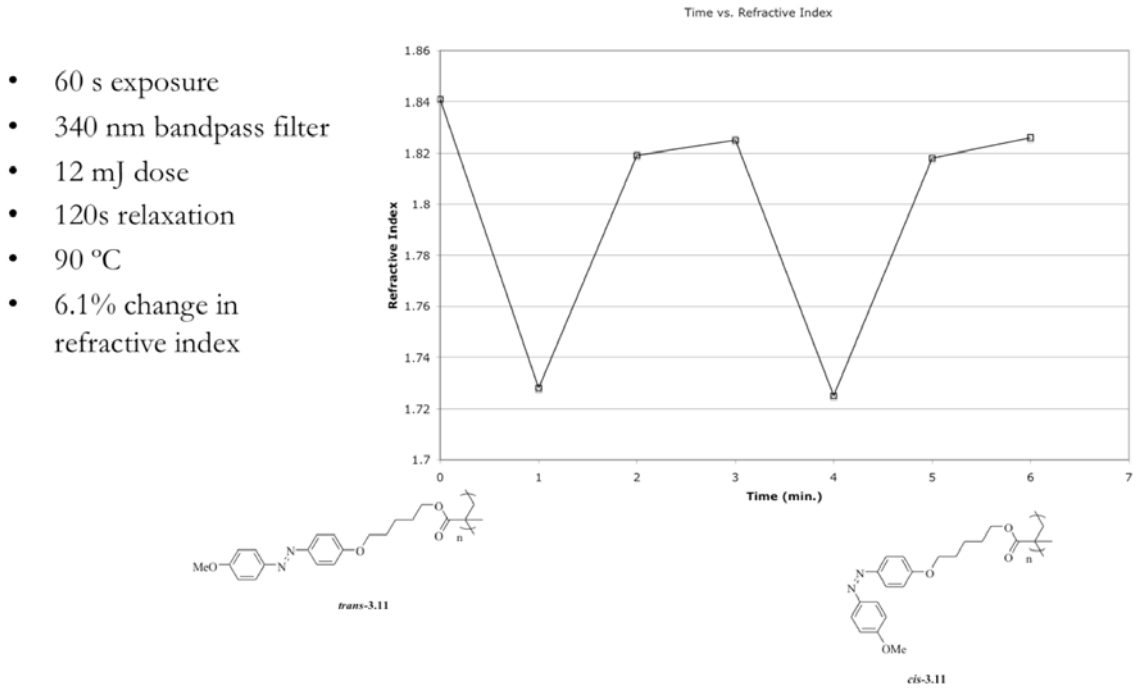


Figure 3.18. Reversible refractive index change by UV exposure of polymer **3.11**

This indicated that polymers **3.11** and **3.12** had transition temperatures too high for reliable measurement of the photochemical permeability switch due to the rapid reversal of the isomerization from exposure.

## 3.12 SYNTHESIS OF ROOM TEMPERATURE LC MATERIALS

Having found success in measurement of diffusion properties in LC systems as well as observing the reversible isomerization in films, work then began on finding LC systems that could operate at room temperature to test the photochemical diffusion switching and avoid issues of thermal reverse isomerization. Two solutions to this problem were found: one being a siloxane-based polymer[48] and the other being acrylate based.[49] Both used known mesogens,

however both also required the use of an azobenzene dopant, as neither mesogen contained a photochromic group (Figure 3.19).

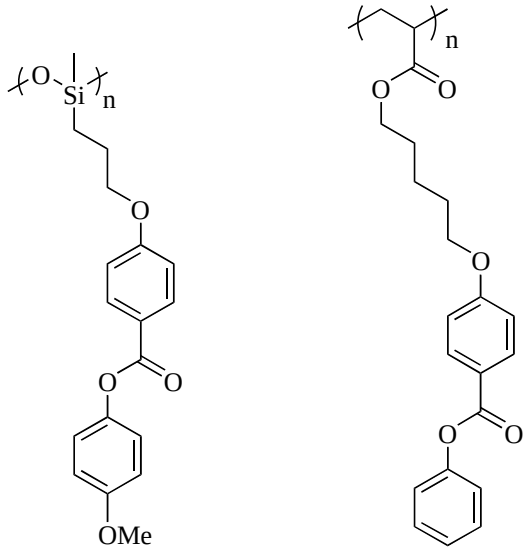

**3.15** **3.21**

Figure 3.19. Homopolymer targets for room temperature LC

The desired materials were synthesized (Scheme 3.8 and Scheme 3.9). Siloxane polymer **3.15** was synthesized from 4-hydroxy ethyl benzoate in five steps, beginning with allylation[50] and saponification of the ethyl ester to obtain **3.13**. Acid chloride formation using thionyl chloride and esterification with 4-methoxyphenol in presence of catalytic DMAP afforded the hydrosilylation precursor **3.14** in 80% yield over two steps.[48] Hydrosilylation using Karsted's catalyst (platinum(divinylsilane)) proceeded smoothly to afford the desired polymer **3.15**.[48]

The synthetic route to polymer **3.21** was altered to include a protection and deprotection of the aliphatic alcohol to improve yields and monomer **3.20** purity over the published route.[49] Alkylation of 4-hydroxybenzoic acid using 6-chloro-1-hexanol under basic conditions afforded **3.16** in moderate yield.[49]

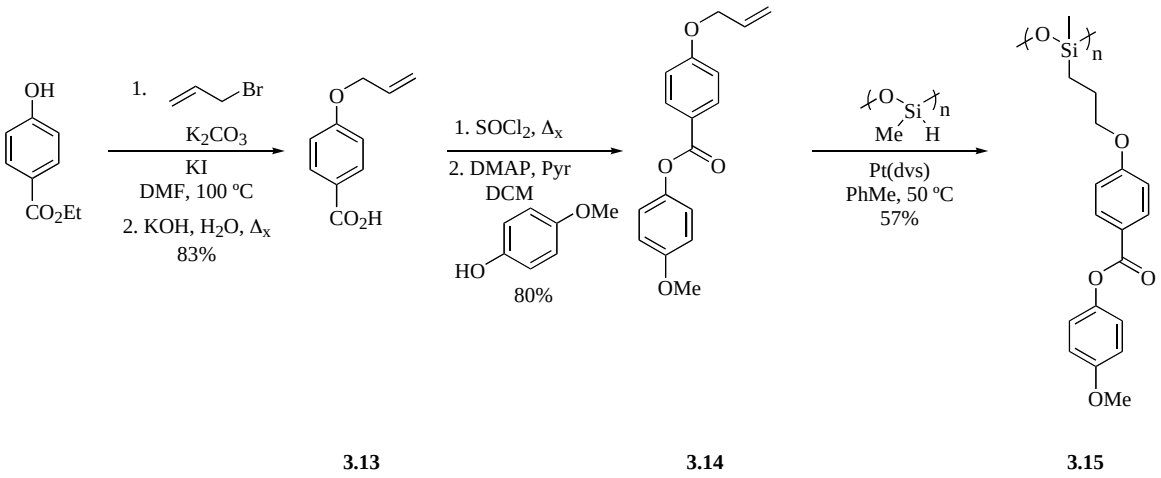


Scheme 3.8. Synthesis of siloxane polymer **3.15**

Protection of the aliphatic alcohol with TBSCl and imidazole, followed by DCC coupling with phenol gave the protected alcohol benzoic ester **3.18** in 70% yield over two steps. The TBS was then removed using 1 M HCl and the free alcohol used to esterify acryloyl chloride to obtain the monomer **3.20** in good yield. Polymerization using benzoyl peroxide (BPO) gave polymer **3.21** in 54% yield.

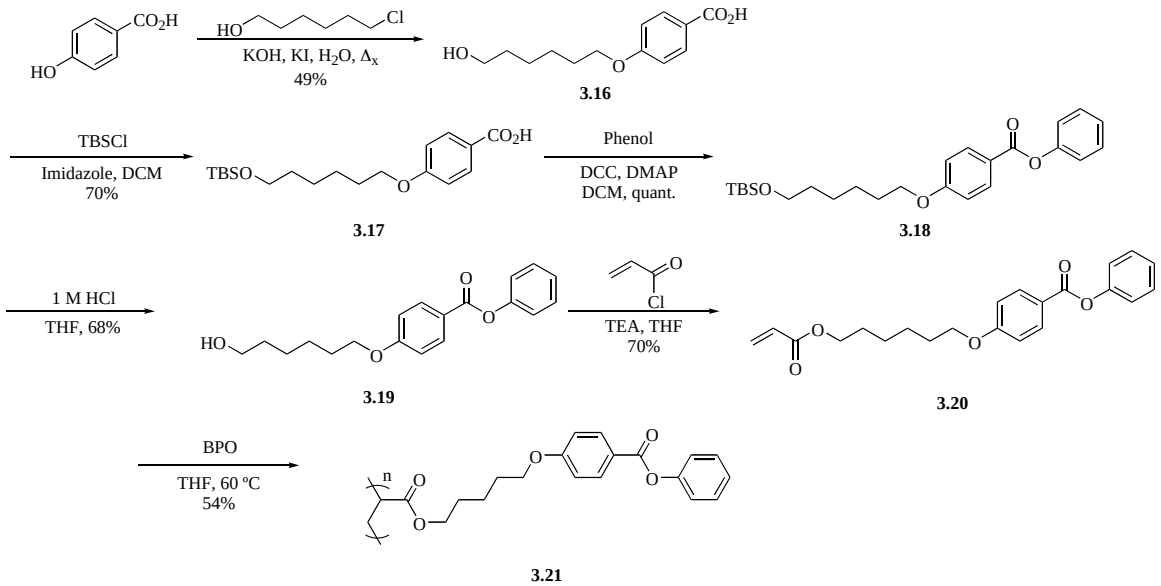


Scheme 3.9. Synthesis of acrylate polymer **3.21**

With the desired polymers in hand, a suitable azobenzene dopant molecule was then synthesized (Scheme 3.10). The hexyl variant **3.23** was chosen as it was thought that the long chain would increase the bulk of the molecule and in turn, the difference in size between the *trans* and *cis* isomers.

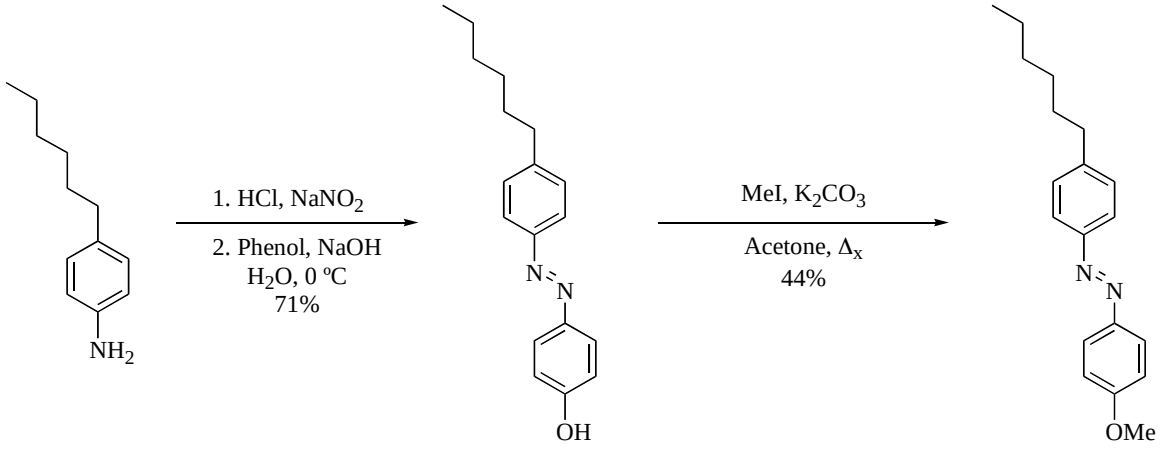


**3.22** **3.23**

Scheme 3.10. Synthesis of azobenzene dopant **3.23**

On its own, compound **3.23** was a LC, as demonstrated by DSC and POM analysis. Its liquid crystalline range was near room temperature (13-47 ºC), bolstering the prospects of obtaining a mixture that could successfully meld a room temperature liquid crystalline state and the ability to be photochemically switched to the isotropic liquid state (Figure 3.20).

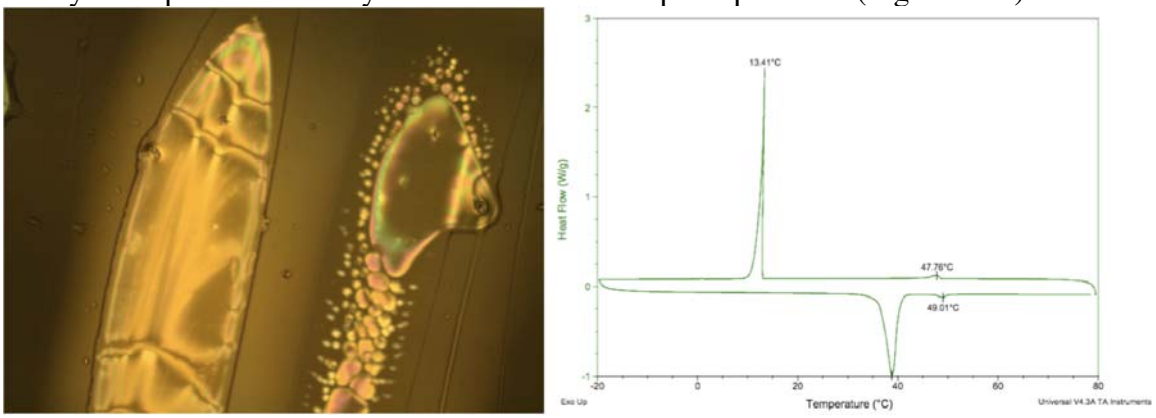


Figure 3.20. POM image and DSC thermogram for **3.23**

### 3.13 CHARACTERIZATION OF LC MIXTURES AND DIFFUSION STUDIES

Attention was shifted to showing the disruption of the LC phase in our synthesized polymers **3.15** and **3.23**. In both cases, a 1:9 mixture of the azobenzene dopant:host LC polymer ratio was used, as this was the smallest value that allowed for weighable quantities of the dopant in test scale mixtures of the polymer. After spin coating these mixtures onto silicon wafer shards, they were tested for liquid crystalline properties. Gratifyingly, both polymers containing 10% by weight azobenzene dopant exhibited LC properties (Figure 3.21).

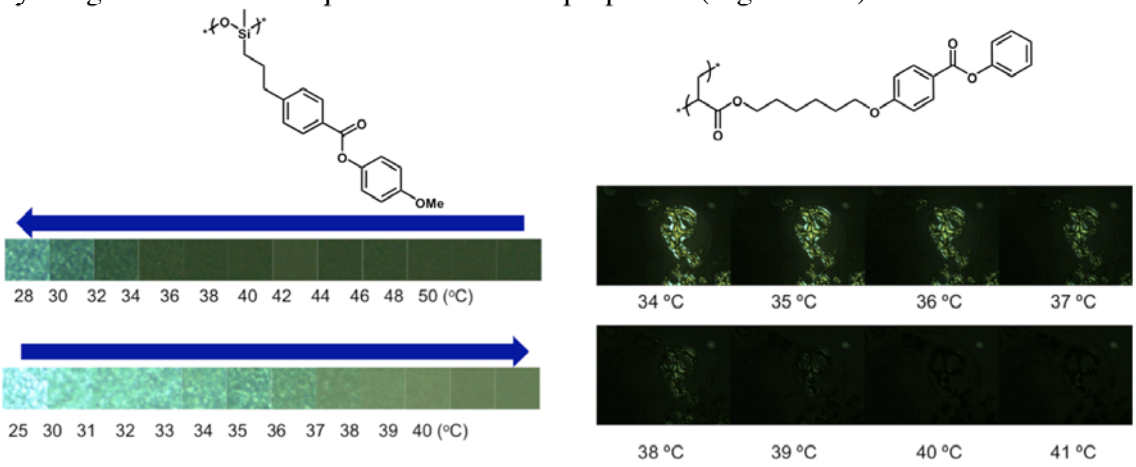


Figure 3.21. LC phases from doped polymers

With successful demonstration of LC phases from both polymer mixtures, acid diffusion studies were then commenced. Unfortunately, when attempting to coat the trilayer system, it was discovered the solubility of the barrier layer mixture was too broad to afford for easy coating of the detector (PPHA) above it. This instigated additional thought on the methods by which the film stack was coated. After significant effort, it was determined an intermediate layer above and below the barrier layer would be necessary to prevent the barrier layer from dissolving when coating the PPHA layer. For this, poly(octadecylmethacrylate) (PODMA) was used, as it had already been synthesized for testing. It has a melting temperature of its side-chains that is below the transition temperatures of both LC mixtures, hopefully mitigating any ill effects that might arise from the addition of layers.

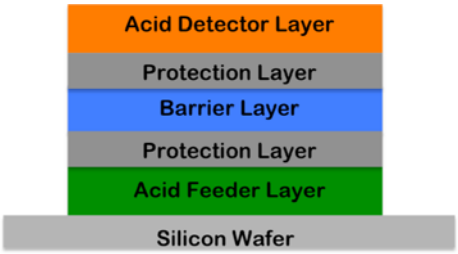


Figure 3.22. Five layer film stack for diffusion testing of LC polymers

This film stack was then generated for the siloxane polymer/dopant mixture. During this process, it was noticed some of the dopant molecule was leeching into the casting solvent for the protection layer (nonane). The amount of leeching was difficult to quantify on this scale, and in spite of this issue, photochemical disruption of the film stack was tested. As expected, this test was successful. By optical microscopy, the phase was determined to disappear upon 365 nm irradiation in the exposed areas (Figure 3.23, left image). Further, exposure at 436 nm into a small area of both unexposed and exposed areas (Figure 3.23, center image) showed some change, which followed by a low temperature bake (35 ºC) were able to largely reverse the isomerization reaction (Figure 3.23, right image).


Figure 3.23. Liquid crystal photochemical switch demonstration

In order to solve the leeching issue, it was decided to synthesize a copolymer of similar composition for both the acrylate and siloxane polymer. In both cases, the mesogen would be paired with an azobenzene containing monomer, with both moieties being incorporated into the same polymer chain. Using previously synthesized **3.22**, alkylation with 1-heptene gave

hydrosilylation precursor **3.24** in excellent yield. Hydrosilylation using **3.24** and **3.14** in a 1:9 ratio afforded copolymer **3.25** (Scheme 3.11).

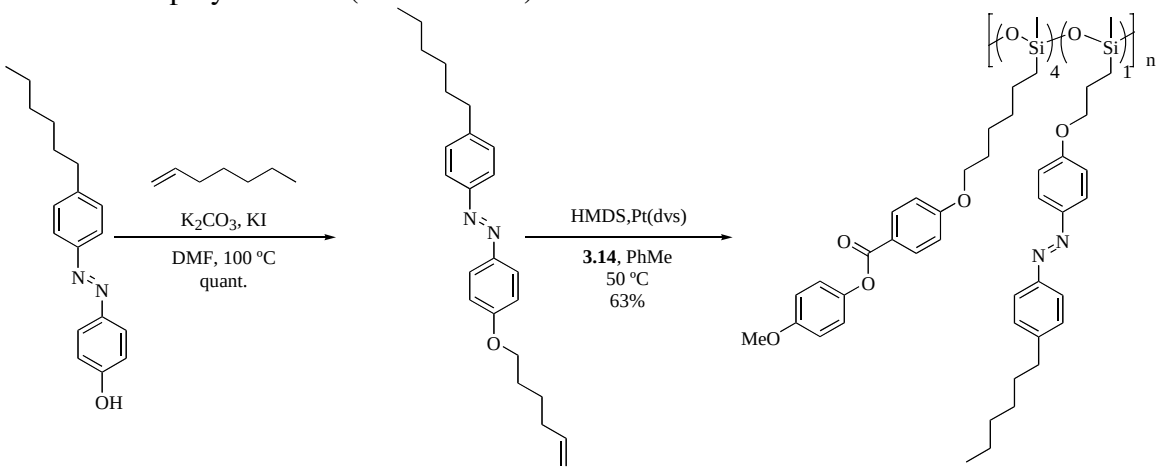


Scheme 3.11. Synthesis of copolymer **3.25**

Upon completion of the synthetic work, the LC transitions of the polymer were tested. Fortunately, solubility testing revealed the dissolution of the azobenzene compound in nonpolar solvents had been prevented. This allowed for the successful coating of the protection layer (PODMA).

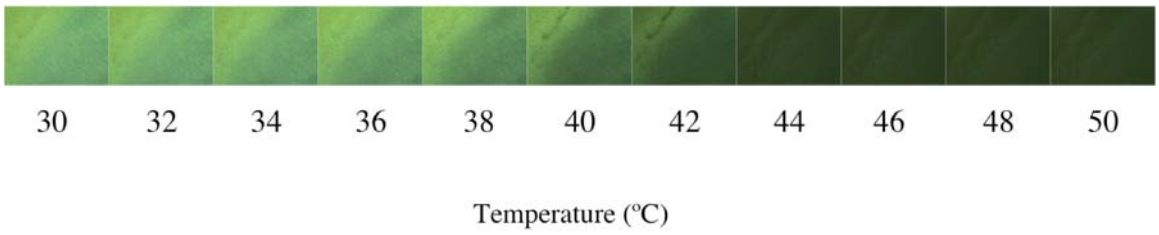


Figure 3.24. LC to isotropic liquid transition for **3.25**

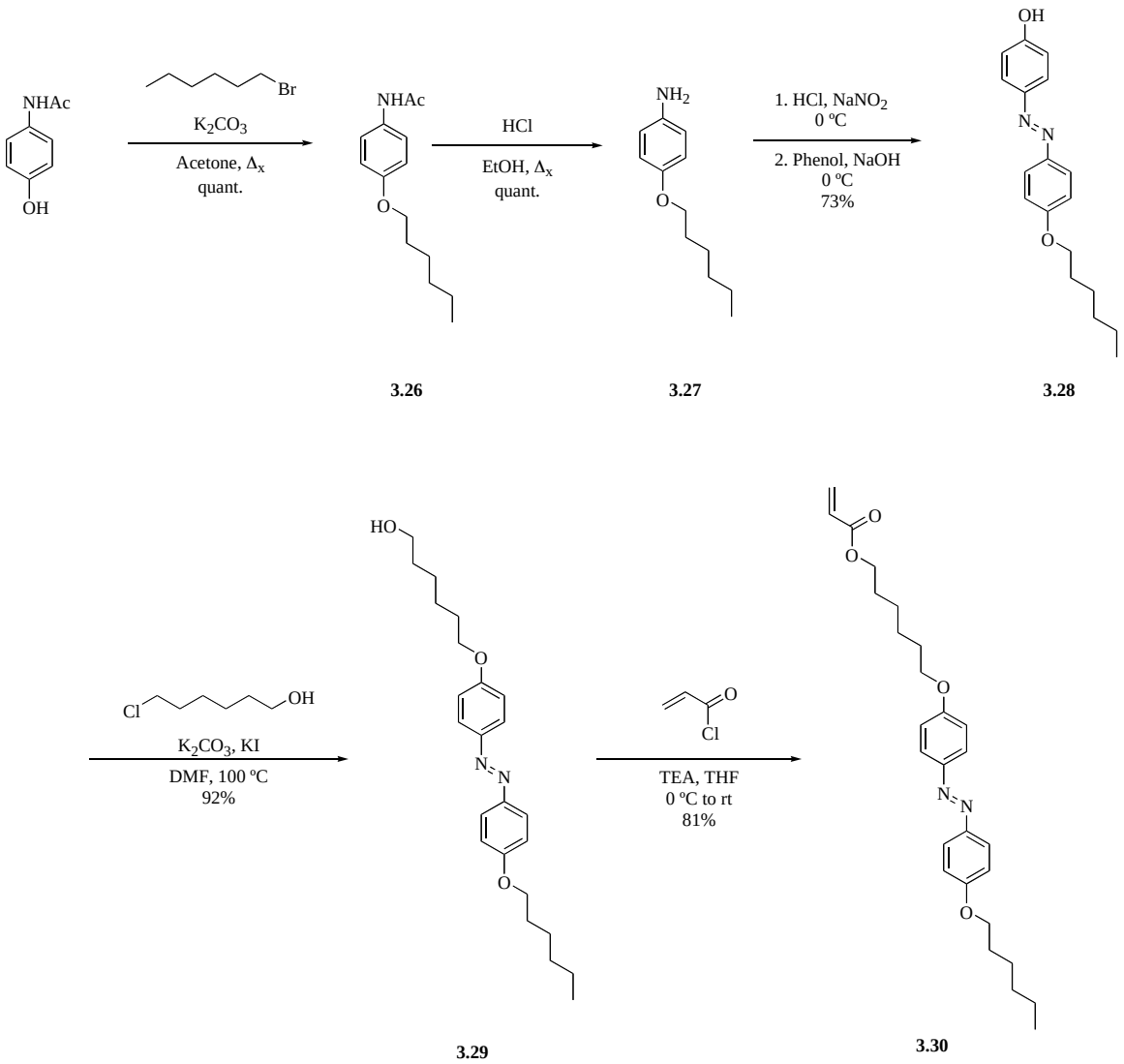


Scheme 3.12. Synthesis of monomer **3.30**

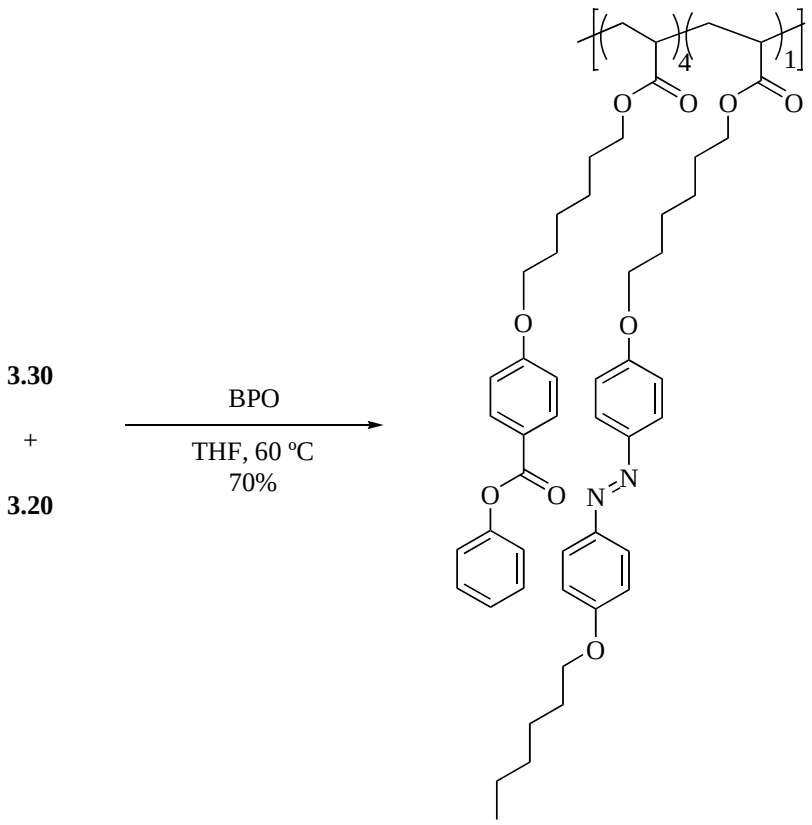


Scheme 3.13. Synthesis of copolymer **3.31**

Synthesis of the acrylate-based copolymer (Scheme 3.12) employed the azobenzene containing monomer that initially came from 4-hydroxyaminophenol (acetaminophen). Alkylation with bromohexane proceeded in quantitative yield, followed by acid catalyzed deprotection of the aniline nitrogen to afford **3.27**. Diazonium formation and quenching with phenolate anion gave the azobenzene **3.28** in 73% yield. Alkylation with 6-chloro-1-hexanol and subsequent esterification with acryloyl chloride provided monomer **3.30** in excellent yield. Polymerization of **3.30** with **3.20** (1:9 feed ratio) using BPO gave the desired copolymer **3.31** (Scheme 3.13). POM of the copolymer indicated an LC phase, as anticipated. Buoyed by this success, work was then initiated to determine whether the diffusion characteristics could be altered through photoisomerization.

### 3.14 EXPOSURE AND IMAGING STUDIES

After assembling the five-layer film stack necessary for this study using copolymer **3.25**, the film stack was exposed to 248 nm irradiation to generate acid from the PAG in the acid-feeder layer, and then subjected to 365 nm exposure through a contact mask to generate the isotropic liquid state in the exposed areas. These two exposures should allow for diffusion of the acid through the areas subjected to exposure in the second pass. Intriguingly, after baking at 45 ºC (above the liquid crystalline to isotropic liquid phase transition) for several minutes, acid was observed to have diffused through the unexposed areas, but not through those where the *trans* to *cis* isomerization had taken place (Figure 3.25).

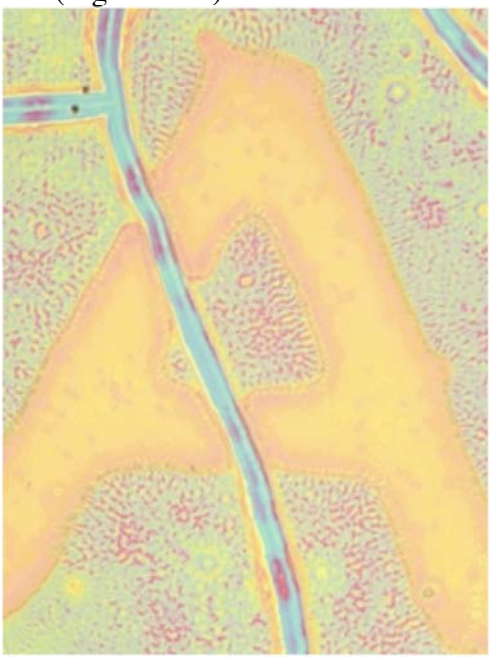

Figure 3.25. Image obtained from exposure of five layer film stack with polymer **3.25**

Perhaps most interesting was the failure of any acid diffusion to take place below the LC to I transition, as was anticipated. Attempts were made at 38 and 40 ºC, but with no acid diffusion was observed, prompting the attempt at 48 ºC. The change in the LC polymer barrier layer is also reversible, making this result quite interesting and worthy of further study. At this time, it is unclear what occurred in these experiments, though due to the reversibility of the isomerization, it would appear that cross-linking or decomposition of the polymer are unlikely.

Furthermore, an experiment conducted with flood exposure at 365 nm to the film followed by 436 nm exposure through a contact mask was able to obtain the reverse tone image (Figure 3.26). Attempts to determine the origin of this surprising result are ongoing as of this writing.

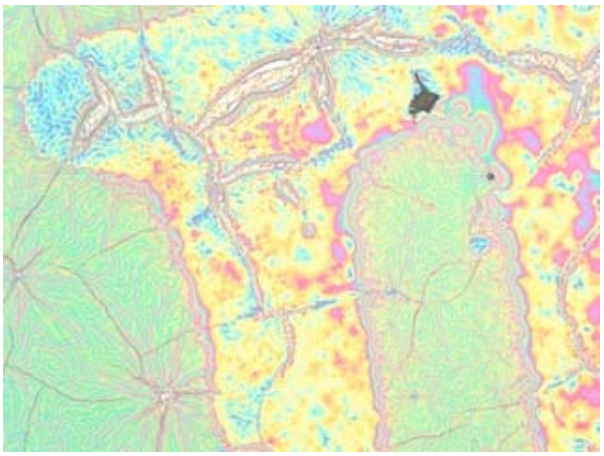

Figure 3.26. Reverse tone image from polymer **3.25**

### 3.15 CONCLUSION AND FUTURE WORK

Through this study, it has been shown the isomerization of azobenzenes from their *trans* to *cis* forms can alter the physical state of the material in some systems. This physical state change in the systems has also been shown to be accompanied by a corresponding change in the permeability of films of these polymers, which can indeed be used to produce an image in an acid-sensitive polymer. More study must be conducted on copolymer **3.25** to determine the origin of the unusual diffusion observations. Additionally, further testing of copolymer **3.31** could provide some insight if the phenomenon is also observed if detection setups utilizing **3.31** as the barrier layer.

With the successful demonstration of single exposure imaging in both side-chain crystalline and side-chain LC polymers containing azobenzene photochromic components, experiments can now be conducted to determine if similar systems can function in a double exposure sense. Successful demonstration of this concept would then allow for the investigation

of 193 nm photochromic materials with the ultimate goal of DEL work being conducted at 193 nm in a fabrication facility.

## 3.16 EXPERIMENTAL

### General Methods

All experiments were carried out under nitrogen atmosphere in flame-dried glassware unless otherwise noted. Tetrahydrofuran (THF) was dried using sodium/benzophenone ketyl radical. Dichloromethane, triethylamine and toluene were dried over calcium hydride. Dimethyl formamide (DMF) and acetone were dried over molecular sieves. Flash column chromatography was run according to the procedure of Still.[51] $^{1}$H NMR spectra were obtained on Varian Mercury (400 MHz), Varian MR (400 MHz) or Unity (300 MHz) instruments and referenced to deuteriochloroform (7.26 ppm), the center of the DMSO-*d*6 quintet (2.54 ppm) or acetone-*d*6 (2.04 ppm) unless otherwise noted. Coupling constants are reported in Hertz (Hz). $^{13}$C spectra were obtained on Varian Mercury (100 MHz), Varian Unity (75 MHz) and Varian MR (100 MHz) spectrometers. $^{19}$F spectra obtained on Varian MR (376 MHz) spectrometer and are unreferenced. Chemical shifts are reported in delta (δ) units, parts per million (ppm) relative to the center of the triplet at 77.00 ppm for deuteriochloroform or 39.5 ppm for DMSO-*d*6 unless otherwise noted. $^{13}$C NMR spectra were routinely collected with broadband decoupling. FT-IR spectra were obtained on a Nicolet Avatar 360 FT-IR instrument. UV-Visible spectra were obtained on Varian Cary 1E UV-Visible spectrometer instrument. All molecular weights were measured using an Agilent 1100 Series Isopump, Autosampler, and Refractometer and the following Pgel GPC columns: guard, 104 Å and 100 Å. Melting points were obtained on a Meltemp II apparatus in open capillary tubes and are uncorrected.

#### *4-(4-Hydroxy-phenylazo)-benzonitrile (3.1)*

Synthesized according to the procedure of Ringsdorf.[37] To a round bottom flask charged with 4-aminobenzonitrile (5.00 g, 42.32 mmol) was added concentrated sulfuric acid (11.75 mL), and deionized water (12 mL). The reaction mixture was cooled in an ice-water bath. A solution

of sodium nitrite (2.92 g, 42.32 mmol) in water (17 mL) was added dropwise via addition funnel at a rate to maintain the flask temperature below 5 ºC. The reaction was stirred until consumption of the amine was observed by TLC. A solution of phenol (3.98 g, 42.32 mmol) and sodium hydroxide (3.38 g, 84.64 mmol) in water (43 mL) was added dropwise via addition funnel. The reaction was warmed to room temperature and was stirred for 1 h. The reaction was then filtered and the filter cake washed with water until the filtrate was clear. The solid was then dissolved in 1:1 absolute ethanol/water (v:v) and acidified with concentrated hydrochloric acid. The mixture was filtered and dried to obtain the product as an orange solid (6.41 g, 68%). **$^{1}$HNMR** (400 MHz, $CDCl_3$): 7.93 (t, 4H, *J* = 8.6 Hz), 7.79 (d, 2H, *J* = 8.5 Hz), 6.97 (d, 2H, *J* = 8.8 Hz). **$^{13}$CNMR** (100 MHz, $CDCl_3$): 159.4, 154.7, 147.0, 133.6, 133.2, 125.7, 123.1, 118.6, 116.0, 113.2. **FTIR** (thin film): 3853, 3837, 3801(b), 3743, 3419, 1733, 1683, 1652, 1635, 1576, 1558, 1506, 1456 $cm^{-1}$. **mp**: 198-200 ºC (lit. 203 ºC).

***11-[4-(4-cyanophenylazo)-phenoxy]-undecyl alcohol (3.2)***

In a round bottom flask was added *p*-nitrile azobenzene **3.1** (1.22 g, 5.50 mmol), potassium carbonate (1.52 g, 11.0 mmol), catalytic amount of potassium iodide and DMF (30 mL). The mixture was heated to 100 ºC and 11-bromo-1-undecanol (1.65 g, 6.60 mmol) in DMF (15 ml) was added dropwise. The solution was stirred at 100 ºC overnight. After cooling to ambient temperature, the mixture was poured onto water. The precipitate was filtered and washed with water. The resulting solid was dried under high vacuum to afford the desired product as a brown solid (2.12 g, 98%). **$^{1}$HNMR** (400 MHz, $CDCl_3$): 7.90-7.93 (d, 4H, *J* = 6.8 Hz), 7.75-7.77 (d, 2H, *J* = 8.2 Hz), 6.99-7.01(d, 2H, *J* = 8.9 Hz), 4.02-4.05 (t, 2H, *J* = 6.5 Hz), 3.62 (s, 2H), 1.75-1.85 (m, 2H), 1.25-1.55 (m, 16H). **$^{13}$CNMR** (75 MHz, $CDCl_3$): 163.0, 155.0, 146.9, 133.4, 125.7, 123.3, 118.9, 115.1, 113.3, 68.7, 63.2, 33.0, 29.81, 29.77, 29.74, 29.66, 29.59, 29.4, 26.2, 26.0. **FTIR** (thin film): 3526, 2917, 2850, 2233, 1600, 1582, 1499, 1417, 1251, 1141, 1046, 843, 559 $cm^{-1}$. **HRMS** (CI+) calculated for $C_{24}H_{31}N_3O_2$: 393.2495; found: 394.2492. **mp**: 115-116 ºC.

***2-Methyl-acrylic acid 11-[4-(4-cyanophenylazo)-phenoxy]-undecyl ester (3.3)***

In a dry round bottom flask was added *p*-nitrile azobenzene undecyl alcohol (1.77 g, 4.50 mmol), triethylamine (0.82 mL, 5.85 mmol) and THF (15 mL). The mixture was cooled in an ice water bath and freshly distilled methacryloyl chloride (0.53 mL, 5.40 mmol) was added dropwise. The solution was warmed to ambient temperature overnight. The reaction mixture was diluted with chloroform (30 mL) and extracted with water (3 x 50 mL). The organic was dried over sodium sulfate and concentrated on a rotary evaporator. The resulting solid was recrystallized from ethanol to afford the desired product as an orange, powdery solid (1.77 g, 85%). **$^{1}$HNMR** (400 MHz, $CDCl_3$): 7.91-7.93 (d, 4H, *J* = 8.2 Hz), 7.76-7.78 (d, 2H, *J* = 8.9 Hz), 6.98-7.01 (d, 2H, *J* = 8.9 Hz), 6.08 (s, 1H), 5.52-5.53 (t, 1H, *J* = 1.7 Hz), 4.10-4.13 (t, 2H, *J* = 6.5 Hz), 4.02-4.05 (t, 2H, *J* = 6.5 Hz), 1.92 (s, 3H), 1.77-1.85 (m, 2H), 1.61-1.69 (m, 2H), 1.25-1.5 (m, 14H). **$^{13}$CNMR** (75 MHz, $CDCl_3$): 167.8, 163.0, 155.0, 146.9, 136.8, 133.4, 125.7, 125.4, 123.3, 118.9, 115.1, 113.3, 68.7, 65.0, 29.7, 29.6, 29.5, 29.4, 28.8, 26.2, 18.6. **FTIR** (thin film): 2916, 2850, 2229, 1704, 1602, 1583, 1504, 1474, 1419, 1397, 1327, 1255, 1141, 854 $cm^{-1}$. **HRMS** (CI+) calculated for $C_{28}H_{35}N_3O_3$:462.2757; found: 462.2751. **mp**: 83-84 ºC.

***Poly(2-Methyl-acrylic acid 11-[4-(4-cyanophenylazo)-phenoxy]-undecyl ester) (3.5)***

In a round bottom flask containing monomer **3.3** (184 mg, 0.40 mmol), monomer **3.4** (541 mg, 1.60 mmol), and AIBN (16 mg, 0.10 mmol) was added THF (3 mL). After three freeze-pump-thaw cycles, the mixture was placed into a preheated oil bath at 60 ºC and stirred overnight. The resulting mixture was then precipitated into methanol (30 mL) and the resulting solid filtered and dried under high vacuum to afford an orange solid (340 mg, 47%). $M_W$=24,000 kDa (determine from PMMA calibration standard using refractive index detector).

***4-(4-Methoxy-phenylazo)-phenol (3.6)***

Synthesized according to the procedure of Boden *et al.*[52] To a round bottom flask containing *p*-anisidine (2.00 g, 16.23 mmol) was added 2 M hydrochloric acid (33 mL) and the resulting solution cooled in an ice water bath. Sodium nitrite (1.56 g, 22.73 mmol) was added in

four portions over 20 min. Phenol (1.52 g, 16.23 mmol) dissolved in 2 M sodium hydroxide solution (33 mL) and added dropwise to the acid solution. The resulting mixture was warmed to room temperature at which time the solution was acidified using 2M hydrochloric acid solution. The mixture was filtered and the resulting solid recrystallized from a minimal amount of EtOH, followed by addition of $H_2O$ until cloudy and allowing to stand overnight to obtain the desired product as a yellow solid (3.20 g, 86%). **$^1$HNMR** (400 MHz, $CDCl_3$): 7.82-7.88 (dd, 4H, *J* = 8.9, 7.5 Hz), 6.92-7.01 (dd, 4H, *J* = 18.4, 8.9 Hz), 3.88 (s, 3H). **$^{13}$CNMR** (75 MHz, $CDCl_3$): 161.6, 157.8, 147.0, 129.6, 124.5, 124.3, 115.7, 115.2, 114.2, 55.5. Melting point (129-131ºC) matched literature value.

***4-[4-(6-Hydroxy-hexyloxy)-phenylazo]-benzonitrile (3.7)***

Synthesized according to the procedure of Ikeda et al.[40] In a round bottom flask containing *p*-CN azobenzene (1.13 g, 5.06 mmol) was added potassium carbonate (700 mg, 5.06 mmol), 6-chloro-1-hexanol (0.90 mL, 6.73 mmol), potassium iodide (2 mg), and DMF (6.3 mL). The reaction mixture was heated to 120 ºC and stirred overnight. The reaction was then cooled to ambient temperature and poured onto water (60 mL). The mixture was filtered and concentrated. The solid was extracted with ethyl acetate, dried over magnesium sulfate and filtered. Concentration on a rotary evaporator and recrystallization from methanol afforded the desired alcohol as an orange solid (1.2 g, 73%). **$^1$HNMR** (400 MHz, $CDCl_3$): 7.92-7.95 (dd, 4H, *J* = 9.2, 1.0 Hz), 7.77-7.80 (dt, 2H, *J* = 8.9, 1.0 Hz), 7.00-7.02 (dt, 2H, *J* = 8.9, 1.0 Hz), 4.05-4.08 (t, 2H, *J* = 6.5 Hz), 3.66-3.69 (t, 2H, *J* = 6.5 Hz), 1.46-1.85 (m, 10 H). **$^{13}$CNMR** (75 MHz, $CDCl_3$): 162.6, 154.7, 146.6, 133.1, 125.4, 123.0, 118.6, 114.8, 113.0, 68.2, 62.8, 32.6, 29.0, 25.8, 25.5. **FTIR** (thin film): 3498 (br), 2928, 2232, 1601, 1581, 1499, 1471, 1415, 1398, 1256, 1136, 846 $cm^{-1}$. **mp** 149-152 ºC.

***6-[4-(4-Methoxy-phenylazo)-phenoxy]-hexan-1-ol (3.8)***

Prepared according to the procedure of Sadagopan *et al.*[53] To a round bottom flask containing *p*-MeO azobenzene (4.55 g, 19.93 mmol) was added anhydrous potassium carbonate

(5.51 g, 39.86 mmol) and potassium iodide (198 mg, 1.19 mmol), followed by DMF (40 mL). The mixture was heated to 100 ºC and stirred for 30 min. 6-Chloro-1-hexanol (3.99 mL, 29.90 mmol) was added dropwise and the solution stirred at 100 ºC for 24 h. The mixture was poured over ice water (400 mL) and filtered. The resulting solid was recrystallized from ethanol to provide the product as an orange solid (5.54 g, 70%). **$^1$HNMR** (400 MHz, $CDCl_3$): 7.84-7.88 (dd, 4H, *J* = 4.4, 2.4 Hz), 6.97-7.01 (m, 4H), 4.02-4.05 (t, 2H, *J* = 6.5 Hz), 3.88 (s, 3H), 3.65-3.68 (t, 2H, *J* = 6.5 Hz), 1.41-1.85 (m, 8H). **$^{13}$CNMR** (75 MHz, $CDCl_3$): 166.1, 162.1, 155.2, 146.7, 131.4, 130.4, 125.1, 122.2, 114.6, 68.1, 65.3, 62.6, 32.5, 31.3, 29.0, 28.6, 25.7, 25.6, 25.4, 22.4, 13.9. **FTIR** (thin film): 3298, 2934, 1600, 1581, 1496, 1464, 1315, 1247, 1151, 1108, 1025, 1009, 842 $cm^{-1}$. **HRMS** (CI+) calculated for $C_{19}H_{24}N_2O_3$: 329.1866; found: 329.1865. **mp** 128-132 ºC.

***2-Methyl-acrylic acid 6-[4-(4-cyano-phenylazo)-phenoxy]-hexyl ester (3.9)***

Synthesized according to the procedure of Ringsdorf.[37] To a round bottom flask was added *p*-CN azobenzene (1.11 g, 3.44 mmol), triethylamine (0.53 mL, 3.78 mmol) and THF (6 mL). The mixture was cooled in an ice bath and methacryloyl chloride (0.37 mL, 3.78 mmol) was added dropwise. The solution was warmed to ambient temperature overnight. The reaction mixture was then concentrated on a rotary evaporator and the remaining solid washed with saturated sodium carbonate. The solid was filtered and washed with water and allowed to dry to afford the desired product as an orange solid (1.216 g, 90%). **$^1$HNMR** (400 MHz, $CDCl_3$): 7.92-7.95 (d, 4H, *J* = 8.5 Hz), 7.77-7.79 (d, 2H, *J* = 8.2Hz), 6.99-7.02 (d, 2H, *J* = 8.9 Hz), 6.10 (s, 1H), 5.55 (s, 1H), 4.15-4.18 (t, 2H, *J* = 6.5 Hz), 4.05-4.08 (t, 2H, *J* = 6.1 Hz), 1.94 (s, 3H), 1.46-1.85 (m, 10 H). **$^{13}$CNMR** (100 MHz, $CDCl_3$): 167.5, 162.6, 154.7, 146.7, 136.4, 133.1, 125.4, 125.2, 123.0, 114.8, 113.1, 68.2, 64.5, 29.0, 28.5, 25.7, 25.6, 18.3. **FTIR** (thin film): 2939, 2867, 2220, 1711, 1600, 1561, 1497, 1471, 1416, 1324, 1297, 1252, 1187, 1141, 1110, 1015, 840 $cm^{-1}$. **mp** 92-94 ºC.

***2-Methyl-acrylic acid 6-[4-(4-methoxy-phenylazo)-phenoxy]-hexyl ester (3.10)***

To a round bottom flask was added *p*-MeO azobenzene (2.323 g, 7.07 mmol), triethylamine (1.05 mL, 7.56 mmol) and THF (23 mL). The mixture was cooled in an ice water bath and methacryloyl chloride (0.69 mL, 7.07 mmol) was added dropwise. The solution was warmed to ambient temperature overnight. The reaction mixture was diluted with chloroform (40 mL) and extracted with water (3 x 50 mL). The organic layers were dried over sodium sulfate and concentrated on a rotary evaporator. The resulting solid was recrystallized from ethanol to afford the desired product as a yellow, powdery solid (1.173 g, 42%). **$^{1}$HNMR** (400 MHz, $CDCl_3$): 7.85-7.88 (m, 4H), 6.97-7.01 (t, 4H, *J* = 8.8 Hz), 6.10 (s, 1H), 5.54-5.55 (t, 1H, *J* = 1.3 Hz), 4.15-4.18 (t, 2H, *J* = 6.8 Hz), 4.02-4.05 (t, 2H, *J* = 6.5 Hz), 3.88 (s, 3H), 1.94 (s, 3H), 1.71-1.83 (m, 8H). **$^{13}$CNMR** (75 MHz, $CDCl_3$): 137.4, 161.4, 161.0, 146.9, 146.8, 136.3, 125.1, 124.2, 124.2, 114.5, 114.0, 67.9, 64.5, 55.4, 28.9, 28.4, 25.7, 25.6, 18.2. **FTIR** (thin film): 2960, 1714, 1688, 1588, 1504, 1465, 1432, 1405, 1280, 1223, 1137, 862, 843, 733, 694 $cm^{-1}$. **HRMS** (CI+) calculated for $C_{23}H_{28}N_2O_4$:397.2125; found:397.2127. **mp** 87-89 ºC.

***Homopolymerization of Azobenzene methacrylates (3.11, 3.12)***

To a round bottom flask charged with azobenzene methacrylate monomer (750 mg, 1.91 mmol) was added AIBN (0.3 mg, 0.001 mmol) and toluene (2 mL). The reaction mixture was sparged with nitrogen gas for 15 min, then placed into a preheated 80 ºC oil bath and stirred for 48 h. The reaction was cooled to ambient temperature and then added dropwise to methanol (30 mL). The precipitated orange /yellow solid was filtered and dried under high vacuum overnight.

***p*-MeO azobenzene homopolymer (3.11)**: (546 mg, 73%) $M_N$: 26,000 kDa, $M_W$: 47,700 kDa, PDI: 1.83. DSC K to N phase transition: 77.8 ºC, N to I phase transition: 121.7 ºC.

***p*-CN azobenzene homopolymer (3.12)**: (410 mg, 55%) $M_N$:29,000 kDa, $M_W$:54,000 kDa, PDI: 1.87. DSC K to N phase transition: 53.7 ºC, N to I phase transition: 164.6 ºC.

***4-allyloxybenzoic acid (3.13)***

To a round bottom flask charged with ethyl 4-hydroxybenzoate (16.61 g, 100 mmol), allyl bromide (20 mL, 231 mmol), potassium carbonate (20.73 g, 150 mmol), potassium iodide (1.26 g, 7.60 mmol), and anhydrous DMF (300 mL). The mixture was stirred under nitrogen at 100 ºC for 24 h, additional allyl bromide (20 mL, 231 mmol) was added and stirred for another 24 h. After being cooled to room temperature, a solution of potassium hydroxide (113.69 g, 2.38 mol, in 300 mL of $H_2O$) was added to the reaction mixture and refluxed for 24 h. After being cooled, the mixture was poured into water and adjusted to pH=2-3 using conc. hydrochloric acid. The product, a white precipitate was filtered, washed with water and dried (14.60 g, 82%) **$^1$HNMR** (400 MHz, $CDCl_3$): 8.03-8.08 (d, 2H, *J* = 8.4 Hz), 6.93-6.95 (d, 2H, *J* = 8.8 Hz), 5.99-6.07 (m, 1H), 5.39-5.43 (d, 1H, *J* = 17.6 Hz), 5.30-5.32 (d, 1H, *J* = 10.4 Hz), 4.59-4.60 (d, 2H, *J* = 5.2 Hz). **$^{13}$CNMR** (75 MHz, DMSO): 167.0, 161.8, 133.2, 131.3, 123.1, 117.8, 114.5, 68.4. **FTIR** (KBr): 1678, 1606, 1428, 1319, 1304, 1290, 1252, 1174, 1819, 999, 950, 850, 770 $cm^{-1}$. **HRMS** (CI+) calculated for $C_{10}H_{11}O_3$:179.0708; found:179.0711. **mp** 160-162 ºC.

***4-methoxyphenyl 4-allyloxybenzoate (3.14)***

A round bottom flask was charged with 4-allyloxybenzoic acid **3.13** (4.30 g, 24.2 mmol) and thionyl chloride (17.4 mL, 242 mmol). The mixture was refluxed for 5 h. After being cooled, the remaining thionyl chloride was evaporated, then, 4-methoxyphenol (3.00 g, 24.2 mmol), pyridine (7.8 mL, 96.7 mmol), dimethylaminopyridine (0.183 g, 0.967 mmol) and dichloromethane (50 mL ) were added. The mixture was stirred at 40 ºC for 24 h. After being cooled to room temperature, ethyl acetate was added into the reaction mixture, and washed with water, dilute hydrochloric acid, saturated sodium carbonate, and brine. After concentration on a rotary evaporator, the white powder obtained was recrystalized with ethyl acetate:hexanes (5.52 g, 80%). **$^1$HNMR** (300 MHz, $CDCl_3$): 8.11-8.13 (d, 2H, *J* = 8.7 Hz), 7.08-7.24 (dd, 2H, *J* = 2.0 Hz, 6.8Hz), 6.90-6.99 (m, 4H), 5.40-5.46 (d, 1H, *J* = 18.6 Hz), 5.30-5.34 (d, 1H, *J* = 10.5 Hz), 4.60-4.62 (d, 2H, *J* = 5.4 Hz), 3.78 (s, 3H). **$^{13}$CNMR** (75 MHz, $CDCl_3$): 165.1, 162.7, 157.1,

144.4, 132.4, 132.1, 122.4, 121.9, 118.0, 114.4, 114.3, 68.7, 55.4. **FTIR** (KBr): 1737, 1609, 1510, 1419, 1272, 1257, 1196, 1167, 1078, 1028, 1007, 943, 772, 845, 764 $cm^{-1}$. **HRMS** (CI+) calculated for $C_{17}H_{17}O_4$:285.1127; found:285.1128. **mp** 144-146 ºC.

***poly((3-(4-(4-methoxyphenyloxycarbonyl)phenyloxy)propyl)methyl siloxane) (3.15)***

A round bottom flask was charged with 4-methoxyphenyl 4-allyloxybenzoate (3.00 g, 10.5 mmol), polyhydromethylsiloxane (0.632 g, Mw = 4100), platinum (0) divinyltetramethyldisiloxane (0.3 mL, 0.1 M solution in xylene, 0.0264 mmol) and toluene (20 mL). The mixture was stirred under nitrogen at 50 ºC for 24 h, and stirred 6 more hours after adding 1-decane to quench all Si-H moieties. The mixture was filtered using Celite and reprecipitated by dissolving in a minimal amount of THF and dropwise addition to methanol (1.97 g, 57%). DSC LC to I phase transition 38 ºC.

***4-(6-Hydroxy-hexyloxy)-benzoic acid (3.16)***

Synthesized according to the procedure of Horvath.[49] In a 3-neck flask containing 4-hydroxybenzoic acid (20.0 g, 144 mmol) and potassium hydroxide (18.6 g, 333 mmol) was added deionized water (29 mL) and potassium iodide (144 mg, 0.86 mmol). The mixture was heated to reflux, and 6-chloro-1-hexanol (21.2 mL, 159 mmol) was added dropwise. The resulting solution was stirred overnight at reflux and then cooled to room temperature. Deionized water (150 mL) was added and the solution extracted with ethyl ether (50 mL). The aqueous layer was then acidified to pH=2 using concentrated hydrochloric acid and filtered. The solid was recrystallized from absolute ethanol to obtain the product as a white solid (15.5 g, 45%). **$^1$HNMR** (400 MHz, DMSO-*d*6): 7.84-7.87 (d, 2H, *J* = 8.9 Hz), 6.96-6.98 (d, 2H, *J* = 8.9 Hz), 4.35 (br s, 1H), 3.98-4.01 (t, 2H, *J* = 6.4 Hz), 3.36-3.39 (t, 2H, *J* = 6.3 Hz), 1.68-1.71 (quin, 2H, *J* = 6.7 Hz), 1.31-1.43 (m, 6H). **$^{13}$CNMR** (100 MHz, DMSO-*d*6): 167.0, 162.3, 131.3, 122.8, 114.2, 67.7, 60.6, 32.5, 28.6, 25.4, 25.3. **HRMS** (CI-) calculated for $C_{13}H_{17}O_4$: 237.1132; found: 237.1131. **FTIR** (Nujol mull): 2923, 2853, 2723, 1506, 1457, 1376, 1249, 1174, 1107, 1051, 722 $cm^{-1}$. **mp** 128-136 ºC.

***4-[6-(tert-Butyl-dimethyl-silanyloxy)-hexyloxy]-benzoic acid (3.17)***

To a round bottom flask containing alkylated *p*-hydroxybenzoic acid **3.16** (5.00 g, 20 mmol) was added chloro-*t*-butyldimethylsilane (3.79 g, 25 mmol) and imidazole (441 g, 63 mmol). Dichloromethane (70 mL) was added and the mixture stirred for 24 h. The solution was then concentrated by rotary evaporator, and after flash column chromatography (1:1 ethyl acetate:hexanes) a white solid was obtained (3.68 g, 49%). **$^{1}$HNMR** (400 MHz, $CDCl_3$): 8.04-8.06 (d, 2H, *J* = 8.2 Hz), 6.91-6.93 (d, 2H, *J* = 8.5 Hz), 4.00-4.03 (t, 2H, *J* = 6.1 Hz), 3.61-3.64 (t, 2H, *J* = 6.1 Hz), 1.80-1.83 (t, 2H, *J* = 6.5 Hz), 1.41-1.57 (m, 6H), 0.89 (s, 9H), 0.05 (s, 6H). **$^{13}$CNMR** (100 MHz, $CDCl_3$): 172.0, 163.6, 132.3, 121.4, 114.1, 68.1, 63.0, 32.6, 29.0, 25.9, 25.7, 25.5, 18.3, -5.2. **HRMS** (CI+) calculated for $C_{19}H_{33}O_4Si$: 353.2148; found: 353.2151. **FTIR** (thin film): 3076, 2926, 2856, 2677, 1675, 1605, 1432, 1307, 1254, 1171, 645 $cm^{-1}$. **mp** 140-142 ºC.

***4-[6-(tert-Butyl-dimethyl-silanyloxy)-hexyloxy]-benzoic acid phenyl ester (3.18)***

To a round bottom flask was added substituted benzoic acid **3.17** (3.50 g, 9.9 mmol), phenol (934 mg, 9.9 mmol), dicyclohexylcarbodiimide (2.25 g, 10.9 mmol) and *N*, *N*-dimethylaminopyridine (121 mg, 0.9 mmol), followed by dichloromethane (100 mL). The reaction mixture was stirred until consumption of starting material was observed by TLC (~20 h). The mixture was then filtered and the mother liquor concentrated by rotary evaporation. Column chromatography (1:1 ethyl acetate:hexanes) afforded the desired product as a white solid (4.30 g, quantitative). **$^{1}$HNMR** (400 MHz, acetone-*d*6): 8.06-8.08 (dt, 2H, *J* = 8.9, 2.1 Hz), 7.39-7.43 (m, 2H), 7.20-7.26 (m, 3H), 7.04-7.06 (dt, 2H, *J* = 8.9, 2.1 Hz), 4.07-4.10 (t, 2H, *J* = 6.4 Hz), 3.59-3.63 (t, 2H, *J* = 6.4 Hz), 1.99-2.01 (m, 2H), 1.77-1.81 (quintet, 2H, *J* = 6.6 Hz), 1.41-1.53 (m, 4H), 0.85 (s, 9H), 0.05 (m, 6H). **$^{13}$CNMR** (100 MHz, $CDCl_3$): 164.8, 163.3, 150.9, 132.1, 129.3, 125.5, 121.7, 121.4, 114.1, 68.0, 62.9, 34.8, 32.6, 28.9, 26.1, 25.8, 25.7, 25.4, 18.2, -5.3. **HRMS** (CI+): calculated for $C_{25}H_{37}O_4Si$: 429.2461; found: 429.2466. **FTIR** (thin film): 3060, 2929, 2895, 2856, 2119, 1724, 1701, 1684, 1652, 1606, 1510, 1496, 1471, 1456, 1386,

1360, 1283, 1254, 1218, 1206, 1167, 1074, 1029, 1004, 836, 811, 772, 761, 744, 731, 692, 660, 630, 614 $cm^{-1}$. **mp** 59-60 ºC.

***4-(6-Hydroxy-hexyloxy)-benzoic acid phenyl ester (3.19)***

The TBS protected substrate **3.18** (3.50 g, 8.1 mmol) was added to a round bottom flask, followed by THF (41 mL) and the mixture stirred to complete dissolution. A 1 M hydrochloric acid solution (5 mL) was added and the mixture stirred until consumption of starting material was observed by TLC (~ 90 min). The mixture was then diluted with ethyl ether (150 mL) and extracted with distilled water (100 mL). The organic layer was then dried over sodium sulfate and adsorbed to silica gel. Column chromatography (1:3 ethyl acetate:hexanes) gave the desired product as a white solid (1.71 g, 67%). **$^{1}$HNMR** (400 MHz, $CDCl_3$): 8.05-8.07 (d, 2H, *J* = 8.8 Hz), 7.32-7.36 (t, 2H, *J* = 7.6 Hz), 7.11-7.19 (m, 3H), 6.87-6.90 (d, 2H, *J* = 8.8 Hz), 3.95-3.98 (t, 2H, *J* = 6.4 Hz), 3.56-3.60 (t, 2H, *J* = 6.4 Hz), 1.01-1.85 (m, 8H). **$^{13}$CNMR** (100 MHz, $CDCl_3$): 164.9, 163.4, 151.0, 132.2, 129.3, 125.6, 121.7, 121.5, 114.2, 68.0, 62.7, 32.5, 29.0, 25.7, 25.4. **HRMS** (CI+) calculated for $C_{19}H_{23}O_4$: 315.1596; found: 315.1600. **FTIR** (thin film): 3334 (br), 2930, 2867, 1728, 1607, 1511, 1470, 1315, 1259, 1191, 1164, 1076, 1007, 762, 747, 692 $cm^{-1}$. **mp** 81-82 ºC.

***4-(6-Acryloyloxy-hexyloxy)-benzoic acid phenyl ester (3.20)***

To a round bottom flask containing alcohol **3.19** (1.00 g, 3.18 mmol) was added THF (11 mL) and triethylamine (0.48 mL, 3.49 mmol) and the resulting mixture cooled to 0 ºC in an ice bath. Freshly distilled acryloyl chloride (0.26 mL, 3.18 mmol) was added dropwise, the ice bath removed, and the mixture stirred for 3 h. The resulting suspension was concentrated by rotary evaporation. Ethyl acetate (30 mL) was added and extracted with sodium carbonate solution (20 mL). The aqueous layer was then back extracted with ethyl acetate (2 x 30 mL) and the organic fractions combined and concentrated. The resulting solid was then recrystallized from absolute ethanol to obtain the product as an off-white solid (749 mg, 64%). **$^{1}$HNMR** (400 MHz, $CDCl_3$): 8.13-8.15 (dt, 2H, *J* = 8.9, 2.1 Hz), 7.40-7.44 (m, 2H), 7.19-7.27 (m, 3H), 6.95-6.97 (dt, 2H, *J* =

8.9, 1.9 Hz), 6.38-6.43 (dd, 1H, *J* = 17.4, 1.5 Hz), 6.09-6.16 (dd, 1H, *J* = 17.2, 10.3 Hz), 5.81-5.84 (dd, 1H, *J* = 10.3, 1.3 Hz), 4.16-4.20 (t, 2H, *J* = 6.6 Hz), 4.03-4.06 (t, 2H, *J* = 6.4 Hz), 1.81-1.88 (quintet. 2H, *J* = 6.6 Hz), 1.69-1.76 (quintet, 2H, *J* = 6.8 Hz), 1.43-1.57 (m, 4H). **$^{13}$CNMR** (100 MHz, $CDCl_3$): 166.3, 164.9, 163.3, 151.0, 132.2, 130.5, 129.4, 128.5, 125.6, 121.7, 121.6, 114.2, 68.0, 28.9, 28.5, 25.7. **HRMS** (CI+) calculated for $C_{22}H_{25}O_5$: 369.1702; found: 369.1708. **FTIR** (thin film): 3056, 2944, 2867, 1717, 1700, 1652, 1635, 1604, 1473, 1277, 1201, 1178, 1068, 763, 748, 691 $cm^{-1}$. **mp** 52-55 ºC.

***Poly(4-(6-Acryloyloxy-hexyloxy)-benzoic acid phenyl ester) (3.21)***

To a round bottom flask containing monomer **3.20** (680 mg, 1.84 mmol) was added benzoyl peroxide (9 mg, 0.03 mmol) and THF (7.4 mL). The resulting solution was subjected to three freeze pump thaw cycles and then placed into a preheated 60 ºC oil bath and stirred 15 h. After cooling to room temperature, the polymer was precipitated into chilled ether (0 ºC, 75 mL) and filtered to obtain a colorless semisolid (195 mg, 29%). $M_N$=5,200, $M_W$=7,066, PDI=1.35. DSC transition K to LC: 14.6 ºC, LC to I: 32.6 ºC.

***4-(4-Hexyl-phenylazo)-phenol (3.22)***

Prepared according to the method of Deindoerfer *et al.*[54] To a round bottom flask containing 4-hexylaniline (3.26 mL, 16.9 mmol) was added distilled water (7 mL) and the mixture cooled in an ice bath. A solution of 2.6 M hydrochloric acid (21 mL) was added dropwise, followed by dropwise addition of sodium nitrite (1.16 g, 16.9 mmol) in distilled water (7 mL). The resulting mixture was stirred for 2 h in an ice bath. A mixture of phenol (1.59 g, 16.9 mmol), sodium carbonate (2.51 g, 23.6 mmol) and sodium hydroxide (676 mg, 16.9 mmol) in distilled water (21 mL) was then added dropwise. The pH of the resulting solution was then adjusted to pH 8 using 1 M hydrochloric acid and then filtered. The solid was then dissolved in ethyl ether and dried over sodium sulfate. The solution was then filtered and concentrated to yield the product as a brown solid (3.42 g, 71%). **$^{1}$HNMR** (400 Mhz, $CDCl_3$): 7.79-7.84 (dd, 4H, *J* = 13.3, 8.5 Hz), 7.29-7.31 (d, 2H, *J* = 8.2 Hz), 6.89-6.91 (d, 2H, *J* = 8.5 Hz), 2.65-2.69 (t,

2H, *J* = 7.5 Hz), 1.63-1.65 (quintet, 2H, *J* = 6.5 Hz), 1.31-1.37 (m, 6H), 0.88-0.91 (t, 3H, *J* = 6.1 Hz). **$^{13}$CNMR** (100 MHz, $CDCl_3$): 158.3, 150.7, 146.9, 145.9, 129.0, 124.7, 122.4, 115.8, 35.8, 31.6, 31.2, 28.9, 22.5, 14.0. **HRMS** (CI+): calculated for $C_{18}H_{23}N_2O$: 283.1810; found: 283.1808. **FTIR** (thin film): 3393 (br), 2953, 2923, 2853, 1593, 1498, 1465, 1249, 841 $cm^{-1}$. **mp** 68-71 ºC.

***(4-Hexyl-phenyl)-(4-methoxy-phenyl)-diazene (3.23)***

Prepared according to the method of Deindoerfer *et al.*[54] To a round bottom flask containing 4-hexylaniline (3.26 mL, 16.9 mmol) was added distilled water (7 mL) and the mixture cooled in an ice bath. A solution of 2.6 M hydrochloric acid (21 mL) was added dropwise, followed by dropwise addition of sodium nitrite (1.16 g, 16.9 mmol) in distilled water (7 mL). The resulting mixture was then stirred for 2 h in an ice bath. A mixture of phenol (1.59 g, 16.9 mmol), sodium carbonate (2.51 g, 23.6 mmol) and sodium hydroxide (676 mg, 16.9 mmol) in distilled water (21 mL) was then added dropwise. The pH of the resulting solution was then adjusted to 8 using 1 M hydrochloric acid and then filtered. The solid was then dissolved in ethyl ether and dried over sodium sulfate. The solution was filtered and concentrated to yield the product as a brown solid (3.42 g, 71%). **$^{1}$HNMR** (400 MHz, $CDCl_3$): 7.79-7.84 (dd, 4H, *J* = 13.3, 8.5 Hz), 7.29-7.31 (d, 2H, *J* = 8.2 Hz), 6.89-6.91 (d, 2H, *J* = 8.5 Hz), 2.65-2.69 (t, 2H, *J* = 7.5 Hz), 1.63-1.65 (quintet, 2H, *J* = 6.5 Hz), 1.31-1.37 (m, 6H), 0.88-0.91 (t, 3H, *J* = 6.1 Hz). **$^{13}$CNMR** (100 MHz, $CDCl_3$): 158.3, 150.7, 146.9, 145.9, 129.0, 124.7, 122.4, 115.8, 35.8, 31.6, 31.2, 28.9, 22.5, 14.0. **HRMS** (CI+): calculated for $C_{18}H_{23}N_2O$: 283.1810; found: 283.1808. **FTIR** (thin film): 3393 (br), 2953, 2923, 2853, 1593, 1498, 1465, 1249, 841 $cm^{-1}$. **mp** 68-71 ºC.

***6-(p-(p-hexylphenyldiazenyl)phenoxy)-1-hexene (3.24)***

To a round bottom flask charged with p-(p-hexylphenyldiazenyl)phenol (565 mg, 2.00 mmol) was added 6-chlorohexene (313 mg, 2.64 mmol), potassium carbonate (828 mg, 5.99 mmol), potassium iodide (0.112 g, 0.675 mmol), and anhydrous DMF (20 mL). The mixture was stirred under nitrogen atmosphere at 100 ºC for 24 h. After being cooled to room temperature,

ethyl acetate was added and the organic layer was washed with water, dilute hydrochloric acid, saturated sodium carbonate, water, and brine. The product, a red, thick liquid was obtained after concentration *in vacuo* (708 mg, 97%). **$^1$HNMR** (300 MHz, $CDCl_3$): 7.89-7.92 (d, 2H, *J* = 9.0 Hz), 7.80-2.83 (d, 2H, *J* = 8.1 Hz), 7.29-7.31 (d, 2H, *J* = 8.4 Hz), 6.97-7.00 (d, 2H, *J* = 9.0 Hz), 5.76-5.91 (m, 1H), 4.98-5.09 (m, 2H), 4.00-4.05 (t, 2H, *J* = 6.6 Hz), 2.65-2.70 (t, 2H, *J* = 7.7 Hz), 2.11-2.18 (m, 2H), 1.79-1.88 (m, 2H), 1.54-1.68 (m, 4H), 1.33-1.40 (m, 6H), 0.88-0.92 (t, 3H, *J* = 6.3 Hz). **$^{13}$CNMR** (75 MHz, $CDCl_3$): 161.4, 151.0, 146.9, 145.7, 138.4, 129.0, 124.5, 122.5, 144.8, 144.6, 68.0, 35.8, 33.4, 31.7, 31.3, 28.9, 28.6, 25.2, 22.6, 14.1. **FTIR** (KBr): 2928, 2856, 1601, 1501, 1251, 1153, 1142, 840 $cm^{-1}$. **HRMS** (CI+) calculated for $C_{24}H_{33}N_2O$: 365.2593; found: 365.2594.

***poly((6-(p-(p-hexylphenyldiazenyl)phenoxy)-1-hexyl)methyl siloxane)-co -((3-(4-(4-methoxyphenyloxycarbonyl)phenyloxy)propyl)methyl siloxane) (3.25)***

To a round bottom flask charged with 6-(p-(p-hexylphenyldiazenyl)phenoxy)-1-hexene **3.24** (74 mg, 0.203 mmol), 4-methoxyphenyl 4-allyloxybenzoate **3.14** (248 mg, 0.789 mmol), polyhydroxymethylsiloxane (60.1 mg, Mw = 4100), platinum (0) divinyltetramethyldisiloxane (0.029 mL, 0.1 M solution in xylene, 3.0 mmol) and anhydrous toluene (10 mL). The mixture was stirred at 50 ºC for 24 h, and 6 additional hours after adding 1-decane (0.60 ml) to quench all remaining Si-H moieties. The mixture was precipitated with methanol and then centrifuged to obtain the product as an orange semisolid (243 mg, 63%). DSC LC to I phase transition: 43 ºC.

***4-hexyloxyacetanilide (3.26)***

Synthesized according to the procedure of Hansch.[55] In a flask containing 4-acetamidophenol (9.0 g, 59 mmol) was added 1-bromohexane (8.3 mL, 59 mmol) and potassium carbonate (8.2 g, 59 mmol). Freshly distilled acetone (60 mL) was added, the mixture heated to reflux and stirred for 48 h. The resulting mixture was then concentrated by rotary evaporator and a 2% sodium hydroxide solution (30 mL) was added and the solution stirred for 1 h. The solid was filtered and dried to afford the desired product as a white solid (13.5 g, 97%). **$^1$HNMR** (400 MHz, $CDCl_3$): 7.75 (br s, 1H), 7.34-7.7.38 (dt, 2H, *J* = 8.9, 2.0 Hz), 6.79-6.81 (dt, 2H, *J* = 8.9,

2.0 Hz), 3.88-3.91 (t, 2H, *J* = 6.5 Hz), 2.10 (s, 3H), 1.72-1.76 (quintet, 2H, *J* = 7.1 Hz), 1.30-1.43 (m, 6H), 0.81-0.90 (t, 3H, *J* = 6.8 Hz). **$^{13}$CNMR** (100 MHz, $CDCl_3$): 168.5, 155.8, 130.8, 121.9, 114.6, 68.1, 31.5, 29.1, 25.6, 24.1, 22.5, 13.9. **FTIR** (thin film): 3281, 3133, 2927, 2867, 1654, 1602, 1540, 1507, 1475, 1456, 1411, 1369, 1313, 1240, 829 $cm^{-1}$. **HRMS** (CI+): calculated for $C_{14}H_{22}NO_2$: 236.1651; found: 236.1649. **mp**: 107-109 ºC.

***4-hexyloxyaniline (3.27)***

Prepared according to the method of Hansch.[55] To a flask containing 4-hexyloxyacetanilide **3.26** (10.0 g, 42 mmol) was added absolute ethanol (42 mL) and concentrated hydrochloric acid (42 mL). The solution was heated to reflux and stirred for 24 h. After cooling to room temperature, the solution was adjusted to pH=7 using saturated sodium bicarbonate. The solution was then extracted with dichloromethane (2x75 mL), the organic layers dried over magnesium sulfate, filtered, and concentrated to yield the product as an off-white solid (8.70 g, quant.). **$^{1}$HNMR** (400 MHz, $CDCl_3$): 7.15 (br s, 2H), 6.95-6.97 (d, 2H, *J* = 8.8 Hz), 6.75-6.77 (d, 2H, *J* = 8.8 Hz), 3.85-3.88 (t, 2H, *J* = 6.6 Hz), 1.70-1.75 (quintet, 2H, *J* = 7.8 Hz), 1.31-1.45 (m, 6H), 0.88-0.92 (t, 3H, *J* = 6.6 Hz). **$^{13}$CNMR** (100 MHz, $CDCl_3$): 155.4, 131.8, 119.9, 115.5, 68.4, 31.5, 29.2, 25.6, 22.5, 13.9. **FTIR** (thin film): 3407, 2954, 2932, 2860, 2608, 1623, 1577, 1511, 1471, 1237, 1118, 1086, 1030, 821, 804 $cm^{-1}$. **HRMS** (CI+) calculated for $C_{12}H_{20}NO$: 194.1545; found: 194.1546. **mp**: 81-85 ºC.

***4-(4-Hexyloxy-phenylazo)-phenol (3.28)***

To a flask containing 4-hexyloxyaniline (6.00 g, 31 mmol) was added 2 M hydrochloric acid (62 mL) and the resulting mixture cooled to 0 ºC in an ice bath. Sodium nitrite (2.99 g, 43 mmol) was added in 5 portions over 20 minutes. Upon completion addition, a solution of phenol (2.92 g, 31 mmol) in 2 M sodium hydroxide (62 mL) was added dropwise, and the reaction then allowed to warm to room temperature. The mixture was then acidified to pH=2 using 2 M hydrochloric acid and the solid filtered and dried under high vacuum. After recrystallization from EtOH/water, the product was obtained as a light orange solid (6.80 g, 73%). **$^{1}$HNMR** (400

MHz, $CDCl_3$): 7.81-7.87 (m, 4H), 6.97-6.99 (dd, 2H, *J* = 8.9, 2.1 Hz), 6.90-6.92 (d, 2H, *J* = 8.8 Hz), 4.01-4.04 (t, 2H, *J* = 6.6 Hz), 1.77-1.84 (quintet, 2H, *J* = 6.6 Hz), 1.33-1.49 (m, 6H), 0.90-0.93 (m, 3H). **$^{13}$CNMR** (100 MHz, $CDCl_3$): 161.2, 157.8, 147.0, 146.7, 124.5, 124.3, 115.7, 114.7, 68.3, 31.5, 29.1, 25.6, 22.5, 14.0. **FTIR** (thin film): 2935, 1684, 1652, 1598, 1558, 1495, 1472, 1394, 1247, 1149, 1101, 1026, 842, 825 $cm^{-1}$. **HRMS** (CI+): calculated for $C_{18}H_{23}N_2O_2$: 299.1760; found: 299.1765. **mp** 96-97 ºC.

***6-[4-(4-Hexyloxy-phenylazo)-phenoxy]-hexan-1-ol (3.29)***

To a round bottom flask containing **3.28** (4.00 g, 13.4 mmol) was added 6-chloro-1-hexanol (2.68 mL, 20.1 mmol), potassium carbonate (3.70 g, 26.8 mmol), and potassium iodide (133 mg, 0.8 mmol), followed by dimethylformamide (27 mL). The mixture was heated to 100 ºC and stirred for 24 h, at which time the reaction was poured over ice water (270 mL). The resulting solid was then filtered and dried under high vacuum. Recrystallization from toluene afforded the product as an orange solid (4.91 g, 92%). **$^{1}$HNMR** (400 MHz, $CDCl_3$): 7.85-7.87 (dt, 4H, *J* = 8.9, 2.1 Hz), 6.96-6.99 (dd, 4H, *J* = 8.9, 1.7 Hz), 4.00-4.04 (t, 4H, *J* = 6.4 Hz), 3.63-3.68 (q, 2H, *J* = 6.4 Hz), 1.79-1.84 (quintet, 4H, *J* = 6.0 Hz), 1.33-1.63 (m, 12H), 0.89-0.93 (t, 3H, *J* = 6.8 Hz). **$^{13}$CNMR** (100 MHz, $CDCl_3$): 161.1, 161.0, 146.9, 146.8, 124.2, 114.6, 114.6, 68.2, 68.0, 62.8, 32.6, 31.5, 29.1, 25.8, 25.6, 25.5, 22.5, 14.0. **FTIR** (thin film): 3297 (br), 2937, 2861, 1652, 1601, 1558, 1496, 1248, 842 $cm^{-1}$. **HRMS** (CI+): calculated for $C_{24}H_{34}N_2O_3$: 398.2569; found: 398.2569. **mp** 116-119 ºC.

***Acrylic acid 6-[4-(4-hexyloxy-phenylazo)-phenoxy]-hexyl ester (3.30)***

A round bottom flask containing **3.29** (2.00 g, 5.04 mmol) and THF (17 mL) was cooled to 0 ºC using an ice bath. Triethylamine (0.78 mL, 5.54 mmol) was added and the mixture stirred an additional 5 minutes. Freshly distilled acryloyl chloride (0.41 mL, 5.04 mmol) was added and the mixture was warmed to room temperature overnight. The resulting suspension was concentrated by rotary evaporator and saturated sodium carbonate solution was added. The mixture was then filtered and washed with distilled water. The yellow solid was then dried

under high vacuum to afford the product (1.85 g, 81%). **$^{1}$HNMR** (400 MHz, $CDCl_3$): 7.84-7.87 (dt, 4H, *J* = 8.8, 1.9 Hz), 6.96-6.99 (dt, 4H, *J* = 6.8, 1.9 Hz), 6.38-6.42 (dd, 1H, *J* = 17.2, 1.3 Hz), 6.09-6.16 (dd, 1H, *J* = 17.4, 10.3 Hz), 5.80-5.83 (dd, 1H, *J* = 10.3, 1.3 Hz), 4.16-4.19 (t, 2H, *J* = 6.6 Hz), 4.01-4.05 (td, 4H, *J* = 6.4, 2.3 Hz), 1.69-1.85 (m, 6H), 1.33-1.57 (m, 10H), 0.89-0.93 (t, 3H, *J* = 7.0 Hz). **$^{13}$CNMR** (100 MHz, $CDCl_3$): 166.3, 161.1, 161.0, 146.9, 146.8, 130.5, 128.5, 124.2, 114.6, 144.6, 68.3, 68.0, 64.4, 31.5, 29.1, 29.0, 28.5, 25.7, 25.6, 22.5, 14.0. **FTIR** (thin film): 2940, 2864, 1718, 1603, 1582, 1503, 1472, 1406, 1249, 1204, 1149, 1107, 843 $cm^{-1}$. **HRMS** (CI+): calculated for $C_{27}H_{37}N_2O_4$: 453.2753; found: 453.2746. **mp**: 80-84 ºC.

***Poly(Acrylic acid 6-[4-(4-hexyloxy-phenylazo)-phenoxy]-hexyl ester)***

To a flask containing **3.30** (500 mg, 1.10 mmol) and AIBN (0.3 mg, 0.002 mmol) was added toluene (2 mL) and the resulting solution subjected to three freeze-pump-thaw cycles. The solution was then placed into an oil bath preheated to 80 ºC and stirred for 48 h. The solution was then concentrated, redissolved into THF (2 mL), and precipitated into chilled methanol (20 mL). The suspension was filtered to obtain a yellow solid, which was dried under high vacuum (300 mg, 60%). $M_N$=14,903, $M_W$=20,088, PDI=1.35. DSC transitions K to LC at 59 ºC, LC to LC at 106 ºC, and LC to I at 126 ºC.

***Copolymerization of 4-(6-Acryloyloxy-hexyloxy)-benzoic acid phenyl ester and Acrylic acid 6-[4-(4-hexyloxy-phenylazo)-phenoxy]-hexyl ester***

To a flask containing **3.20** (300 mg, 0.81 mmol), **3.30** (41 mg, 0.09 mmol) and benzoyl peroxide (1.9 mg, 0.008 mmol) was added THF (3 mL) and the resulting solution subjected to three freeze-pump-thaw cycles. The solution was then placed into an oil bath preheated to 60 ºC and stirred for 19 h. The reaction mixture was cooled to room temperature and precipitated into chilled methanol (20 mL) and filtered through a chilled fritted funnel to obtain the desired polymer as an orange amorphous solid (240 mg, 70%). $M_N$=4100, $M_W$=5000, PDI=1.22. DSC transitions: K to LC 10.3 ºC, LC to I 37.1 ºC.

***Procedure for testing of $T_m$ shift of 3.5***

Compound **3.5** was dissolved in nonane and spin coated onto a clean silicon wafer, then baked at 110 ºC for 60 s. Measurements were taken on a spectroscopic ellipsometer (J. A. Woolam) using CompletEASE software connected to a temperature controller and Peltier device. The temperature was ramped and measurements of thickness taken at 1 ºC intervals.

***Control Experiment for Diffusion Switching of 3.5***

A solution of PBMA containing 7.7 wt% triphenylsulfonium triflate (TPS-Tf) was spin-coated onto a clean silicon wafer from PGMEA, followed by coating of poly(octadecylmethacrylate) (PODMA) from nonane. Oxygen plasma etching for 2 s was followed by coating of PPHA from a cooled solution in PGMEA. Flood exposure was then conducted at 248 nm (200 mJ/cm$^2$) using a Cymer KrF excimer laser source and the film baked at 35 ºC for 60 s. The film was then inspected using optical microscopy.

***Procedure for Diffusion Switching Experiment of 3.5***

A solution of PBMA containing 7.7 wt% triphenylsulfonium triflate (TPS-Tf) was spin-coated onto a clean silicon wafer from PGMEA, followed by coating of **3.5** from nonane, 2 s treatment with oxygen plasma, and finally a cooled mixture of 1:1 by wt. of PPHA:PBMA from PGMEA. The film stack was baked at 30 ºC for 60 s. The resulting film thickness were: 200 nm for PPHA, 82 nm for **3.5**, and 173 nm for PBMA+PAG as measured by ellipsometry. Flood exposure of 248 nm light (200 mJ/cm$^2$) from a Cymer KrF excimer laser source followed by exposure through a contact mask using 365 nm light (210 mJ/cm$^2$)from a Novacure broadband mercury arc lamp source fitted with a 365 nm bandpass filter. Post exposure bake at various temperatures were then conducted and the film observed with optical spectroscopy.

***Procedure for Diffusion Measurement of 3.11***

A solution of PBMA containing 10 wt% TPS-Tf was spin coated onto a clean aluminum-backed silicon wafer from PGMEA. Polymer **3.11** was coated from a solution in chlorobenzene. A film of PPHA/PBMA (1:1 by weight) was coated onto a polished disc of sodium chloride and

floated into water at ambient temperature, which was then lifted from the surface using the wafer coated with PBMA and **3.11** in accordance with the procedure published previously.[24] The film was baked and dried, then flood exposed at 248 nm (200 mJ/cm$^2$) from a Cymer KrF excimer laser. FT-IR measurements were then taken in reflectance mode and data recorded for later analysis.

***Morphology of LC Barrier Layer confirmation***

A solution of PODMA in nonane was coated onto a clean silicon wafer. Oxygen plasma etching for 2 s was followed by coating of the polymer from PGMEA. A second layer of PODMA was coated from nonane and the film then viewed under POM to confirm LC phase. Exposure through a contact mask at 365 nm (150 mJ/cm$^2$) from a Novacure broadband mercury arc lamp source through a 365 nm bandpass filter was followed by POM observation to confirm loss of LC phase in exposed areas.

***Procedure for Diffusion Switching Experiments for 3.25 and 3.31***

A solution of PBMA containing 10 wt% TPS-Tf was spin coated onto a clean silicon wafer from PGMEA. PODMA was spin coated from nonane, followed by oxygen plasma etching for 2 s. Polymers were coated from cooled solution of PGMEA. A second layer of PODMA was cast from nonane and was treated with oxygen plasma for 2 s after coating. Finally, spin coating of PPHA from a cooled solution in PGMEA afforded the final film stack with film thicknesses of: 176 nm for PBMA+PAG, 69 nm for PODMA, 104 nm for LC polymer, 71 nm for PODMA, and 196 nm for PPHA as measured by spectroscopic ellipsometry. Flood exposure at 248 nm (200 mJ/cm$^2$) from a Cymer KrF excimer laser was followed by exposure through a contact mask at 365 nm (150 mJ/cm$^2$) from a Novacure broadband mercury arc lamp source through a 365 nm bandpass filter. Post exposure bake was conducted at various temperatures and the wafers inspected using optical microscopy. When used, 436 nm exposures (~100 mJ/cm$^2$) were conducted using a Novacure broadband mercury arc lamp source through a bandpass filter.

### 3.17 REFERENCES


(1) Dykes, J. M.; Plesa, C.; Choo, C.; Chapman, G. H. *Proc. SPIE-Int. Soc. Opt. Eng.* **2007**, *6730*, 673040/1-673040/10.
(2) Chapman, G.; Poon, D.; Choo, C.; Tu, Y.; Dykes, J.; Wang, J.; Peng, J.; Lennard, W.; Kavanagh, K. *Proc. SPIE-Int. Soc. Opt. Eng.* **2005**, *5753*, 976-987.
(3) Chapman, G. H.; Dykes, J.; Poon, D.; Choo, C.; Wang, J.; Peng, J.; Tu, Y. *Proc. SPIE-Int. Soc. Opt. Eng.* **2005**, *5713*, 247-258.
(4) Barachevsky, V. A. *J. Photochem. Photobiol., A* **2008**, *196*, 180-189.
(5) Ikeda, T. *J. Mater. Chem.* **2003**, *13*, 2037-2057.
(6) Ikeda, T.; Horiuchi, S.; Karanjit, D. B.; Kurihara, H.; Tazuke, S. *Macromolecules* **1990**, *23*, 42-48.
(7) Ikeda, T.; Horiuchi, S.; Karanjit, D. B.; Kurihara, S.; Tazuke, S. *Macromolecules* **1990**, *23*, 36-42.
(8) Ikeda, T.; Yoneyama, S.; Yamamoto, T.; Hasegawa, M. *Mol. Cryst. Liq. Cryst.* **2002**, *375*, 45-60.
(9) Kurihara, H.; Shishido, A.; Ikeda, T.; Tsutsumi, O.; Shiono, T. *Mol. Cryst. Liq. Cryst.* **2005**, *441*, 173-184.
(10) Okano, K.; Shishido, A.; Ikeda, T. *Macromolecules* **2006**, *39*, 145-152.
(11) Sung, J.-H.; Hirano, S.; Tsutsumi, O.; Kanazawa, A.; Shiono, T.; Ikeda, T. *Chem. Mater.* **2002**, *14*, 385-391.
(12) Kim, J. Y. F., T. *Mol. Cryst. Liq. Cryst.* **2006**, *449*, 71-80.
(13) Legge, C. H.; Mitchell, G. R. *J. Phys. D: Appl. Phys.* **1992**, *25*, 492-499.
(14) Prasad, S. K.; Nair, G. G.; Sandhya, K. L.; Rao, D. S. S. *Curr. Sci.* **2004**, *86*, 815-823.
(15) Crano, J. C.; Flood, T.; Knowles, D.; Kumar, A.; Van Gemert, B. *Pure Appl. Chem.* **1996**, *68*, 1395-1398.
(16) Natansohn, A.; Rochon, P. *Chem. Rev.* **2002**, *102*, 4139-4175.
(17) Mogri, Z., Dissertation, University of Texas at Austin, 2001.
(18) Mogri, Z.; Paul, D. R. *Polymer* **2001**, *42*, 7765-7780.
(19) Mogri, Z.; Paul, D. R. *Polymer* **2001**, *42*, 2531-2542.
(20) O'Leary, K. A., Dissertation, University of Texas at Austin, 2005.
(21) O'Leary, K. A.; Paul, D. R. *Polymer* **2004**, *45*, 6575-6585.
(22) O'Leary, K. A.; Paul, D. R. *Polymer* **2006**, *47*, 1245-1258.
(23) O'Leary, K. A.; Paul, D. R. *Polymer* **2006**, *47*, 1226-1244.
(24) Stewart, M. D., Dissertation, University of Texas at Austin, 2003.
(25) Postnikov, S. V.; Stewart, M. D.; Vi Tran, H.; Nierode, M. A.; Medeiros, D. R.; Cao, T.; Byers, J.; Webber, S. E.; Willson, C. G. *J. Vac. Sci. Technol., B* **1999**, *17*, 3335-3338.
(26) Willson, C. G.; Ito, H.; Frechet, J. M. J.; Tessier, T. G.; Houlihan, F. M. *J. Electrochem. Soc.* **1986**, *133*, 181-7.
(27) Odian, G. In *Principles of Polymerization*; 4th ed.; John Wiley & Sons: Hoboken, NJ, 2004, p 279-281.
(28) Ito, H.; Willson, C. G. *Polymer Engineering and Science* **1983**, *23*, 1012-1018.
(29) Reinitzer, F. *Monatsch. Chem.* **1888**, *9*, 421.
(30) Lehmann, O. *Z. Physikal Chem.* **1889**, *4*, 462.
(31) Singh, S. In *Liquid Crystals: Fundamentals*; World Scientific Publishing: Singapore, 2002, p 1-27.
(32) Medeiros, D. R. Dissertation, Univeristy of Texas at Austin, 1998.

(33) Kumar, G. S.; Neckers, D. C. *Chem. Rev.* **1989**, *89*, 1915-1925.
(34) Eich, M.; Wendorff, J. H.; Reck, B.; Ringsdorf, H. *Makromolekulare Chemie, Rapid Communications* **1987**, *8*, 59-63.
(35) Portugall, M.; Ringsdorf, H.; Zentel, R. *Makromolecular Chemie* **1982**, *183*, 2311-2321.
(36) Reck, B.; Ringsdorf, H. *Makromolekulare Chemie, Rapid Communications* **1985**, *6*, 291-299.
(37) Ringsdorf, H.; Schmidt, H.-W. *Makromolecular Chemie* **1984**, *185*, 1327-1334.
(38) Kondo, M.; Maeda, T.; Shishido, A.; Ikeda, T.; Yu, Y.; Nakano, M.; Shiono, T. *Mol. Cryst. Liq. Cryst.* **2005**, *441*, 297-305.
(39) Kurihara, S.; Ikeda, T.; Tazuke, S. *Japanese Journal of Applied Physics* **1988**, *27*, L1791-L1792.
(40) Saishoji, A.; Sato, D.; Shishido, A.; Ikeda, T. *Langmuir* **2007**, *23*, 320-326.
(41) Tazuke, S.; Kurihara, S.; Ikeda, T. *Chem. Lett.* **1987**, 911-914.
(42) Ichimura, K. *Chem. Rev.* **2000**, *100*, 1847-1873.
(43) Akiyama, H.; Kudo, K.; Ichimura, K. *Makromolekulare Chemie, Rapid Communications* **1995**, *16*, 35-41.
(44) Haas, W. E.; Nelson, K. F.; Adams, J. E.; Dir, G. A. *J. Electrochem. Soc.* **1974**, *121*, 1667-1669.
(45) Chiou, J. S.; Paul, D. R. *J. Polym. Sci., Part B: Polym. Phys.* **1987**, *25*, 1699-1707.
(46) Weinkauf, D. H.; Paul, D. R. *J. Polym. Sci., Part B: Polym. Phys.* **1992**, *30*, 817-835.
(47) Weinkauf, D. H.; Paul, D. R. *J. Polym. Sci., Part B: Polym. Phys.* **1992**, *30*, 837-849.
(48) Zhang, B.; Guo, S.; Shao, B. *J. Appl. Polym. Sci.* **1998**, *68*, 1555-1561.
(49) Horvath, J.; Nyitrai, K.; Cser, F.; Hardy, G. *Eur. Polym J.* **1985**, *21*, 251-257.
(50) Chien, G. C.; Kuo, J. F.; Chen, C. *J. Polym. Sci. Polym. Chem.* **1993**, *31*, 2423.
(51) Still, W. C.; Kahn, M.; Mitra, A. *J. Org. Chem.* **1978**, *43*, 2923-2925.
(52) Boden, N.; Bushby, R. J.; Clark, L. D. *J. Chem. Soc. Perkin Trans. 1* **1983**, 543-551.
(53) Sadagopan, K.; Rekha, A. S.; Ratna, D.; Samui, A. B. *J. Appl. Polym. Sci.* **2007**, *104*, 3497-3504.
(54) Deindoerfer, P.; Geiger, T.; Schollmeyer, D.; Ye, J. H.; Zentel, R. *J. Mater. Chem.* **2006**, *16*, 351-358.
(55) Selassie, C. D.; Hansch, C.; Khwaja, T. A.; Dias, C. B.; Pentecost, S. *J. Med. Chem.* **1984**, *27*, 347-357.

# *Chapter 4 Mechanistic Dichotomy of the Methyl Gilman Reagent*

## 4.1 INTRODUCTION

Conjugate addition reactions to α,β-unsaturated carbonyl compounds represent a common motif in organic chemistry (Scheme 4.1). [1] One common reagent for effecting these transformations is the lithium dialkylcuprate, or Gilman reagent, named after the author detailing its discovery. While such reactions utilizing Gilman reagents have been known for some time, the mechanism by which these reactions occur has been subject to a great deal of debate in the literature.

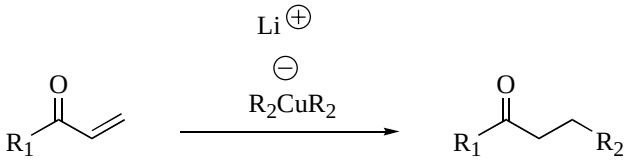


Scheme 4.1. Example of Gilman reagent addition to α,β-unsaturated carbonyl

Mechanisms have been proposed for both single and two electron processes, with much scrutiny applied to the results. In many cases, the evidence cited for a single electron process was inconclusive and later refuted.[2-4] Such cases include (a) *E*/*Z* isomerization of enones when subjected to $Me_2CuLi•LiI$, which was initially attributed to anion radical formation by the Gilman reagent and accompanying cleavage of the alkene double bond to form the diradical, followed by bond rotation and recombination, but later proved to be catalyzed by LiI at temperatures as low as -78 ºC.[5] (b) A correlation of reduction potentials of the substrate and its ability to undergo conjugate addition using $Me_2CuLi•LiI$,[6] which has subsequently proved to be superficial, and thus not good evidence of a rate-determining electron transfer step.[7] (c) A number of studies that employed chemical probes to test for and found the intermediacy of anion radicals, including elimination products from γ-heteroatom substituents,[8-10] enones with leaving groups at the δ-position that give products of internal substitution,[10-12] and enones that possessed

γ,δ-cyclopropyl groups (radical clocks), which are subject to ring opening (Scheme 4.2).[13,14] Although cleavage of a cyclopropyl ring is often indicative of radical formation, it has also been found that cyclopropyl esters and ketones may be opened by nucleophilic attack directly on the cyclopropyl ring by the Gilman reagent.[15-20]

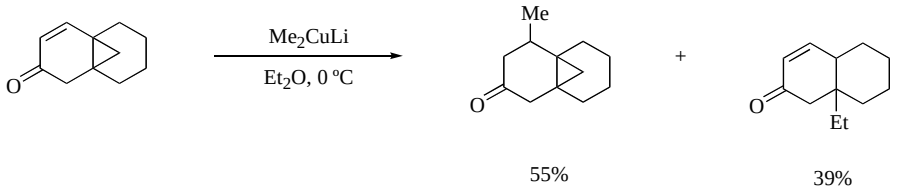


Scheme 4.2. Cyclopropyl ring opening with methyl Gilman reagent

Additional studies conducted by Casey displayed a stereospecific alkylative ring opening reaction on a γ,δ-cyclopropyl containing enone, which would appear to preclude an anion radical mechanism.[21] While Casey's study concluded that the cyclopropane ring opening was proceeding via nucleophilic addition from the Gilman reagent, Bertz later conducted further experiments that would seem to suggest that an intial β-cuprio adduct formed in the initial step would undergo stereospecific rearrangement.[22] (d) The final example that seemed to eliminate the possibility of an electron transfer mechanism has been the failure to detect any anion radicals utilizing either electron spin resonance (ESR) or chemically induced dynamic nuclear polarization (CIDNP) techniques.[23,24]

## 4.2 ACCEPTED MECHANISM OF 1,4 ADDITION USING GILMAN REAGENTS

It has now been generally accepted that Gilman reagents in conjugate addition reactions react through the reversible formation of a copper complex with the enone and a subsequent rate determining carbon-carbon bond forming reductive elimination (Scheme 4.3). Kinetic isotope effect studies are supportive of reductive elimination as the rate determining step,[25] a conclusion also supported by experiments performed by Krauss and Smith.[7] It has also been possible to observe enones complexed to the copper species through nuclear magnetic resonance,[26-29] although the exact nature of the complex itself has remained unclear.

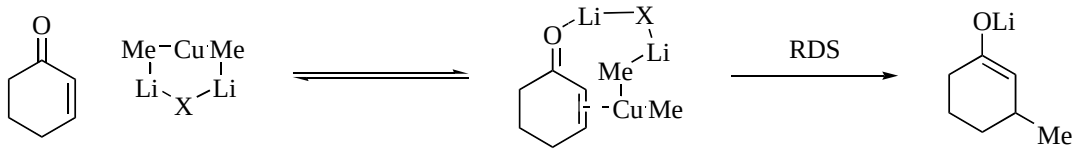


Scheme 4.3. 1,4 Addition Mechanism

The structure of the intermediate species in the reaction is thought to reside between unsymmetrical mesomeric forms, including π-complexes, oxy-π-allyls, enyls (σ+π), and β-cuprio adducts.[30-35] Boche has also suggested the that Gilman reagent is complexed with the enone prior to reaction and exists as a contact ion pair (CIP) and not a solvent separated ion pair (SSIP), even in cases where the latter would be the predominant species in the solution.[36]

However, despite the large body of evidence suggesting that anion radicals are not involved in most Gilman type conjugate addition reactions, evidence for the electron transfer properties of these reagents is nonetheless present in reactions where the substrate is easily reducible, as is the case in doubly activated olefins,[37,38] bromonaphthoquinone,[39,40] and the formation of ketyl anion radicals and subsequent pinacol reaction of fluorenone,[41] among others. With this in mind, it does remain possible that a rapid pre-equilibrium formation of anion radicals, especially in cases utilizing easily reduced substrates, could exist. This information, coupled with experiments conducted noting that *bis*(enone) substrates can undergo intramolecular [2+2] cycloaddition reactions upon cathodic reduction[42,43] afforded an opportunity to detect anion radicals. With possession of this knowledge, work began to examine the possibility of using this reaction as a mechanistic probe to determine the conditions under which electron transfer might occur with $Me_2CuLi$•LiI reagents.

## 4.3 USE OF *BIS*(ENONES) AS MECHANISTIC PROBES

Previously, we had sought to find suitable reagents for use in [2+2] cycloaddition reactions that would be useful in natural product synthesis.[44,45] This led to a series of studies with various methods of generating anion radicals in the tethered *bis*(enone) systems. The first of these studies were conducted with cathodic reduction[42] and were later followed by the use of

chrysene anion radical.[43] It was with these studies that work began in earnest to look into the use of these substrates for detecting anion radical intermediates in reactions utilizing Gilman reagents. The studies using the methyl Gilman reagent and the *bis*(enone) substrates established that one does indeed see both the products of tandem conjugate addition-Michael cyclization and [2+2] cycloaddition (Scheme 4.4). Modulation of this bifurcated reaction manifold can be achieved through control of the concentration of the Gilman reagent in solution. Through this study, it was postulated that this concentration dependence arose from the different aggregate(s) present in higher and lower concentration solutions, with the aggregate(s) present at lower concentration responsible for the [2+2] cycloaddition manifold.[36]

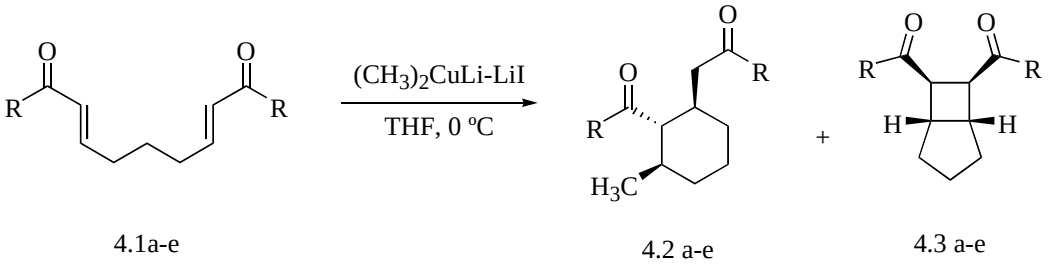


4.1a-e 4.2 a-e 4.3 a-e

a. R = 4-Biphenylyl; b. R = 2-Naphthyl; c. R = 4-Chlorophenyl;
d. R = 3,4-Dichlorophenyl; e. R = Phenyl

Scheme 4.4. Reaction of *bis*(enone) substrate with the Gilman Reagent

As these easily reduced *bis*(enone) substrates had been demonstrated in the laboratory to be capable of undergoing electron transfer and subsequent cyclization, testing began for the possibility of a radical anion mechanism for the formation of the [2+2] cycloaddition product. From the available evidence in the cathodic reduction and chrysene anion radical experiments, a stepwise cycloaddition mechanism was proposed involving electron transfer to form a distonic anion radical intermediate which would then cyclize, forming the cyclobutanation product and resulting in an anion radical that would be localized on the carbonyl and its exocyclic constituent. Following electron transfer, the product of [2+2] cycloaddition is then generated (Scheme 4.5). As electron transfer to substrate **4.1a** is much more favorable due to the more stable anion radical formed than that of **4.1e**, it would be expected that formation of the

cyclobutanation product of the former would be more efficient, and indeed this is borne out through experimentation. For this reason, substrate **4.1a** was chosen as the anion radical probe for more extensive study.

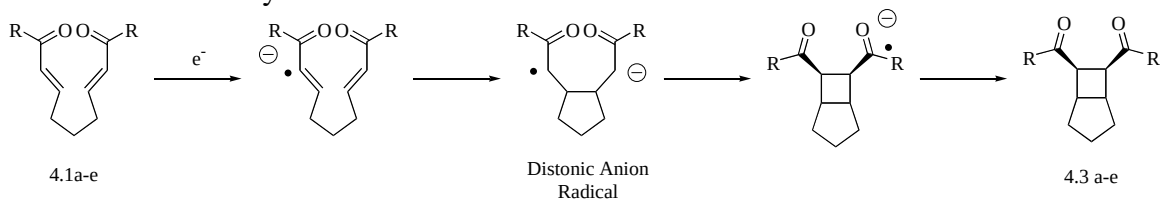


a. R = 4-Biphenylyl; b. R = 2-Naphthyl; c. R = 4-Chlorophenyl;
d. R = 3,4-Dichlorophenyl; e. R = Phenyl

Scheme 4.5. Postulated Mechanism for Anion Radical [2+2] Cycloaddition Reaction

## 4.4 BIFURCATION OF REACTIVITY BASED ON CATALYST LOADING

For the entirety of the study, the standard Gilman reagent, $Me_2CuLi•LiI$, was generated using copper(I) iodide in THF by addition of methyllithium solution. Experiments conducted with the anion radical probe were designed to gain insight into the effect of catalyst loading on the product distribution. Using a standard solution (0.01M in THF) of *bis*(enone) **4.1a** at 0 ºC, upon addition of 2 equivalents of the Gilman reagent, an 85% yield of the tandem conjugate addition-Michael cyclization product **4.3a** was obtained (Table 4.1, Entry 1). When the loading of Gilman reagent was reduced to a single equivalent, the [2+2] cycloaddition adduct was then generated in a yield of 13%, though the Michael cyclization product remained the dominant product at 64%. Further reduction in the stoichiometry of the Gilman reagent (25 mol%) led to higher yields of the cyclobutanation product. The best result was obtained when the addition time of the Gilman reagent was increased from the standard 5 s to 60 s (Table 4.1, Entry 5), where a 91% yield of the desired cyclobutanation product was generated as a single diastereomer. Further decreases in loading of the Gilman reagent resulted in increased recovered starting material and lower yields of the cyclobutanation product as well as increased yield of the Michael cyclization adduct. These results offer good evidence that the aggregate(s) present at lower concentration can effectively catalyze the [2+2] cycloaddition reaction and become less effective at methylation.

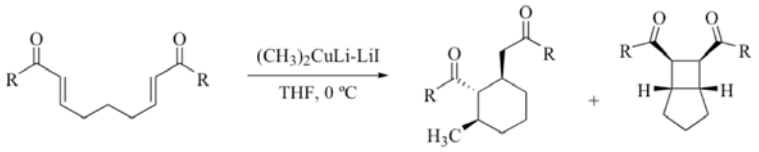


4.1a 4.2 a 4.3 a

| Entry | $(CH_3)_2CuLi$ | Conc. 4.1a | Recovered 4.1a[c] | 4.2a yield[c] | 4.3a yield[c] |
|---|---|---|---|---|---|
| 1 | 200 mol%[a] | 0.01 M | 5% | 85% | - |
| 2 | 100 mol%[a] | 0.01 M | 5% | 64% | 13% |
| 3 | 50 mol%[a] | 0.01 M | - | 38% | 40% |
| 4 | 25 mol%[a] | 0.01 M | - | 13% | 84% |
| 5 | 25 mol%[b] | 0.01 M | 3% | - | 91% |
| 6 | 10 mol%[a] | 0.01 M | 16% | 7% | 72% |
| 7 | 100 mol%[a] | 1.25 mM | - | 10% | 60% |

(a) A 0.5 M solution of the Gilman reagent in THF added over 5 s. (b) A 0.5 M solution of the Gilman reagent in THF added over 60 s. (c) Isolated yields after chromatographic separation.

Table 4.1. Cuprate loading and concentration effects on product distribution

## 4.5 SUBSTRATE SCOPE DETERMINATION

Having optimized the reaction conditions for obtaining the tandem conjugate addition-Michael cyclization and cyclobutanation products, work began to apply these conditions to other *bis*(enone) substrates in order to generalize the results. In almost all cases tested in this set of experiments, the partitioning of the two reaction manifolds was complete, with none of the unwanted product isolated from the reactions while simultaneously obtaining good to excellent yields of the desired products (Table 4.2). Most interestingly, both 3,4-dichlorophenyl and the parent phenyl system undergo efficient tandem conjugate addition-Michael cyclization reactions, but unfortunately also form a minor amount of this same product when using the conditions optimized for the cyclobutanation reaction, with the parent phenyl system having especially inefficient conversion even under these optimized conditions.

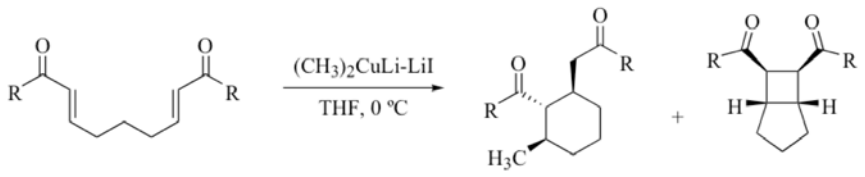


| Substrate | R | Conditions[a] | 4.2 yield[b] | 4.3 yield[b] |
|---|---|---|---|---|
| **4.1a** | **4-Biphenylyl** | **A** | **91%** | **-** |
| | | **B** | **-** | **91%** |
| **4.1b** | **2-Naphthyl** | **A** | **89%** | **-** |
| | | **B** | **-** | **90%** |
| **4.1c** | **4-Chlorophenyl** | **A** | **93%** | **-** |
| | | **B** | **-** | **80%** |
| **4.1d** | **3,4-Dichlorophenyl** | **A** | **85%** | **-** |
| | | **B** | **4%** | **70%** |
| **4.1e** | **Phenyl** | **A** | **90%** | **-** |
| | | **B** | **12%** | **43%** |

(a) Condition A: 5 s addition of $Me_2CuLi$ (200 mol%) to solution of substrate in THF at 0°C. Condition B: 60 s addition of $Me_2CuLi$ (25 mol%) to solution of substrate in THF at 0°C. (b) Isolated yields after column chromatography. *Cis*/*trans* ratios for 4.2a-e are >99:1, 44:1, 9:1, 13:1, and 17:1 respectively.

Table 4.2. Partitioned pathway yields for various substrates

The poor partitioning of substrate **4.1e** suggests that only very easily reduced substrates are capable of undergoing this reaction in an efficient manner. Indeed, when this reaction was tried using unsymmetrically substituted *bis*(enone) systems, as in the case of phenyl-methyl, no cyclobutanation product was observed, despite efficient conversion in the tandem conjugate addition-Michael cyclization pathway. This additional information suggests that both substituents in the *bis*(enone) system must be capable of effectively stabilizing the anion radical for [2+2] cycloaddition utilizing Gilman reagents to be a viable reaction manifold.

## 4.6 REACTION KINETICS STUDIES

In addition to the data suggesting that lower loadings of the Gilman reagent in solution lead to a greater level or cyclobutanation product being formed, we then set out to investigate

this same effect as a function of reaction time, as one can reasonably assume that as more tandem conjugate addition-Michael cyclization product is generated, a corresponding amount of the Gilman reagent is used up and thereby reduces the effective concentration of the reagent in solution. To this end, we again used our standard biphenylyl *bis*(enone) substrate at standard concentration and added the cuprate solution (0.01 M) with a 25 mol% relation to the *bis*(enone) injected rapidly and monitored the product distribution using $^{1}$H NMR (Table 4.3). In the beginning stages of the reaction, product **4.2a** was formed as essentially the exclusive product, as would be expected. As the reaction progressed, an increasing amount of the cyclobutanation product **4.3a** is formed. After time ~60 s, the amount of the conjugate addition-Michael cyclization product had reached its peak and no additional amount of this product is observed within experimental error (Table 4.3, entry 4). The cyclobutanation product began to dominate the product distribution after roughly 180 s (Table 4.3, entry 5).

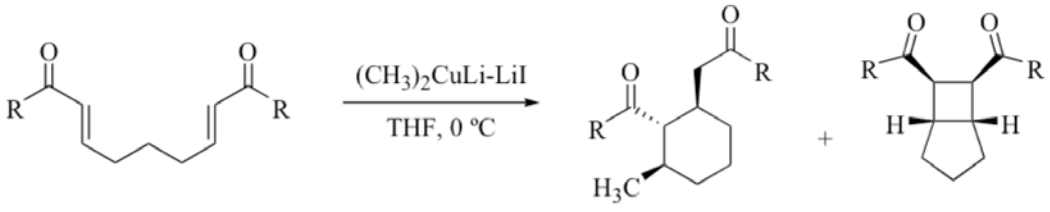


4.1a-e

R = Biphenylyl

4.2 a-e

4.3 a-e

| Entry | Time (s) | 4.1a (mol%) | 4.2a (mol%) | 4.3a (mol%) |
|---|---|---|---|---|
| 1 | 0 | 100 | 0 | 0 |
| 2 | 10 | 76 | 16 | 5.1 |
| 3 | 30 | 66 | 19 | 11 |
| 4 | 60 | 63 | 20 | 12 |
| 5 | 180 | 42 | 18 | 33 |
| 6 | 480 | 33 | 20 | 43 |
| 7 | 1200 | 24 | 22 | 54 |

Conversion was determined by $^1$H NMR analysis and values given are the average of two trials. Total values are under 100 mol% as small quantities of hetero-Diels-Alder cycloadducts are produced

Table 4.3. Reaction kinetics experimental results

This result would indicate again that the reaction pathway is reagent concentration dependent.

## 4.7 MECHANISTIC PROPOSAL FOR REACTION PATHWAYS

Given the available experimental evidence shown in Table 4.1 and Table 4.3, one can reasonably assert that the cyclobutanation reaction is a catalytic or chain process, but with a low turnover number, given that nearly complete conversion to the desired [2+2] cycloaddition product with 25 mol% loading of the cuprate. It also became clear through the course of this study that concentration plays a very significant role in the mechanistic pathway that is followed.

Higher concentrations and their associated cuprate complexes favor methyl group transfer, whereas lower concentrations and the corresponding complexes clearly generate a cyclobutanation product that can reasonably be assigned to an electron transfer or oxidative cyclization pathway (Scheme 4.6). For this to be the case, varying concentration of the cuprates with respect to the concentration of the overall solution utilizing a constant loading of the added Gilman reagent must then correlate to the product distribution, which is what by the data obtained in Table 4.3 show. In particular, substrate **4.1a** afforded a 64% yield of **4.2a** at 0.01 M, but only 10% at 1.25 mM, while **4.3a** was formed in only a 13% yield in the former case, but at 60% in the latter. This would indicate that the reactive action of the Gilman reagent is concentration dependent, and this would presumably arise via the formation of a different aggregate upon decreasing concentration.

It should be noted that lithium iodide does not appear to play an active role in either reaction pathway nor in the differentiation of the two pathways, a distinction that is important to note in light of previously detailed experimental evidence of isomerization of enone substrates.[5] We carried out a reaction identical to previous experiments with 100 mol% of cuprate added in slow fashion, but in this case containing 100 mol% of added lithium iodide, but observed neither a difference in the rate of reaction nor in the product distribution.

## 4.8 MECHANISM OF [2+2] CYCLOADDITION REACTION

The final remaining question in this system was the mechanism by which the cyclobutanation product is generated. Two possibilities seemed reasonable: either an anion radical chain mechanism, or an oxidative cyclization catalyzed by a copper(I) species (Scheme 4.6). In the case of an oxidative cyclization pathway, the Gilman intermediate, whether a π-complex, oxy-π-allyl, enyl (σ+π), or β-cuprio adduct, would insert into the double bond of the appendant enone of the substrate. In this mode of action, we would expect that the rate of reaction as well as the efficiency of the process to be nearly identical for all *bis*(enone) substrates

in this study, as the enone substituent would play little role electronically in the oxidative addition or subsequent reductive elimination steps.

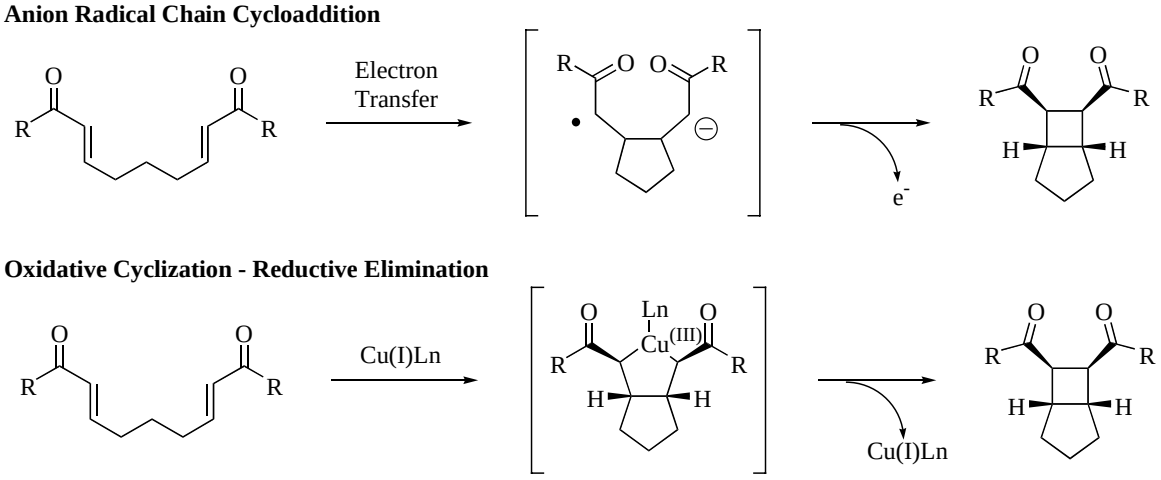


Scheme 4.6. Mechanistic pathways for cyclobutanation

However, *bis*(enone) **4.1a** undergoes much more facile [2+2] cycloaddition than do the related **4.1d** or **4.1e** substrates, indicating that the substituent does indeed play a role in the reaction mechanism. These results parallel those of the electrochemical and chrysene anion radical studies previously conducted.[42,43] This would be attributable to the greater conjugation present in the biphenylyl substituent in **4.1a**, which would afford enhanced stability of the anion radical moiety. We believe that polar effects would be negligible, as substrates **4.1a** and **4.1e** differ only in their level of conjugation and not in electron withdrawing abilities. Additionally, cyclobutanation reactions conducted with cathodic reduction typically proceed via short chains in an analogous manner to our system. Finally, in THF solvent, the chemically initiated anion radical cyclobutanation reaction affords exclusively the *exo*, *cis* product **4.3a**, just as observed in this work. These high levels of stereoselectivity suggest that the anion radical intermediates derived from substrate **4.1a** exist as contact ion pairs.

## 4.9 CONCENTRATION DEPENDENCE OF REACTIVE SPECIES

The second important consideration of the Gilman reagent and its reactivity involves the composition of the active species at high and low concentration. In THF solution, it has been determined that the Gilman reagent exists predominately as the solvent-separated ion pair ($Li^+$ and $CuMe_2^-$), which is in rapid equilibrium with the cyclic dimer (Scheme 4.7).[36] Evidence presented to date indicates that the dimeric form is the more active of the two as relates to methylation.[36] In either form, the cuprate is not closely associated with the lithium halide generated during formation of the cuprate, which is also consistent with our findings that product distribution is independent of added lithium iodide. The combination of the above findings leads us to postulate that the monomeric SSIP form, which is known to be unreactive in methylation relative to the dimeric form, to be the active species in the electron transfer pathway, while the dimeric form is responsible for methylation. This conclusion would provide adequate explanation for the observed product distribution in the course of this study, as well as to provide evidence for both radical-type reactions as well as the standard reactivity generally associated with cuprates. In addition, since the conjugate addition-Michael cyclization product and cyclobutanation product can be formed in exclusion of one another, it stands to reason that the pathways are mechanistically distinct, as we have postulated. We have also considered the possibility of impurities and byproducts being responsible for the anion radical pathway. We have tested methyllithium, methylcopper and lithium iodide independently under otherwise identical conditions using substrate **4.1a** and have found no evidence of anion radical chemistry taking place. Additionally, we specifically tested lithium trimethyldicuprate, as it can be generated from methylcopper formed during methylation and lithium dimethylcuprate, and it has been found to possess analogous reactivity to lithium dimethylcuprate in 1,4-addition reactions as well as [2+2] cycloaddition reactions, thus eliminating the most likely impurities and possible byproducts from implication in the anion radical pathway.

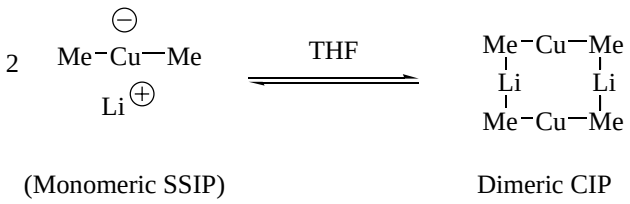


Scheme 4.7. Solvent-separated ion pair - contact ion pair equilibrium

## 4.10 CONCLUSION

This work has established that the previously known anion radical chain [2+2] cycloaddition reactions of *bis*(enone) substrates can be employed as anion radical probes in reactions with the Gilman reagent. Lower concentrations of this reagent, whether arising from slow addition of the reagent itself to a solution of *bis*(enone) or through the use of a sub-stoichiometric amount (specifically 25 mol%), lead to cyclobutanation products in good to excellent yield in easily reduced *bis*(enone) substrates. Higher concentrations, conversely, through rapid addition or stoichiometric amounts, result in tandem conjugate addition-Michael cyclization products in similarly high yield for all substrates tested. When using optimized conditions for either cyclobutanation or conjugate addition-Michael cyclization, nearly complete partitioning can be achieved between the reaction manifolds. These data also lead to the postulation that the two reaction pathways are mechanistically distinct and competing under some reaction conditions. Coupled with the known evidence for the dimeric form of the Gilman reagent being of higher reactivity with respect to methylation, we postulate that the monomeric Gilman reagent is the active species for the anion radical pathway.

## 4.11 EXPERIMENTAL

### General Methods

Commercial reagents were used without further purification, unless otherwise stated. Tetrahydrofuran was distilled from sodium benzophenone ketyl radical immediately prior to use. All reactions were conducted in oven-dried glassware, under an inert atmosphere of nitrogen or argon. High-resolution mass spectra (HRMS) are reported as *m*/*z* (relative intensity). Accurate

masses are reported for the molecular ion (M+1) or a suitable fragment ion. Proton NMR spectra were recorded with a Varian Unity (300 MHz ) or Varian Unity Plus (500 MHz) spectrometer. Carbon NMR spectra were recorded with a Varian Unity (75 MHz MHz) spectrometer.

***Dimethyllithium Cuprate-Lithium Iodide ($Me_2CuLi$-LiI) reagent***

Reagent was prepared by adding 200 mol% MeLi (1.6 M in $Et_2O$) to a suspension of 100 mol% CuI in 0 °C THF. Stirring for approximately 30 minutes at 0 °C resulted in a homogeneous solution.

***Table 4.1***

Data were obtained using the following procedure: $Me_2CuLi$-LiI reagent solution (0.5 M in $Et_2O$/THF) was added at the indicated rate to a solution of bis-enone substrate (0.25 mmol) in 25 mL 0 °C THF. The reaction was stirred at 0 °C for 25 minutes, and then quenched with several drops of saturated aqueous $NH_4Cl$ solution. The residue was concentrated and purified via silica gel chromatography, eluting with a mixture of ethyl acetate and hexane.

***Table 4.2***

Data were obtained using the following representative procedures:

**A.** $Me_2CuLi$-LiI (15.7 mL; 3.2 mM in $Et_2O$/THF; 200 mol%) was added over 5 s to a solution of substrate (0.26 mmol; 100 mol%) in 5 mL 0 °C THF. Stirring was maintained for 25 minutes and then was worked up and purified as described above.

**B**. $Me_2CuLi$-LiI (1.0 mL; 0.5 M in $Et_2O$/THF; 25 mol%) was added over 60 s to a solution of substrate (0.25 mmol; 100 mol%) in 25 mL 0 °C THF. Stirring was maintained for 25 minutes and then quenched and purified as described above.

***Table 4.3***

Data represents measurements from separate, parallel reactions, conducted using the following procedure: $Me_2CuLi$-LiI (0.98 mL; 0.034 M in $Et_2O$/THF; 25 mol%) was added over 5 s to a solution of substrate (0.13 mmol; 100 mol%) in 3.5 mL 0 °C THF. Stirring was maintained for the indicated time before work up and purification as described above.

**Product Characterization**

***2-[2-(Biphenyl-4-carbonyl)-3-methyl-cyclohexyl]-1-biphenyl-4-yl-ethanone (4.2a)***

**$^1$HNMR** (300 MHz, $CDCl_3$): δ 8.10-8.12 (d, *J* = 8.4 Hz, 2H), 7.89-7.86 (d, *J* = 8.4 Hz, 2H), 7.66-7.67 (d, *J* = 8.4 Hz, 2H), 7.55-7.63 (m, 6H), 7.36-7.47 (m, 6H), 3.12-3.19 (t, *J* = 9.9 Hz, 1H), 2.90-3.00 (q, *J* = 8.7 Hz, 1H), 2.42-2.57 (m, 2H), 1.72-1.87 (m, 4H), 1.36-1.49 (m, 1H), 1.06-1.27 (m, 2H), 0.80-0.82 (d, *J* = 6.3 Hz, 3H). **$^{13}$CNMR** (75 MHz, $CDCl_3$): δ 205.7, 198.9, 145.9, 145.5, 139.9, 139.7, 137.9, 135.4, 128.9, 128.8, 128.2, 128.1, 127.4, 127.3, 127.2, 127.2, 56.6, 44.1, 38.5, 36.9, 34.9, 31.5, 25.4, 21.1 **HRMS**: Calc. [M+1] for $C_{34}H_{32}O_2$: 473.2481; Found: 473.2460. **FTIR** (KBr): 3060, 3031, 2950, 2921, 2848, 1674, 1601, 1601, 1553, 1403, 1212, 1193, 1003, 761, 746, 695 $cm^{-1}$.

***1,9-Di-naphthalen-2-yl-nona-2,7-diene-1,9-dione (4.2b)***

**$^1$HNMR** (300 MHz, $CDCl_3$): δ 8.56 (s, 1H), 8.27 (s, 1H), 8.12-8.15 (dd, *J* = 8.7 Hz, 1.8 Hz, 1H), 7.99-8.03 (m, 1H), 7.77-7.91 (m, 6H), 7.46-7.61 (m, 4H), 3.28-3.34 (t, *J* = 9.9 Hz, 1H), 3.02-3.09 (q, *J* = 9 Hz, 1H), 2.52-2.66 (m, 2H), 1.72-1.97 (m, 4H), 1.14-1.45 (m, 3H), 0.80-0.83 (d, *J* = 6.9 Hz, 3H). **$^{13}$CNMR** (75 MHz, $CDCl_3$): δ 206.1, 199.4, 136.6, 135.6, 135.4, 133.9, 132.6, 132.4, 130.1, 129.7, 129.7, 128.7, 128.6, 128.3, 128.3, 127.7, 127.6, 126.8, 126.5, 123.9, 56.6, 44.2, 38.7, 37.1, 34.9, 31.5, 25.4, 21.1. **HRMS**: Calc. [M+1] for $C_{30}H_{28}O_2$: 421.2168; Found: 421.2168. **FTIR** (KBr): 3453, 3057, 2950, 2925, 2848, 1674, 1626, 1461, 1373, 1270, 1179, 1120, 819, 753 $cm^{-1}$.

***2-[2-(4-Chloro-benzoyl)-3-methyl-cyclohexyl]-1-(4-chloro-phenyl)-ethanone (4.2c)***

**$^1$HNMR** (300 MHz, $CDCl_3$): δ 7.96-7.93 (d, *J* = 8.7 Hz, 2H), 7.70-7.73 (d, *J* = 8.7 Hz, 2H), 7.42-7.45 (d, *J* = 8.7 Hz, 2H), 7.35-7.38 (d, *J* = 8.7 Hz, 2H), 3.10-3.08 (t, *J* = 9.9 Hz, 1H), 2.75-2.82 (q, *J* = 11.1Hz, 1H), 2.38-2.45 (m, 2H), 1.70-1.84 (m, 4H), 1.31-1.40 (m, 1H), 1.10-1.23 (m, 2H), 0.73-0.75 (d, *J* = 6.6 Hz, 3H). **$^{13}$CNMR** (75 MHz, $CDCl_3$): δ 204.9, 197.9, 139.8, 139.4, 137.4, 134.9, 129.6, 129.1, 128.8, 56.3, 43.8, 38.2, 37.0, 34.8, 31.3, 25.3, 21.0. **HRMS**:

Calc. [M+1] for $C_{22}H_{22}O_2Cl_2$: 389.1075; Found: 389.1081. **FTIR** (KBr): 3071, 2955, 1932, 2850, 1877, 1850, 1685, 1662, 1588, 1565, 1401, 1211, 1087, 982, 898, 815 $cm^{-1}$.

***2-[2-(3,4-Dichloro-benzoyl)-3-methyl-cyclohexyl]-1-(3,4-dichloro-phenyl)-ethanone (4.2d)***

**$^1$HNMR** (300 MHz, $CDCl_3$): δ 8.05-8.05 (d, *J* = 2.1 Hz, 1H), 7.84-7.85 (d, *J* = 2.1 Hz, 1H), 7.79-7.83 (dd, *J* = 8.4 Hz, 2.1 Hz, 1H), 7.46-7.60 (m, 3H), 2.98-3.05 (t, *J* = 10.2 Hz, 1H), 2.71-2.77 (dd, *J* = 14.1 Hz, 2 Hz, 1H), 2.34-2.51 (m, 2H), 1.70-1.78 (m, 4H), 1.33-1.46 (m, 1H), 1.03-1.24 (m, 2H), 0.73-0.76 (d, *J* = 6.3 Hz, 3H). **$^{13}$CNMR** (75 MHz, $CDCl_3$): δ 203.8, 196.8, 138.4, 138.1, 137.6, 136.2, 133.6, 133.3, 130.9, 130.7, 130.2, 130.1, 127.2, 127.2, 56.3, 43.5, 38.1, 37.2, 34.8, 31.4, 25.3, 21.0. **HRMS**: Calc. [M+1] for $C_{22}H_{20}O_2Cl_4$: 457.0296; Found: 457.0299. **FTIR** (film): 3423, 3090, 3068, 2950, 2928, 2848, 1681, 1678, 1652, 1582, 1557, 1454, 1381, 1204, 1028 $cm^{-1}$.

***2-(2-Benzoyl-3-methyl-cyclohexyl)-1-phenyl-ethanone (4.2e)***

**$^1$HNMR** (300 MHz, $CDCl_3$): δ 7.99-8.03 (d, *J* = 8.4 Hz, 2H), 7.77-7.79 (d, *J* = 8.7 Hz, 2H), 7.36-7.58 (m, 6H), 3.06-3.13 (t, *J* = 9.9 Hz, 1H), 2.82-2.92 (q, *J* = 11.1 Hz, 1H), 2.38-2.51 (m, 2H), 1.63-1.88 (m, 4H), 1.32-1.42 (m, 1H), 1.02-1.23 (m, 2H ), 0.75-0.77 (d, *J* = 6.6 Hz, 3H). **$^{13}$CNMR** (75 MHz, $CDCl_3$): δ 206.2, 199.3, 139.3, 136.7, 133.2, 132.9, 128.7, 128.5, 128.2, 56.5, 44.0, 38.3, 36.9, 34.9, 31.4, 25.3, 21.0. **HRMS**: Calc. [M+1] for $C_{22}H_{24}O_2$: 321.1855; Found: 321.1853. **FTIR** (KBr): 3082, 3067, 3024, 2958, 2939, 2932, 2914, 2851, 2833, 1678, 970, 889, 786, 750, 706, 684 $cm^{-1}$.

***[7-(Biphenyl-4-carbonyl)-bicyclo[3.2.0]hept-6-yl]-biphenyl-4-yl-methanone (4.3a)***

**$^1$HNMR**: (500 MHz, $CDCl_3$): δ 1.69-1.77 (m, 2H), 1.86-1.90 (ddd, *J* = 13.0, 5.5, 1.5 Hz, 2H), 2.04-2.11 (m, 2H), 3.26-3.28 (m, 2H), 3.92-3.93 (d, *J* = 4.2 Hz, 2H), 7.34-7.37 (tt, *J* = 7.5, 1.0 Hz, 2H), 7.39-7.43 ((tt, *J* = 8.0, 1.5 Hz, 4H), 7.82-7.84 (dt, *J* = 9.0, 2.0 Hz, 4H), 8.22 (s, 2H). **$^{13}$CNMR** (75 MHz, $CDCl_3$): δ 198.3, 145.2, 139.9, 135.1, 128.8, 128.3, 128.0, 127.2, 127.1, 48.4, 39.0, 32.5, 25.3. **HRMS**: Calc. [M+1] for $C_{33}H_{29}O_2$: 457.2168; Found: 457.2174. **FTIR**

(KBr): 3025, 2928, 2846, 1681, 1603, 1479, 1401, 1347, 1266, 1219, 1176, 1005, 838, 765, 691 $cm^{-1}$.

***[7-(Naphthalene-2-carbonyl)-bicyclo[3.2.0]hept-6-yl]-naphthalen-2-yl-methanone (4.3b)***

**$^{1}$HNMR**: (300 MHz, $CDCl_3$): δ 1.69-1.78 (m, 2H), 1.90-1.97 (dd, *J* = 14.1, 5.4 Hz, 2H), 2.08-2.22 (m, 2H), 3.29-3.30 (d, *J* = 2.4 Hz, 2H), 4.07-4.09 (d, *J* = 4.2 Hz, 2H), 7.40-7-51 (m, 4H), 7.73-7.74 (m, 4H), 7.80-7.83 (m, 4H), 8.22 (s, 2H). **$^{13}$CNMR** (75 MHz, $CDCl_3$): δ 198.6, 135.2, 133.7, 132.3, 129.3, 128.9, 128.3, 127.6, 126.4, 123.9, 48.4, 39.1, 32.5, 25.3. **HRMS**: Calc. [M+1] for $C_{29}H_{25}O_2$: 485.1855; Found: 405.1858. **FTIR** (KBr): 3053, 2921, 2848, 1678, 1623, 1461, 1362, 1274, 1362, 1274, 1182, 1127, 819, 746 $cm^{-1}$.

***[7-(4-Chloro-benzoyl)-bicyclo[3.2.0]hept-6-yl]-(4-chloro-phenyl)-methanone (4.3c)***

**$^{1}$HNMR**: (300 MHz, $CDCl_3$): δ 1.66-1.70 (m, 2H), 1.80-1.83 (dd, *J* = 9.9, 2.4 Hz, 2H), 1.97-2.04 (m, 2H), 3.15-3.17 (m, 2H), 3.77-3.78 (d, *J* = 3.9 Hz, 2H), 7.31-7.33 (d, *J* = 8.4 Hz, 4H), 7.65-7.68 (dd, *J* = 9 Hz, 4H). **$^{13}$CNMR** (75 MHz, $CDCl_3$): δ 197.3, 138.9, 134.5, 129.1, 128.8, 48.1, 39.0, 32.3, 25.1. **HRMS**: Calc. [M+1] for $C_{22}H_{19}O_2Cl_2$: 373.0762; Found: 373.0762. **FTIR** (KBr): 3064, 2961, 2925, 2899, 2859, 1681, 1586, 1487, 1399, 1340, 1234, 1094, 1010, 922, 841, 812 $cm^{-1}$.

***[7-(3,4-Dichloro-benzoyl)-bicyclo[3.2.0]hept-6-yl]-(3,4-dichloro-phenyl)-methanone (4.3d)***

**$^{1}$HNMR**: (300 MHz, $CDCl_3$): δ 1.65-1.73 (m, 2H), 1.80-1.85 (dd, *J* = 11.7, 3.3 Hz, 2H), 2.00-2.06 (m, 2H), 3.15-3.16 (d, *J* = 2.4 Hz, 2H), 3.74-3.76 (d, *J* = 3.9 Hz, 2H), 7.42-7.45 (d, *J* = 8.4 Hz, 2H), 7.53-7.56 (dd, *J* = 8.7, 2.2 Hz, 2H), 7.79-7.80 (d, *J* = 1.8 Hz, 2H). **$^{13}$CNMR** (75 MHz, $CDCl_3$): δ 196.3, 137.2, 135.6, 133.2, 130.7, 129.7, 126.7, 48.0, 39.0, 32.3, 25.1. **HRMS**: Calc. [M+1] for $C_{22}H_{17}O_2Cl_4$: 440.9983; Found: 440.9979. **FTIR** (KBr): 3086, 2936, 2848, 1681, 1579, 1557, 1465, 1381, 1201, 1028, 827, 680 $cm^{-1}$.

## 4.12 REFERENCES


(1) House, H. O. *Acc. Chem. Res.* **1976**, *9*, 59-67.
(2) Nakamura, E.; Mori, S. *Angew. Chem. Int. Ed.* **2000**, *39*, 3750-3771.
(3) Perlmutter, P. *Conjugate Addition Reactions in Organic Synthesis*; Pergamon Press: Oxford, 1992.
(4) Smith, R. A. J.; Vellekoop, S. *Advances in Detailed Reaction Mechanisms*; JAI: Greenville, CT, 1994; Vol. 3.
(5) Corey, E. J.; Hannon, F. J.; Boaz, N. W. *Tetrahedron* **1989**, *45*, 545-555.
(6) House, H. O.; Umen, M. J. *J. Am. Chem. Soc.* **1972**, *94*, 5495-5497.
(7) Krauss, S. R.; Smith, S. G. *J. Am. Chem. Soc.* **1981**, *103*, 141-148.
(8) Ibuka, T.; Chu, G.-N.; Yoneda, F. *Tetrahedron Lett.* **1984**, *25*, 3247-3250.
(9) Logusch, E. W. *Tetrahedron Lett.* **1979**, *20*, 3365-3366.
(10) Ruden, R. A.; Litterer, W. E. *Tetrahedron Lett.* **1975**, *16*, 2043-2044.
(11) Hannah, D. J.; Smith, R. A. J.; Teoh, I.; Weavers, R. T. *Aust. J. Chem.* **1981**, *34*, 181-188.
(12) Smith, R. A. J.; Vellekoop, A. S. *Tetrahedron* **1989**, *45*, 517-522.
(13) Marshall, J. A.; Ruden, R. A. *J. Org. Chem.* **1972**, *37*, 659-664.
(14) House, H. O.; Snoble, K. A. J. *J. Org. Chem.* **1976**, *41*, 3076-3083.
(15) Corey, E. J.; Fuchs, P. L. *J. Am. Chem. Soc.* **1972**, *94*, 4014-4015.
(16) Daviaud, G.; Migniac, P. *Tetrahedron Lett.* **1972**, *13*, 997-1000.
(17) Grieco, P. A.; Finkelhor, R. *J. Org. Chem.* **1973**, *38*, 2100-2101.
(18) Miyaura, N.; Itoh, M.; Sasaki, N.; Suzuki, A. *Synthesis* **1975**, 317-318.
(19) House, H. O.; Prabhu, A. V.; Wilkins, J. M.; Lee, L. F. *J. Org. Chem.* **1976**, *41*, 3067-3076.
(20) House, H. O.; McDaniel, W. C.; Sieloff, R. F.; Vanderveer, D. *J. Org. Chem.* **1978**, *43*, 4316-4323.
(21) Casey, C. P.; Cesa, M. C. *J. Am. Chem. Soc.* **1979**, *101*, 4236-44.
(22) Bertz, S. H.; Dabbagh, G.; Cook, J. M.; Honkan, V. *J. Org. Chem.* **1984**, *49*, 1739-43.
(23) Hannah, D. J.; Smith, R. A. J. *Tetrahedron Lett.* **1975**, 187-90.
(24) Smith, R. A. J.; Hannah, D. J. *Tetrahedron* **1979**, *35*, 1183-9.
(25) Frantz, D. E.; Singleton, D. A.; Snyder, J. P. *J. Am. Chem. Soc.* **1997**, *119*, 3383-3384.
(26) Bertz, S. H.; Carlin, C. M.; Deadwyler, D. A.; Murphy, M. D.; Ogle, C. A.; Seagle, P. H. *J. Am. Chem. Soc.* **2002**, *124*, 13650-13651.
(27) Vellekoop, A. S.; Smith, R. A. J. *J. Am. Chem. Soc.* **1994**, *116*, 2902-13.
(28) Bertz, S. H.; Smith, R. A. J. *J. Am. Chem. Soc.* **1989**, *111*, 8276-7.
(29) Ullenius, C.; Christenson, B. *Pure Appl. Chem.* **1988**, *60*, 57-64.
(30) Snyder, J. P. *J. Am. Chem. Soc.* **1995**, *117*, 11025-6.
(31) Snyder, J. P.; Bertz, S. H. *J. Org. Chem.* **1995**, *60*, 4312-13.
(32) Mori, S.; Nakamura, E. *Chem.--Eur. J.* **1999**, *5*, 1534-1543.
(33) Nakamura, E.; Mori, S.; Morokuma, K. *J. Am. Chem. Soc.* **1997**, *119*, 4900-4910.
(34) Nakamura, E.; Yamanaka, M. *J. Am. Chem. Soc.* **1999**, *121*, 8941-8942.
(35) Yamanaka, M.; Kato, S.; Nakamura, E. *J. Am. Chem. Soc.* **2004**, *126*, 6287-6293.
(36) John, M.; Auel, C.; Behrens, C.; Marsch, M.; Harms, K.; Bosold, F.; Gschwind, R. M.; Rajamohanan, P. R.; Boche, G. *Chem. Eur. J.* **2000**, *6*, 3060-3068.
(37) Chounan, Y.; Horino, H.; Ibuka, T.; Yamamoto, Y. *Bull. Chem. Soc. Jpn.* **1997**, *70*, 1953-1959.

(38) Yamamoto, Y.; Nishii, S.; Ibuka, T. *J. Am. Chem. Soc.* **1988**, *110*, 617-18.
(39) Wigal, C. T.; Grunwell, J. R.; Hershberger, J. *J. Org. Chem.* **1991**, *56*, 3759-61.
(40) Anderson, S. J.; Hopkins, W. T.; Wigal, C. T. *J. Org. Chem.* **1992**, *57*, 4304-5.
(41) House, H. O.; Respess, W. L.; Whitesides, G. M. *J. Org. Chem.* **1966**, *31*, 3128-41.
(42) Roh, Y.; Jang, H.-Y.; Lynch, V.; Bauld, N. L.; Krische, M. J. *Org. Lett.* **2002**, *4*, 611-613.
(43) Yang, J.; Felton, G. A. N.; Bauld, N. L.; Krische, M. J. *J. Am. Chem. Soc.* **2004**, *126*, 1634-1635.
(44) Baik, T.-G.; Luis, A. L.; Wang, L.-C.; Krische, M. J. *J. Am. Chem. Soc.* **2001**, *123*, 6716-6717.
(45) Wang, L.-C.; Jang, H.-Y.; Roh, Y.; Lynch, V.; Schultz, A. J.; Wang, X.; Krische, M. J. *J. Am. Chem. Soc.* **2002**, *124*, 9448-9453.

# Chapter 5 *Enantioselective Allylic Substitution Reactions Using Chiral Phosphine Catalysis*

## 5.1 INTRODUCTION

Catalytic reactions have found extensive use in organic chemistry, as they allow for the use of more expensive reagents to promote a reaction without the expense of using a full equivalent of that reagent. In particular, they allow for enantioselective functional group manipulation using expensive, difficult to synthesize chiral reagents that would ordinarily be untenable in stoichiometric amounts. Traditionally, these reactions have involved transition metal catalysts, such as palladium or platinum, in conjunction with a phosphine ligand used to increase the reactivity, solubility and stability of the active complex.[1,2] However, in recent years, in particular in the pharmaceutical industry, there has been a substantial push into organocatalysis,[3] using an amine or phosphine to accomplish the same transformation as a transition metal. This not only eliminates heavy metal waste streams, but also simplifies purification and allows for expanded use of the desired reaction, as the Food and Drug Administration has stringent heavy metal content constraints.[4] To this end, a great deal of research has been conducted in organocatalysis, with the majority of the work being done on two types of compounds: amine-based catalysts and phosphorus-based catalysts.[3]

Organocatalysis has been reported as a viable alternative to transition metal catalysis in asymmetric reactions where previously it was not possible including the following: aldol condensation,[5] Mannich reaction,[6,7] epoxidation,[8] [3+2] and [4+2] cycloaddition,[9-13] and transfer hydrogenations,[14] among many others. Specifically, many of these reactions use amines as the nucleophilic component of the structure, drawing upon the chiral pool to obtain asymmetric reactions. This is exemplified perhaps most prominently in the asymmetric aldol and Mannich reactions, which most often employ catalysts derived from L-proline such as the MacMillan catalysts (Figure 5.1).[15]

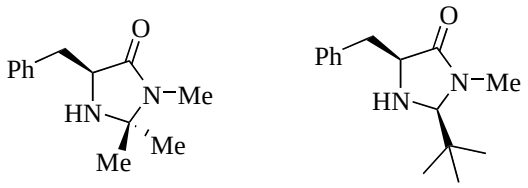


Figure 5.1. MacMillan generation 1 and generation 2 catalysts

More recently, however, phosphorus based nucleophilic catalysts have been receiving more attention in search of new organic-based catalysts. It has been argued that organophosphorus compounds are better suited for nucleophilic catalysis than a comparable amine because of the balance of nucleophilicity and leaving group ability. It has been shown that the $S_N2$ reaction of ethyl iodide with $Et_2PhP$ proceeds at a rate 500 times faster than the corresponding amine,[16,17] showing the phosphine to be considerably better nucleophile. Leaving group ability is generally considered to be inversely related to the basicity of the compound in question. The $pK_A$ of triethylphosphonium cation versus the triethylammonium cation are 8.7[18] and 10.7[19] respectively, which would indicate by inference that the phosphorus compound should be a better leaving group. For these reasons, a specifically tailored phosphine should provide better reactivity than the corresponding amine analog.

The first use of phosphines as nucleophilic catalysts[20] was demonstrated in 1963 by Rauhut and Currier (Scheme 5.1).[21] More recently, Morita[22] discovered that phosphines can add in a Michael fashion to an enone or enoate. Subsequently Baylis and Hillman[23] found the same reaction could proceed with tertiary amine catalysts. This intermediate can then subsequently attack an aldehyde in either inter- or intramolecular fashion and provide a β-hydroxy ketone or ester while maintaining the alkene upon elimination of the catalyst (Scheme 5.2).[24]

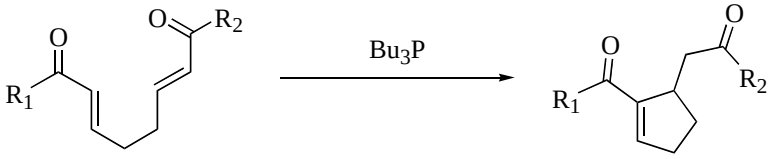


Scheme 5.1. Intramolecular Rauhut-Currier reaction

The Morita-Baylis-Hillman (MBH) reaction affords high functional group density, which allows for subsequent manipulation to generate scaffolds of increasing complexity. It was hoped that these adducts would allow for an allylic amination reaction, catalyzed by a nucleophilic phosphine, as well as perhaps other transformations that could provide useful building blocks for natural products, as well as compounds of interest to the pharmaceutical industry. In particular, an early goal was to generate β-amino acids, which could be obtained from an allylic amination reaction of a MBH product derivative.

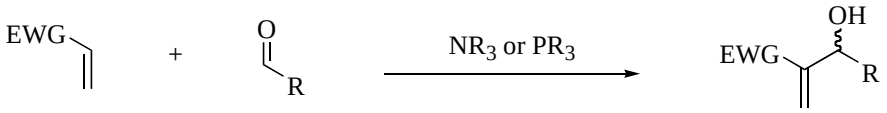


Scheme 5.2. Morita-Baylis-Hillman reaction

β-amino acids were interesting targets due to considerable interest in synthesis.[25-27] These compounds provide useful precursor molecules for β-peptides[28-30] and β-lactams,[29,31] and have been shown to possess antibiotic, antifungal, and cytotoxic properties in either monomeric form or as part of a larger peptide.[32-36] Recently, Kim and coworkers published a two-step synthesis of β-amino acids utilizing the MBH reaction adduct with stoichiometric DABCO to provide allylic amination products.[37] Subsequently, Kim also published a catalytic, asymmetric allylic amination of MBH adducts using cinchona alkaloid derived $(DHQD)_2PHAL$ and $(DHQ)_2PHAL$ (Scheme 5.3), which suffered from low yield (12%) but with promising enantioselectivity (70%).[38] Additionally, the reaction only proceeded with a single substrate although others had been tried, allowing an opportunity for work to improve upon many facets of this reaction.

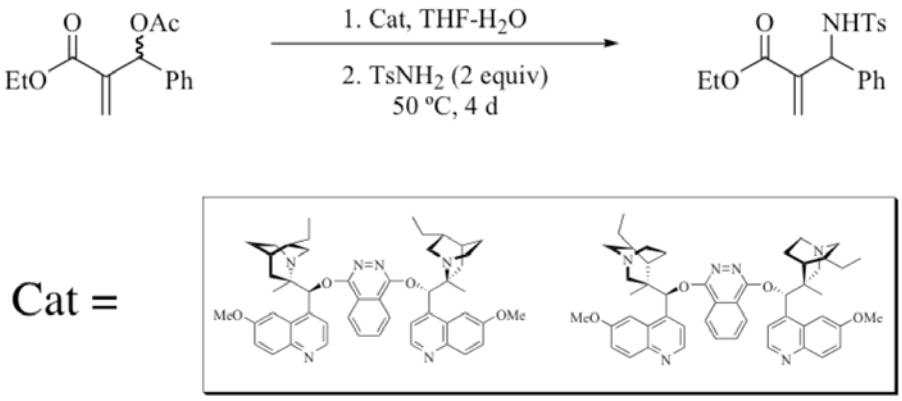


Scheme 5.3. Amination reaction performed by Kim *et al.*

## 5.2 DEVELOPMENT OF PHOSPHINE CATALYZED ALLYLIC AMINATION

To this end, work was undertaken to first develop a phosphine-catalyzed variant of the racemic reaction, with later work to focus on an enantioselective version. In 2004, the first regioselective allylic amination of MBH acetates using a phosphine catalyst was published.[39] It should also be noted that a similar allylic substitution reaction had been attempted by Trost *et al.* using palladium π-allyl chemistry, but the product was a mixture of regioisomers.[40] Triphenylphosphine proved to be a suitable catalyst for the reaction, and phthalimide or 4,5-dichlorophthalimide were used as the amine source. The reaction proved to be amenable to a variety of substrates, including enones and enoates, as well as both aromatic and aliphatic substituents (Table 5.1), with reactions utilizing 4,5-dichlorophthalimide proceeding more rapidly than the corresponding phthalimide reaction.

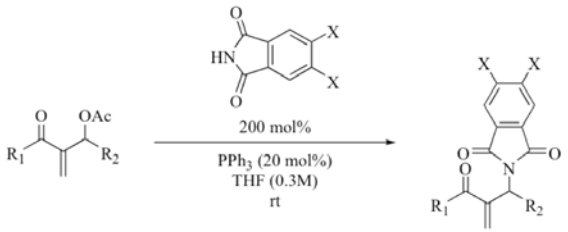


5.1a-f 5.2a-f

| Entry | Substrate | $R_1$ | $R_2$ | X | Yield |
|---|---|---|---|---|---|
| 1 | 5.1a | OMe | *p*-$NO_2$-Ph | H | 8% |
| 2 | 5.1a | OMe | *p*-$NO_2$-Ph | Cl | 90% |
| 3 | 5.1b | OMe | Ph | H | 76%[a] |
| 4 | 5.1b | OMe | Ph | Cl | 95%[a] |
| 5 | 5.1c | OMe | Pr | H | 15%[a] |
| 6 | 5.1c | OMe | Pr | Cl | 73% |
| 7 | 5.1d | Me | *p*-$NO_2$-Ph | H | 91% |
| 8 | 5.1d | Me | *p*-$NO_2$-Ph | Cl | 92% |
| 9 | 5.1e | Me | Ph | H | 92% |
| 10 | 5.1e | Me | Ph | Cl | 95% |
| 11 | 5.1f | Me | Pr | H | 20% |
| 12 | 5.1f | Me | Pr | Cl | 86% |

[a] Reaction performed at 50 °C

Table 5.1. Allylic amination using $PPh_3$ catalyst

A deuterium labeling study was then conducted in order to help elucidate a plausible mechanism for the reaction (Scheme 5.4).

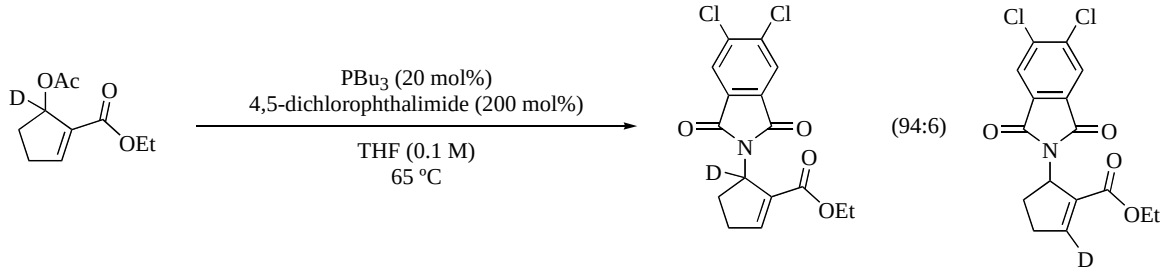


Scheme 5.4. Deuterium labeling study

Using a cyclic MBH acetate and $PBu_3$ as catalyst,[1] it was shown that the amination reaction occurs with a 94:6 ratio of retention to inversion of regiochemistry, making it reasonable to suggest a tandem $S_N2'$-$S_N2'$ reaction sequence (Figure 5.2). The phosphine first adds in Michael fashion to the α,β-unsaturated carbonyl with elimination of the acetate to afford an ion pair. At this point, it is believed that the acetate anion then deprotonates the pronucleophile, in this case phthalimide, to generate a second ion pair, this time with the desired nucleophile and the substrate. A second $S_N2'$ reaction then occurs, followed by elimination of the phosphine to generate the observed product. Direct nucleophilic substitution ($S_N2$) at the site of phosphine addition would be quite difficult in this case with the bulky triphenylphosphine, making the regioisomeric product a much less competitive route in comparison to the Trost palladium catalyzed system.

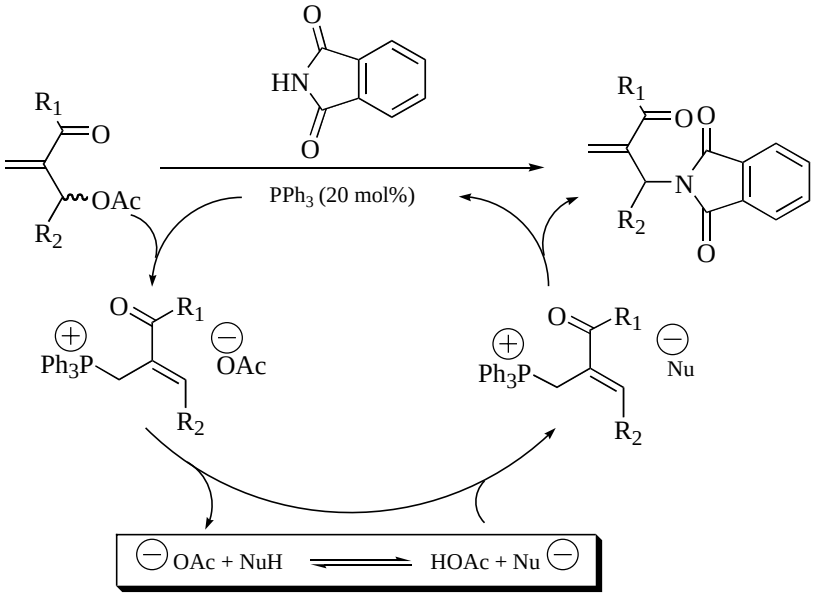


Figure 5.2. Proposed catalytic cycle of allylic amination

## 5.3 DERACEMIZATION OF MORITA-BAYLIS-HILLMAN ACETATES

Having successfully demonstrated a racemic version of the allylic amination reaction with triphenylphosphine, attention was then turned to the development of an enantioselective

[1] β-substituents on the enone in this work do not react with triarylphosphines, necessitating the use of the more nucleophilic trialkylphosphines.

variant. In order for an enantioselective variant of this reaction to be viable, one must be able to obtain the intermediate phosphonium salt of our reaction as a single alkene isomer, and then have attack of the nucleophile with high facial selectivity (Figure 5.3). This seemed like a viable conversion based on previous work which formed γ-butenolide products from the reaction of a Baylis-Hillman acetate and 2-trimethylsilyloxyfuran.[41]

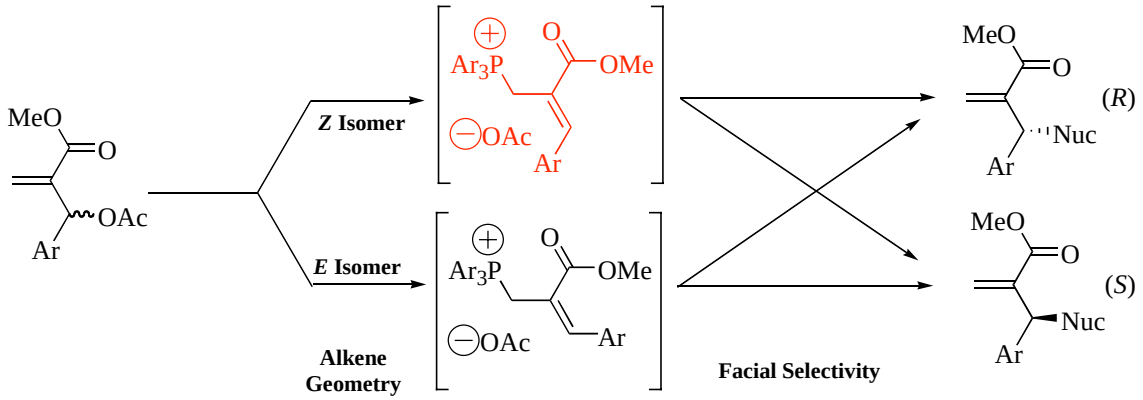


Figure 5.3. Origin of selectivity in allylic substitution of MBH acetates

The product of this reaction was obtained as a single diastereomer, indirectly suggesting that the intermediate alkene species in these allylic substitution reactions was being formed as a single isomer (Scheme 5.5). Based on these results, it seemed likely that other allylic substitution reactions, specifically the allylic amination reaction, would follow a similar path, which would provide enantiocontrol of this reaction.

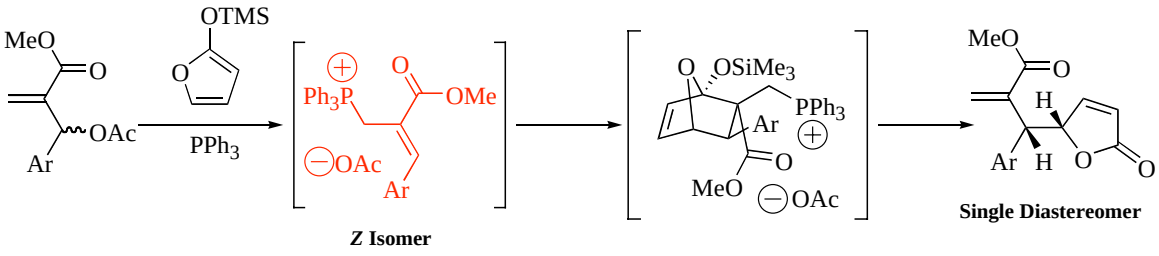


Scheme 5.5. Proposed reaction pathway for single diastereomer in the allylic substitution reaction

After screening a variety of commercially available chiral phosphines (Table 5.2), it was found that (*R*)-Cl-MeO-BIPHEP (Table 5.2, Entry 1) provided the best enantioselectivity, affording a ratio of 78:22 of the enantiomeric compounds.

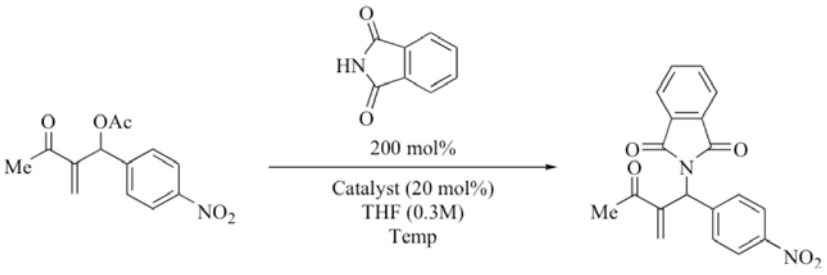


| Entry | Temp (°C) | Catalyst | Yield (%) | ee (%) |
|---|---|---|---|---|
| 1 | 25 | (*R*)-Cl-MeO-BIPHEP | 37 | 56 |
| 2 | 25 | (*R*)-MOP | 49 | 17 |
| 3 | 25 | (*R*)-QUINAP | 79 | 9 |
| 4 | 25 | NMDPP | 73 | 37 |
| 5 | 25 | (*S*)-BINAP | 25 | 7 |
| 6 | 25 | (*S*),(*S*)-Trost Ligand | 61 | 7 |

Table 5.2. Screen of commercial phosphines

Although 56% ee is an encouraging start, it is too low to be synthetically useful, directing work towards the synthesis of chiral monophosphines more suitable for this purpose. From this study, in can be seen that in general, monophosphines (NMDPP and MOP) outperform the bisphosphines, with the exception of Cl-MeO-BIPHEP. NMDPP also provided the highest yield

of the phosphines screened, which provided some direction for synthesis of phosphines to improve yield.

Unfortunately, few chiral monophosphines exist in the literature, as they in general provide lower selectivity in most transition metal catalyzed reactions than their bisphosphine counterparts. This is due in large part to the reduced level of chelation derived from interaction with one site versus two in the bisphosphine systems.

Work started based on a previously known scaffold of BINOL derived phosphines previously synthesized by Hayashi (Scheme 5.6).[42,43] This skeleton is attractive due to the tunability of the phenol substituents, but also due to the generally good results obtained from commercially available chiral phosphines of similar structure.

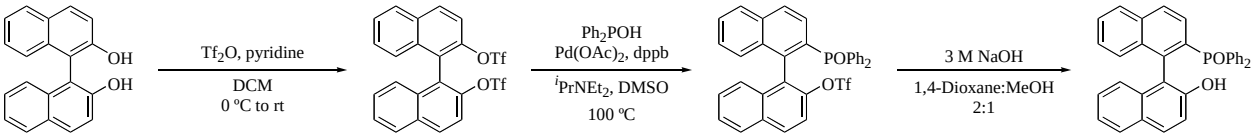


Scheme 5.6. Synthesis of MOP-type phosphine precursor

These chiral compounds are readily obtained from cheap and commercially available 2-naphthol using a copper catalyzed Ullman coupling,[44] followed by chiral resolution using a cinchona-based alkaloid.[45] The resolved BINOL is then converted to the *bis*-triflate and following palladium-catalyzed coupling to diphenyl phosphine oxide to yield the phosphine oxide precursor required for further modification (Scheme 5.6). It should be noted that at this point, synthesis of derivatives using transition metal catalyzed coupling methods was attempted, however these reactions all failed to afford the desired adducts, presumably due to the steric bulk of the diphenylphosphine oxide moiety on the neighboring aromatic ring. However, removal of the triflate using NaOH solution does provide the free phenol, which can be alkylated with a variety of aliphatic and benzylic halides, as well as with aromatic substituents using triarylbismuth arylation methodology inspired by Barton[46] that had been applied to arylate

enones.[47,48] Following alkylation of the phenol, the phosphine oxide functionality was reduced using trichlorosilane in a sealed tube to afford the desired phosphine (Scheme 5.7).

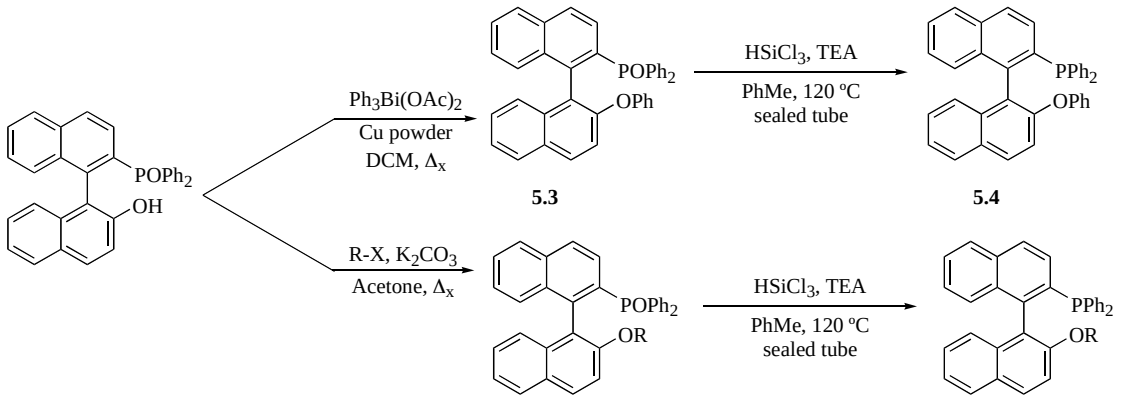


Scheme 5.7. Alkylation and reduction of phosphine catalysts

With the desired phosphines in hand, work began to find optimal reaction parameters, including the leaving group, solvent, and reaction temperature. The standard substrate for screening became the *p*-nitrophenyl substrate because of its relatively high reactivity in the reaction, as had been determined in the racemic variant (Table 5.1). Enones and enoates were then screened, using the *t*-butyl enoate, which provided higher levels of selectivity than the methyl enone or methyl enoate substrates (Table 5.3).

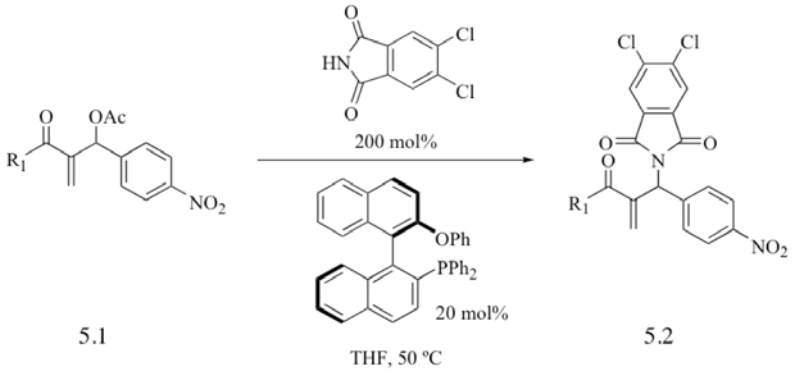


| Entry | Substrate | $R_1$ | Yield (%) | ee (%) |
|---|---|---|---|---|
| 1 | 5.1a | Me | 97 | 29 |
| 2 | 5.1d | OMe | 27 | 33 |
| 3 | 5.1g | O-*t*-Bu | 31 | 44 |

Reaction Details: Reactions were run for 18 h and then adsorbed to silica gel and chromatographed
%ee determined via chiral HPLC using Chiracel OD-H column with IPA:Hexanes as eluent

Table 5.3. $R_1$ substituent screen

Having settled upon the substrate for optimization, reaction solvents were then screened (Table 5.4). THF was found to be the best solvent, as it provided the optimal balance of yield and selectivity in this particular class of phosphine catalysts. While ethyl acetate provided higher selectivity in this particular reaction, the result was not as general for all scaffolds tested. Highly polar solvents such as DMSO offered poor selectivity in all cases, while 1,4-dioxane gave results similar to that of THF. Through the course of this screening, it was determined that increasing temperature in this system affords higher yields of the desired product and had no deleterious effect on the selectivity.

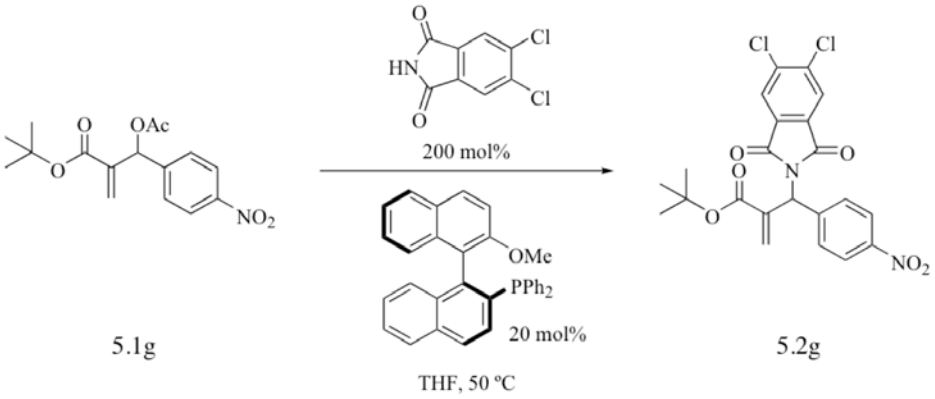


| Entry | Solvent | Temp (°C) | Yield (%) | ee (%) |
|---|---|---|---|---|
| 1 | THF | 50 | 45 | 33 |
| 2 | DCE | 50 | 20 | 40 |
| 3 | EtOH | 50 | 14 | 40 |
| 4 | EtOAc | 50 | 34 | 50 |
| 5 | DMSO | 50 | 56 | 20 |
| 6 | 1,4-Dioxane | Reflux | 87 | 25 |

Table 5.4. Solvent screen

It is interesting to note that while BINAP provides only 7% ee, MOP provides a much higher level of selectivity. Indeed, this structural scaffold showed a greater level of selectivity while maintaining adequate yield in reaction with the more challenging ester substrates. Further modification of the ether substituent allowed for alteration of the enantioselectivity of the system, as all of the catalysts of this type tested provided 15-60% ee, with larger substituents seeming to favoring higher selectivity (Table 5.5). Also of note is the fact that the isopropyl ether of the MOP scaffold (Table 5.5, entry 4) has achieved a higher level of selectivity than previously observed during the commercial phosphine screen (Table 5.2).

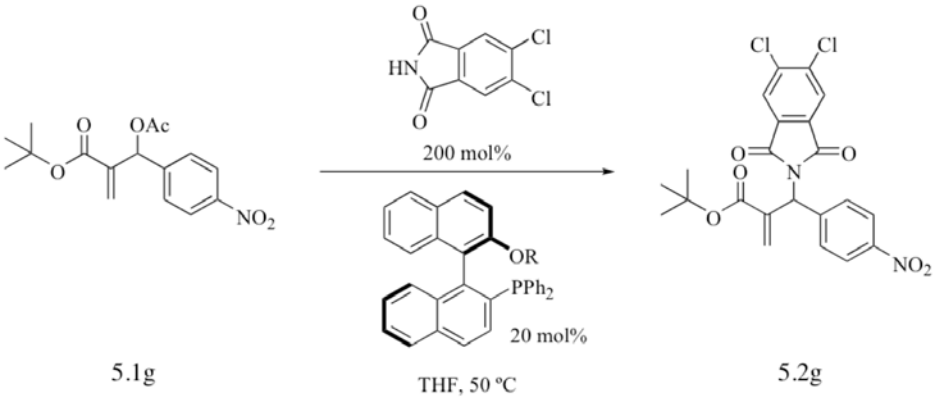


5.1g 5.2g

| Entry | R | Yield (%) | ee (%) |
|---|---|---|---|
| 1 | Me | 45 | 33 |
| 2 | Bn | 27 | 33 |
| 3 | Ph | 31 | 44 |
| 4 | *i*-Pr | 48 | 60 |
| 5 | H | Trace | 30 |

Table 5.5. MOP-type phosphine screen

These selectivities however were still not sufficient for a synthetically useful transformation. It was therefore decided to explore a set of novel phosphines based on a diphenylphosphinobenzoic acid (DPPBA) core. The benzoic acid group would provide a functional handle to which a variety of chiral amines and alcohols could be attached to provide selectivity, while maintaining the reactive triarylphosphine as the nucleophile. Attachment of the chiral portion of the molecule was accomplished using DCC coupling as described by Trost.[49] This route was attractive not only because of the modular nature of the synthesis, but also because of the large number of known chiral amines and alcohols in the chiral pool from which we could choose in order to quickly alter the structure of our catalyst system. A variety of different representatives for screening were chosen, including reduced amino acids, terpenes, and sugar-based alcohols, as well as diaminocyclohexane, the chiral component of the Trost ligand.

Due to the exploratory nature of this work, the yields for this coupling are not optimized (Table 5.6).

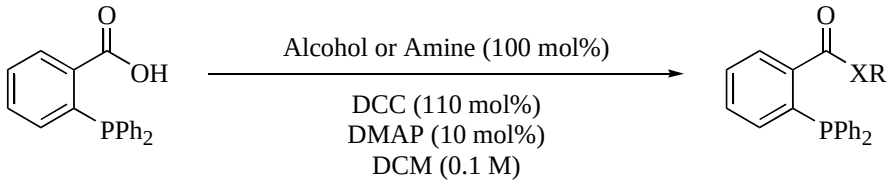


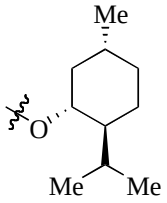


**5.5** (46%)

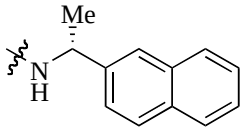


**5.6** (39%)

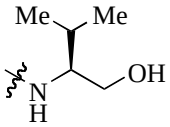


**5.7** (15%)

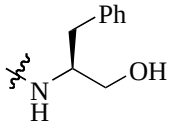


**5.8** (21%)

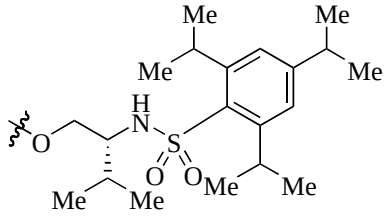


**5.9** (72%)

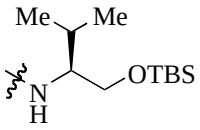


**5.10** (38%)

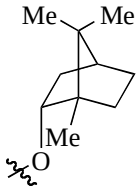


**5.11** (57%)

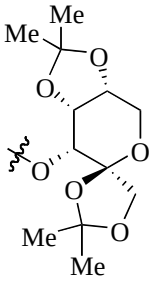


**5.12** (51%)

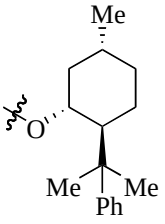


**5.13** (73%)

Table 5.6. DCC coupling results

With the desired phosphine compounds in hand, experiments were conducted to test this scaffold in our allylic amination reaction. As was the case in the BINOL derived phosphines,

higher temperatures favored higher conversion, however in this case, increasing temperature provided higher selectivity in some, but not all systems. When using the phenylmenthol derived phosphine, there is a maximum selectivity at approximately 50 ºC (Table 5.7).

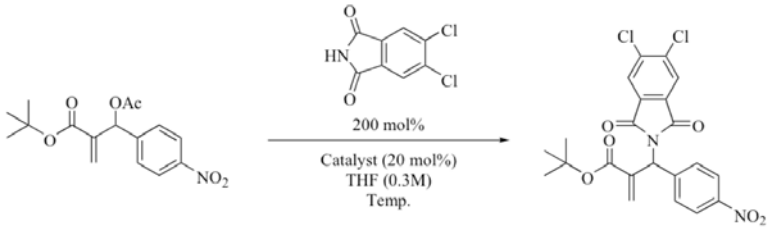


5.1g 5.2g

| Entry | Catalyst | Temp. (ºC) | Yield (%) | ee (%) |
|---|---|---|---|---|
| 1 | **5.5** | 0 | 21 | 39 |
| 2 | **5.5** | 25 | 57 | 51 |
| 3 | **5.5** | 50 | 61 | 23 |
| 4 | **5.11** | 25 | 39 | 12 |
| 5 | **5.11** | 50 | 56 | 11 |
| 6 | **5.12** | 25 | 0 | - |
| 7 | **5.12** | 50 | 10 | 16 |
| 8 | **5.13** | 50 | 56 | 51 |
| 9 | **5.13** | Reflux | 83 | 24 |

Table 5.7. DPPBA phosphine results

For the DPPBA-based catalysts, the steric bulk of the chiral substituent does not appear to relate closely to the enantioselectivity of the system. These systems were tested not only on the *t*-butyl ester substrate **5.1g**, but also on methyl ketone substrate **5.1d** (Table 5.8) to ensure that lower than desired selectivity was not solely a function of the chosen substrate. Selectivities here were moderately lower than those achieved with the *t*-butyl enoate substrate, as was the case in the BINOL based phosphines; however it should be noted that the synthesized phosphines in large part performed much better in terms of yield and enantioselectivity than the commercially available phosphines. It was encouraging to see that the new phosphines were able to compete

with the results of the commercially available material, and with this in mind, work continued toward new catalyst design.

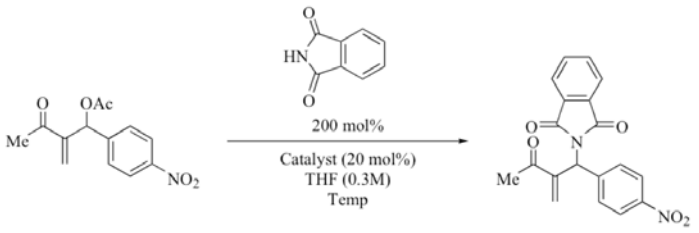


| Entry | Catalyst | Temp. (°C) | Yield (%) | ee (%) |
|---|---|---|---|---|
| 1 | **5.5** | 25 | 74 | 23 |
| 2 | **5.5** | 50 | 61 | 40 |
| 3 | **5.6** | 25 | 0 | - |
| 4 | **5.8** | 25 | 37 | 15 |
| 5 | **5.9** | 25 | 65 | 7 |
| 6 | **5.10** | 25 | 67 | 3 |

Table 5.8. DPPBA phosphines with methyl ketone substrate

It was proposed that moving the chiral center closer to the phosphorus might provide higher levels of selectivity. This could be accomplished in two fashions: First, condensation of an amino alcohol onto an aldehyde adjacent to the phosphorus atom could be accomplished. Second, a chiral alcohol could be attached directly to the aromatic ring. Spurred on by the success of the Buchwald-Hartwig type couplings of amines and alcohols to aromatic halides to achieve this aromatic substitution,[50] work began to apply this methodology to the synthesis of new chiral monophosphines (Scheme 5.8).

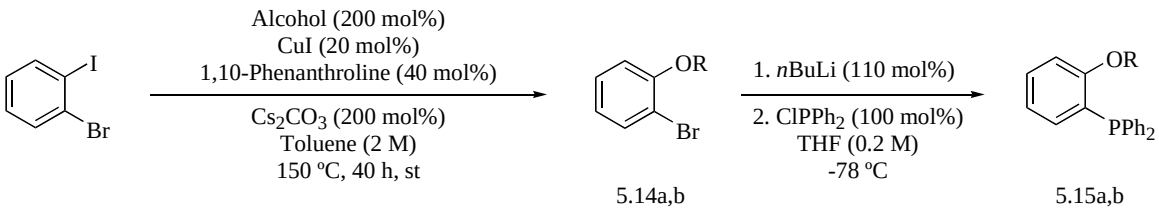


Scheme 5.8. Synthesis of Buchwald-Hartwig coupling based phosphines

| Catalyst | Alcohol | Yield 5.14 (%) | Yield 5.15 (%) |
|---|---|---|---|
| 5.15a | Menthol | 91 | 52 |
| 5.15b | α-Methylnaphthylenemethanol | 75 | 65 |

Table 5.9. Phosphine synthesis yields

A coupling of an *o*-dihalobenzene and a chiral alcohol using the Buchwald-Hartwig reaction was accomplished. Following lithium-halogen exchange on the remaining halide and trapping with chlorodiphenylphosphine, the desired product was synthesized. These couplings work quite well in limited testing, even with the highly hindered alcohol menthol (Table 5.9, entry 1). Notably, coupling occured with these highly hindered chiral alcohols in yields comparable to those obtained by Buchwald using the less hindered 1,3-substituted systems. Known phosphines **5.16**[51] and **5.17**[51] from 2-diphenylphosphino-1-benzaldehyde, as well as PHOX-type ligand **5.18**[52] were synthesized for this study (Figure 5.4).

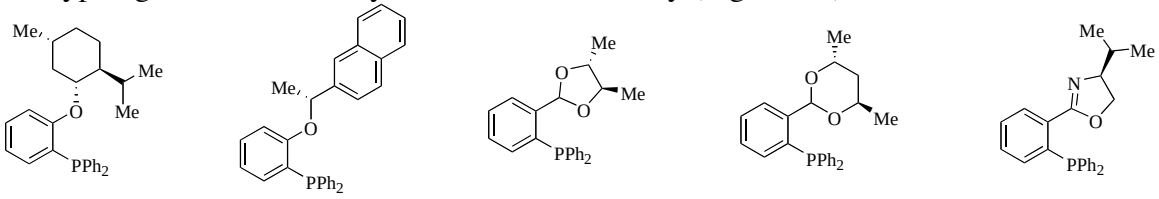


**5.15a** **5.15b** **5.16** **5.17** **5.18**

Figure 5.4. Aryl ether and acetal-type phosphines

With the desired phosphines in hand combined, the allylic amination reaction was attempted. Again, moderate yields of the allylic amination product were obtained, but high levels of selectivity were not achieved (Table 5.10). Indeed, an impasse on our path towards an enantioselective variant of this reaction using chiral phosphines appeared to have been reached. At this point that attention was turned towards molecular modeling. It was thought that by establishing a reasonable model for the observed selectivity, the design of the catalysts tested could be guided to provide a positive outcome.

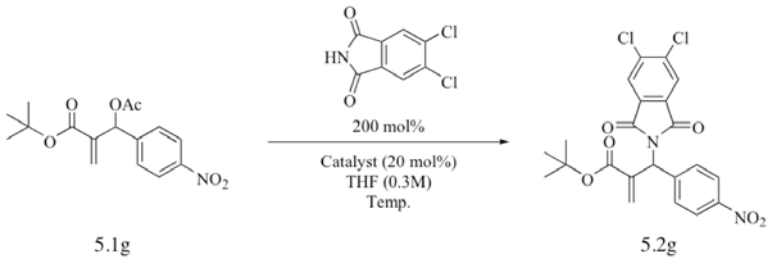


5.1g 5.2g

| Entry | Catalyst | Temp. (°C) | Yield (%) | ee (%) |
|---|---|---|---|---|
| 1 | **5.15a** | 25 | 38 | 20 |
| 2 | **5.15b** | 25 | 59 | 28 |
| 3 | **5.16** | 25 | 61 | Racemic |
| 4 | **5.17** | 25 | 67 | 4 |
| 5 | **5.18** | 50 | 15 | 7 |

Table 5.10. Aryl ether and acetal-type phosphine results

## 5.4 ABSOLUTE STEREOCHEMISTRY DETERMINATION

In order to utilize molecular modeling of the intermediate of this reaction and obtain reliable results, determination of the absolute configuration of our products from the allylic amination reaction was needed. Efforts to crystallize compounds in hand (as well as various derivatives) to homogeneity to acquire a crystal structure proved to be ineffective. These derivatives included the phthalimide derived and 4,5-dichlorophthalimide derived methyl enone products, as well as methyl and *t*-butyl enoates with varying aromatic substituents such as simple phenyl, *p*-$NO_2$-phenyl, and *p*-Br-phenyl.

Considerable effort was spent to crystallize a reactive intermediate of this reaction with various catalysts, but again we were unable to obtain any competent structures in crystalline form. Having exhausted other avenues to establish absolute configuration, pursuit of an independent synthesis of the desired product began. It was envisioned that installation of the 4,5-dichlorophthalimide protecting group on the free amine would come from deprotection of the hydroalumination-electrophilic trapping reaction using DIBAL[53] and a chiral imine could be used (Scheme 5.9).

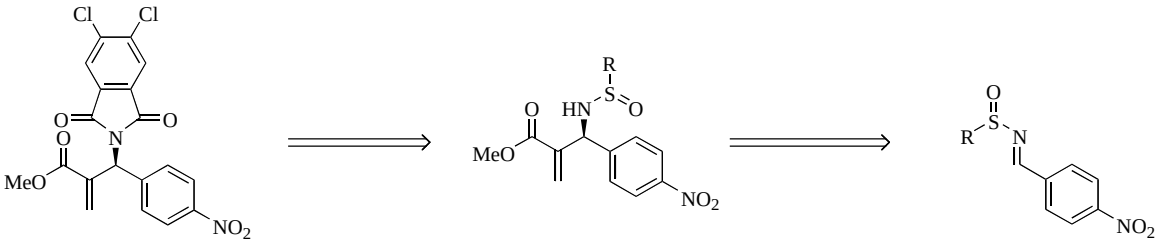


**5.2a-Cl** **5.20** **5.19**

Scheme 5.9. Retrosynthesis of independent synthesis

In order to obtain enantiopure product, the hydroalumination-electrophilic trapping must be done in an enantioselective fashion. It was thought that by use of the chiral *t*-butylsulfinamide, this goal could be accomplished. Ellman and coworkers used chiral *t*-butylsulfinamides to afford enantiopure products in other reactions,[54] and it was thought that this method would work well in this system as well.

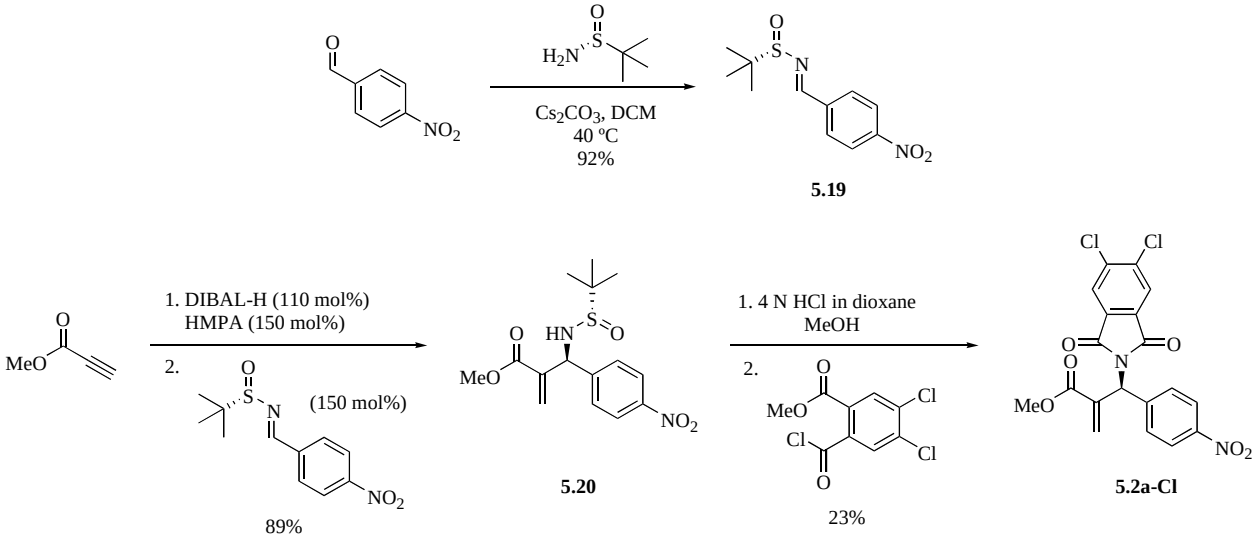


Scheme 5.10. Independent synthesis of amination product

Starting with *p*-nitrobenzaldehyde, the chiral (*R*)-variant **5.19** was formed from the corresponding sulfinamide in excellent yield (Scheme 5.10). Hydroalumination of methyl propiolate with DIBAL, followed by trapping with sulfinimine **5.19** delivered the Baylis-Hillman-type product **5.20** in 89% yield as a single diastereomer as determined by $^{1}$H NMR analysis. Deprotection using 4 N HCl in methanol, followed by reaction with the monoacid

chloride-mono methyl ester of 4,5-dichlorophthalic acid then gave the desired analog **5.2a-Cl** in 23% yield over two steps. This low yield can presumably be attributed to the instability of deprotected **5.20**, as attempts to isolate this intermediate were unsuccessful without significant degradation as observed by $^{1}$H NMR.

Compound **5.2a-Cl** was crystallized from dichloromethane by slow evaporation (see **Appendix B** for details) and determined to be the *S* isomer by single crystal X-ray crystallography (Figure 5.5).

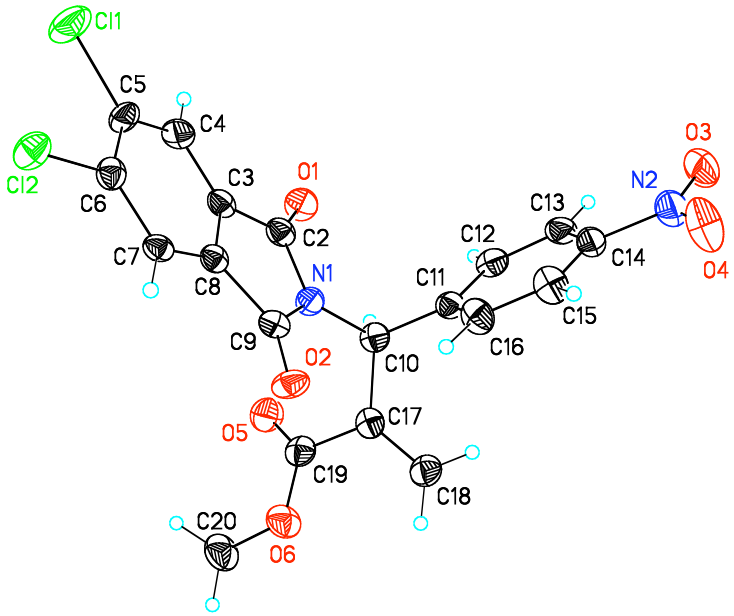


Figure 5.5. Crystal structure of enantiopure amination product **5.2a-Cl**

Having successfully synthesized the allylic amination product in enantiopure form and determined its absolute stereochemistry, we set out to convert the *t*-butyl ester products into the methyl ester analogs in order to determine the absolute stereochemistry of the allylic amination products. For this, an acid-catalyzed deprotection-esterification sequence was followed. Using *p*-toluenesulfonic acid in refluxing benzene, the *t*-butyl esters could be cleanly converted to the acid form **5.21**. Following concentration, freshly dried methanol was added and after refluxing overnight, the methyl ester analog was obtained in a 23% yield over two steps. A two-step

procedure was required for this reaction sequence, as transesterification attempts proved unsuccessful (Scheme 5.11).

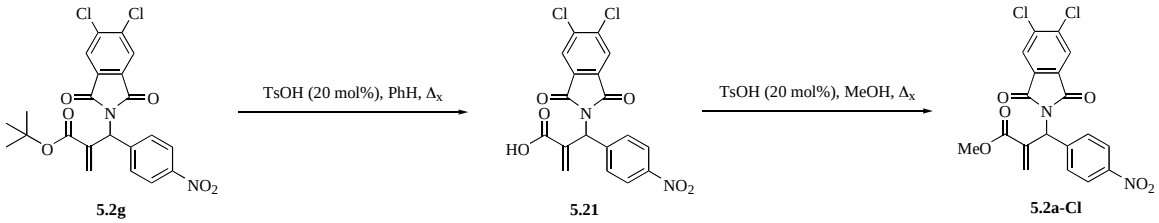


Scheme 5.11. Transesterification sequence

Having now converted the allylic amination products to their methyl ester, the optical rotation of the enantiopure sample could be compared to the enantioenriched samples from the allylic amination reaction to establish the major isomer. This information allows a model of the intermediate of the amination reaction to be generated. For the MOP-type phosphines, the absolute stereochemistry is shown in Table 5.11. There are several trends that appear from these results, the first of which is that the MOP-type catalysts afford products that are the opposite absolute configuration of the catalyst (*R* catalysts providing *S* products and vice versa).

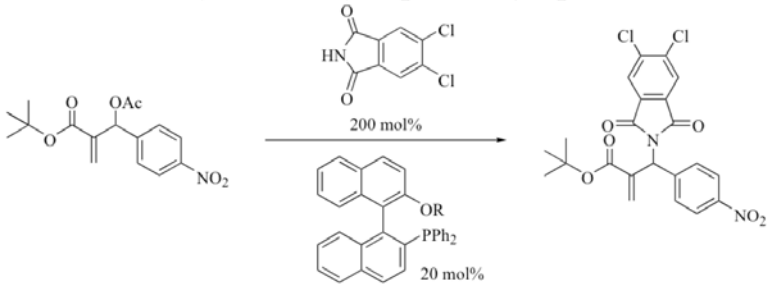


| R | Catalyst Enantiomer | Solvent | Temp. (°C) | ee (%) | Product Enantiomer |
|---|---|---|---|---|---|
| Me | R | THF | 50 | 33 | S |
| *i*-Pr | R | THF | 50 | 60 | S |
| Bn | R | THF | 50 | 33 | S |
| Ph | S | THF | 50 | 44 | R |
| Ph | S | THF | 75 (sealed tube) | 40 | R |
| Ph | S | 1,4-Dioxane | 100 | 25 | R |

Table 5.11. Absolute stereochemistry from MOP-type phosphines

When switching to the DPPBA and aryl ether scaffolds (Table 5.12), a similar pattern emerged (Table 5.11). In the case of the aryl ethers, the (-)-antipode of the catalyst affords the (+) or (*R*)-antipode of the product, though it is unclear whether there is a causative link between the two. Across the aryl ether and DPPBA scaffold, (-)-menthol afforded the (*R*) isomer, indicating that the intermediate conformation across the two scaffolds is similar. The (-)-borneol and (-)-phenylmenthol catalysts in the DPPBA scaffold provide the (*S*) isomer. The radically different shape of (-)-borneol could account for the change in selectivity, and the low selectivity obtained in this transformation indicates that the chirality transfer is inefficient. (-)-Phenylmenthol, however, provides substantially higher selectivity (51% ee) of the (*S*) isomer, which may mean that the additional bulk of the aromatic ring enforces a conformational change in the intermediate structure, leading to the opposite enantiomer of the product, though not in higher selectivity than (-)-menthol at 50 ºC.

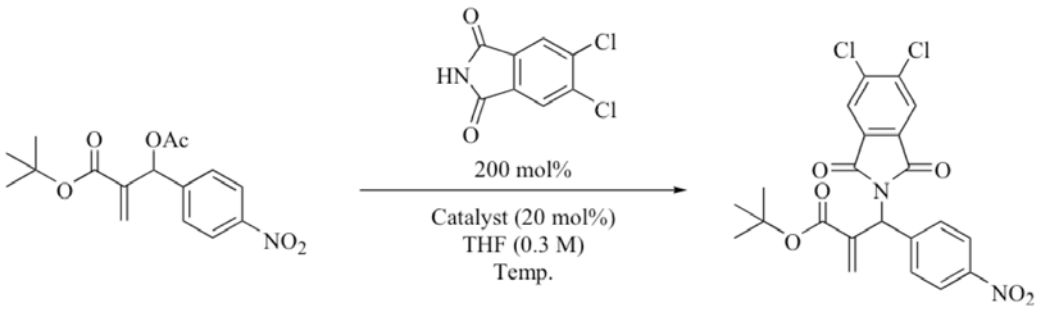


| Catalyst (Isomer) | Temp. (ºC) | ee (%) | Product Enantiomer |
|---|---|---|---|
| **5.5 (-)** | 25 | 51 | R |
| **5.11 (-)** | 25 | 12 | S |
| **5.13 (-)** | 25 | 51 | S |
| **5.13 (-)** | 50 | 51 | S |
| **5.15a (-)** | 25 | 20 | R |
| **5.15b (-)** | 25 | 28 | R |

Table 5.12. Absolute stereochemistry of products from DPPBA and aryl ether catalysts

## 5.5 POSTULATION OF A STEREOCHEMICAL MODEL

In order to continue optimization of the enantioselectivity of this reaction and it is helpful to put forth a model for the existing selectivity to determine which effects can be exploited to enhance the reaction.

It should be noted that the level of selectivity is on the order of 70:30 of the major:minor isomer, roughly equating to a difference in transition state energy of ~0.5 kcal/mol of the diastereomeric intermediates at room temperature (Table 5.13), as calculated from Equation 5.1.[55]

$$\Delta G^{\circ} = RT\ln(K_{eq})$$

Equation 5.1. Free energy at equilibrium

| $\Delta G^{o}$ (kcal/mol) | $K_{eq}$ (B/A) | Percent A at Equilibrium |
|---|---|---|
| 6.0 | $3.95 \times 10^{-5}$ | 99.996 |
| 5.0 | $2.14 \times 10^{-4}$ | 99.98 |
| 4.0 | $1.16 \times 10^{-3}$ | 99.88 |
| 3.0 | $6.29 \times 10^{-3}$ | 99.38 |
| 2.0 | $3.41 \times 10^{-2}$ | 96.71 |
| 1.0 | $1.85 \times 10^{-1}$ | 84.42 |
| 0.5 | $4.3 \times 10^{-1}$ | 69.95 |
| 0.1 | $8.45 \times 10^{-1}$ | 54.21 |

Table 5.13. Selectivity by free energy at equilibrium (25 ºC)

As many of these results are from experiments conducted at 50 ºC, this table can be recalculated to reflect this change in free energy (Table 5.14). The changes to the energy difference of the reactive intermediates between one diastereomeric intermediate and the other are quite small. For a selectivity of roughly 70:30, there is a 0.54 kcal/mol difference.

| $\Delta G^{o}$ (kcal/mol) | $K_{eq}$ (B/A) | Percent A at Equilibrium |
|---|---|---|
| 6.50 | $3.95 \times 10^{-5}$ | 99.996 |
| 5.41 | $2.14 \times 10^{-4}$ | 99.98 |
| 4.33 | $1.16 \times 10^{-3}$ | 99.88 |
| 3.25 | $6.29 \times 10^{-3}$ | 99.38 |
| 2.16 | $3.41 \times 10^{-2}$ | 96.71 |
| 1.08 | $1.85 \times 10^{-1}$ | 84.42 |
| 0.54 | $4.3 \times 10^{-1}$ | 69.95 |
| 0.10 | $8.45 \times 10^{-1}$ | 54.21 |

Table 5.14. Selectivity by free energy at equilibrium (50 ºC)

This amount of energy is lower than the typical value associated with a hydrogen bond (~1.5 kcal/mol).[56] In terms of predicting the effects that are responsible for this difference, there will be a great deal of uncertainty.

In the MOP-type catalysts, increasing the bulk of the ether substituent does appear to influence the selectivity of the reaction, as the larger isopropyl group affords higher selectivity than methyl. Yields are enhanced by heating with no appreciable erosion in the selectivity observed. The MOP-type catalysts also appear to provide the allylic amination product with the opposite chiral sense from the catalyst (Table 5.14). In the DPPBA-type scaffold, a similar phenomenon is also seen with catalysts **5.5**, **5.15a**, and **5.15b**, as these catalysts provide a product with opposite optical rotation from the starting catalyst. These results would seem to indicate that the ether substituent in the MOP-type catalysts and the chiral alcohol or amine in the DPPBA system are placed close to the site of nucleophilic attack, as the larger groups are better able to prevent attack from the face on which the catalyst resides. For the case of the (*R*) MOP-type catalysts, the catalyst would reside on the *Re* face, thus enforcing *Si* face attack (Figure 5.6).

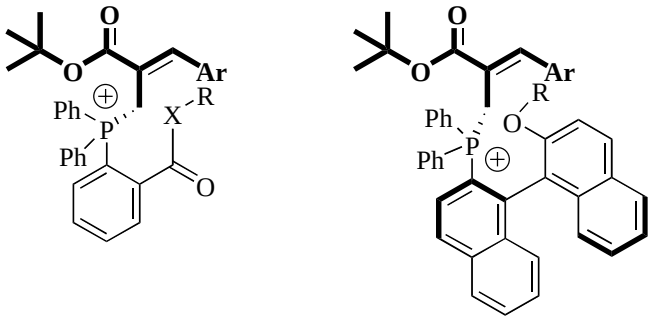


Figure 5.6. Proposed intermediate structure for asymmetric allylic amination

However, in the case of the (-)-phenylmenthol ester (**5.13**), the stereochemistry of the product is opposite from the results for the other catalysts. For both DPPBA and MOP-type catalysts, a model shows that the aromatic ring appears to reside in a similar position relative to the phosphorus center (Figure 5.7).

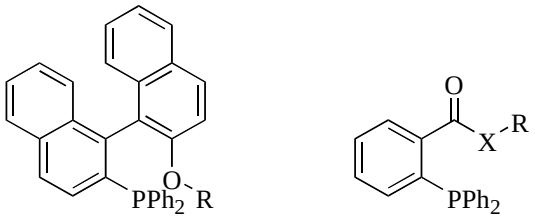


Figure 5.7. Catalyst scaffold comparison (X = O, NH)

This would also help to account for the similar selectivity observed between these two scaffolds, as the steric bulk is located in a similar position, which presumably is carried over into the reactive intermediate. In light of this possible structural similarity, it seems reasonable to suggest that while the chirality is dictated by the R group of the DPPBA scaffold, due to the similarity in location of this group relative to the catalyst nucleophilic center the intermediate structure would remain largely the same between the two types. Thus, it is proposed that the R group of both catalyst structures is responsible for blocking of one face of the intermediate, leading to enantioenrichment. No dative bond is indicated in this intermediate-state model, as X-ray crystal structure analysis of phosphine addition to an enone conducted by Krafft *et al.* has shown no evidence for a dative bond.[57]

## 5.6 CONCLUSIONS

With a model now postulated to account for the enantioselectivity observed in the allylic amination reaction, we believe it possible to develop the enantioselective variant of this reaction. However, it necessitates the synthesis and testing of a variety of new chiral monophosphines in order to adequately validate the proposed model and thus establish its predictive abilities. Work in this area seems promising, though most likely would involve a large effort. This work has established for the first time, to our knowledge, the absolute stereochemistry of the product of asymmetric allylic amination of Morita-Baylis-Hillman adducts, as well as established the viability of the enantioselective variant of the phosphine-catalyzed allylic amination of Morita-Baylis-Hillman adducts. We have synthesized a variety of new chiral monophosphines that could find use as catalysts in other organocatalytic reactions, or as ligands in transition metal-catalyzed reactions that require the use of monophosphines for activity and selectivity purposes, such as enantioselective hydrosilylation and hydroboration.[58]

## 5.7 EXPERIMENTAL

### General Methods

All chemicals were purchased from Sigma-Aldrich, Strem, or Alfa Aesar and used without further purification unless otherwise noted. Tetrahydrofuran was dried over sodium/benzophenone ketyl radical and distilled. Dichloromethane was dried over calcium hydride and distilled. Methanol and benzene were dried over molecular sieves (3Å for MeOH). Chromatography solvents given as volume:volume. Reactions were run in flame-dried glassware under nitrogen atmosphere unless otherwise noted. $^{1}$H NMR spectra obtained on a Varian MR (400 MHz), Varian Mercury (400 MHz), or Varian Unity (300 MHz) spectrometers. $^{1}$H NMR spectra are reported in delta units (δ) and were referenced to solvent peaks (7.26 ppm for $CDCl_3$). $^{13}$CNMR spectra obtained on Varian MR (100 MHz), Varian Mercury (100 MHz), or Varian Unity (75 MHz) spectrometers. $^{13}$C NMR were referenced to the center of the triplet (77.0 ppm for $CDCl_3$). $^{13}$C NMR spectra were routinely run with broadband decoupling. $^{31}$P NMR spectra

were obtained on a Varian Unity (121 MHz) spectrometer. $^{31}$PNMR spectra were referenced to trimethyl phosphite internal standard (141.0 ppm). FTIR values determined using a Nicolet Avatar 360 FT-IR instrument. Melting points were determined on a Meltemp II apparatus in open capillary tubes and are uncorrected. Enantiomeric excess was determined using a Varian HPLC or Shimadzu HPLC (LC20AT pumps, SPD-20A UV/Vis detector, SIL-20A autosampler and CBM-20A controller) equipped with a Chiracel OD-H column. Optical rotations determined on a Perkin-Elmer 241MC polarimeter using sodium D-line (589 nm) in a 10 cm cell with THF as solvent. All known compounds had properties corresponding to known literature values. 2-(Diphenylphosphanyl)-benzoic acid was prepared according to the procedure of Rauchfuss.[59] Reduced amino acids were obtained using the method of Meyers.[60] Substrates **5.1a-5.1f** prepared according to literature procedure.[61-63] Phosphines **5.16** and **5.17** were synthesized according to published procedure.[51] Phosphine **5.18** was synthesized according to literature procedure.[52]

***2-[Hydroxy-(4-nitro-phenyl)-methyl]-acrylic acid tert-butyl ester***

Prepared according to the procedure of Batra[24]. In a round bottom flask under air containing *t*-butyl acrylate (11.32 mL, 78.0 mmol) and *p*-nitrobenzaldehyde (5.89 g, 39.0 mmol) was added DABCO (4.37, 39.00 mmol) and water (40 mL). The reaction was stirred at room temperature until consumption of the aldehyde was observed (~3 days). Column chromatography (1:4 Ethyl Acetate:Hexanes) afforded the desired product as a light yellow solid (10.8 g, 48%). **$^{1}$HNMR** ($CDCl_3$, 400 MHz): 8.18-8.21 (dt, 2H, $J$ = 8.8, 2.5 Hz), 7.54-7.57 (m, 2H), 6.29 (s, 1H), 5.73-5.74 (t, 1H, $J$ = 1 Hz), 5.55-5.56 (d, 1H, $J$ = 6.4 Hz), 1.47 (s, 9H). **$^{13}$CNMR** ($CDCl_3$, 100 MHz): 165.2, 148.9, 147.3, 142.2, 127.2, 126.5, 123.5, 82.3, 73.0, 27.9. **HRMS** (CI+): calculated for $C_{14}H_{17}NO_5$: 280.1185 found: 280.1187. **FTIR** (Nujol mull): 3312 (br), 2924, 2858, 1733, 1715, 1700, 1683, 1652, 1635, 1558, 1539, 1521, 1506, 1488, 1456, 1419, 1375, 1353, 1279, 1154 $cm^{-1}$. **mp**: 80-84 ºC.

***2-[Acetoxy-(4-nitro-phenyl)-methyl]-acrylic acid tert-butyl ester (5.1g)***

In a round bottom flask containing *t*-butyl acrylate Morita-Baylis-Hillman adduct (7.00 g, 25.06 mmol) was added acetic anhydride (29.1 mL), and 2 drops of concentrated sulfuric acid. The resulting mixture was stirred at room temperature for 30 minutes, then poured onto chilled 2 M sodium hydroxide solution (200 mL). The mixture was then stirred for one hour and then extracted with chloroform (3 x 150 mL). The combined organic layers were then washed with saturated sodium bicarbonate solution and dried over magnesium sulfate. The mixture was adsorbed to silica and column chromatography (1:4 Ethyl Acetate:Hexanes) afforded the desired product as a thick yellow oil (6.85 g, 85%). **$^1$HNMR** (300 MHz, $CDCl_3$): 8.18-8.21 (d, 2H, $J$ = 8.9 Hz), 7.53-7.56 (m, 2H), 6.67 (s, 1H), 6.38 (s, 1H), 5.83 (s, 1H), 1.38 (s, 9H). **$^{13}$CNMR** (100 MHz, $CDCl_3$): 169.2, 163.6, 147.6, 145.4, 140.0, 128.5, 125.8, 123.6, 82.0, 72.2, 27.9, 20.9. **HRMS** (CI+) calculated for $C_{16}H_{20}NO_6$: 322.1291; found: 322.1290. **FTIR** (Nujol mull): 2923, 2853, 1456, 1376, 1348, 1222, 1148 $cm^{-1}$. **mp**: 41-43 ºC.

***Allylic Amination of Morita Baylis-Hillman Acetates (5.2a-f and H and Cl)***

Allylic amination was conducted using conditions reported by Krische et al.[39] Morita-Baylis-Hillman acetate (100 mol%), phthalimide or 4,5-dichlorophthalimide (200 mol%) and phosphine catalyst (20 mol%) were added to dried solvent (0.3 M) and stirred at the desired temperature for 24 h. Purification by column chromatography (hexanes:ethyl acetate) yielded the desired product. Compound **5.2g-Cl** enantiomeric excess determined by chiral stationary phase HPLC using hexanes:isopropanol (85:15 v/v, 0.5 mL/min flow rate). (*R*)-isomer (as determined by optical rotation comparison of derivative to compound (*S*)-**5.2a-Cl**) elutes at 16.95 minutes, and (*S*)-isomer elutes at 18.64 minutes.

***2'-(Diphenyl-phosphinoyl)-2-phenoxy-[1,1']binaphthalenyl (5.3)***

To a flask containing 2'-(Diphenyl-phosphinoyl)-[1,1']binaphthalenyl-2-ol[42] (1.19 g, 2.54 mmol) was added triphenylbismuth bisacetate (4.25 g, 7.60 mmol) and copper powder (16 mg, 0.25 mmol), followed by dichloromethane (13 mL). The mixture was heated to reflux with

stirring for 16 h. The mixture was cooled to room temperature and filtered. The filtrate was concentrated to afford the product as an off-white solid (865 mg, 63%). **$^{1}$HNMR** (400 MHz, $CDCl_3$): 7.88-7.93 (m, 2H), 6.86-7.75 (m, 23H), 6.74-6.76 (d, 2H, *J* = 7.8 Hz). **$^{13}$CNMR** (75 MHz, $CDCl_3$): 156.3, 152.8, 134.7, 134.3, 133.2, 132.1, 131.9, 131.5, 131.4, 130.8, 130.0, 129.4, 129.0, 127.9, 127.8, 127.6, 127.3, 127.2, 126.8, 126.3, 125.7, 124.1, 123.2, 119.7, 117.3. **$^{31}$PNMR** (121 MHz, $CDCl_3$): 29.9. **HRMS** (CI+): calculated for $C_{38}H_{28}O_2P$: 547.1827; found 547.1820. **FTIR** (thin film from DCM): 3057, 2220, 1623, 1587, 1558, 1506, 1489, 1466, 1456, 1436, 1373, 1350, 1332, 1311, 1258, 1235, 1204, 1116, 1099, 1068, 1024, 973, 908, 818, 746, 725, 694, 636 $cm^{-1}$. **mp** 99-104 ºC.

***(2'-Phenoxy-[1,1']binaphthalenyl-2-yl)-diphenyl-phosphane (5.4)***

In a pressure vessel under argon containing phosphine oxide (**5.3**) (50 mg, 0.09 mmol) and triethylamine (0.06 mL, 0.45 mmol) was added toluene (1 mL) and the reaction was cooled to 0 ºC. Trichlorosilane (0.03 mL, 0.36 mmol) was added dropwise and the vessel sealed. The mixture was stirred at 0 ºC for 10 minutes, then heated to 120 ºC and stirred overnight. After cooling to room temperature, the mixture was quenched with several drops of saturated sodium bicarbonate and diluted with ethyl ether. The mixture was filtered through Celite and adsorbed to silica gel. Column chromatography (ethyl ether) afforded the product as a white powder (40 mg, 85%). **$^{1}$HNMR** (300 MHz, $CDCl_3$): 7.89-7.98 (m, 4H), 7.00-7.54 (m, 22H), 6.79-6.97 (d, 2H, *J* = 8.2 Hz). **$^{13}$CNMR** (75 MHz, $CDCl_3$): 156.7, 152.8, 141.9, 141.4, 138.0, 137.9, 135.5, 134.4, 133.7, 133.4, 133.1, 132.8, 130.5, 129.8, 129.6, 129.2, 128.2, 128.1, 128.0, 127.9, 127.9, 127.6, 126.7, 126.3, 126.3, 125.9, 125.2, 124.4, 122.8, 119.3, 119.3, 118.2. **$^{31}$PNMR** (121 MHz, $CDCl_3$): -14.2. **HRMS** (CI+) calculated for $C_{38}H_{28}OP$:531.1878 found:531.1871. **FTIR** (Nujol mull): 3853, 3743, 2958, 2723, 1652, 1558, 1540, 1506, 1457, 1419, 1376, 722 $cm^{-1}$. **mp**: 175-177 ºC.

***2-(Diphenylphosphanyl)-benzoic acid-O-(l)-menthol ester (5.5)***

This transformation followed a modified DCC coupling method.[64] To a round bottom flask charged with 2-(Diphenylphosphanyl)-benzoic acid (300 mg, 0.97 mmol) was added menthol (153 mg, 0.97 mmol), dicyclohexylcarbodiimide (222 mg, 1.07 mmol), DMAP (12 mg, 0.09 mmol) and DCM (10 mL). The reaction was stirred overnight, then filtered through a plug of celite and washed with two portions of DCM (2 mL). The resulting solution was adsorbed to silica gel and chromatography (1:4 EtOAc:Hexanes) afforded the product as a clear oil (67 mg, 46%). **$^{1}$HNMR** (400 MHz, $CDCl_3$): 7.88-7.92 (m, 3H), 7.43-7.49 (m, 3H), 7.09-7.32 (m, 8H), 4.91-4.97 (dt, *J* = 6.4, 4.4 Hz, 1H), 2.10-2.18 (m, 1H), 1.96-2.25 (m, 1H), 1.66-1.75 (m, 2H), 1.48-1.58 (m, 3H), 1.06-1.16 (q, 2H, *J* = 10.9 Hz), 0.89-0.92 (dd, 6H, *J* = 4.1, 2.3 Hz), 0.78-0.79 (d, 4H, *J* = 4.1 Hz). **$^{13}$CNMR** (100 MHz, $CDCl_3$): 163.9, 134.1, 133.9, 131.8, 128.4, 123.7, 123.7, 119.4, 119.3, 116.9, 116.7, 75.2, 46.9, 40.7, 34.1, 31.3, 26.0, 23.2, 21.9, 21.8, 20.7, 16.1. **$^{31}$PNMR** (121 MHz, $CDCl_3$): -4.4. **HRMS** (CI+): calculated for $C_{29}H_{34}O_2P$: 445.2296; found: 445.2291. **FTIR** (thin film from DCM): 3053, 2954, 2868, 2118, 1708, 1585, 1477, 1462, 1434, 1386, 1369, 1325, 1289, 1265, 1180, 1139, 1106, 1055, 1037, 981, 960, 910, 744, 696 $cm^{-1}$.

***2-(Diphenyl-phosphanyl)-N-(S)-(1-naphthalen-2-yl-ethyl)-benzamide (5.6)***

Synthesized as above. (*S*)-(+)-1-(1-naphthyl)ethylamine (112 mg, 0.65 mmol), 2-(Diphenylphosphanyl)-benzoic acid (200 mg, 0.65 mmol), dicyclohexylcarbodiimide (135 mg, 0.65 mmol), DMAP (8 mg, 0.06 mmol) in DCM (7 mL). Product obtained as an off-white solid (115 mg, 39%). **$^{1}$HNMR** (400 MHz, $CDCl_3$): 7.74-7.81 (m, 3H), 7.65 (s, 2H), 7.45-7.47 (m, 2H), 7.19-7.38 (m, 13H), 6.93 (m, 1H), 6.40 (s, 1H), 5.35-5.40 (quin, 1H, *J* = 6.8 Hz), 1.46-1.48 (d, 3H, *J* = 6.8 Hz). **$^{13}$CNMR** (100 MHz, $CDCl_3$): 168.0, 140.0, 134.0, 134.0, 133.8, 133.8, 133.6, 133.3, 132.7, 130.2, 128.9, 128.8, 128.7, 128.7, 128.6, 128.5, 128.4, 127.9, 127.5, 126.1, 125.8, 124.8, 124.7, 109.7, 49.6, 21.3. **$^{31}$PNMR** (121 MHz, $CDCl_3$): 3.07. **HRMS** (CI+): calculated for $C_{31}H_{27}NOP$: 460.1830; found: 460.1841. **FTIR** (thin film from DCM): 3055, 2925, 1733, 1716, 1699, 1683, 1652, 1646, 1635, 1558, 1540, 1521, 1506, 1456 $cm^{-1}$. **mp**: 143-146 ºC.

***2-(Diphenyl-phosphanyl)-N-(1-hydroxymethyl-2-methyl-propyl)-benzamide (5.7)***

Synthesized as above. Valinol (67 mg, 0.65 mmol), 2-(Diphenylphosphanyl)-benzoic acid (200 mg, 0.65 mmol), dicyclohexylcarbodiimide (135 mg, 0.65 mmol), DMAP (8 mg, 0.06 mmol) in DCM (7 mL). Product obtained as an off-white solid (38 mg, 15%). **$^{1}$HNMR** (400 MHz, $CDCl_3$): 7.68-7.74 (m, 1H), 7.24-7.48 (m, 12H), 6.60-7.23 (m, 1H), 3.63-3.67 (dd, 2H, *J* = 8.5, 3.4 Hz), 1.67-1.74 (m, 1H), 1.20-1.21 (d, 1H, *J* = 5.4 Hz), 0.86-0.87 (d, 3H, *J* = 6.8 Hz), 0.76-0.78 (d, 3H, *J* = 6.8 Hz). $^{13}$CNMR (100 MHz, $CDCl_3$): 169.6, 142.0, 141.7, 136.4, 136.3, 136.1, 136.0, 134.5, 134.3, 133.7, 133.5, 130.0, 129.0, 128.9, 128.8, 128.7, 128.5, 128.5, 128.0, 127.9, 62.9, 57.5, 28.6, 19.2, 18.5. **$^{31}$PNMR** (121 MHz, $CDCl_3$): -16.0. **HRMS** (CI+): calculated for $C_{24}H_{27}NO_2P$: 392.1779; found 392.1774. **FTIR** (Nujol mull): 2923, 2853, 1652, 1558, 1506, 1456, 1375 $cm^{-1}$. **mp** 123-128 ºC.

***2-(Diphenyl-phosphanyl)-N-(1-hydroxymethyl-2-phenyl-ethyl)-benzamide (5.8)***

Synthesized as above. Phenylalanol (99 mg, 0.65 mmol), 2-(Diphenylphosphanyl)-benzoic acid (200 mg, 0.65 mmol), dicyclohexylcarbodiimide (148 mg, 0.71 mmol), DMAP (8 mg, 0.06 mmol) in DCM (7 mL). Product obtained as an off-white solid (50 mg, 21%). **$^{1}$HNMR** (300 MHz, $CDCl_3$): 7.00-7.34 (m, 17H), 6.84-6.85 (m, 1H), 6.08-6.18 (m, 1H), 4.01-4.09 (m, 1H), 4.08-4.09 (m, 1H), 3.29-3.35 (m, 2H), 2.56-2.70 (t, 1H, *J* = 13 Hz), 2.56-2.70 (q, 1H, *J* = 13 Hz). **$^{13}$CNMR** (75 MHz, $CDCl_3$): 169.2, 137.2, 136.2, 135.2, 134.0, 133.9, 133.8, 133.6, 133.5, 133.0, 129.3, 129.1, 128.9, 128.8, 128.8, 128.7, 128.6, 128.5, 128.4, 128.3, 127.7, 127.6, 126.3, 62.9, 53.3, 36.4. **$^{31}$PNMR** (121 MHz, $CDCl_3$): -11.29. **HRMS** (CI+): calculated for $C_{28}H_{27}NO_2P$: 440.1779; found: 440.1777. **FTIR** (Nujol mull): 2923, 2723, 1652, 1635, 1558, 1540, 1521, 1506, 1496, 1456, 1376, 722 $cm^{-1}$. **mp**: 133-140 ºC.

***2-Diphenylphosphanyl-benzoic acid 3-methyl-2-(2,4,6-triisopropyl-benzenesulfonylamino)-butyl ester (5.9)***

Synthesized as above. Protected valinol[65] (241 mg, 0.65 mmol), 2-(Diphenylphosphanyl)-benzoic acid (200 mg, 0.65 mmol), dicyclohexylcarbodiimide (148 mg, 0.71 mmol), DMAP (8 mg, 0.06 mmol) in DCM (7 mL). Product obtained as a yellow oil (310 mg, 72%). **$^{1}$HNMR**

(400 MHz, $CDCl_3$): 7.98-8.02 (m, 1H), 7.13-7.40 (m, 14H), 6.94-6.95 (m, 1H), 4.25-4.29 (dd, 1H, *J* = 11.2, 3.7 Hz), 4.02-4.14 (m, 3H), 3.40 (br s, 1H N-H), 2.85-2.92 (quintet, 1H, *J* = 6.8 Hz), 1.60-1.65 (m, 1H), 1.21-1.25 (m, 18H), 0.76-0.83 (dd, 6H, *J* = 17.7, 6.8 H). **$^{13}$CNMR** (75 MHz, $CDCl_3$): 166.5, 152.3, 149.5, 139.7, 137.3, 137.3, 137.2, 137.1, 134.4, 134.1, 134.0, 133.8, 133.7, 133.6, 133.4, 132.1, 130.9, 130.8, 128.7, 128.5, 128.4, 128.4, 128.3, 123.6, 65.2, 57.4, 33.9, 29.7, 29.7, 29.5, 24.8, 24.8, 23.4, 18.9, 18.8. **$^{31}$PNMR** (121 MHz, $CDCl_3$): -4.9. **HRMS** (CI+): calculated for $C_{39}H_{49}NO_4SP$: 658.3120; found: 658.3126. **FTIR** (thin film from DCM): 3291 (br), 3055, 2959, 2869, 1716, 1652, 1646, 1635, 1600, 1586, 1559, 1540, 1521, 1506, 1463, 1435, 1384, 1363, 1253, 1157, 1058, 1041, 998, 972, 910, 882, 806, 734, 697, 663, 623 $cm^{-1}$.

***N-[1-(tert-Butyl-dimethyl-silanyloxymethyl)-2-methyl-propyl]-2-diphenylphosphanyl-benzamide (5.10)***

Synthesized as above. TBS protected valinol (71 mg, 0.32 mmol), 2-(Diphenylphosphanyl)-benzoic acid (100 mg, 0.32 mmol), dicyclohexylcarbodiimide (74 mg, 0.36 mmol), DMAP (4 mg, 0.03 mmol) in DCM (3 mL). Product obtained as a colorless oil (63 mg, 38%). **$^{1}$HNMR** (300 MHz, $CDCl_3$): 7.57-7.60 (ddd, 1H, *J* = 7.6, 3.9, 1.1 Hz), 7.21-7.38 (m, 12H), 6.92-6.95 (ddd, 1H, *J* = 7.6, 3.9, 0.9 Hz), 6.20-6.22 (d, 1H, *J* = 8.7 Hz), 3.81-3.87 (m, 1H), 3.66-3.69 (dd, 1H, *J* = 10.1, 2.9 Hz), 3.46-3.50 (d, 1H, *J* = 10.1, 4.6 Hz), 1.82-1.90 (sextet, 1H, *J* = 7.0 Hz), 0.82-0.89 (dd, 6H, *J* = 23.0, 6.4 Hz), 0.86 (s, 9H), 0.02 (d, 6H, *J* = 2.9 Hz). **$^{13}$CNMR** (100 MHz, $CDCl_3$): 168.5, 142.0, 141.8, 137.4, 137.3, 137.2, 135.9, 135.7, 134.2, 133.8, 133.6, 133.6, 130.0, 128.6, 128.6, 128.6, 128.5, 128.5, 128.4, 128.4, 127.5, 127.5, 62.4, 55.9, 28.5, 25.8, 19.5, 18.6, 18.1, -3.6, -5.5. **$^{31}$PNMR** (121 MHz, $CDCl_3$): -9.0**.** **HRMS** (CI+): calculated for $C_{30}H_{41}NO_2PSi$ 506.2644: found 506.2641. **FTIR** (thin film from DCM): 3053, 2927, 1652, 1585, 1506, 1462, 1433, 1388, 1257, 1104, 835 $cm^{-1}$.

***2-Diphenylphosphanyl-benzoic acid 1,7,7-trimethyl-bicyclo[2.2.1]hept-2-yl ester (5.11)***

Synthesized as above. Borneol (50 mg, 0.32 mmol), 2-(diphenylphosphanyl)-benzoic acid (100 mg, 0.32 mmol), dicyclohexylcarbodiimide (67 mg, 0.32 mmol), DMAP (2 mg, 0.01 mmol) in DCM (2 mL). Product was obtained as an off-white solid (83 mg, 57%). **$^{1}$HNMR**

(400 MHz, $CDCl_2$): 8.04-8.06 (m, 1H), 7.24-7.42 (m, 12H), 6.90-6.93 (m, 1H), 5.00-5.03 (m, 1H), 2.29-2.32 (m, 1H), 1.96-2.17 (m, 1H), 1.63-1.73 (m, 2H), 1.15-1.32 (m, 2H) 0.81-0.87 (m, 10H). **$^{13}$CNMR** (100 MHz, $CDCl_3$): 166.9, 166.9, 140.3, 140.0, 138.2, 138.1, 138.1, 138.0, 135.2, 135.0, 134.3, 133.9, 133.8, 133.7, 131.6, 130.2, 130.2, 128.4, 128.4, 128.3, 128.1, 80.8, 48.9, 47.7, 44.8, 36.5, 27.9, 27.3, 19.6, 18.8, 13.5. **$^{31}$PNMR** (121 MHz, $CDCl_3$): -5.1. **HRMS** (CI+): calculated for $C_{29}H_{32}O_2P$: 443.2140; found 443.2148. **FTIR** (Nujol mull): 2923, 1716, 1700, 1684, 1652, 1558, 1506, 1456, 1376, 1303, 1115, 748, 722, 695 $cm^{-1}$. **mp**: 101-108 ºC.

***2-Diphenylphosphanyl-benzoic acid 1,2:4,5-di-O-isopropylidene-β–D-Fructopyranose ester (5.12)***

1,2:4,5-Di-*O*-isopropylidene-β–D-fructopyranose was prepared according to literature procedure.[66] In a round bottom flask containing 2-diphenylphosphanyl-benzoic acid (100 mg, 0.32 mmol) was added dichloromethane (1 mL). The mixture was cooled to 0 ºC. Dicyclohexylcarbodiimide (67 mg, 0.32 mmol), DMAP (8 mg, 0.06 mmol) and 1,2:4,5-di-*O*-isopropylidene-β–D-fructopyranose (85 mg, 0.32 mmol) were added, the reaction was removed from the ice bath and stirred at room temperature for 48 h. The mixture was then concentrated and redissolved in ethyl acetate. The resulting solution was placed in the freezer at -5 ºC for 30 minutes, then filtered. The filtrate was then washed with saturated sodium bicarbonate, 10% citric acid, and brine, then dried over magnesium sulfate. Column chromatography (15% EtOAc in Hexanes as eluent) afforded the product as a fluffy, white solid (92 mg, 51%). **$^{1}$HNMR** (400 MHz, $CDCl_3$) 8.04-8.06 (m, 1H), 7.25-7.43 (m, 12H), 6.85-6.95 (m, 1H), 4.55-4.58 (m, 2H), 4.31 (s, 1H), 4.20-4.22 (d, 1H, $J$ = 7.8 Hz), 4.07-4.10 (d, 1H, $J$ = 11.6 Hz), 3.88-3.91 (d, 1H, $J$ = 12.9 Hz), 3.73-3.76 (d, 1H, $J$ = 12.9Hz), 1.42-1.50 (d, 6H, $J$ = 33.1 Hz), 1.28-1.34 (d, 6H, $J$ = 24.2 Hz). **$^{13}$CNMR** (100 MHz, $CDCl_3$): 165.8, 165.8, 140.9, 140.6, 137.7, 137.6, 137.5, 134.2, 134.0, 133.9, 133.8, 133.7, 133.7, 131.9, 130.7, 128.5, 128.4, 128.4, 128.4, 128.3, 128.0, 108.9, 101.5, 70.7, 70.4, 70.0, 65.4, 61.2, 26.4, 25.8, 25.3, 24.0. **$^{31}$PNMR** (121 MHz, $CDCl_3$): -4.8. **HRMS** (CI+): calculated for $C_{31}H_{34}O_7P$: 549.2042; found: 549.2046. **FTIR** (Nujol mull): 2924, 2723, 1652, 1558, 1506, 1456, 1419, 1376, 722 $cm^{-1}$. **mp**: 67-78 ºC.

***2-Diphenylphosphanyl-benzoic acid 5-methyl-2-(1-methyl-1-phenyl-ethyl)-cyclohexyl ester (5.13)***

In a round bottom flask cooled to 0 ºC containing phenylmenthol (592 mg, 2.55 mmol) and THF (10 mL) was added *n*-butyllithium (3.16 mL, 1.61M). The resulting mixture was stirred for 10 minutes, followed by the addition of 2-diphenylphosphinobenzoic acid *p*-nitrophenyl ester[67] in THF (10 mL). The reaction was stirred at 0 ºC until complete by TLC. The mixture was then adsorbed to silica gel and column chromatography (1:5 EtOAc:Hexanes) to afford the product as a thick, yellow oil (970 mg, 73%). **$^{1}$HNMR** (400 MHz, $CDCl_3$): 7.12-7.32 (m, 17H), 6.98-7.02 (t, 1H, $J$ = 6.8 Hz), 6.78-6.79 (m, 1H), 4.91-4.97 (dt, 1H, $J$ = 10.6, 4.4 Hz), 2.04-2.09 (m, 1H), 1.60-1.74 (m, 1H), 0.73-1.18 (m, 13 H). **$^{13}$CNMR** (100 MHz, $CDCl_3$) 165.5, 165.5, 151.7, 140.9, 140.6, 138.4, 138.4, 138.3, 134.2, 134.0, 133.8, 133.7, 133.6, 131.8, 131.5, 130.7, 128.5, 128.4, 128.4, 128.3, 128.3, 128.0, 127.7, 125.3, 124.9, 75.1, 50.3, 41.5, 39.7, 34.5, 31.2, 27.5, 26.6, 25.4, 21.7. **HRMS** (CI+): calculated for $C_{35}H_{38}O_2P$: 521.2609; found: 521.2611. **$^{31}$PNMR** (121 MHz, $CDCl_3$): -3.6. **FTIR** (thin film from DCM): 3056, 3018, 2923, 1733, 1716, 1700, 1599, 1586, 1569, 1505, 1495, 1472, 1456, 1436, 1388, 1370, 1258, 1217, 1142, 1116, 1057, 1029, 990, 978, 907, 787, 696, 666 $cm^{-1}$.

***1-Bromo-2-(2-isopropyl-5-methyl-cyclohexyloxy)-benzene (5.14a)***

Prepared using a modified procedure from Buchwald.[50] In a heavy wall pressure vessel containing 2-bromoiodobenzene (0.13 mL, 1.00 mmol) and menthol (312 mg, 2.00 mmol) was added 1,10-phenanthroline (72 mg, 0.40 mmol), cesium carbonate (652 mg, 2.00 mmol) and copper (I) iodide (38 mg, 0.20 mmol) and toluene (0.5 mL). The vessel was sealed, heated to 150 ºC and stirred for 40 h. After cooling to room temperature, the solution was filtered through a small amount of silica gel and washed with ethyl ether. Concentration of the filtrate, followed by column chromatography (Hexanes) afforded the product as a thick, colorless oil (283 mg, 91%). **$^{1}$HNMR** (300 MHz, $CDCl_3$): 7.50-7.53 (dd, 1H, $J$ = 7.9, 1.6 Hz), 7.19-7.25 (m, 1H), 6.80-6.91 (m, 1H), 6.75-6.78 (dt, 1H, $J$ = 7.4, 1.3 Hz), 4.03-4.11 (dt, 1H, $J$ = 10.6, 4.1 Hz), 2.29-2.30

(m, 1H), 2.09-2.13 (m, 1H), 1.71-1.76 (m, 3H), 1.62-1.63 (m, 1H), 0.96-1.17 (m, 3H), 0.90-0.95 (t, 6H, *J* = 7.1 Hz), 0.75-0.77 (d, 3H, *J* = 7.0 Hz). **$^{13}$CNMR** (75 MHz, $CDCl_3$): 133.5, 128.2, 121.3, 114.3, 78.9, 47.8, 40.1, 34.4, 31.4, 25.9, 23.6, 22.1, 20.8, 16.5. **HRMS** (CI+): calculated for $C_{16}H_{23}OBr$ 310.0932: found 310.0934. **FTIR** (thin film from DCM): 2955, 2924, 2869, 1584, 1474, 1442, 1369, 1278, 1246, 1124, 1047, 1030, 992, 745 $cm^{-1}$.

***(R)-2-[1-(2-Bromo-phenoxy)-ethyl]-naphthalene (5.14b)***

Prepared as above. 2-bromoiodobenzene (0.13 mL, 1.00 mmol) and alcohol (344 mg, 2.00 mmol) was added 1,10-phenanthroline (72 mg, 0.40 mmol), cesium carbonate (652 mg, 2.00 mmol) and copper (I) iodide (38 mg, 0.20 mmol) and toluene (0.5 mL). Product obtained as a brown solid (334 mg, 75%). **$^{1}$HNMR** (300 MHz, $CDCl_3$): 7.80-7.85 (m, 4H), 7.45-7.56 (m, 4H), 6.91-7.07 (m, 1H), 6.72-6.79 (m, 2H), 5.47-5.51 (m, 1H), 1.75-1.78 (d, 3H, *J* = 6.4 Hz). **$^{13}$CNMR** (75 MHz, $CDCl_3$): 133.3, 129.3, 128.6, 128.1, 127.9, 127.7, 126.1, 125.9, 124.5, 123.6, 121.9, 115.9, 115.6, 77.5, 24.3. **HRMS** (CI+) calculated for $C_{18}H_{15}OBr$: 326.0306 found: 326.0309. **FTIR** (thin film from DCM): 3509, 3056, 3022, 2976, 2928, 2900, 2871, 1633, 1599, 1586, 1571, 1559, 1506, 1494, 1473, 1455, 1441, 1419, 1374, 1307, 1274, 1243, 1174, 1143, 1127, 1069, 1047, 1029, 1002, 949, 931, 894, 857, 819, 745, 708, 691, 666, 621 $cm^{-1}$. **mp**: 45-47 ºC.

***[2-(2-Isopropyl-5-methyl-cyclohexyloxy)-phenyl]-diphenyl-phosphane (5.15a)***

To a round bottom flask containing aryl bromide **5.14a** (100 mg, 0.32 mmol) was added THF (1.6 mL). The mixture was cooled to -78 ºC in a dry ice/acetone bath and then *n*-butyllithium (0.14 mL, 2.5M) was added dropwise. The mixture was then stirred at -78 ºC for 15 minutes. Chlorodiphenylphosphine (0.06 mL, 0.32 mmol) was added and the solution warmed to room temperature and stirred overnight. The resulting mixture was adsorbed to silica gel and column chromatography (Hexanes) afforded the product as a thick, colorless oil (70 mg, 52%). **$^{1}$HNMR** (300 MHz, $CDCl_3$): 7.24-7.32 (m, 10H), 6.67-6.86 (m, 4H), 4.01-4.04 (dt, 1H, *J* = 6.4, 3.8 Hz), 2.05-2.09 (d, 1H, *J* = 12.5 Hz), 1.09-1.64 (m, 5H), 0.68-0.97 (m, 3H), 0.82-0.84 (d, 3H,

*J* = 6.4 Hz), 0.47-0.61 (dd, 6H, *J* = 35.6, 6.9 Hz). **$^{13}$CNMR** (75 MHz, $CDCl_3$): 159.1, 158.9, 137.0, 136.9, 136.8, 134.4, 134.2, 134.0, 133.7, 133.5, 129.8, 128.4, 128.3, 128.3, 128.2, 128.2, 128.1, 126.6, 126.5, 119.9, 110.8, 76.2, 47.2, 39.2, 34.3, 31.3, 24.8, 22.9, 22.0, 20.8, 15.8. **$^{31}$PNMR** (121 MHz, $CDCl_3$): 1.33. **HRMS** (CI+): calculated for $C_{28}H_{34}OP$: 417.2347; found: 417.2352. **FTIR** (thin film from DCM): 3054, 2954, 2925, 2868, 2361, 2338, 1733, 1699, 1683, 1652, 1576, 1558, 1540, 1465, 1457, 1436, 1279, 1238, 1012, 993, 745, 696, 667 $cm^{-1}$.

***(R)-[2-(1-Naphthalen-2-yl-ethoxy)-phenyl]-diphenyl-phosphane (5.15b)***

Prepared as above. Aryl bromide **5.14b** (100 mg, 0.30 mmol), *n*-butyllithium (0.14 mL, 2.5 M), chlorodiphenylphosphine (0.06 mL, 0.30 mmol), THF (1.5 mL). Product isolated as a white solid (86 mg, 65%). **$^{1}$HNMR** (300 MHz, $CDCl_3$): 7.53-7.79 (m, 3H), 7.35-7.42 (m, 12H), 7.06-7.21 (m, 3H), 6.68-6.91 (m, 3H), 5.35-5.38 (q, 1H, *J* = 6.1 Hz), 1.39-1.42 (d, 3H, *J* = 6.4 Hz). **$^{13}$CNMR** (75 MHz, $CDCl_3$): 159.0, 158.8, 157.9, 140.7, 140.5, 136.9, 136.7, 136.6, 134.5, 134.2, 133.9, 132.7, 129.8, 129.3, 128.7, 128.5, 128.4, 128.3, 128.3, 127.8, 127.6, 126.6, 126.4, 126.1, 125.9, 125.6, 124.2, 124.0, 123.6, 120.6, 115.9, 112.3, 24.1. **$^{31}$PNMR** (121 MHz, $CDCl_3$): -14.0. **HRMS** (CI+): calculated for $C_{30}H_{26}OP$: 433.1721; found 433.1727. **FTIR** (thin film from DCM): 3054, 2976, 2927, 1791, 1772, 1750, 1733, 1716, 1699, 1683, 1652, 1646, 1635, 1616, 1575, 1569, 1540, 1533, 1521, 1506, 1496, 1489, 1471, 1465, 1456, 1419, 1394, 1374, 1276, 1234, 1177, 1128, 1071 $cm^{-1}$. **mp**: 77-85 ºC.

***(R)-2-Methyl-propane-2-sulfinic acid 4-nitro-benzylideneamide (5.19)***

Prepared according to the procedure of Nakata.[68] 4-Nitrobenzaldehyde (5.61 g, 37.1 mmol), (*R*)-(+)-2-methyl-2-propanesulfinamide (4.50 g, 37.1 mmol), and cesium carbonate (12.09 g, 37.1 mmol) were added to a round bottom flask, followed by dichloromethane (185 mL). The resulting suspension was heated to 40 ºC and stirred for approximately 8 hours. The solution was then filtered through Celite and the filter cake washed with dichloromethane. The liquid was concentrated and column chromatography (1:4 ethyl acetate:hexanes v:v) afforded the product as a yellow solid (8.66 g, 92%). **$^{1}$HNMR** (400 MHz, $CDCl_3$): 8.62 (s, 1H), 8.26-8.29

(dt, 2H, *J* = 8.8, 2.1 Hz), 7.97-8.00 (dt, 2H, *J* = 8.8, 2.1 Hz), 1.24 (s, 9H). **$^{13}$CNMR** (100 MHz, $CDCl_3$): 160.5, 149.6, 138.7, 129.9, 124.0, 58.3, 22.5. **HRMS** (CI+): calculated for $C_{11}H_{15}N_2O_3S$: 255.0803; found: 255.0800. **FTIR** (thin film from DCM): 3106, 2979, 2948, 2862, 1585, 1515, 1340, 1084 $cm^{-1}$. **mp** 139-140 ºC.

***2-[(2-Methyl-propane-2-sulfinylamino)-(4-nitro-phenyl)-methyl]-acrylic acid methyl ester (5.20)***

To a round bottom flask charged with hexamethylphosphoramidite (2.05 mL, 11.80 mmol) was added tetrahydrofuran (41 mL) and the resulting solution was cooled to 0 ºC. Diisobutylaluminum hydride (1.5 M in toluene, 5.7 mL, 8.65 mmol) was added and the mixture stirred for 30 minutes. Methyl propiolate (0.70 mL, 7.87 mmol) was added to the solution dropwise and stirred for 1 h. Sulfinimide **5.19** (3.00 g, 11.80 mmol) was added in one portion, the ice bath removed and the reaction stirred overnight. 1 M HCl (20 mL) was added and the solution was extracted with ethyl ether. The organic layer was washed with 1 M HCl (3 x 20 mL) and saturated sodium bicarbonate (20 mL), dried over magnesium sulfate and concentrated. Flash column chromatography (ethyl acetate) afforded the product as a viscous yellow oil that solidified upon standing (2.39 g, 89%). **$^{1}$HNMR** (400 MHz, $CDCl_3$): 8.09-8.12 (dd, 2H, *J* = 8.8, 1.3 Hz), 7.53-7.56 (d, 2H, *J* = 8.8 Hz), 6.43 (s, 1H), 5.99 (s, 1H), 5.43-5.44 (d, 1H, *J* = 6.8 Hz), 4.11-4.13 (d, 1H, *J* = 6.8 Hz), 3.64 (s, 3H). **$^{13}$CNMR** (100 MHz, $CDCl_3$): 165.5, 147.4, 147.2, 139.6, 128.1, 127.8, 123.7, 59.9, 56.3, 52.0, 22.4. **HRMS** (CI+) calculated for $C_{15}H_{21}N_2O_5S$: 341.1171; found: 341.1179. **FTIR** (thin film from DCM): 3207, 2955, 2926, 2867, 1719, 1632, 1606, 1598, 1521, 1493, 1473, 1456, 1439, 1391, 1347, 1267, 1195, 1153, 1109, 1063, 1014, 963, 901, 857, 823, 736, 715, 697 $cm^{-1}$. **mp** 77-81 ºC.

***2-[(5,6-Dichloro-1,3-dioxo-1,3-dihydro-isoindol-2-yl)-(4-nitro-phenyl)-methyl]-acrylic acid (5.21)***

Ester substrate **5.2g** (100 mg, 0.209 mmol) was added to a round bottom flask, followed by *p*-toluenesulfonic acid (8 mg, 0.042 mmol) and benzene (1.0 mL). The mixture was heated to reflux and stirred for approximately 30 minutes. The reaction mixture was cooled to room

temperature and filtered to afford the desired product as a white solid (92 mg, quant.). **$^1$HNMR** (400 MHz, $CDCl_3$): 8.21-8.23 (d, 2H, *J* = 8.9 Hz), 7.93 (s, 2H), 7.57-7.59 (d, 2H, *J* = 8.5 Hz), 6.74 (d, 1H, *J* = 1.3 Hz), 6.41 (s, 1H), 5.71-5.72 (d, 1H, *J* = 1.7 Hz). **$^{13}$CNMR** (100 MHz, $CDCl_3$): 168.7, 165.8, 165.7, 147.8, 143.3, 139.6, 139.4, 135.4, 132.4, 131.6, 130.5, 129.5, 125.8, 125.7, 124.0, 53.8. **HRMS** (CI+): calculated for $C_{18}H_{11}N_2O_6Cl_2$: 420.9994; found 420.9998. **FTIR** (Nujol mull): 2925 (br), 2723, 2688, 1715, 1700, 1684, 1520, 1458, 1376, 1345, 1303, 1263, 723 $cm^{-1}$. **mp**: 216 ºC (decomp).

***(S)-2-[(5,6-Dichloro-1,3-dioxo-1,3-dihydro-isoindol-2-yl)-(4-nitro-phenyl)-methyl]-acrylic acid methyl ester ((S)-5.2a-Cl)***

Deprotection of the sulfinamide protecting group was conducted using a modified procedure of Ellman.[54] Protected amine **5.20** (1.93 g, 5.68 mmol) was added to a round bottom flask followed by methanol (28 mL) and 4 N HCl in dioxane (10 mL) and the mixture stirred until consumption of starting material was observed by TLC (~1 h). The mixture was concentrated *in vacuo* and redissolved in THF (7 mL). Triethylamine (1.58 mL, 11.36 mL) was added and the mixture cooled to 0 ºC. A solution of dichlorophthalic acid mono methyl ester mono acid chloride[69] (1.35 g, 6.81 mmol) in THF (7 mL) was added dropwise and the solution warmed to room temperature and stirred overnight. The mixture was adsorbed to silica gel and column chromatography (1:4 ethyl acetate:hexanes) yielded the product as a light yellow solid (580 mg, 23%). **$^1$HNMR** (400 MHz, $CDCl_3$): 8.20-8.22 (d, 2H, *J* = 9.0 Hz), 7.92 (s, 2H), 7.57-7.59 (d, 2H, *J* = 8.5 Hz), 6.62-6.63 (d, 1H, *J* = 1.4 Hz), 6.45 (s, 1H), 5.61-5.62 (d, 1H, *J* = 1.7 Hz), 3.72 (s, 3H). **$^{13}$CNMR** (75 MHz, $CDCl_3$): 165.7, 165.4, 147.7, 143.5, 139.5, 135.9, 130.5, 130.2, 129.6, 125.7, 123.9, 54.2, 52.4. **HRMS** (CI+) calculated for $C_{19}H_{13}N_2O_6Cl_2$; 435.015067; found: 435.014595 **FTIR** (thin film from DCM): 3095, 2925, 1723, 1524, 1377, 1346, 1144, 1104, 910, 733 $cm^{-1}$. **mp**: 165-176 ºC

***2-[(5,6-Dichloro-1,3-dioxo-1,3-dihydro-isoindol-2-yl)-(4-nitro-phenyl)-methyl]-acrylic acid methyl ester (5.2a-Cl)***

In a round bottom flask charged with 2-[(5,6-dichloro-1,3-dioxo-1,3-dihydro-isoindol-2-yl)-(4-nitro-phenyl)-methyl]-acrylic acid **5.21** (25 mg, 0.05 mmol) and *p*-toluenesulfonic acid (2 mg, 0.01 mmol) was added methanol (1 mL) and the reaction was heated to reflux and stirred overnight. The reaction mixture was cooled to room temperature and filtered to obtain a light yellow solid (12 mg, 46%). Properties matched those of **(*S*)-5.2a-Cl**.

## 5.8 REFERENCES


(1) Tolman, C. A. *Chem Rev* **1977**, *77*, 313-348.
(2) Collman, J. P.; Hegedus, L. S.; Norton, J. R.; Finke, R. G. *Principles and Applications of Organotransition Metal Chemistry*; University Science Books: Sausalito, 1987, p. 66-80.
(3) Dondoni, A.; Massi, A. *Angew. Chem., Int. Ed.* **2008**, *47*, 4638-4660.
(4) Kemsley, J. *Chem. Eng. News* **2008**, *86*, 32-34.
(5) Guillena, G.; Najera, C.; Ramon, D. J. *Tetrahedron: Asymmetry* **2007**, *18*, 2249-2293.
(6) Ting, A.; Schaus, S. E. *Eur. J. Org. Chem.* **2007**, 5797-5815.
(7) Verkade, J. M. M.; vanHemert, L. J. C.; Quaedflieg, P. J. L. M.; Rutjes, F. P. J. T. *Chem. Soc. Rev.* **2008**, *37*, 29-41.
(8) Wong, O. A.; Shi, Y. *Chem. Rev.* **2008**, *108*, 3958-3987.
(9) Xu, Z.; Lu, X. *Tetrahedron Lett.* **1997**, *38*, 3461-3464.
(10) Xu, Z.; Lu, X. *J. Org. Chem.* **1998**, *63*, 5031-5041.
(11) Xu, Z.; Lu, X. *Tetrahedron Lett.* **1999**, *40*, 549-552.
(12) Zhu, G.; Chen, Z.; Jiang, Q.; Xiao, D.; Cao, P.; Zhang, X. *J. Am. Chem. Soc.* **1997**, *119*, 3836-3837.
(13) Zhu, X.-F.; Lan, J.; Kwon, O. *J. Am. Chem. Soc.* **2003**, *125*, 4716-4717.
(14) Ouellet, S. G.; Walji, A. M.; Macmillan, D. W. C. *Acc. Chem. Res.* **2007**, *40*, 1327-1339.
(15) MacMillan, D. W. C. *Nature* **2008**, *455*, 304-308.
(16) White, D. A.; Baizer, M. M. *Tetrahedron Lett.* **1973**, 3597-600.
(17) Davies, W. C.; Lewis, W. P. G. *J. Chem. Soc.* **1934**, 1599.
(18) Henderson, W. A.; Streuli, C. A. *J. Am. Chem. Soc.* **1960**, *82*, 5791-5794.
(19) Smith, J. W. *The Chemistry of the Amino Group*; Interscience: New York, 1968,161.
(20) Methot, J. L.; Roush, W. R. *Adv. Synth. Catal.* **2004**, *346*, 1035-1050.
(21) Rauhut, M. M.; Currier, H. US Patent 19630122.
(22) Morita, K.; Suzuki, Z.; Hirose, H. *Bull. Chem. Soc. Jap.* **1968**, *41*, 2815.
(23) Baylis, A. B.; Hillman, M. E. D.DE19720510.
(24) Patra, A.; Roy, A. K.; Joshi, B. S.; Roy, R.; Batra, S.; Bhaduri, A. P. *Tetrahedron* **2003**, *59*, 663-670.
(25) Juaristi, E.; Soloshonok, V. A.; Editors *Enantioselective Synthesis of beta-Amino Acids, Second Edition*, 2005.
(26) Cardillo, G.; Tomasini, C. *Chem. Soc. Rev.* **1996**, *25*, 117-128.
(27) Cole, D. C. *Tetrahedron* **1994**, *50*, 9517-82.
(28) Gellman, S. H. *Acc. Chem. Res.* **1998**, *31*, 173-180.
(29) Salzmann, T. N.; Ratcliffe, R. W.; Christensen, B. G.; Bouffard, F. A. *J. Am. Chem. Soc.* **1980**, *102*, 6161-3.
(30) Miyachi, N.; Shibasaki, M. *J. Org. Chem.* **1990**, *55*, 1975-6.
(31) Juaristi, E.; Quintana, D.; Escalante, J. *Aldrichimica Acta* **1994**, *27*, 3-11.
(32) Fulop, F. *Chem. Rev.* **2001**, *101*, 2181-204.
(33) Harmat, N. J. S.; Di Bugno, C.; Criscuoli, M.; Giorgi, R.; Lippi, A.; Martinelli, A.; Monti, S.; Subissi, A. *Bioorg. Med. Chem. Lett.* **1998**, *8*, 1249-1254.
(34) Knapp, S. *Chem. Rev.* **1995**, *95*, 1859-76.
(35) Porter, E. A.; Wang, X.; Lee, H.-S.; Weisblum, B.; Gellman, S. H. *Nature* **2000**, *404*, 565.
(36) Cheng, R. P.; Gellman, S. H.; DeGrado, W. F. *Chem. Rev.* **2001**, *101*, 3219-3232.

(37) Kim, J. N.; Lee, H. J.; Lee, K. Y.; Gong, J. H. *Synlett* **2002**, 173-175.
(38) Kim, J. N.; Lee, H. J.; Gong, J. H. *Tetrahedron Lett.* **2002**, *43*, 9141-9146.
(39) Cho, C.-W.; Kong, J.-R.; Krische, M. J. *Org. Lett.* **2004**, *6*, 1337-1339.
(40) Trost, B. M.; Tsui, H.-C.; Toste, F. D. *J. Am. Chem. Soc.* **2000**, *122*, 3534-3535.
(41) Cho, C.-W.; Krische, M. J. *Angew. Chem. Int. Ed. Engl.* **2004**, *43*, 6689-91.
(42) Uozumi, Y.; Kawatsura, M.; Hayashi, T. *Org. Synth.* **2002**, *78*, 363-369.
(43) Uozumi, Y.; Tanahashi, A.; Lee, S. Y.; Hayashi, T. *J. Org. Chem.* **1993**, *58*, 1945-1948.
(44) Schanz, H.-J.; Linseis, M. A.; Gilheany, D. G. *Tetrahedron: Asymmetry* **2003**, *14*, 2763-2769.
(45) Cai, D.; Hughes, D. L.; Verhoeven, T. R.; Reider, P. J. *Tetrahedron Lett.* **1995**, *36*, 7991-4.
(46) Barton, D. H. R.; Finet, J. P.; Khamsi, J.; Pichon, C. *Tetrahedron Lett.* **1986**, *27*, 3619-22.
(47) Koech, P. K.; Krische, M. J. *J. Am. Chem. Soc.* **2004**, *126*, 5350-5351.
(48) Koech, P. K.; Krische, M. J. *Tetrahedron* **2006**, *62*, 10594-10602.
(49) Trost, B. M.; Van Vranken, D. L.; Bingel, C. *J. Am. Chem. Soc.* **1992**, *114*, 9327-43.
(50) Wolter, M.; Nordmann, G.; Job, G. E.; Buchwald, S. L. *Org. Lett.* **2002**, *4*, 973-976.
(51) Frost, C. G.; Williams, J. M. J. *Synlett* **1994**, 551-2.
(52) Peer, M.; de Jong, J. C.; Kiefer, M.; Langer, T.; Rieck, H.; Schell, H.; Sennhenn, P.; Sprinz, J.; Steinhagen, H.; et al. *Tetrahedron* **1996**, *52*, 7547-7583.
(53) Tsuda, T.; Yoshida, T.; Saegusa, T. *J. Org. Chem.* **2002**, *53*, 1037-1040.
(54) Tang, T. P.; Ellman, J. A. *J. Org. Chem.* **1999**, *64*, 12-13.
(55) Lowry, T. H.; Richardson, K. S. *Mechanism and Theory in Organic Chemistry*; 3rd Edition ed.; HarperCollins Publishers: New York, 1987, p. 211-212.
(56) Anslyn, E. V.; Dougherty, D. A. In *Modern Physical Organic Chemistry*; University Science Books: Sausalito, 2006, p 168-174.
(57) Krafft, M. E.; Haxell, T. F. N.; Seibert, K. A.; Abboud, K. A. *J. Am. Chem. Soc.* **2006**, *128*, 4174-4175.
(58) Hayashi, T. *Acc. Chem. Res.* **2000**, *33*, 354-362.
(59) Hoots, J. E.; Rauchfuss, T. B.; Wrobleski, D. A. *Inorg. Synth.* **1982**, *21*, 175.
(60) McKennon, M. J.; Meyers, A. I.; Drauz, K.; Schwarm, M. *J. Org. Chem.* **1993**, *58*, 3568-3571.
(61) Nilov, D.; Racker, R.; Reiser, O. *Synthesis* **2002**, 2232-2242.
(62) Annunziata, R.; Benaglia, M.; Cinquini, M.; Cozzi, F.; Raimondi, L. *J. Org. Chem.* **1995**, *60*, 4697-706.
(63) Still, W. C.; Kahn, M.; Mitra, A. *J. Org. Chem.* **1978**, *43*, 2923-5.
(64) Trost, B. M.; Van Vranken, D. L.; Bingel, C. *J. Am. Chem. Soc.* **1992**, *114*, 9327-9343.
(65) Bowman, W. R.; Coghlan, D. R. *Tetrahedron* **1997**, *53*, 15787-15798.
(66) Kang, J.; Lim, G. J.; Yoon, S. K.; Kim, M. Y. *J. Org. Chem.* **1995**, *60*, 564-577.
(67) Lin, F. L.; Hoyt, H. M.; van Halbeek, H.; Bergman, R. G.; Bertozzi, C. R. *J. Am. Chem. Soc.* **2005**, *127*, 2686-2695.
(68) Higashibayashi, S.; Tohmiya, H.; Mori, T.; Hashimoto, K.; Nakata, M. *Synlett* **2004**, *2004*, 457-460.
(69) Allison, B. D.; Hack, M. D.; Phuong, V. K.; Rabinowitz, M. H.; Rosen, M. D. US Patent 20050038032.

# Appendix A (Crystallographic Data for 4.2e)

**X-RAY EXPERIMENTAL.**

Table A.1. Crystallographic Data for **4.2e**.

Table A.2. Fractional coordinates and equivalent isotropic thermal parameters (Å2) for the non- hydrogen atoms of **4.2e**.

Table A.3. Bond Lengths (Å) and Angles (o) for the non-hydrogen atoms of **4.2e**.

Table A.4. Anisotropic thermal parameters for the non-hydrogen atoms of **4.2e**.

Table A.5. Fractional coordinates and isotropic thermal parameters (Å2) for the hydrogen atoms of **4.2e**.

Table A.6. Torsion Angles (o) for the non-hydrogen atoms of **4.2e**.

Table A.7. Observed and calculated structure factor amplitudes for **4.2e**. Values for Fo, Fc and σ(Fo) have been multiplied by 10.

Figure A.1. View of molecule 1 in **4.2e** showing the atom labeling scheme. Displacement ellipsoids are scaled to the 50% probability level.

Figure A.2. View of molecule 2 in **4.2e** showing the atom labeling scheme. Displacement ellipsoids are scaled to the 50% probability level.

Figure A.3. Fit by least-squares of selected atoms of molecule 1 (solid lines) onto the equivalent atoms of molecule 2 (dashed lines). The atoms of molecule 1 used in the fit are labeled.

Figure A.4. Unit cell packing diagram for **4.2e**. The view is approximately down the **b** axis.

Molecules 1 are shown in ball-and-stick form while molecules 2 are in wire frame form.

X-ray Experimental for $C_{22}H_{24}O_2$: Crystals grew as long, colorless needles by slow evaporation from $CH_3CN$: $CH_2Cl_2$**:** MeOH( 4: 1: 0.2). The data crystal was cut from a much longer needle and had approximate dimensions; 0.60 x 0.17 x 0.12 mm. The data were collected

on a Nonius Kappa CCD diffractometer using a graphite monochromator with MoKα radiation ($\lambda = 0.71073$Å). A total of 327 frames of data were collected using ω-scans with a scan range of 1° and a counting time of 62 seconds per frame. The data were collected at 223 K using an Oxford Cryostream low temperature device. Details of crystal data, data collection and structure refinement are listed in Table 1. Data reduction were performed using DENZO-SMN.[1] The structure was solved by direct methods using SIR97[2] and refined by full-matrix least-squares on $F^2$ with anisotropic displacement parameters for the non-H atoms using SHELXL-97.[3] The hydrogen atoms on carbon were calculated in ideal positions with isotropic displacement parameters set to 1.2xUeq of the attached atom (1.5xUeq for methyl hydrogen atoms). There are two crystallographically unique molecules per asymmetric unit. The molecules are nearly

identical in conformation (Figure 3). The function, $\Sigma w(|F_o|^2 - |F_c|^2)^2$, was minimized, where $w = 1/[(\sigma(F_o))^2 + (0.0578*P)^2]$ and $P = (|F_o|^2 + 2|F_c|^2)/3$. $R_w(F^2)$ refined to 0.132, with R(F) equal to 0.0574 and a goodness of fit, S, = 0.956. Definitions used for calculating R(F), $R_w(F^2)$ and the goodness of fit, S, are given below.[4] The data were corrected for secondary extinction effects. The correction takes the form: $F_{corr} = kF_c/[1 + (1.17(9)x10^{-5})* F_c^2 \lambda^3/(\sin 2\theta)]^{0.25}$ where k is the overall scale factor. The absolute direction of the **c-**axis could not be determined from the X- ray results. Neutral atom scattering factors and values used to calculate the linear absorption

coefficient are from the International Tables for X-ray Crystallography (1992).[5] All figures were generated using SHELXTL/PC.[6] Tables of positional and thermal parameters, bond lengths and angles, torsion angles, figures and lists of observed and calculated structure factors are located in tables 1 through 7.

**References**

1) DENZO-SMN. (1997). Z. Otwinowski and W. Minor, Methods in Enzymology, **276**: Macromolecular Crystallography, part A, 307 – 326, C. W. Carter, Jr. and R. M. Sweets, Editors, Academic Press.

2) SIR97. (1999). A program for crystal structure solution. Altomare A., Burla M.C., Camalli M., Cascarano G.L., Giacovazzo C. , Guagliardi A., Moliterni

A.G.G., Polidori G.,Spagna R. J. Appl. Cryst. 32, 115-119.

3) Sheldrick, G. M. (1994). SHELXL97. Program for the Refinement of Crystal Structures. University of Gottingen, Germany.

4) Rw(F2) = {Σw(|Fo|2 - |Fc|2)2/Σw(|Fo|)4}1/2 where w is the weight given each reflection. R(F) = Σ(|Fo| - |Fc|)/Σ|Fo|} for reflections with Fo > 4(σ(Fo)).
S = [Σw(|Fo|2 - |Fc|2)2/(n - p)]1/2, where n is the number of reflections and p is the number of refined parameters.

5) International Tables for X-ray Crystallography (1992). Vol. C, Tables 4.2.6.8 and 6.1.1.4, A. J. C. Wilson, editor, Boston: Kluwer Academic Press.

6) Sheldrick, G. M. (1994). SHELXTL/PC (Version 5.03). Siemens Analytical X-ray Instruments, Inc., Madison, Wisconsin, USA.

Table A.1. Crystal data and structure refinement for 2e.

Empirical formula C22 H24 O2

Formula weight 320.41

Temperature 223(2) K

Wavelength 0.71073 Å

Crystal system Orthorhombic

Space group Pca21

Unit cell dimensions a = 16.9116(3) Å α= 90°.

b = 5.56190(10) Å β= 90°.

c = 36.4494(8) Å γ = 90°.

Volume 3428.45(11) $Å^3$

Z 8

Density (calculated) 1.242 $Mg/m^3$

Absorption coefficient 0.078 $mm^{-1}$

F(000) 1376

Crystal size 0.60 x 0.17 x 0.12 mm

Theta range for data collection 2.93 to 27.48°.

Index ranges -21<=h<=21, -7<=k<=7, -47<=l<=46

Reflections collected 7195

Independent reflections 7195 [R(int) = 0.0000]

Completeness to theta = 27.48° 99.0 %

Absorption correction None

Refinement method Full-matrix least-squares on $F_2$

Data / restraints / parameters 7195 / 1 / 434

Goodness-of-fit on $F_2$ 0.956

Final R indices [I>2sigma(I)] R1 = 0.0574, wR2 = 0.1037

R indices (all data) R1 = 0.1559, wR2 = 0.1319

Extinction coefficient $1.17(9)x10^{-5}$

Largest diff. peak and hole 0.225 and -0.202 e.$Å^{-3}$

Table A.2. Atomic coordinates ( x $10^4$) and equivalent isotropic displacement parameters ($Å^2$x $10^3$) for 1. U(eq) is defined as one third of the trace of the orthogonalized $U_{ij}$ tensor.

| | x | y | z | U(eq) |
|---|---|---|---|---|
| C1 | 7472(2) | 2523(5) | 3805(1) | 23(1) |
| C2 | 7504(2) | 572(6) | 3503(1) | 24(1) |
| C3 | 8336(2) | 281(6) | 3339(1) | 28(1) |
| C4 | 8942(2) | -178(6) | 3643(1) | 33(1) |
| C5 | 8922(2) | 1791(6) | 3930(1) | 33(1) |
| C6 | 8100(2) | 2037(7) | 4096(1) | 32(1) |
| C7 | 6648(2) | 2645(6) | 3975(1) | 27(1) |
| C8 | 6491(2) | 4827(6) | 4212(1) | 26(1) |

O9 6963(2) 6497(4) 4224(1) 36(1)

C10 5742(2) 4933(6) 4428(1) 23(1)

C11 5632(2) 6833(7) 4674(1) 30(1)

C12 4940(2) 6967(7) 4879(1) 34(1)

C13 4363(2) 5261(7) 4840(1) 33(1)

C14 4463(2) 3399(7) 4592(1) 36(1)

C15 5146(2) 3218(6) 4389(1) 30(1)

C16 6936(2) 1208(7) 3194(1) 24(1)

O17 7047(1) 3069(4) 3022(1) 34(1)

C18 6246(2) -369(6) 3099(1) 25(1)

C19 5807(2) 214(7) 2788(1) 32(1)

C20 5169(2) -1213(7) 2685(1) 33(1)

C21 4968(2) -3200(7) 2890(1) 31(1)

C22 5400(2) -3773(6) 3198(1) 33(1)

C23 6033(2) -2359(6) 3304(1) 29(1)

C24 8362(2) -1699(6) 3050(1) 34(1)

C1' 4537(2) 7435(6) 6144(1) 24(1)

C2' 4515(2) 5481(6) 6445(1) 24(1)

C3' 3675(2) 5209(6) 6606(1) 29(1)

C4' 3071(2) 4781(6) 6303(1) 31(1)

C5' 3087(2) 6758(6) 6016(1) 33(1)

C6' 3912(2) 6966(6) 5853(1) 29(1)

C7' 5370(2) 7594(6) 5973(1) 25(1)

C8' 5523(2) 9793(6) 5741(1) 25(1)

O9' 5050(2) 11447(4) 5728(1) 36(1)

C10' 6270(2) 9936(6) 5524(1) 25(1)

C11' 6373(2) 11818(6) 5277(1) 29(1)

C12' 7060(2) 11991(6) 5072(1) 34(1)

C13' 7657(2) 10296(6) 5112(1) 35(1)

C14' 7559(2) 8418(7) 5354(1) 35(1)

C15' 6873(2) 8231(7) 5561(1) 32(1)

C16' 5080(2) 6142(6) 6751(1) 26(1)

O17' 4956(1) 8006(4) 6924(1) 35(1)

C18' 5776(2) 4627(6) 6854(1) 25(1)

C19' 6230(2) 5305(6) 7155(1) 31(1)

C20' 6864(2) 3929(7) 7270(1) 36(1)

C21' 7056(2) 1850(7) 7082(1) 39(1)

C22' 6623(2) 1150(6) 6779(1) 35(1)

C23' 5980(2) 2543(6) 6663(1) 32(1)

C24' 3648(2) 3221(6) 6895(1) 38(1)

Table A.3. Bond lengths [Å] and angles [°] for 1.

---

C1-C6 1.525(5)

C1-C7 1.526(5)

C1-C2 1.548(5)

C1-H1 0.96

C2-C16 1.521(5)

C2-C3 1.537(5)

C2-H2 0.96

C3-C24 1.525(5)

C3-C4 1.531(5)

C3-H3 0.96

C4-C5 1.515(5)

C4-H4A 0.96

C4-H4B 0.96

C5-C6 1.523(5)

C5-H5A 0.96

C5-H5B 0.96

C6-H6A 0.96

C6-H6B 0.96

C7-C8 1.514(5)

C7-H7A 0.96

C7-H7B 0.96

C8-O9 1.225(4)

C8-C10 1.492(5)

C10-C15 1.395(5)

C10-C11 1.400(5)

C11-C12 1.389(5)

C11-H11 0.96

C12-C13 1.368(5)

C12-H12 0.96

C13-C14 1.387(5)

C13-H13 0.96

C14-C15 1.375(5)

C14-H14 0.96

C15-H15 0.96

C16-O17 1.225(4)

C16-C18 1.501(5)

C18-C23 1.383(5)

C18-C19 1.395(5)

C19-C20 1.390(5)

C19-H19 0.96

C20-C21 1.376(5)

C20-H20 0.96

C21-C22 1.377(5)

C21-H21 0.96

C22-C23 1.383(5)

C22-H22 0.96

C23-H23 0.96

C24-H24A 0.96

C24-H24B 0.96

C24-H24C 0.96

C1'-C6' 1.520(5)

C1'-C7' 1.544(5)

C1'-C2' 1.544(5)

C1'-H1' 0.96

C2'-C16' 1.514(5)

C2'-C3' 1.544(4)

C2'-H2' 0.96

C3'-C4' 1.524(5)

C3'-C24' 1.528(5)

C3'-H3' 0.96

C4'-C5' 1.518(5)

C4'-H4'A 0.96

C4'-H4'B 0.96

C5'-C6' 1.521(5)

C5'-H5'A 0.96

C5'-H5'B 0.96

C6'-H6'A 0.96

C6'-H6'B 0.96

C7'-C8' 1.510(5)

C7'-H7'A 0.96

C7'-H7'B 0.96

C8'-O9' 1.220(4)

C8'-C10' 1.492(5)

C10'-C11' 1.392(5)

C10'-C15' 1.398(5)

C11'-C12' 1.384(5)

C11'-H11' 0.96

C12'-C13' 1.388(5)

C12'-H12' 0.96

C13'-C14' 1.377(5)

C13'-H13' 0.96

C14'-C15' 1.389(5)

C14'-H14' 0.96

C15'-H15' 0.96

C16'-O17' 1.232(4)

C16'-C18' 1.495(5)

C18'-C19' 1.390(5)

C18'-C23' 1.396(5)

C19'-C20' 1.383(5)

C19'-H19' 0.96

C20'-C21' 1.384(5)

C20'-H20' 0.96

C21'-C22' 1.381(6)

C21'-H21' 0.96

C22'-C23' 1.401(5)

C22'-H22' 0.96

C23'-H23' 0.96

C24'-H24D 0.96

C24'-H24E 0.96

C24'-H24F 0.96

C6-C1-C7 111.3(3)

C6-C1-C2 110.3(3)

C7-C1-C2 110.6(3)

C6-C1-H1 108.1

C7-C1-H1 108.0

C2-C1-H1 108.4

C16-C2-C3 108.4(3)

C16-C2-C1 110.0(3)

C3-C2-C1 112.5(3)

C16-C2-H2 108.9

C3-C2-H2 108.2

C1-C2-H2 108.7

C24-C3-C4 111.2(3)

C24-C3-C2 111.7(3)

C4-C3-C2 110.5(3)

C24-C3-H3 108.5

C4-C3-H3 107.9

C2-C3-H3 107.0

C5-C4-C3 111.4(3)

C5-C4-H4A 110.7

C3-C4-H4A 109.6

C5-C4-H4B 108.1

C3-C4-H4B 108.7

H4A-C4-H4B 108.4

C4-C5-C6 111.0(3)

C4-C5-H5A 107.6

C6-C5-H5A 108.8

C4-C5-H5B 110.7

C6-C5-H5B 110.6

H5A-C5-H5B 108.1

C5-C6-C1 112.1(3)

C5-C6-H6A 109.0

C1-C6-H6A 107.6

C5-C6-H6B 109.4

C1-C6-H6B 110.5

H6A-C6-H6B 108.2

C8-C7-C1 115.3(3)

C8-C7-H7A 108.3

C1-C7-H7A 106.9

C8-C7-H7B 109.4

C1-C7-H7B 109.0

H7A-C7-H7B 107.8

O9-C8-C10 120.3(3)

O9-C8-C7 120.9(3)

C10-C8-C7 118.8(3)

C15-C10-C11 119.0(3)

C15-C10-C8 122.2(3)

C11-C10-C8 118.7(3)

C12-C11-C10 119.8(3)

C12-C11-H11 120.3

C10-C11-H11 119.9

C13-C12-C11 120.5(4)

C13-C12-H12 119.4

C11-C12-H12 120.0

C12-C13-C14 119.9(3)

C12-C13-H13 120.5

C14-C13-H13 119.6

C15-C14-C13 120.5(3)

C15-C14-H14 119.0

C13-C14-H14 120.4

C14-C15-C10 120.2(3)

C14-C15-H15 119.1

C10-C15-H15 120.7

O17-C16-C18 119.7(3)

O17-C16-C2 118.6(3)

C18-C16-C2 121.7(3)

C23-C18-C19 119.1(3)

C23-C18-C16 123.1(3)

C19-C18-C16 117.8(3)

C20-C19-C18 119.9(3)

C20-C19-H19 121.2

C18-C19-H19 118.9

C21-C20-C19 120.3(4)

C21-C20-H20 119.9

C19-C20-H20 119.8

C20-C21-C22 119.8(3)

C20-C21-H21 120.8

C22-C21-H21 119.4

C21-C22-C23 120.5(3)

C21-C22-H22 121.3

C23-C22-H22 118.2

C22-C23-C18 120.4(3)

C22-C23-H23 120.9

C18-C23-H23 118.7

C3-C24-H24A 111.3

C3-C24-H24B 108.4

H24A-C24-H24B 109.5

C3-C24-H24C 108.7

H24A-C24-H24C 109.5

H24B-C24-H24C 109.5

C6'-C1'-C7' 111.2(3)

C6'-C1'-C2' 111.0(3)

C7'-C1'-C2' 110.5(3)

C6'-C1'-H1' 107.8

C7'-C1'-H1' 108.7

C2'-C1'-H1' 107.5

C16'-C2'-C3' 108.9(3)

C16'-C2'-C1' 109.6(3)

C3'-C2'-C1' 111.2(3)

C16'-C2'-H2' 110.3

C3'-C2'-H2' 108.4

C1'-C2'-H2' 108.3

C4'-C3'-C24' 111.5(3)

C4'-C3'-C2' 110.8(3)

C24'-C3'-C2' 111.2(3)

C4'-C3'-H3' 107.5

C24'-C3'-H3' 108.3

C2'-C3'-H3' 107.4

C5'-C4'-C3' 112.0(3)

C5'-C4'-H4'A 109.7

C3'-C4'-H4'A 109.0

C5'-C4'-H4'B 109.3

C3'-C4'-H4'B 108.2

H4'A-C4'-H4'B 108.4

C4'-C5'-C6' 109.9(3)

C4'-C5'-H5'A 109.3

C6'-C5'-H5'A 108.0

C4'-C5'-H5'B 110.9

C6'-C5'-H5'B 110.3

H5'A-C5'-H5'B 108.3

C1'-C6'-C5' 112.2(3)

C1'-C6'-H6'A 108.0

C5'-C6'-H6'A 107.6

C1'-C6'-H6'B 109.9

C5'-C6'-H6'B 111.0

H6'A-C6'-H6'B 108.0

C8'-C7'-C1' 115.4(3)

C8'-C7'-H7'A 109.1

C1'-C7'-H7'A 108.2

C8'-C7'-H7'B 108.3

C1'-C7'-H7'B 108.0

H7'A-C7'-H7'B 107.6

O9'-C8'-C10' 119.7(3)

O9'-C8'-C7' 121.3(3)

C10'-C8'-C7' 119.0(3)

C11'-C10'-C15' 118.9(3)

C11'-C10'-C8' 119.2(3)

C15'-C10'-C8' 122.0(3)

C12'-C11'-C10' 120.3(3)

C12'-C11'-H11' 120.6

C10'-C11'-H11' 119.0

C11'-C12'-C13' 120.5(3)

C11'-C12'-H12' 119.1

C13'-C12'-H12' 120.4

C14'-C13'-C12' 119.6(4)

C14'-C13'-H13' 120.0

C12'-C13'-H13' 120.4

C13'-C14'-C15' 120.4(4)

C13'-C14'-H14' 119.5

C15'-C14'-H14' 120.1

C14'-C15'-C10' 120.3(3)

C14'-C15'-H15' 120.8

C10'-C15'-H15' 118.9

O17'-C16'-C18' 118.6(3)

O17'-C16'-C2' 118.3(3)

C18'-C16'-C2' 123.1(3)

C19'-C18'-C23' 118.8(3)

C19'-C18'-C16' 118.7(3)

C23'-C18'-C16' 122.4(3)

C20'-C19'-C18' 121.3(3)

C20'-C19'-H19' 120.0

C18'-C19'-H19' 118.7

C19'-C20'-C21' 119.5(4)

C19'-C20'-H20' 119.9

C21'-C20'-H20' 120.6

C22'-C21'-C20' 120.6(3)

C22'-C21'-H21' 119.8

C20'-C21'-H21' 119.6

C21'-C22'-C23' 119.8(4)

C21'-C22'-H22' 119.8

C23'-C22'-H22' 120.4

C18'-C23'-C22' 120.0(4)

C18'-C23'-H23' 119.6

C22'-C23'-H23' 120.4

C3'-C24'-H24D 110.8

C3'-C24'-H24E 108.5

H24D-C24'-H24E 109.5

C3'-C24'-H24F 109.1

H24D-C24'-H24F 109.5

H24E-C24'-H24F 109.5

Table A.4. Anisotropic displacement parameters ($Å^2 \times 10^3$) for 4.2e. The anisotropic displacement factor exponent takes the form: $-2\pi^2[ h^2 a^{*2} U_{11} + ... + 2 h k a^* b^* U_{12} ]$

| | $U_{11}$ | $U_{22}$ | $U_{33}$ | $U_{23}$ | $U_{13}$ | $U_{12}$ |
|---|---|---|---|---|---|---|
| C1 | 24(2) | 22(2) | 23(2) | -1(1) | 3(2) | -2(2) |
| C2 | 27(2) | 24(2) | 21(2) | 3(2) | 0(2) | -2(2) |
| C3 | 31(2) | 24(2) | 28(2) | 0(2) | 3(2) | -2(2) |
| C4 | 26(2) | 30(2) | 43(3) | -1(2) | 5(2) | 6(2) |
| C5 | 22(2) | 39(2) | 36(2) | 2(2) | -2(2) | -1(2) |
| C6 | 30(2) | 38(2) | 29(2) | -2(2) | -2(2) | -3(2) |
| C7 | 29(2) | 29(2) | 23(2) | 1(2) | 1(2) | -3(2) |
| C8 | 32(2) | 22(2) | 25(2) | 2(2) | -3(2) | 3(2) |
| O9 | 39(2) | 28(1) | 40(2) | -5(1) | 8(1) | -8(1) |
| C10 | 27(2) | 22(2) | 20(2) | 3(2) | -1(2) | 3(2) |
| C11 | 31(2) | 32(2) | 25(2) | -2(2) | -2(2) | 1(2) |
| C12 | 36(2) | 37(2) | 28(2) | -4(2) | 0(2) | 7(2) |
| C13 | 32(2) | 43(2) | 25(2) | 3(2) | 2(2) | 2(2) |
| C14 | 27(2) | 37(2) | 44(3) | 0(2) | 2(2) | 2(2) |
| C15 | 33(2) | 26(2) | 31(2) | 0(2) | 1(2) | 1(2) |
| C16 | 32(2) | 21(2) | 20(2) | -3(2) | 3(2) | 3(2) |
| O17 | 38(2) | 32(2) | 31(2) | 7(1) | -1(1) | -1(1) |
| C18 | 24(2) | 25(2) | 25(2) | -2(2) | 4(2) | 4(2) |
| C19 | 34(2) | 35(2) | 26(2) | 2(2) | -1(2) | -1(2) |
| C20 | 35(2) | 39(2) | 26(2) | -3(2) | -1(2) | 3(2) |
| C21 | 26(2) | 35(2) | 32(2) | -4(2) | -4(2) | -2(2) |

C22 34(2)  29(2) 37(2)  2(2) -2(2)  -9(2)

C23 29(2)  32(2) 27(2)  0(2) -2(2)  0(2)

C24 36(2)  29(2) 37(2)  -4(2) 3(2)  -1(2)

C1' 28(2)  23(2) 21(2)  -1(1) 0(2)  0(2)

C2' 22(2)  25(2) 24(2)  -2(2) 2(2)  2(2)

C3' 28(2)  27(2) 30(2)  0(2) 4(2)  -2(2)

C4' 30(2)  28(2) 36(2)  0(2) -3(2)  0(2)

C5' 29(2)  31(2) 37(2)  1(2) -8(2)  -2(2)

C6' 31(2)  29(2) 27(2)  3(2) -6(2)  2(2)

C7' 24(2)  29(2) 22(2)  0(2) -2(2)  0(2)

C8' 32(2)  23(2) 20(2)  -5(2) 1(2)  -1(2)

O9' 37(2)  31(1) 41(2)  2(1) 9(1)  8(1)

C10' 29(2)  23(2) 23(2)  -3(2) -2(2)  -3(2)

C11' 34(2)  28(2) 24(2)  0(2) -6(2)  1(2)

C12' 38(2)  35(2) 27(2)  3(2) 0(2)  -5(2)

C13' 33(2)  41(2) 32(2)  -1(2) 5(2)  -5(2)

C14' 31(2)  36(2) 37(3)  1(2) 8(2)  4(2)

C15' 34(2)  32(2) 29(2)  4(2) 4(2)  3(2)

C16' 28(2)  29(2) 20(2)  0(2) 6(2)  0(2)

O17' 40(2)  31(1) 34(2)  -9(1) -5(1)  6(1)

C18' 31(2)  23(2) 21(2)  2(2) 1(2)  -2(2)

C19' 32(2)  35(2) 27(2)  2(2) 1(2)  -2(2)

C20' 31(2)  46(3) 31(3)  6(2) -5(2)  0(2)

C21' 31(2)  42(2) 43(3)  16(2) 1(2)  4(2)

C22' 31(2)  31(2) 43(3)  -2(2) 3(2)  -3(2)

C23' 30(2)  30(2) 35(3)  -4(2) -6(2)  1(2)

C24' 37(2)  39(2) 38(2)  9(2) 3(2)  -6(2)

Table A.5. Hydrogen coordinates ( x $10^4$) and isotropic displacement parameters ($Å^2$x $10^3$) for 4.2e.

| | x | y | z | U(eq) |
|---|---|---|---|---|
| H1 | 7583 | 4053 | 3695 | 28 |
| H2 | 7348 | -940 | 3607 | 29 |
| H3 | 8468 | 1779 | 3224 | 33 |
| H4A | 9460 | -315 | 3538 | 40 |
| H4B | 8815 | -1672 | 3761 | 40 |
| H5A | 9058 | 3273 | 3811 | 39 |
| H5B | 9307 | 1492 | 4119 | 39 |
| H6A | 7963 | 560 | 4217 | 39 |
| H6B | 8103 | 3296 | 4276 | 39 |
| H7A | 6586 | 1234 | 4123 | 33 |
| H7B | 6261 | 2573 | 3782 | 33 |
| H11 | 6028 | 8063 | 4696 | 36 |
| H12 | 4862 | 8271 | 5048 | 40 |
| H13 | 3892 | 5328 | 4987 | 40 |
| H14 | 4051 | 2235 | 4555 | 43 |
| H15 | 5202 | 1914 | 4218 | 36 |
| H19 | 5952 | 1609 | 2648 | 38 |
| H20 | 4862 | -792 | 2473 | 40 |
| H21 | 4533 | -4206 | 2820 | 37 |
| H22 | 5261 | -5119 | 3349 | 40 |

H23 6344 -2770 3515 35

H24A 7986 -1406 2858 51

H24B 8885 -1754 2948 51

H24C 8244 -3206 3166 51

H1' 4415 8944 6259 29

H2' 4665 3976 6336 28

H3' 3542 6703 6723 34

H4'A 2553 4680 6410 37

H4'B 3189 3269 6188 37

H5'A 2959 8264 6130 39

H5'B 2706 6454 5826 39

H6'A 4034 5460 5737 35

H6'B 3932 8201 5669 35

H7'A 5454 6180 5827 30

H7'B 5749 7569 6169 30

H11' 5958 12983 5249 35

H12' 7117 13287 4900 40

H13' 8143 10459 4978 43

H14' 7964 7216 5375 41

H15' 6800 6922 5730 38

H19' 6104 6777 7279 37

H20' 7163 4412 7482 43

H21' 7489 875 7164 47

H22' 6762 -295 6650 42

H23' 5685 2095 6448 38

H24D 3129 3093 7000 58

H24E 3787 1727 6780 58

H24F 4023 3578 7085 58

Table A.6. Torsion angles [°] for 4.2e.

C6-C1-C2-C16 -174.1(3)

C7-C1-C2-C16 62.4(4)

C6-C1-C2-C3 -53.2(4)

C7-C1-C2-C3 -176.7(3)

C16-C2-C3-C24 -59.9(4)

C1-C2-C3-C24 178.3(3)

C16-C2-C3-C4 175.8(3)

C1-C2-C3-C4 54.0(4)

C24-C3-C4-C5 179.7(3)

C2-C3-C4-C5 -55.7(4)

C3-C4-C5-C6 57.3(4)

C4-C5-C6-C1 -56.9(4)

C7-C1-C6-C5 177.3(3)

C2-C1-C6-C5 54.2(4)

C6-C1-C7-C8 70.0(4)

C2-C1-C7-C8 -167.1(3)

C1-C7-C8-O9 9.1(5)

C1-C7-C8-C10 -172.0(3)

O9-C8-C10-C15 172.2(3)

C7-C8-C10-C15 -6.8(5)

O9-C8-C10-C11 -7.3(5)

C7-C8-C10-C11 173.8(3)

C15-C10-C11-C12 0.7(5)

C8-C10-C11-C12 -179.8(3)

C10-C11-C12-C13 -0.2(6)

C11-C12-C13-C14 -0.9(6)

C12-C13-C14-C15 1.6(6)

C13-C14-C15-C10 -1.1(6)

C11-C10-C15-C14 -0.1(5)

C8-C10-C15-C14 -179.5(3)

C3-C2-C16-O17 -61.2(4)

C1-C2-C16-O17 62.1(4)

C3-C2-C16-C18 119.3(3)

C1-C2-C16-C18 -117.3(3)

O17-C16-C18-C23 -173.0(3)

C2-C16-C18-C23 6.5(5)

O17-C16-C18-C19 7.3(5)

C2-C16-C18-C19 -173.3(3)

C23-C18-C19-C20 -0.7(5)

C16-C18-C19-C20 179.1(3)

C18-C19-C20-C21 0.1(6)

C19-C20-C21-C22 0.1(6)

C20-C21-C22-C23 0.4(6)

C21-C22-C23-C18 -1.0(6)

C19-C18-C23-C22 1.1(5)

C16-C18-C23-C22 -178.6(3)

C6'-C1'-C2'-C16' -173.9(3)

C7'-C1'-C2'-C16' 62.2(4)

C6'-C1'-C2'-C3' -53.4(4)

C7'-C1'-C2'-C3' -177.2(3)

C16'-C2'-C3'-C4' 174.6(3)

C1'-C2'-C3'-C4' 53.6(4)

C16'-C2'-C3'-C24' -60.8(4)

C1'-C2'-C3'-C24' 178.2(3)

C24'-C3'-C4'-C5' 179.5(3)

C2'-C3'-C4'-C5' -56.2(4)

C3'-C4'-C5'-C6' 57.3(4)

C7'-C1'-C6'-C5' 179.0(3)

C2'-C1'-C6'-C5' 55.6(4)

C4'-C5'-C6'-C1' -57.1(4)

C6'-C1'-C7'-C8' 69.9(4)

C2'-C1'-C7'-C8' -166.4(3)

C1'-C7'-C8'-O9' 8.4(5)

C1'-C7'-C8'-C10' -171.8(3)

O9'-C8'-C10'-C11' -7.7(5)

C7'-C8'-C10'-C11' 172.5(3)

O9'-C8'-C10'-C15' 172.3(3)

C7'-C8'-C10'-C15' -7.4(5)

C15'-C10'-C11'-C12' 0.0(5)

C8'-C10'-C11'-C12' -180.0(3)

C10'-C11'-C12'-C13' -0.2(6)

C11'-C12'-C13'-C14' 0.6(6)

C12'-C13'-C14'-C15' -0.9(6)

C13'-C14'-C15'-C10' 0.7(6)

C11'-C10'-C15'-C14' -0.2(5)

C8'-C10'-C15'-C14' 179.8(4)

C3'-C2'-C16'-O17' -59.4(4)

C1'-C2'-C16'-O17' 62.5(4)

C3'-C2'-C16'-C18' 119.9(3)

C1'-C2'-C16'-C18' -118.2(3)

O17'-C16'-C18'-C19' 3.5(5)

C2'-C16'-C18'-C19' -175.7(3)

O17'-C16'-C18'-C23' -177.2(3)

C2'-C16'-C18'-C23' 3.5(5)

C23'-C18'-C19'-C20' -1.5(6)

C16'-C18'-C19'-C20' 177.8(3)

C18'-C19'-C20'-C21' 0.7(6)

C19'-C20'-C21'-C22' 0.4(6)

C20'-C21'-C22'-C23' -0.5(6)

C19'-C18'-C23'-C22' 1.3(5)

C16'-C18'-C23'-C22' -178.0(3)

C21'-C22'-C23'-C18' -0.3(6)

---

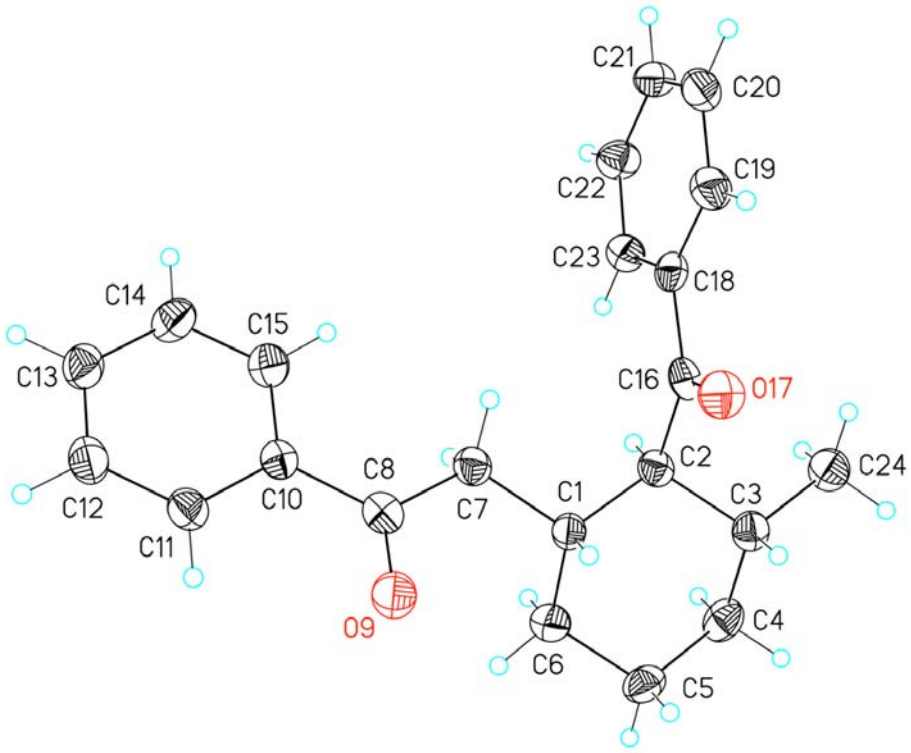


Figure A.1. View of molecule 1 in **4.2e** showing the atom labeling scheme. Displacement ellipsoids are scaled to the 50% probability level.

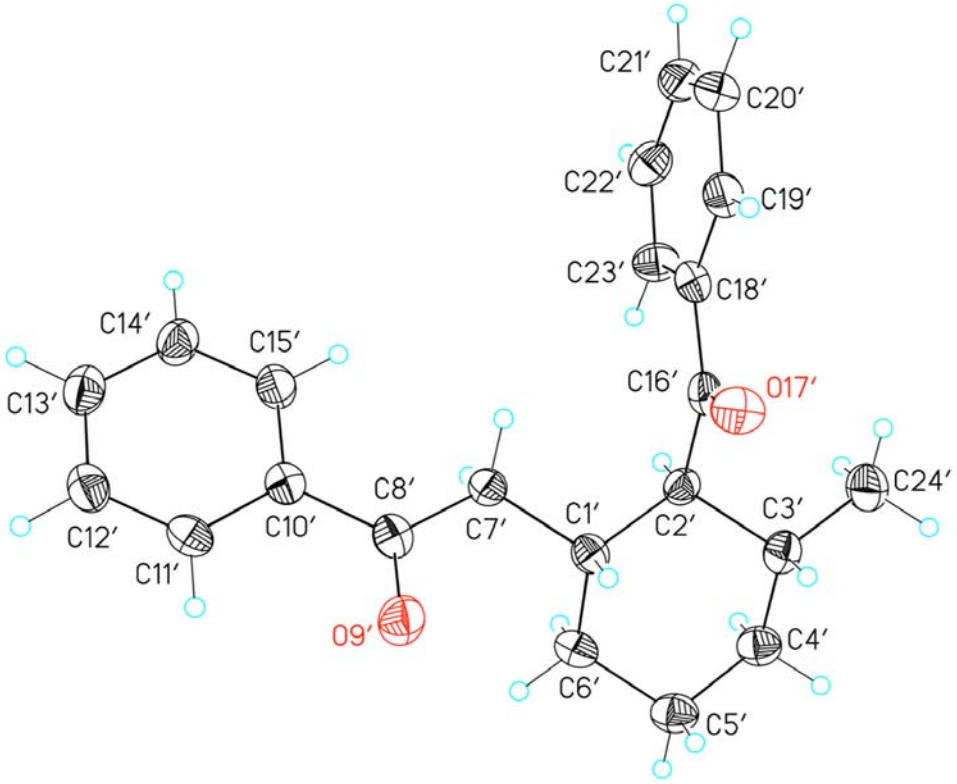


Figure A.2. View of molecule 2 in **4.2e** showing the atom labeling scheme. Displacement ellipsoids are scaled to the 50% probability level.

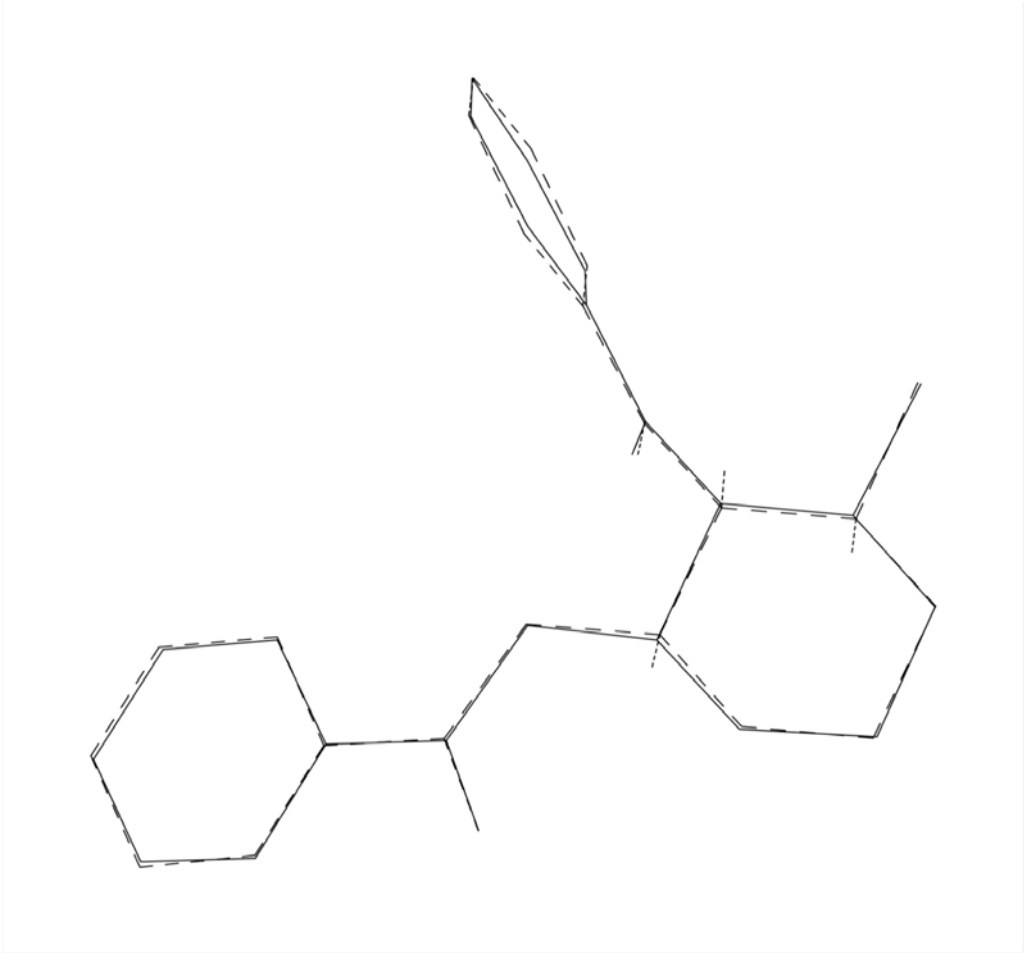

Figure A.3. Fit by least-squares of selected atoms of molecule 1 (solid lines) onto the equivalent atoms of molecule 2 (dashed lines). The atoms of molecule 1 used in the fit are labeled.

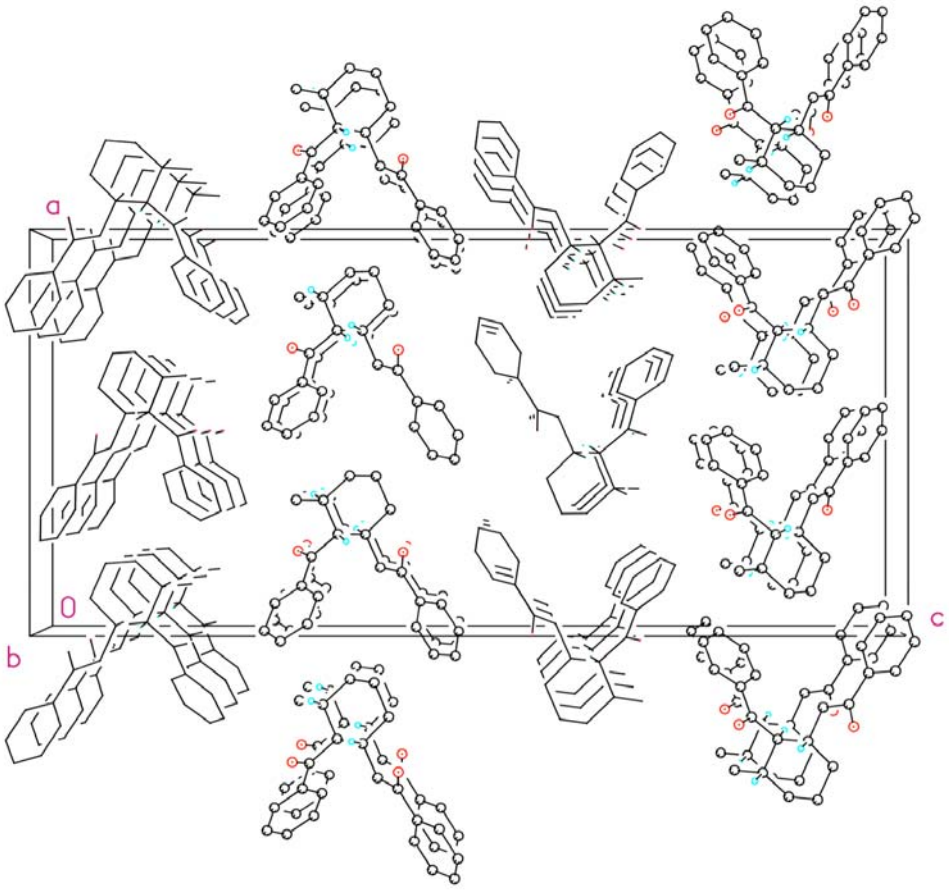


Figure A.4. Unit cell packing diagram for **4.2e**. The view is approximately down the **b** axis. Molecules 1 are shown in ball-and-stick form while molecules 2 are in wire frame form.

# Appendix B (Crystallographic Material for 5.2a-Cl)

## X-RAY EXPERIMENTAL

Table B.1. Crystallographic Data for **5.2a-Cl**.

Table B.2. Fractional coordinates and equivalent isotropic thermal parameters ($Å^2$) for the non-hydrogen atoms of **5.2a-Cl**.

Table B.3. Bond Lengths (Å) and Angles ($^o$) for the non-hydrogen atoms of **5.2a-Cl**.

Table B.4. Anisotropic thermal parameters for the non-hydrogen atoms of **5.2a-Cl**.

Table B.5. Fractional coordinates and isotropic thermal parameters ($Å^2$) for the hydrogen atoms of **5.2a-Cl**.

Table B.6. Torsion Angles ($^o$) for the non-hydrogen atoms of **5.2a-Cl**.

Table B.7. Observed and calculated structure factor amplitudes for **5.2a-Cl**. Values for Fo, Fc and $\sigma$(Fo) have been multiplied by 10.

Figure B.1. View of molecule 1 of **5.2a-Cl** showing the atom labeling scheme. Displacement ellipsoids are scaled to the 50% probability level.

Figure B.2. View of molecule 2 of **5.2a-Cl** showing the atom labeling scheme. Displacement ellipsoids are scaled to the 50% probability level.

Figure B.3. View of the fit by least-squares of selected atoms from molecule 1 (dashed lines) onto the equivalent atoms of molecule 2 (solid lines). The atoms from molecule 2 used in the fit are labeled.

Table B.7. Observed and calculated structure factor amplitudes for **5.2a-Cl**. Values for Fo, Fc and σ(Fo) have been multiplied by 10.

X-ray Experimental for $C_{19}H_{12}N_2O_6Cl_2$: Crystals grew as colorless plates by slow evaporation from dichloromethane. The data crystal was cut from a larger crystal and had approximate dimensions; 0.20 x 0.15 x 0.12 mm. The data were collected on a Nonius Kappa CCD diffractometer using a graphite monochromator with MoKα radiation (λ = 0.71073Å). A total of 218 frames of data were collected using ω-scans with a scan range of 2° and a counting time of 70 seconds per frame. The data were collected at 153 K using an Oxford Cryostream low temperature device. Details of crystal data, data collection and structure refinement are listed in Table 1. Data reduction were performed using DENZO-SMN.[1] The structure was solved by direct methods using SIR97[2] and refined by full-matrix least-squares on $F^2$ with anisotropic displacement parameters for the non-H atoms using SHELXL-97.[3] The hydrogen atoms on carbon were calculated in ideal positions with isotropic displacement parameters set to 1.2xUeq of the attached atom (1.5xUeq for methyl hydrogen atoms). The function, $\Sigma w(|F_o|^2 - |F_c|^2)^2$, was minimized, where $w = 1/[(\sigma(F_o))^2 + (0.0163*P)^2 + (0.4186*P)]$ and $P = (|F_o|^2 + 2|F_c|^2)/3$. $R_w(F^2)$ refined to 0.0831, with R(F) equal to 0.0390 and a goodness of fit, S, = 1.05. Definitions used for calculating R(F), $R_w(F^2)$ and the goodness of fit, S, are given below.[4] The data were checked for secondary extinction effects but no correction was necessary. Neutral atom scattering factors and values used to calculate the linear absorption coefficient are from the International Tables for X-ray Crystallography (1992).[5] All figures were generated using SHELXTL/PC.[6] Tables of positional and thermal parameters, bond lengths and angles, torsion angles, figures and lists of observed and calculated structure factors are located in tables 1 through 7.

**References**


1) DENZO-SMN. (1997). Z. Otwinowski and W. Minor, Methods in Enzymology, **276**: Macromolecular Crystallography, part A, 307 – 326, C. W. Carter, Jr. and R. M. Sweets, Editors, Academic Press.

2) SIR97. (1999). A program for crystal structure solution. Altomare A., Burla M.C., Camalli M., Cascarano G.L., Giacovazzo C. , Guagliardi A., Moliterni A.G.G., Polidori G.,Spagna R. J. Appl. Cryst. 32, 115-119.

3) Sheldrick, G. M. (1994). SHELXL97. Program for the Refinement of Crystal Structures. University of Gottingen, Germany.

4) $R_w(F^2) = \{\Sigma w(|F_o|^2 - |F_c|^2)^2/\Sigma w(|F_o|)^4\}^{1/2}$ where w is the weight given each reflection.
$R(F) = \Sigma(|F_o| - |F_c|)/\Sigma|F_o|\}$ for reflections with $F_o > 4(\sigma(F_o))$.
$S = [\Sigma w(|F_o|^2 - |F_c|^2)^2/(n - p)]^{1/2}$, where n is the number of reflections and p is the number of refined parameters.

5) International Tables for X-ray Crystallography (1992). Vol. C, Tables 4.2.6.8 and 6.1.1.4, A. J. C. Wilson, editor, Boston: Kluwer Academic Press.

6) Sheldrick, G. M. (1994). SHELXTL/PC (Version 5.03). Siemens Analytical X-ray Instruments, Inc., Madison, Wisconsin, USA.

Table B.1. Crystal data and structure refinement for **5.2a-Cl**.

| | | |
|---|---|---|
| Empirical formula | C19 H12 Cl2 N2 O6 | |
| Formula weight | 435.21 | |
| Temperature | 153(2) K | |
| Wavelength | 0.71070 Å | |
| Crystal system | Triclinic | |
| Space group | P1 | |
| Unit cell dimensions | a = 7.8573(6) Å | $\alpha$= 98.224(3)°. |
| | b = 9.2391(7) Å | $\beta$= 98.324(3)°. |
| | c = 14.0284(14) Å | $\gamma$ = 111.640(3)°. |
| Volume | 915.02(13) Å$^3$ | |
| Z | 2 | |
| Density (calculated) | 1.580 Mg/m$^3$ | |
| Absorption coefficient | 0.397 mm$^{-1}$ | |
| F(000) | 444 | |
| Crystal size | 0.20 x 0.15 x 0.12 mm | |
| Theta range for data collection | 1.50 to 27.50°. | |
| Index ranges | -9<=h<=10, -10<=k<=11, -17<=l<=18 | |
| Reflections collected | 6316 | |
| Independent reflections | 6316 | |
| Completeness to theta = 27.50° | 97.3 % | |
| Absorption correction | Semi-empirical from equivalents | |
| Max. and min. transmission | 0.957 and 0.883 | |
| Refinement method | Full-matrix least-squares on F$^2$ | |
| Data / restraints / parameters | 6316 / 3 / 523 | |
| Goodness-of-fit on F$^2$ | 1.049 | |
| Final R indices [I>2sigma(I)] | R1 = 0.0390, wR2 = 0.0787 | |
| R indices (all data) | R1 = 0.0499, wR2 = 0.0831 | |
| Absolute structure parameter | -0.06(4) | |
| Largest diff. peak and hole | 0.301 and -0.286 e.Å$^{-3}$ | |

Table B.2. Atomic coordinates ( x $10^4$) and equivalent isotropic displacement parameters ($Å^2$x$10^3$) for **5.2a-Cl**. U(eq) is defined as one third of the trace of the orthogonalized $U^{ij}$ tensor.

| | x | y | z | U(eq) |
|---|---|---|---|---|
| Cl1A | 8136(1) | 6375(1) | -1195(1) | 38(1) |
| Cl2A | 4493(1) | 6816(1) | -2045(1) | 46(1) |
| O1A | 5563(3) | 3695(3) | 2077(2) | 32(1) |
| O2A | 280(3) | 4353(3) | 766(2) | 35(1) |
| O3A | 4063(4) | 8663(3) | 6309(2) | 50(1) |
| O4A | 2186(4) | 9336(3) | 5373(2) | 48(1) |
| O5A | -1554(4) | -678(3) | 983(2) | 68(1) |
| O6A | 1398(3) | 74(3) | 1791(2) | 33(1) |
| N1A | 2683(3) | 3805(3) | 1597(2) | 25(1) |
| N2A | 2962(4) | 8443(3) | 5537(2) | 32(1) |
| C2A | 4523(4) | 4016(4) | 1518(2) | 25(1) |
| C3A | 4814(4) | 4695(4) | 615(2) | 24(1) |
| C4A | 6371(4) | 5135(4) | 196(2) | 26(1) |
| C5A | 6238(5) | 5801(4) | -631(2) | 29(1) |
| C6A | 4627(5) | 5998(4) | -1012(2) | 30(1) |
| C7A | 3071(5) | 5535(4) | -585(2) | 28(1) |
| C8A | 3220(4) | 4883(4) | 227(2) | 25(1) |
| C9A | 1820(4) | 4332(4) | 858(2) | 27(1) |
| C10A | 1911(4) | 3208(4) | 2433(2) | 25(1) |
| C11A | 2084(4) | 4562(3) | 3246(2) | 23(1) |
| C12A | 3057(4) | 4712(4) | 4193(2) | 26(1) |
| C13A | 3326(4) | 5957(4) | 4951(2) | 28(1) |
| C14A | 2615(4) | 7062(4) | 4756(2) | 26(1) |
| C15A | 1596(4) | 6936(4) | 3837(2) | 30(1) |
| C16A | 1333(4) | 5682(4) | 3080(2) | 30(1) |
| C17A | -25(4) | 1886(4) | 2066(2) | 27(1) |
| C18A | -1599(5) | 2015(4) | 2192(3) | 36(1) |
| C19A | -165(5) | 311(4) | 1544(3) | 34(1) |
| C20A | 1270(5) | -1503(4) | 1364(3) | 41(1) |

| | | | | |
|---|---|---|---|---|
| Cl1 | 4691(1) | -9(1) | 10065(1) | 48(1) |
| Cl2 | 1312(1) | 729(1) | 9167(1) | 33(1) |
| O1 | 9583(3) | 2750(3) | 7558(2) | 34(1) |
| O2 | 4463(3) | 3445(3) | 6049(2) | 31(1) |
| O3 | 7979(4) | -2375(3) | 2869(2) | 54(1) |
| O4 | 5191(4) | -2486(3) | 2373(2) | 55(1) |
| O5 | 9843(3) | 6877(3) | 6987(2) | 40(1) |
| O6 | 7871(3) | 7526(2) | 5978(2) | 37(1) |
| N1 | 7289(3) | 3269(3) | 6632(2) | 25(1) |
| N2 | 6745(5) | -1881(3) | 2921(2) | 41(1) |
| C2 | 8043(4) | 2750(4) | 7416(2) | 26(1) |
| C3 | 6537(4) | 2188(4) | 7972(2) | 24(1) |
| C4 | 6486(5) | 1460(4) | 8768(2) | 30(1) |
| C5 | 4844(5) | 994(4) | 9108(2) | 28(1) |
| C6 | 3314(4) | 1295(4) | 8688(2) | 26(1) |
| C7 | 3379(4) | 2028(3) | 7884(2) | 22(1) |
| C8 | 5000(4) | 2437(3) | 7529(2) | 22(1) |
| C9 | 5449(4) | 3121(4) | 6646(2) | 25(1) |
| C10 | 8356(4) | 3720(4) | 5856(2) | 26(1) |
| C11 | 7919(4) | 2245(3) | 5076(2) | 26(1) |
| C12 | 9328(5) | 1710(4) | 4951(2) | 31(1) |
| C13 | 8949(5) | 344(4) | 4259(3) | 33(1) |
| C14 | 7158(5) | -449(4) | 3690(2) | 30(1) |
| C15 | 5726(5) | 43(4) | 3800(3) | 34(1) |
| C16 | 6123(4) | 1385(4) | 4505(2) | 32(1) |
| C17 | 8089(4) | 5088(3) | 5463(2) | 26(1) |
| C18 | 7598(4) | 5087(4) | 4522(3) | 32(1) |
| C19 | 8703(4) | 6580(4) | 6234(2) | 29(1) |
| C20 | 8473(6) | 9035(4) | 6656(3) | 43(1) |

Table B.3. Bond lengths [Å] and angles [°] for **5.2a-Cl**.

| | | | |
|---|---|---|---|
| Cl1A-C5A | 1.735(3) | C14A-C15A | 1.380(4) |
| Cl2A-C6A | 1.735(3) | C15A-C16A | 1.386(5) |
| O1A-C2A | 1.197(4) | C15A-H15A | 0.95 |
| O2A-C9A | 1.206(4) | C16A-H16A | 0.95 |
| O3A-N2A | 1.225(4) | C17A-C18A | 1.320(4) |
| O4A-N2A | 1.221(3) | C17A-C19A | 1.490(5) |
| O5A-C19A | 1.206(4) | C18A-H18A | 0.95 |
| O6A-C19A | 1.332(4) | C18A-H18B | 0.95 |
| O6A-C20A | 1.455(4) | C20A-H20A | 0.98 |
| N1A-C9A | 1.398(4) | C20A-H20B | 0.98 |
| N1A-C2A | 1.409(4) | C20A-H20C | 0.98 |
| N1A-C10A | 1.480(4) | Cl1-C5 | 1.730(3) |
| N2A-C14A | 1.469(4) | Cl2-C6 | 1.732(3) |
| C2A-C3A | 1.502(4) | O1-C2 | 1.197(3) |
| C3A-C8A | 1.373(4) | O2-C9 | 1.202(3) |
| C3A-C4A | 1.384(4) | O3-N2 | 1.221(4) |
| C4A-C5A | 1.396(4) | O4-N2 | 1.223(4) |
| C4A-H4A | 0.95 | O5-C19 | 1.206(4) |
| C5A-C6A | 1.387(4) | O6-C19 | 1.327(4) |
| C6A-C7A | 1.391(4) | O6-C20 | 1.441(4) |
| C7A-C8A | 1.373(4) | N1-C2 | 1.401(4) |
| C7A-H7A | 0.95 | N1-C9 | 1.405(4) |
| C8A-C9A | 1.500(4) | N1-C10 | 1.483(4) |
| C10A-C17A | 1.514(4) | N2-C14 | 1.481(4) |
| C10A-C11A | 1.518(4) | C2-C3 | 1.486(4) |
| C10A-H10A | 1.00 | C3-C4 | 1.382(4) |
| C11A-C12A | 1.394(4) | C3-C8 | 1.388(4) |
| C11A-C16A | 1.397(4) | C4-C5 | 1.380(5) |
| C12A-C13A | 1.380(4) | C4-H4 | 0.95 |
| C12A-H12A | 0.95 | C5-C6 | 1.399(4) |
| C13A-C14A | 1.373(4) | C6-C7 | 1.394(4) |
| C13A-H13A | 0.95 | C7-C8 | 1.377(4) |

| | | | |
|---|---|---|---|
| C7-H7 | 0.95 | C14-C15 | 1.380(4) |
| C8-C9 | 1.498(4) | C15-C16 | 1.373(5) |
| C10-C11 | 1.514(4) | C15-H15 | 0.95 |
| C10-C17 | 1.519(4) | C16-H16 | 0.95 |
| C10-H10 | 1.00 | C17-C18 | 1.320(4) |
| C11-C16 | 1.388(4) | C17-C19 | 1.495(4) |
| C11-C12 | 1.392(4) | C18-H18C | 0.95 |
| C12-C13 | 1.383(5) | C18-H18D | 0.95 |
| C12-H12 | 0.95 | C20-H20D | 0.98 |
| C13-C14 | 1.379(5) | C20-H20E | 0.98 |
| C13-H13 | 0.95 | C20-H20F | 0.98 |

| | | | |
|---|---|---|---|
| C19A-O6A-C20A | 114.5(3) | C6A-C7A-H7A | 121.7 |
| C9A-N1A-C2A | 112.0(2) | C7A-C8A-C3A | 122.6(3) |
| C9A-N1A-C10A | 126.8(2) | C7A-C8A-C9A | 128.8(3) |
| C2A-N1A-C10A | 121.0(2) | C3A-C8A-C9A | 108.5(3) |
| O4A-N2A-O3A | 123.4(3) | O2A-C9A-N1A | 126.6(3) |
| O4A-N2A-C14A | 118.5(3) | O2A-C9A-C8A | 127.8(3) |
| O3A-N2A-C14A | 118.0(3) | N1A-C9A-C8A | 105.7(3) |
| O1A-C2A-N1A | 124.6(3) | N1A-C10A-C17A | 110.5(2) |
| O1A-C2A-C3A | 130.1(3) | N1A-C10A-C11A | 111.6(2) |
| N1A-C2A-C3A | 105.3(2) | C17A-C10A-C11A | 116.0(2) |
| C8A-C3A-C4A | 121.6(3) | N1A-C10A-H10A | 106.0 |
| C8A-C3A-C2A | 108.5(3) | C17A-C10A-H10A | 106.0 |
| C4A-C3A-C2A | 129.9(3) | C11A-C10A-H10A | 106.0 |
| C3A-C4A-C5A | 116.4(3) | C12A-C11A-C16A | 118.5(3) |
| C3A-C4A-H4A | 121.8 | C12A-C11A-C10A | 118.8(2) |
| C5A-C4A-H4A | 121.8 | C16A-C11A-C10A | 122.7(3) |
| C6A-C5A-C4A | 121.6(3) | C13A-C12A-C11A | 121.3(3) |
| C6A-C5A-Cl1A | 119.7(2) | C13A-C12A-H12A | 119.3 |
| C4A-C5A-Cl1A | 118.8(2) | C11A-C12A-H12A | 119.3 |
| C5A-C6A-C7A | 121.2(3) | C14A-C13A-C12A | 118.6(3) |
| C5A-C6A-Cl2A | 120.6(2) | C14A-C13A-H13A | 120.7 |
| C7A-C6A-Cl2A | 118.1(2) | C12A-C13A-H13A | 120.7 |
| C8A-C7A-C6A | 116.6(3) | C13A-C14A-C15A | 122.0(3) |
| C8A-C7A-H7A | 121.7 | C13A-C14A-N2A | 119.7(3) |

| | | | |
|---|---|---|---|
| C15A-C14A-N2A | 118.2(3) | C5-C4-H4 | 121.4 |
| C14A-C15A-C16A | 118.9(3) | C3-C4-H4 | 121.4 |
| C14A-C15A-H15A | 120.5 | C4-C5-C6 | 121.6(3) |
| C16A-C15A-H15A | 120.5 | C4-C5-Cl1 | 118.5(2) |
| C15A-C16A-C11A | 120.5(3) | C6-C5-Cl1 | 120.0(2) |
| C15A-C16A-H16A | 119.8 | C7-C6-C5 | 120.7(3) |
| C11A-C16A-H16A | 119.8 | C7-C6-Cl2 | 119.8(2) |
| C18A-C17A-C19A | 117.4(3) | C5-C6-Cl2 | 119.5(2) |
| C18A-C17A-C10A | 124.8(3) | C8-C7-C6 | 117.2(3) |
| C19A-C17A-C10A | 117.8(3) | C8-C7-H7 | 121.4 |
| C17A-C18A-H18A | 120.0 | C6-C7-H7 | 121.4 |
| C17A-C18A-H18B | 120.0 | C7-C8-C3 | 121.7(3) |
| H18A-C18A-H18B | 120.0 | C7-C8-C9 | 130.0(3) |
| O5A-C19A-O6A | 122.8(3) | C3-C8-C9 | 108.2(3) |
| O5A-C19A-C17A | 124.5(3) | O2-C9-N1 | 126.0(3) |
| O6A-C19A-C17A | 112.6(3) | O2-C9-C8 | 128.7(3) |
| O6A-C20A-H20A | 109.5 | N1-C9-C8 | 105.2(2) |
| O6A-C20A-H20B | 109.5 | N1-C10-C11 | 109.3(2) |
| H20A-C20A-H20B | 109.5 | N1-C10-C17 | 112.3(2) |
| O6A-C20A-H20C | 109.5 | C11-C10-C17 | 114.8(2) |
| H20A-C20A-H20C | 109.5 | N1-C10-H10 | 106.6 |
| H20B-C20A-H20C | 109.5 | C11-C10-H10 | 106.6 |
| C19-O6-C20 | 115.3(3) | C17-C10-H10 | 106.6 |
| C2-N1-C9 | 112.2(3) | C16-C11-C12 | 119.3(3) |
| C2-N1-C10 | 119.5(2) | C16-C11-C10 | 121.3(3) |
| C9-N1-C10 | 127.9(2) | C12-C11-C10 | 119.4(3) |
| O3-N2-O4 | 124.2(3) | C13-C12-C11 | 120.4(3) |
| O3-N2-C14 | 118.0(3) | C13-C12-H12 | 119.8 |
| O4-N2-C14 | 117.8(3) | C11-C12-H12 | 119.8 |
| O1-C2-N1 | 124.6(3) | C14-C13-C12 | 118.4(3) |
| O1-C2-C3 | 129.6(3) | C14-C13-H13 | 120.8 |
| N1-C2-C3 | 105.8(2) | C12-C13-H13 | 120.8 |
| C4-C3-C8 | 121.5(3) | C13-C14-C15 | 122.7(3) |
| C4-C3-C2 | 130.0(3) | C13-C14-N2 | 119.1(3) |
| C8-C3-C2 | 108.5(3) | C15-C14-N2 | 118.2(3) |
| C5-C4-C3 | 117.2(3) | C16-C15-C14 | 118.0(3) |

| | | | |
|---|---|---|---|
| C16-C15-H15 | 121.0 | H18C-C18-H18D | 120.0 |
| C14-C15-H15 | 121.0 | O5-C19-O6 | 125.0(3) |
| C15-C16-C11 | 121.2(3) | O5-C19-C17 | 123.0(3) |
| C15-C16-H16 | 119.4 | O6-C19-C17 | 111.9(3) |
| C11-C16-H16 | 119.4 | O6-C20-H20D | 109.5 |
| C18-C17-C19 | 120.6(3) | O6-C20-H20E | 109.5 |
| C18-C17-C10 | 125.2(3) | H20D-C20-H20E | 109.5 |
| C19-C17-C10 | 113.7(3) | O6-C20-H20F | 109.5 |
| C17-C18-H18C | 120.0 | H20D-C20-H20F | 109.5 |
| C17-C18-H18D | 120.0 | H20E-C20-H20F | 109.5 |

Table B.4. Anisotropic displacement parameters ($Å^2 x\ 10^3$) for **5.2a-Cl**. The anisotropic displacement factor exponent takes the form: $-2\pi^2[\ h^2\ a^{*2}U^{11} + ...\ + 2\ h\ k\ a^*\ b^*\ U^{12}\ ]$

| | $U^{11}$ | $U^{22}$ | $U^{33}$ | $U^{23}$ | $U^{13}$ | $U^{12}$ |
|---|---|---|---|---|---|---|
| Cl1A | 37(1) | 38(1) | 36(1) | 7(1) | 16(1) | 7(1) |
| Cl2A | 58(1) | 53(1) | 32(1) | 23(1) | 14(1) | 23(1) |
| O1A | 30(1) | 45(1) | 30(1) | 11(1) | 6(1) | 23(1) |
| O2A | 29(1) | 50(1) | 34(1) | 16(1) | 6(1) | 22(1) |
| O3A | 62(2) | 48(2) | 36(2) | -5(1) | -5(1) | 28(1) |
| O4A | 60(2) | 46(2) | 47(2) | 2(1) | 7(1) | 36(1) |
| O5A | 43(2) | 42(2) | 100(2) | -14(2) | -23(2) | 20(1) |
| O6A | 35(1) | 29(1) | 36(1) | 6(1) | 3(1) | 15(1) |
| N1A | 26(1) | 27(1) | 29(2) | 10(1) | 6(1) | 16(1) |
| N2A | 32(2) | 32(2) | 32(2) | 6(1) | 11(1) | 11(1) |
| C2A | 29(2) | 23(2) | 25(2) | 3(1) | 8(1) | 13(1) |
| C3A | 29(2) | 20(2) | 23(2) | 3(1) | 4(1) | 9(1) |
| C4A | 25(2) | 21(2) | 29(2) | 0(1) | 4(1) | 7(1) |
| C5A | 31(2) | 24(2) | 26(2) | 1(1) | 8(1) | 6(2) |
| C6A | 42(2) | 25(2) | 23(2) | 8(1) | 9(2) | 13(2) |
| C7A | 27(2) | 30(2) | 26(2) | 6(1) | 4(1) | 12(1) |
| C8A | 26(2) | 22(2) | 25(2) | 3(1) | 5(1) | 9(1) |
| C9A | 30(2) | 25(2) | 26(2) | 2(1) | 4(1) | 14(1) |
| C10A | 29(2) | 28(2) | 26(2) | 10(1) | 7(1) | 18(1) |
| C11A | 20(2) | 28(2) | 26(2) | 12(1) | 10(1) | 11(1) |
| C12A | 26(2) | 26(2) | 31(2) | 11(1) | 5(1) | 15(1) |
| C13A | 26(2) | 32(2) | 24(2) | 10(1) | 1(1) | 10(1) |
| C14A | 23(2) | 26(2) | 27(2) | 6(1) | 9(1) | 8(1) |
| C15A | 33(2) | 33(2) | 33(2) | 11(2) | 10(2) | 22(2) |
| C16A | 33(2) | 39(2) | 23(2) | 11(2) | 4(1) | 20(2) |
| C17A | 28(2) | 33(2) | 26(2) | 14(1) | 4(1) | 16(1) |
| C18A | 30(2) | 43(2) | 37(2) | 13(2) | 5(2) | 15(2) |
| C19A | 31(2) | 31(2) | 39(2) | 10(2) | 3(2) | 13(2) |
| C20A | 49(2) | 34(2) | 46(2) | 11(2) | 8(2) | 22(2) |

| | | | | | | |
|---|---|---|---|---|---|---|
| Cl1 | 56(1) | 66(1) | 34(1) | 29(1) | 11(1) | 32(1) |
| Cl2 | 29(1) | 40(1) | 32(1) | 14(1) | 11(1) | 11(1) |
| O1 | 26(1) | 46(1) | 36(1) | 10(1) | 5(1) | 21(1) |
| O2 | 27(1) | 41(1) | 34(1) | 18(1) | 6(1) | 19(1) |
| O3 | 76(2) | 55(2) | 46(2) | 5(1) | 12(1) | 48(2) |
| O4 | 43(2) | 49(2) | 59(2) | -14(1) | 9(1) | 14(1) |
| O5 | 42(2) | 39(1) | 32(1) | 3(1) | -1(1) | 15(1) |
| O6 | 39(1) | 24(1) | 40(1) | 1(1) | 3(1) | 9(1) |
| N1 | 24(1) | 30(1) | 25(1) | 7(1) | 6(1) | 13(1) |
| N2 | 53(2) | 35(2) | 38(2) | 7(1) | 18(2) | 19(2) |
| C2 | 25(2) | 26(2) | 28(2) | 3(1) | 2(1) | 13(1) |
| C3 | 25(2) | 24(2) | 25(2) | 1(1) | 1(1) | 13(1) |
| C4 | 31(2) | 38(2) | 28(2) | 8(2) | -1(2) | 23(2) |
| C5 | 35(2) | 32(2) | 16(2) | 7(1) | 1(1) | 14(2) |
| C6 | 25(2) | 24(2) | 25(2) | 3(1) | 7(1) | 8(1) |
| C7 | 23(2) | 20(2) | 23(2) | 2(1) | -1(1) | 10(1) |
| C8 | 22(2) | 19(2) | 21(2) | 0(1) | 0(1) | 8(1) |
| C9 | 24(2) | 21(2) | 29(2) | 5(1) | 3(1) | 10(1) |
| C10 | 22(2) | 29(2) | 30(2) | 9(1) | 9(1) | 10(1) |
| C11 | 28(2) | 26(2) | 28(2) | 10(1) | 10(1) | 12(1) |
| C12 | 30(2) | 35(2) | 30(2) | 13(2) | 7(1) | 15(2) |
| C13 | 42(2) | 37(2) | 36(2) | 17(2) | 18(2) | 27(2) |
| C14 | 39(2) | 25(2) | 29(2) | 8(1) | 14(2) | 13(2) |
| C15 | 26(2) | 32(2) | 40(2) | 4(2) | 10(2) | 8(2) |
| C16 | 26(2) | 36(2) | 40(2) | 7(2) | 15(2) | 14(2) |
| C17 | 21(2) | 24(2) | 30(2) | 6(1) | 9(1) | 5(1) |
| C18 | 34(2) | 29(2) | 32(2) | 10(1) | 12(2) | 9(2) |
| C19 | 27(2) | 28(2) | 31(2) | 10(2) | 11(2) | 6(1) |
| C20 | 51(2) | 27(2) | 46(2) | 0(2) | 11(2) | 13(2) |

_____

_

Table B.5. Hydrogen coordinates ( x $10^4$) and isotropic displacement parameters (Å$^2$x $10^3$) for **5.2a-Cl**.

| | x | y | z | U(eq) |
|---|---|---|---|---|
| H4A | 7469 | 4992 | 456 | 31 |
| H7A | 1961 | 5665 | -843 | 33 |
| H10A | 2731 | 2703 | 2724 | 30 |
| H12A | 3545 | 3942 | 4319 | 31 |
| H13A | 3989 | 6048 | 5594 | 34 |
| H15A | 1084 | 7697 | 3726 | 36 |
| H16A | 636 | 5583 | 2444 | 36 |
| H18A | -2762 | 1124 | 1953 | 44 |
| H18B | -1570 | 3000 | 2521 | 44 |
| H20A | 2468 | -1583 | 1583 | 62 |
| H20B | 980 | -1676 | 643 | 62 |
| H20C | 275 | -2312 | 1577 | 62 |
| H4 | 7538 | 1288 | 9070 | 36 |
| H7 | 2347 | 2237 | 7594 | 27 |
| H10 | 9714 | 4113 | 6175 | 32 |
| H12 | 10558 | 2287 | 5343 | 37 |
| H13 | 9898 | -39 | 4178 | 40 |
| H15 | 4502 | -529 | 3401 | 40 |
| H16 | 5151 | 1731 | 4604 | 39 |
| H18C | 7633 | 6041 | 4329 | 38 |
| H18D | 7210 | 4133 | 4037 | 38 |
| H20D | 7784 | 9646 | 6408 | 65 |
| H20E | 9820 | 9633 | 6719 | 65 |
| H20F | 8225 | 8851 | 7303 | 65 |

Table B.6. Torsion angles [°] for **5.2a-Cl**.

| | | | |
|---|---|---|---|
| C9A-N1A-C2A-O1A | 178.0(3) | C2A-N1A-C10A-C17A | -132.4(3) |
| C10A-N1A-C2A-O1A | 2.5(5) | C9A-N1A-C10A-C11A | -77.9(4) |
| C9A-N1A-C2A-C3A | -2.0(3) | C2A-N1A-C10A-C11A | 96.9(3) |
| C10A-N1A-C2A-C3A | -177.6(3) | N1A-C10A-C11A-C12A | -122.6(3) |
| O1A-C2A-C3A-C8A | -178.8(3) | C17A-C10A-C11A-C12A | 109.6(3) |
| N1A-C2A-C3A-C8A | 1.3(3) | N1A-C10A-C11A-C16A | 56.3(4) |
| O1A-C2A-C3A-C4A | -0.4(6) | C17A-C10A-C11A-C16A | -71.5(3) |
| N1A-C2A-C3A-C4A | 179.7(3) | C16A-C11A-C12A-C13A | -1.7(4) |
| C8A-C3A-C4A-C5A | 0.9(5) | C10A-C11A-C12A-C13A | 177.3(3) |
| C2A-C3A-C4A-C5A | -177.3(3) | C11A-C12A-C13A-C14A | -0.1(4) |
| C3A-C4A-C5A-C6A | -0.4(5) | C12A-C13A-C14A-C15A | 2.0(4) |
| C3A-C4A-C5A-Cl1A | -179.8(2) | C12A-C13A-C14A-N2A | -176.9(3) |
| C4A-C5A-C6A-C7A | -0.1(5) | O4A-N2A-C14A-C13A | -173.9(3) |
| Cl1A-C5A-C6A-C7A | 179.3(3) | O3A-N2A-C14A-C13A | 8.3(4) |
| C4A-C5A-C6A-Cl2A | -179.6(2) | O4A-N2A-C14A-C15A | 7.2(4) |
| Cl1A-C5A-C6A-Cl2A | -0.2(4) | O3A-N2A-C14A-C15A | -170.7(3) |
| C5A-C6A-C7A-C8A | 0.1(5) | C13A-C14A-C15A-C16A | -2.0(5) |
| Cl2A-C6A-C7A-C8A | 179.6(3) | N2A-C14A-C15A-C16A | 176.9(3) |
| C6A-C7A-C8A-C3A | 0.4(5) | C14A-C15A-C16A-C11A | 0.1(4) |
| C6A-C7A-C8A-C9A | 177.7(3) | C12A-C11A-C16A-C15A | 1.7(4) |
| C4A-C3A-C8A-C7A | -1.0(5) | C10A-C11A-C16A-C15A | -177.3(3) |
| C2A-C3A-C8A-C7A | 177.6(3) | N1A-C10A-C17A-C18A | -109.2(3) |
| C4A-C3A-C8A-C9A | -178.7(3) | C11A-C10A-C17A-C18A | 19.2(4) |
| C2A-C3A-C8A-C9A | -0.2(4) | N1A-C10A-C17A-C19A | 72.2(3) |
| C2A-N1A-C9A-O2A | -177.1(3) | C11A-C10A-C17A-C19A | -159.4(3) |
| C10A-N1A-C9A-O2A | -1.8(5) | C20A-O6A-C19A-O5A | -2.6(5) |
| C2A-N1A-C9A-C8A | 1.9(3) | C20A-O6A-C19A-C17A | 175.0(3) |
| C10A-N1A-C9A-C8A | 177.2(3) | C18A-C17A-C19A-O5A | 23.3(5) |
| C7A-C8A-C9A-O2A | 0.4(6) | C10A-C17A-C19A-O5A | -158.0(3) |
| C3A-C8A-C9A-O2A | 177.9(3) | C18A-C17A-C19A-O6A | -154.2(3) |
| C7A-C8A-C9A-N1A | -178.6(3) | C10A-C17A-C19A-O6A | 24.5(4) |
| C3A-C8A-C9A-N1A | -1.1(4) | C9-N1-C2-O1 | 179.5(3) |
| C9A-N1A-C10A-C17A | 52.8(4) | C10-N1-C2-O1 | 6.0(5) |

| | | | |
|---|---|---|---|
| C9-N1-C2-C3 | 1.2(3) | C9-N1-C10-C11 | -86.3(3) |
| C10-N1-C2-C3 | -172.3(3) | C2-N1-C10-C17 | -145.3(3) |
| O1-C2-C3-C4 | -3.1(6) | C9-N1-C10-C17 | 42.3(4) |
| N1-C2-C3-C4 | 175.1(3) | N1-C10-C11-C16 | 63.8(3) |
| O1-C2-C3-C8 | 179.8(3) | C17-C10-C11-C16 | -63.4(3) |
| N1-C2-C3-C8 | -2.0(3) | N1-C10-C11-C12 | -114.1(3) |
| C8-C3-C4-C5 | -0.1(5) | C17-C10-C11-C12 | 118.7(3) |
| C2-C3-C4-C5 | -177.0(3) | C16-C11-C12-C13 | 0.5(4) |
| C3-C4-C5-C6 | -2.2(5) | C10-C11-C12-C13 | 178.5(3) |
| C3-C4-C5-Cl1 | 176.9(2) | C11-C12-C13-C14 | 1.1(4) |
| C4-C5-C6-C7 | 2.4(5) | C12-C13-C14-C15 | -1.6(5) |
| Cl1-C5-C6-C7 | -176.7(2) | C12-C13-C14-N2 | 177.8(3) |
| C4-C5-C6-Cl2 | -178.3(3) | O3-N2-C14-C13 | 5.4(4) |
| Cl1-C5-C6-Cl2 | 2.6(4) | O4-N2-C14-C13 | -174.2(3) |
| C5-C6-C7-C8 | -0.1(5) | O3-N2-C14-C15 | -175.2(3) |
| Cl2-C6-C7-C8 | -179.4(2) | O4-N2-C14-C15 | 5.3(4) |
| C6-C7-C8-C3 | -2.3(4) | C13-C14-C15-C16 | 0.3(5) |
| C6-C7-C8-C9 | 175.1(3) | N2-C14-C15-C16 | -179.1(3) |
| C4-C3-C8-C7 | 2.5(5) | C14-C15-C16-C11 | 1.4(5) |
| C2-C3-C8-C7 | 179.9(3) | C12-C11-C16-C15 | -1.9(4) |
| C4-C3-C8-C9 | -175.4(3) | C10-C11-C16-C15 | -179.8(3) |
| C2-C3-C8-C9 | 2.0(3) | N1-C10-C17-C18 | -128.6(3) |
| C2-N1-C9-O2 | -178.3(3) | C11-C10-C17-C18 | -2.9(4) |
| C10-N1-C9-O2 | -5.4(5) | N1-C10-C17-C19 | 59.9(3) |
| C2-N1-C9-C8 | 0.0(3) | C11-C10-C17-C19 | -174.5(2) |
| C10-N1-C9-C8 | 172.8(3) | C20-O6-C19-O5 | 2.5(4) |
| C7-C8-C9-O2 | -0.8(6) | C20-O6-C19-C17 | -176.4(3) |
| C3-C8-C9-O2 | 176.9(3) | C18-C17-C19-O5 | -148.2(3) |
| C7-C8-C9-N1 | -178.9(3) | C10-C17-C19-O5 | 23.8(4) |
| C3-C8-C9-N1 | -1.3(3) | C18-C17-C19-O6 | 30.7(4) |
| C2-N1-C10-C11 | 86.1(3) | C10-C17-C19-O6 | -157.3(2) |

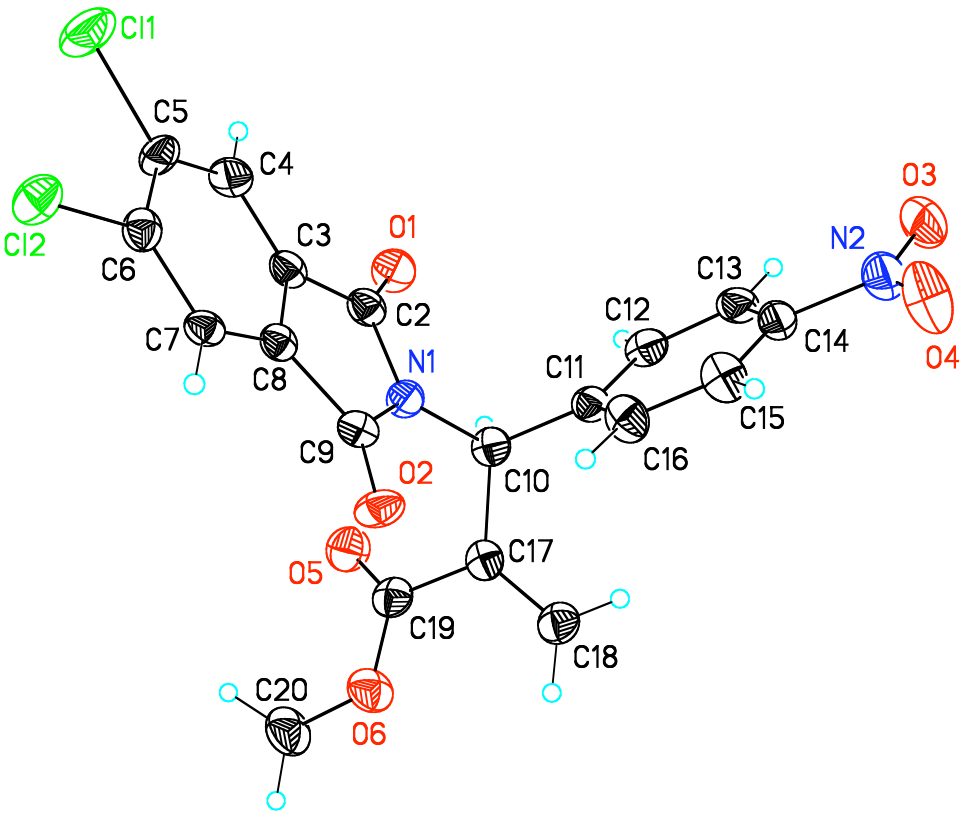


Figure B.1. View of molecule 1 of **5.2a-Cl** showing the atom labeling scheme. Displacement ellipsoids are scaled to the 50% probability level.

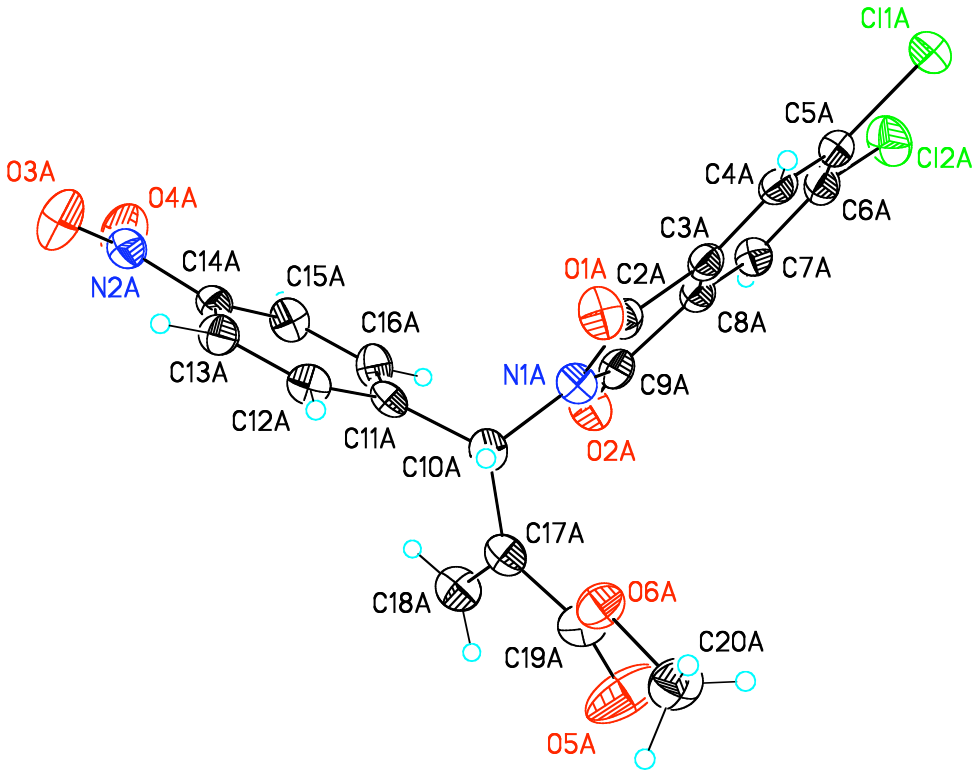


Figure B.2. View of molecule 2 of **5.2a-Cl** showing the atom labeling scheme. Displacement ellipsoids are scaled to the 50% probability level.

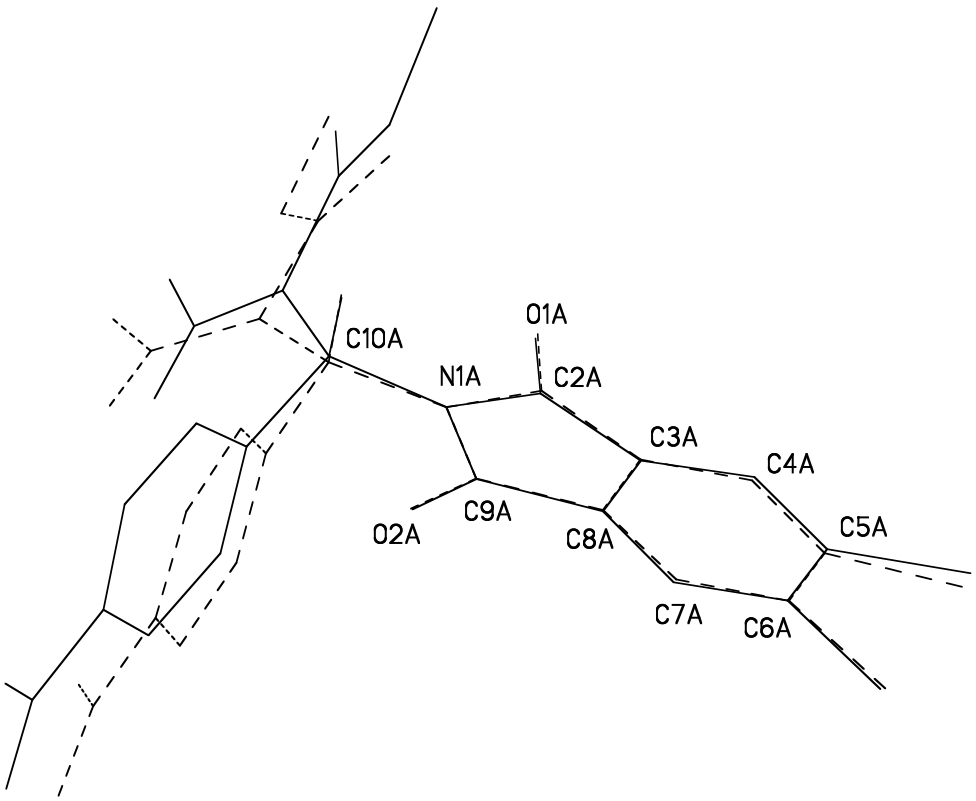


Figure B.3. View of the fit by least-squares of selected atoms from molecule 1 (dashed lines) onto the equivalent atoms of molecule 2 (solid lines). The atoms from molecule 2 used in the fit are labeled.

## Glossary of Common Abbreviations

| | |
|---|---|
| AIBN | Azobisisobutyronitrile |
| BARC | Bottom Antireflective Coating |
| BINOL | 2,2'-dihydroxy binaphthyl |
| BPO | Benzoyl Peroxide |
| CAR | Chemically Amplified Resist |
| CIDNP | Chemically Induced Dynamic Nuclear Polarization |
| CIP | Contact Ion Pair |
| CPU | Central Processing Unit |
| DCC | Dicyclohexyl carbodiimide |
| DEL | Double Exposure Lithography |
| DMAP | *N,N*-Dimethylamino pyridine |
| DMF | Dimethyl formamide |
| DMSO | Dimethyl Sulfoxide |
| DNQ | Diazonaphthoquinone |
| DOF | Depth of Focus |
| DPL | Double Patterning Lithography |
| DPPBA | Diphenylphosphino benzoic acid |
| DSC | Differential Scanning Calorimetry |
| DUV | Deep Ultraviolet |
| ESR | Electron Spin Resonance |
| EUVL | Extreme Ultraviolet |
| FT-IR | Fourier Transform Infrared |
| GPC | Gel Permiation Chromatography |
| IC | Integrated Circuit |

| | |
|---|---|
| ISTP | Intermediate-State Two Photon PAG |
| LC | Liquid Crystal |
| MBH | Morita-Baylis-Hillman reaction |
| $M_N$ | Number average Molecular Weight |
| MOP | 2-Methoxy-2'-diphenylphosphino binaphthyl |
| *NA* | Numerical Aperture |
| NMDPP | *Neo*-menthol diphenylphosphine |
| Nuc | Nucleophile |
| ODMA | Octadecyl Methacrylate |
| OTL | Optical Threshold Layer |
| PAG | Photoacid Generator |
| PBMA | Poly(butyl methacrylate) |
| PGMEA | Propylene Glycol Methyl Ether Acetate |
| PODMA | Poly(octadecyl methacrylate) |
| POM | Polarized Optical Microscopy |
| PPHA | Poly(phthaldialdehyde) |
| Pyr | Pyridine |
| rCEL | Reversible Contrast Enhancement Layer |
| $SOCl_2$ | Thionyl Chloride |
| SSIP | Solvent-Separated Ion Pair |
| *t*-BOC | *tert*-Butoxycarbonyl |
| TBSCl | *tert*-Butyl dimethylsilyl chloride |
| $T_g$ | Glass transition |
| $T_m$ | Melting Temperature |
| UV | Ultraviolet |

# BIBLIOGRAPHY


Akiyama, H.; Kudo, K.; Ichimura, K. *Makromolekulare Chemie, Rapid Communications* **1995**, *16*, 35-41.

Barachevsky, V. A. *J. Photochem. Photobiol., A* **2008**, *196*, 180-189.

Bard, A. J. *private communication*.

Birney, D.; Tang, K. L.; Koh, J. H. P.; Pool, B. R.; White, J. M. *J. Am. Chem. Soc.* **2002**, *124*, 5091-5099.

Boden, N.; Bushby, R. J.; Clark, L. D. *J. Chem. Soc. Perkin Trans. 1* **1983**, 543-551.

Bradshaw, J. S.; Hammond, G. S. *J. Am. Chem. Soc.* **1963**, *85*, 3953-3955.

Byers, J.; Lee, S.; Jen, K.; Zimmerman, P.; Turro, N. J.; Willson, C. G. *J. Photopolym. Sci. Technol.* **2007**, *20*, 707-717.

Chapman, G. H.; Dykes, J.; Poon, D.; Choo, C.; Wang, J.; Peng, J.; Tu, Y. *Proc. SPIE-Int. Soc. Opt. Eng.* **2005**, *5713*, 247-258.

Chapman, G.; Poon, D.; Choo, C.; Tu, Y.; Dykes, J.; Wang, J.; Peng, J.; Lennard, W.; Kavanagh, K. *Proc. SPIE-Int. Soc. Opt. Eng.* **2005**, *5753*, 976-987.

Chien, G. C.; Kuo, J. F.; Chen, C. *J. Polym. Sci. Polym. Chem.* **1993**, *31*, 2423.

Chiou, J. S.; Paul, D. R. *J. Polym. Sci., Part B: Polym. Phys.* **1987**, *25*, 1699-1707.

Crano, J. C.; Flood, T.; Knowles, D.; Kumar, A.; Van Gemert, B. *Pure Appl. Chem.* **1996**, *68*, 1395-1398.

Crivello, J. V. *J. Polym. Sci., Part A: Polym. Chem.* **1999**, *37*, 4241-4254.

Crivello, J. V. US Patent 19760921.

Deindoerfer, P.; Geiger, T.; Schollmeyer, D.; Ye, J. H.; Zentel, R. *J. Mater. Chem.* **2006**, *16*, 351-358.

Dill, F. H. *IEEE Transactions on Electron Devices* **1975**, *22*, 440-444.

Dill, F. H.; Hornberger, W. P.; Hauge, P. S.; Shaw, J. M. *IEEE Transactions on Electron Devices* **1975**, *22*, 445-452.

Dykes, J. M.; Plesa, C.; Choo, C.; Chapman, G. H. *Proc. SPIE-Int. Soc. Opt. Eng.* **2007**, *6730*, 673040/1-673040/10.

Eich, M.; Wendorff, J. H.; Reck, B.; Ringsdorf, H. *Makromolekulare Chemie, Rapid Communications* **1987**, *8*, 59-63.

Elderfield, R. C.; Hydorn, A. E.; Schenker, E.; Wyckoff, K. K. *J. Org. Chem.* **1959**, *24*, 1296-1301.

Frechet, J. M. J.; Eichler, E.; Ito, H.; Willson, C. G. *Polymer* **1983**, *24*, 995-1000.

Grant, B. D.; Clecak, N. J.; Twieg, R. J.; Willson, C. G. *IEEE Transactions on Electron Devices* **1985**, *28*, 1300-1305.

Haas, W. E.; Nelson, K. F.; Adams, J. E.; Dir, G. A. *J. Electrochem. Soc.* **1974**, *121*, 1667-1669.

Hoffmann, N. *J. Photochem. Photobiol., C* **2008**, *9*, 43-60.

Horvath, J.; Nyitrai, K.; Cser, F.; Hardy, G. *Eur. Polym J.* **1985**, *21*, 251-257.

Ichimura, K. *Chem. Rev.* **2000**, *100*, 1847-1873.

Ikeda, T. *J. Mater. Chem.* **2003**, *13*, 2037-2057.

Ikeda, T.; Horiuchi, S.; Karanjit, D. B.; Kurihara, S.; Tazuke, S. *Macromolecules* **1990**, *23*, 36-42.

Ikeda, T.; Horiuchi, S.; Karanjit, D. B.; Kurihara, H.; Tazuke, S. *Macromolecules* **1990**, *23*, 42-48.

Ikeda, T.; Yoneyama, S.; Yamamoto, T.; Hasegawa, M. *Mol. Cryst. Liq. Cryst.* **2002**, *375*, 45-60.

Ito, H. *Adv. Polym. Sci.* **2005**, *172*, 37-245.

Ito, H.; Willson, C. G. *Polymer Engineering and Science* **1983**, *23*, 1012-1018.

Iwaki, J.; Suzuki, S.; Park, C.; Miyagawa, N.; Takahara, S.; Yamaoka, T. *J. Photopolym. Sci. Technol.* **2004**, *17*, 123-124.

Jiang, Q.; Spehar, A.-M.; Hakansson, M.; Suomi, J.; Ala-Kleme, T.; Kulmala, S. *Electrochim. Acta* **2006**, *51*, 2706-2714.

Kawabe, Y.; Tan, S.; Nishiyama, F.; Sakaguchi, S.; Kokubo, T.; Blakeney, A. J.; Ferreira, L. *Proc. SPIE Int. Soc. Opt. Eng.* **1996**, *2724*, 420-437.

Kim, J. Y. F., T. *Mol. Cryst. Liq. Cryst.* **2006**, *449*, 71-80.

Kondo, M.; Maeda, T.; Shishido, A.; Ikeda, T.; Yu, Y.; Nakano, M.; Shiono, T. *Mol. Cryst. Liq. Cryst.* **2005**, *441*, 297-305.

Kuebler, S. M.; Braun, K. L.; Zhou, W.; Cammack, J. K.; Yu, T.; Ober, C. K.; Marder, S. R.; Perry, J. W. *J. Photochem. Photobiol., A* **2003**, *158*, 163-170.

Kumar, G. S.; Neckers, D. C. *Chem. Rev.* **1989**, *89*, 1915-1925.

Kurihara, H.; Shishido, A.; Ikeda, T.; Tsutsumi, O.; Shiono, T. *Mol. Cryst. Liq. Cryst.* **2005**, *441*, 173-184.

Kurihara, S.; Ikeda, T.; Tazuke, S. *Japanese Journal of Applied Physics* **1988**, *27*, L1791-L1792.

Lee, S.; Byers, J.; Jen, K.; Zimmerman, P.; Rice, B.; Turro, N. J.; Willson, C. G. *Proc. SPIE* **2008**, *6924*, 69242A/1-69242A/12.

Lee, S.; Jen, K.; Willson, C. G.; Byers, J.; Zimmerman, P.; Turro, N. J. *J. Micro/Nanolithogr., MEMS, MOEMS* **2009**, *8*, 011011/1-011011/11.

Legge, C. H.; Mitchell, G. R. *J. Phys. D: Appl. Phys.* **1992**, *25*, 492-499.

Lehmann, O. *Z. Physikal Chem.* **1889**, *4*, 462.

Mack, C. A. In *Fundamental Principles of Optical Lithography*; John Wiley & Sons: West Sussex, 2007, p 15-18.

Mack, C. A. In *Fundamental Principles of Optical Lithography*; John Wiley & Sons: West Sussex, 2007, p 129-140.

Mack, C. A. In *Fundamental Principles of Optical Lithography*; John Wiley & Sons: West Sussex, 2007, p 224-235.

Malval, J.-P.; Morlet-Savary, F.; Allonas, X.; Fouassier, J.-P.; Suzuki, S.; Takahara, S.; Yamaoka, T. *Chem. Phys. Lett.* **2007**, *443*, 323-327.

Malval, J.-P.; Suzuki, S.; Morlet-Savary, F.; Allonas, X.; Fouassier, J.-P.; Takahara, S.; Yamaoka, T. *J. Phys. Chem. A.* **2008**, *112*, 3879-3885.

Matsumoto, K.; Costner, E. A.; Nishimura, I.; Ueda, M.; Willson, C. G. *Macromolecules* **2008**, *41*, 5674-5680.

Medeiros, D. R. Dissertation, Univeristy of Texas at Austin, 1998.

Mogri, Z., Dissertation, University of Texas at Austin, 2001.

Mogri, Z.; Paul, D. R. *Polymer* **2001**, *42*, 2531-2542.

Mogri, Z.; Paul, D. R. *Polymer* **2001**, *42*, 7765-7780.

Moore, G. E. *Electronics* **1965**, *38*, 114-117.

Morneau, W. M. In *Semiconductor Lithography*; Plenum Press: New York, 1988, p 259-327.

Morneau, W. M. In *Semiconductor Lithography*; Plenum Press: New York, 1988, p 329-353.

Morneau, W. M. In *Semiconductor Lithography*; Plenum Press: New York, 1988, p 355-408.

Morneau, W. M. In *Semiconductor Lithography*; Plenum Press: New York, 1988, p 631-777.

Morneau, W. M. In *Semiconductor Lithography*; Plenum Press: New York, 1988, p 779-812.

Morneau, W. M. In *Semiconductor Lithography*; Plenum Press: New York, 1988, p 409-458.

Natansohn, A.; Rochon, P. *Chem. Rev.* **2002**, *102*, 4139-4175.

O'Connor, N. A.; Berro, A. J.; Lancaster, J. R.; Gu, X.; Jockusch, S.; Nagai, T.; Ogata, T.; Lee, S.; Zimmerman, P.; Willson, C. G.; Turro, N. J. *Chem. Mater.* **2008**, *20*, 7374-7376.

O'Leary, K. A., Dissertation, University of Texas at Austin, 2005.

O'Leary, K. A.; Paul, D. R. *Polymer* **2004**, *45*, 6575-6585.

O'Leary, K. A.; Paul, D. R. *Polymer* **2006**, *47*, 1226-1244.

O'Leary, K. A.; Paul, D. R. *Polymer* **2006**, *47*, 1245-1258.

Odian, G. In *Principles of Polymerization*; 4th ed.; John Wiley & Sons: Hoboken, NJ, 2004, p 279-281.

Okano, K.; Shishido, A.; Ikeda, T. *Macromolecules* **2006**, *39*, 145-152.

Olah, G. A.; Surya Prakash, G. K. *Superacids*; Wiley: New York, 1985,7-8.

Pohlers, G.; Scaiano, J. C.; Sinta, R. *Chem. Mater.* **1997**, *9*, 3222-3230.

Portugall, M.; Ringsdorf, H.; Zentel, R. *Makromolecular Chemie* **1982**, *183*, 2311-2321.

Postnikov, S. V.; Stewart, M. D.; Vi Tran, H.; Nierode, M. A.; Medeiros, D. R.; Cao, T.; Byers, J.; Webber, S. E.; Wilson, C. G. *J. Vac. Sci. Technol., B* **1999**, *17*, 3335-3338.

Prasad, S. K.; Nair, G. G.; Sandhya, K. L.; Rao, D. S. S. *Curr. Sci.* **2004**, *86*, 815-823.

Reck, B.; Ringsdorf, H. *Makromolekulare Chemie, Rapid Communications* **1985**, *6*, 291-299.

Rehm, D.; Weller, A. *Ber. Bunsen-Ges.* **1969**, *73*, 834-839.

Reinitzer, F. *Monatsch. Chem.* **1888**, *9*, 421.

Ringsdorf, H.; Schmidt, H.-W. *Makromolecular Chemie* **1984**, *185*, 1327-1334.

Sadagopan, K.; Rekha, A. S.; Ratna, D.; Samui, A. B. *J. Appl. Polym. Sci.* **2007**, *104*, 3497-3504.

Saishoji, A.; Sato, D.; Shishido, A.; Ikeda, T. *Langmuir* **2007**, *23*, 320-326.

Selassie, C. D.; Hansch, C.; Khwaja, T. A.; Dias, C. B.; Pentecost, S. *J. Med. Chem.* **1984**, *27*, 347-357.

Singh, S. In *Liquid Crystals: Fundamentals*; World Scientific Publishing: Singapore, 2002, p 1-27.

Smith, G. H. US Patent 19830719.

Stewart, M. D., Dissertation, University of Texas at Austin, 2003.

Still, W. C.; Kahn, M.; Mitra, A. *J. Org. Chem.* **1978**, *43*, 2923-2925.

Sung, J.-H.; Hirano, S.; Tsutsumi, O.; Kanazawa, A.; Shiono, T.; Ikeda, T. *Chem. Mater.* **2002**, *14*, 385-391.

Tazuke, S.; Kurihara, S.; Ikeda, T. *Chem. Lett.* **1987**, 911-914.

Thompson, L. F.; Bowden, M. J. In *Introduction to Microlithography*; Thompson, L. F., Willson, C. G., Bowden, M. J., Eds.; American Chemical Society: Washington, D.C., 1983, p 161-214.

Thompson, L. F. In *Introduction to Microlithography*; Second Edition ed.; Thompson, L. F., Willson, C. G., Bowden, M. J., Eds.; American Chemical Society: Washington, D.C., 1994, p 332-341.

Weinkauf, D. H.; Paul, D. R. *J. Polym. Sci., Part B: Polym. Phys.* **1992**, *30*, 817-835.

Weinkauf, D. H.; Paul, D. R. *J. Polym. Sci., Part B: Polym. Phys.* **1992**, *30*, 837-849.

Willson, C. G. In *Introduction to Microlithography*; Thompson, L. F., Willson, C. G., Bowden, M. J., Eds.; American Chemical Society: Washington, D.C., 1983, p 87-159.

Willson, C. G.; Ito, H.; Frechet, J. M. J.; Tessier, T. G.; Houlihan, F. M. *J. Electrochem. Soc.* **1986**, *133*, 181-7.

Wurm, S. *J. Photopolym. Sci. Technol.* **2009**, *22*(1), 31-42.

Zhang, B.; Guo, S.; Shao, B. *J. Appl. Polym. Sci.* **1998**, *68*, 1555-1561.

Zimmerman, P. A.; Rice, B. J.; Piscani, E. C.; Liberman, V.; Harry, J. L., Mircea, V. D., Eds.; SPIE: 2009; Vol. 7274, p 727420.

# Vita

Adam was born in November 1980 to Emil and Christine Berro in Kalamazoo, Michigan. He grew up in Michigan, and graduated from Portage Northern High School in 1999. He attended the University of Michigan in Ann Arbor, where he worked for Prof. Henry C. Griffin doing research involving γ-ray spectroscopy of metastable protactinium isotopes. He did research as a Junior and Senior for Prof. Dmitri Coucouvanis involving the synthesis of large metal sulfide clusters related to the nitrogenase enzyme and graduated with a BS in chemistry from the University of Michigan in 2003. In addition, he worked two summers at Pharmacia Corp. in Kalamazoo as an undergraduate. In the fall of 2003, he began work on his Ph.D. at the University of Texas at Austin, where he has done research in transition metal and organocatalysis, as well as materials design, synthesis, and application.

Permanent address: 8904 E. Gull Lake Dr. Augusta, MI 49012

This dissertation was typed by the author.